1974

Fracture toughness of bridge steels - phase ii final report, June 1974 (FHWA-RD-74-59, September 1974)

R. Roberts

G. R. Irwin

G. V. Krishna

B. T. Yen

PB-239 188

FRACTURE TOUGHNESS OF BRIDGE STEELS. PHASE II REPORT

LEHIGH UNIVERSITY

PREPARED FOR
FEDERAL HIGHWAY ADMINISTRATION

SEPTEMBER 1974

DISTRIBUTED BY:
NTIS
National Technical Information Service
U. S. DEPARTMENT OF COMMERCE

TECHNICAL REPORT STANDARD TITLE PAGE

1. Report No.	2. Government Accession No.	3. Recipient's Catalog No.
FHWA-RD-74-59		PB 239 188

4. Title and Subtitle	5. Report Date
FRACTURE TOUGHNESS OF BRIDGE STEELS - PHASE II REPORT	September 1974
	6. Performing Organization Code
7. Author(s) R. Roberts, G. R. Irwin, G. V. Krishna, B. T. Yen	8. Performing Organization Report No. Fritz Lab Report 379.2
9. Performing Organization Name and Address Lehigh University Bethlehem, Pa. 18016	10. Work Unit No. FCP 35F2-032
	11. Contract or Grant No. DOT-FH-11-7664
	13. Type of Report and Period Covered Final Report
12. Sponsoring Agency Name and Address Department of Transportation Federal Highway Administration Washington, D. C. 20590	14. Sponsoring Agency Code 34291

15. Supplementary Notes

FHWA Contract Manager for this study: C. F. Galambos (HRS-11)

16. Abstract

The ability of past and present steel highway bridges to withstand brittle fracture has been investigated. To this end, the static fracture toughness (K_{Ic}), the dynamic fracture toughness (K_{ID}), the dynamic tear energy (DT) and the Charpy impact properties (CVN) of eight steels common to bridge constructions have been measured over a temperature range of about -200° F to +75° F. The steels studied were A7, A36, A242, A440, A441, A588, A514 and A517. The use of these measures of fracture toughness and fracture mechanics in general are discussed as they apply to design, inspection and fabrication of bridges. The present AASHTO CVN requirements for bridge steels were evaluated in relationship to the finding of the program. These requirements were judged adequate for structures where parallel load paths exist. For structures where the loads are carried by only one load path more detailed material evaluations are recommended in place of the AASHTO CVN requirement.

17. Key Words	18. Distribution Statement
Fracture, Fracture of Steel, Bridge Failure, Bridge Design.	No restrictions. This document is available to the public through the National Technical Information Service, Springfield, Virginia 22151

19. Security Classif. (of this report)	20. Security Classif. (of this page)	21. No. of Pages	22. Price
Unclassified	Unclassified	418	10.50

Form DOT F 1700.7 (8-69)

Form FHWA 121 (Rev. 5-73)

UNITED STATES GOVERNMENT

Memorandum

DEPARTMENT OF TRANSPORTATION
FEDERAL HIGHWAY ADMINISTRATION

DATE:

In reply refer to: HRS-11

SUBJECT: Transmittal of Research Report No. FHWA-RD-74-59, "Fracture Toughness of Bridge Steels - Phase II Report"

FROM : Director
Office of Research
Washington, D. C. 20590

TO : Regional Federal Highway Administrators
Regions 1, 3-10

Distributed with this memorandum is the subject report with significant implementation potential. This report will be of interest to researchers as well as engineers involved in design, maintenance, inspection, and erection of steel highway bridge structures.

This report presents the results of various fracture toughness tests performed on a number of structural steels utilized in past and present bridge construction. These measures of the fracture toughness of tested materials and fracture mechanics in general are discussed as they may apply to the design, inspection and fabrication of bridges.

Distributed with this memorandum are sufficient copies of the report to provide a minimum of one copy to each regional office, division office, and State highway agency. Direct distribution is being made to the division offices. Additional copies for official use may be requested from Mr. F. J. Tamanini, Chief, Structures and Applied Mechanics Division, FHWA (HRS-10), Washington, D. C. 20590. These requests will be filled while our limited supply lasts. Additional copies for the public are available from the National Technical Information Service, Department of Commerce, 5285 Port Royal Road, Springfield, Virginia 22151. A small charge will be imposed for each copy ordered from NTIS.

for F. J. Tamanini
Charles F. Scheffey

Preceding page blank

TABLE OF CONTENTS

TABLE OF CONTENTS (continued)

TABLE OF CONTENTS (continued)

1. INTRODUCTION

The catastrophic failure of the Point Pleasant Bridge in 1967 (1) focused considerable attention on the ability of bridge steels to withstand fracture. In general, the problems associated with fracture are not new to the engineering community. Since the establishment of ASTM committee E-24 approximately thirteen years ago (2), much progress has been made in the understanding of fracture toughness measurements. To date, major emphasis has been placed on high strength aero-space materials. For steel, this normally implies a yield strength greater than 190 ksi. These materials can be characterized for the most part by a plane-strain fracture toughness measurement, K_{Ic} (3). The steels used in bridge construction have yield strengths below 150 ksi. Excepting instances of poor metallurgical quality or large section thickness, their plane-strain resistance to fracturing can be measured only at temperatures well below those of interest.

Recognizing the present limitations of fracture mechanics as applied to steels common to bridge construction, the U. S. Department of Transportation Federal Highway Administration initiated at Lehigh University a research project to study the fracture toughness of bridge steels. The primary objectives of this project were to establish meaningful measures of fracture toughness for bridge steels, practical methods of obtaining these measurements and to collect sufficient data

on past and present bridge steels to establish the fracture resistance of these steels. In particular this research project was separated into three phases.

PHASE 1 - Phase 1 was concerned with the establishment of meaningful measures and tests for fracture toughness. The materials considered in this portion were ASTM grades A36, A441, and A514 in thicknesses of 1/2", 1" and 2".

PHASE 2 - Phase 2 was concerned with the collection of fracture resistance data for ASTM grade steels A7, A242, A440, A588 and SAE 1035 in thicknesses of 1/2", 1" and 2" where possible. Phase 2 also included the fracture testing of four (4) pre-cracked A36 beams.

PHASE 3 - Phase 3 was a study of the applicability to bridge steel weldments of the techniques developed in Phase 1.

This report describes the results of Phase 1 and Phase 2 of the U. S. Department of Transportation Federal Highway Administration Fracture of Bridge Steels Project conducted at Lehigh University.

2. FRACTURE MECHANICS CONCEPTS

2.1 General Comments

The major objective of Phase 1 of this project was to establish a method or methods by which the fracture resistance of bridge steels can be evaluated. Many methods exist which are able to rank the relative fracture resistance of bridge steels. One such test is the well known Charpy V-notch (CVN) test. In past years such tests have not been extensively used by the bridge designer. Although CVN tests have shown that at some temperature steel A is more fracture resistant than steel B, the CVN test did not allow the designer to account for such variables as load level, loading rate, flaw size, etc. in the design of a fracture resistant structure. To overcome this problem with the CVN and similar tests, the body of knowledge known as fracture mechanics was developed over the past 15 years. Through the use of fracture mechanics concepts the designer can account for the effect of load level, loading rate, etc. in his design. However, as already noted in Chapter 1 of this report, linear elastic fracture mechanics as embodied in plane-strain fracture testing does not generally apply to bridge steels in the normal design temperature ranges. It is the intent of the remaining sections of this chapter to examine the limitations of linear elastic fracture mechanics as applied to bridge steels. The various types of tests conducted in Phase 1 and 2 will also be discussed.

2.2 Elementary Fracture Mechanics

The observation, that in the immediate vicinity of a crack the spatial distribution of the stresses are the same from one cracked body to another, forms the basis for a large portion of fracture mechanics theory. The effect of body geometry, crack size, loading, etc. is felt through a term called the stress intensity factor, K, which acts as a scale factor for the magnitude of the stress field. As an example, consider the two specimens which are common to fracture testing shown in Figure 1. If a polar coordinate system is placed at the crack tip of each specimen the state of stress near the tip can be written as (4).

$$\begin{Bmatrix} \sigma_y \\ \sigma_x \\ \sigma_{xy} \end{Bmatrix} = \frac{K \cos \frac{\theta}{2}}{\sqrt{2 \pi r}} \cdot \begin{Bmatrix} 1 + \sin \frac{\theta}{2} \sin \frac{3\theta}{2} \\ 1 - \sin \frac{\theta}{2} \sin \frac{3\theta}{2} \\ \sin \frac{\theta}{2} \cos \frac{3\theta}{2} \end{Bmatrix} \qquad (1)$$

where r and θ are polar coordinates, and K is the stress intensity factor. The values of K for the two specimens (3) shown in Figure 1 are indicated on the figure. Other K values and methods for determining K can be found in Reference 4.

At this point, if consideration is given to the process of fracture beginning at and propagating from the crack tip, it seems reasonable since the state of stress near the crack tips in the two specimens are spatially identical, that fracture will occur for the same material and loading rates when the stress levels local to the crack tip in the

two specimens are equal. This implies that fracture in specimen 1a and specimen 1b will occur at equal K levels. This reasoning leads to the concept of a critical K level or a K_c. If the concept of a critical stress intensity factor, K_c, is valid, once the K_c level is known for a particular material the effect of specimen or body geometry, crack size and load level on fracture can be predicted. All that has to be done is to equate the K value such as found in Figure 1 to the value of K_c to obtain the desired relationship.

Assuming for the time being that a property K_c exists for each material, it is quite simple to demonstrate the usefulness of fracture mechanics in the design process to guard against sudden or unexpected fracture. Basically four things are needed in a fracture control plan once the nominal design is set. These are:

1. K_c values for candidate materials.
2. Locations in the structure where cracks will form due to fabrication, fatigue, stress corrosion or any other cause of cracking.
3. K value calculations or methods for the probable crack configurations.
4. An understanding of available inspection techniques for crack detection applicable to the particular structure being designed.

To illustrate how these four things interact, consider a structure in which it is known that small cracks exist or can form during the expected life of the structure. Furthermore, assume that the

structure's geometry can be represented as a large thin plate subjected to a uniform stress σ and containing a small central crack of length $2a$. This would correspond to specimen 1a where

$$\sigma = \frac{P}{bW}$$

and

$$a << W.$$

For this geometry the K value is given as (4)

$$K = \sigma \sqrt{\pi a} \qquad (2)$$

It will now be assumed that the smallest flaw which can be found by inspection is $2a_i$. One possible method of combining all four items listed above in a fracture resistant design would be to require that the operating stress, σ_o, be limited to half (50%) of the stress level, σ_f, which would cause fracture at the point where the crack length just reaches $2a_i$. For a particular material this gives

$$\sigma_o = \frac{\sigma_f}{2} = \frac{K_c}{2\sqrt{\pi a_i}} \qquad (3)$$

where σ_o is the operating stress and σ_f is the failure stress for K_c and a_i.

It is quite possible that an operating stress given by equation (3) would be too low for practical purposes. This can be changed by going to a material which has a higher toughness or K_c value or going to better inspection techniques so that smaller crack lengths can be detected. Both of these possibilities are shown schematically on Figure 2. Another example of a fracture control plan called the Leak-Before-Burst criterion (27) is given in Appendix I.

The above discussion of a fracture control plan, although it touches on all of the essentials, is a gross oversimplification of fracture behavior. It is intended solely to illustrate how fracture mechanics can be used in design. The major difficulty of such a plan is that a single-valued materials constant K_c does not exist. The value of K_c can be greatly dependent upon loading rate, temperature and thickness as well as upon material quality. In response to these complexities, fracture mechanics initially focused attention on what is called plane-strain fracture testing and the determination of a K_c value called a plane-strain fracture toughness and denoted as K_{Ic} (3). This value represents the minimum toughness possessed by a material for a given temperature and loading speed. The major feature in K_{Ic} testing is that the value is determined for a configuration in which the constraint at the crack tip is great. This is just another way of saying that plasticity effects are small. The concept of constraint will be discussed in more detail later in this chapter.

At this point it is certainly justified to ask, "Why not use K_{Ic} in fracture design for bridge steels since K_{Ic} represents a minimum toughness and would produce a conservative design?" One part of the answer to such a question is simple. Using a conservative design philosophy based on K_{Ic} would place such an undue burden on the materials available that it would preclude the use of almost all past and present bridge steels. Records show that bridges in general do not fail due to fracture. Therefore to understand this past performance record and to guarantee that it continues in the future it is quite necessary to study the fracture behavior of bridge steels under non plane-strain conditions.

Considering the limitations of linear elastic fracture mechanics as briefly described above the series of tasks listed in Chapter 1 were laid out for Phase 1 of this project. The remaining sections of this chapter discuss loading speed and constraint as related to bridge steels. Also described are the types of tests and correlation procedures used in Phases 1 and 2.

2.3 Loading Speed

It might appear from stu' of the vibrational response of heavy bridge components that loading times for the components are generally greater than 0.05 seconds. Correspondingly, loading times equal to and greater than 0.05 seconds could be selected for measurements of fracture toughness. However, since crack extension behavior itself tends to inject high loading rates on a local scale from such things as "pop-in" (3), and since the degree of this influence is difficult to predict, a fracture test loading time of about 10^{-3} seconds can be defended as a reasonable lower limit for loading time.

Since it is impossible to predict the appropriate loading speed for fracture testing of bridge steels without realistic testing of full scale bridge components, loading speeds of 1 and 0.001 seconds were chosen for Phase 1. It was felt that these two loading times represented the possible extremes encountered in actual bridges. Also the K_c testing at the 0.001 loading time was given major emphasis since for the materials being tested this loading time produced minimum toughness values. With regard to loading speed this same philosophy was carried through into Phase 2.

2.4 Constraint

For purposes of selecting appropriate conditions for fracture toughness evaluations, in addition to testing temperature and loading speed, it is necessary to consider "constraint". The term, constraint, is interpreted here as the ratio of the plate thickness to the nominal size of the plastic zone (degree of elevation of the resistance to plastic deformation) close to the leading edge of the crack. For a given temperature, loading speed, and crack sharpness, the resistance to onset of rapid fracturing is minimum when there is a maximum degree of constraint. In situations of relatively small constraint, the resistance to plastic extensional strain is generally close to the uni-axial tensile yield strength, σ_{YS}. Maximum amounts of constraint correspond to a condition of plane-strain relative to relaxation of the stress component parallel to the leading edge of the crack. The resistance to plastic extensional strain for a degree of constraint corresponding to plane-strain is approximately 2 σ_{YS}.

Rough estimates of the degree of constraint can be made by comparing the nominal plastic zone size, 2 r_Y, to the plate thickness for a through-the-thickness crack, or to the net ligament and crack depth for a part-through surface crack. The value of 2 r_Y is given by the equation

$$2\ r_Y = \frac{1}{\pi} \left(\frac{K}{\sigma_Y}\right)^2 \qquad (4)$$

where σ_Y is the tensile yield strength for a given degree of constraint. The value of σ_Y in equation (4) as already indicated is about twice the

uni-axial tensile yield strength, σ_{YS}, under plane-strain conditions and roughly equal to σ_{YS} when the plastic zone is relatively large.

In the case of most bridge fracture occurrences, the fracture toughness can be thought of in terms of resistance to extension of a through-the-thickness crack in a plate-like element of the structure. For situations of this kind the degree of constraint can be estimated in terms of the ratio of the nominal plastic zone size, $2\ r_Y$, to the plate thickness, B. However, $2\ r_Y$ is itself sensitive to degree of constraint and it has been found useful to employ, in place of that ratio, the dimensionless factor, β, where

$$\beta = \frac{1}{B} \left(\frac{K}{\sigma_{YS}}\right)^2 \qquad (3)$$

As a matter of terminology, the symbols β_c or β_{Ic} are used when K is replaced by K_c or K_{Ic}. K_{Ic} is accurately defined by an ASTM testing standard (5) which requires specimen dimensions such that β_{Ic} is 0.4. or less. For a given temperature and loading speed, β_{Ic} depends only upon the plate thickness, B. Loss of constraint by reduction of B causes increase of the value of K_c and is often accompanied by a change in fracture appearance from flat-tensile to oblique-shear. A major portion of the change in fracture toughness from a condition of high constraint (plane-strain) to one of low constraint (plane-stress) occurs across the range of β_{Ic} values from 0.6 to 1.5. For steels with σ_{YS} above 180 ksi, a corresponding factor of 2 increase in K_c would be typical. For steels with σ_{YS} less than 150 ksi, the corresponding increase of K_c may be larger. Since the thicknesses of steel employed in bridge components cover a large range, the effect of constraint upon

resistance to crack extension is a significant consideration. To account for this thickness effect three material thicknesses were tested in Phases 1 and 2; 1/2 in., 1 in., and 2 in.

Elevation of the loading rate, as in dynamic testing, increases the degree of constraint by decreasing the value of β_{Ic}. The value of β_{Ic} is reduced in part because the yield strength of steels increases with strain rate and in part because elevation of yield strength is usually accompanied by loss of fracture toughness independently of the constraint effect. Elevation of the degree of constraint occurs when the testing temperature is lowered for the same pair of reasons.

2.5 R-Curve Testing

Brown and Srawley (6) give a detailed discussion of R-curves and their relationship to K_c measurements. Only a brief review will be given here, primarily to indicate the complexities which pertain to R-curves for rate sensitive structural steels. When crack extension starts from the leading edge of a fatigue crack many small fracture separations occur simultaneously along the crack front. These separations when viewed at a fine scale tend to be abrupt and their speed of joining is inherently fast enough to cause rapid crack propagation. However, under low constraint conditions macroscopic instability can be delayed and can be preceded by significant amounts of slow-stable crack extension. For situations of low constraint the resistance to crack extension is best represented by a graph showing the resistance to crack extension, K_R, as a function of the effective crack size, a (effective), across the entire range of stable crack extension. This is termed an R-curve.

An R-curve which would be typical of a material which is not rate sensitive is shown in Figure 3 as curve S. This curve shows that the resistance to crack extension is increasing as the crack length increases.

To understand how an R-curve is obtained and used, consider a typical expression for K and a/W for a test configuration such as shown in Figure 1. For this case the test would be started out at a fixed or initial a/W and the load would be increased. At a fixed or constant load level the expressions shown in Figure 1 are just curves of K versus a/W for a fixed load. Such a situation is shown as curve L_1, L_2, L_3 and L_4 in Figure 3. Thus as load increases different L curves become operative. As an example, consider the R-curve shown for an initial crack of 2 inches and curve L_1. At the point of intersection of these two curves, A_1, the K levels for the R-curve and the K - a curve are identical. If the crack would try to move further at this load, the K level produced would be less that value required from the R-curve. Thus for load L_1 a stable situation is achieved. As the load is increased to level L_2 the crack will propogate a short distance to the intersection A_2 and will again be stable for the reasons already discussed. At load L_3 the K - a and R-curves are tangent. This point is unstable since an increase in crack length would produce a K level in the K - a curve greater than the R-curve K level. Instability is thus reached. One problem with using a specimen as shown in Figure 1 for the determination of an R-curve is that once point A_3 is reached, instability occurs and only that portion of the R-curve up to A_3 has been determined. Thus many specimens are needed in general in a load controlled test to obtain the complete R-curve. By use of a wedge loading test method such as that introduced by Heyer and McCabe (7), the range of stable crack extension can be

extended over that obtained from load control tests and it can be shown that K_R approaches a plateau value of maximum resistance as shown by curve (S) in Figure 3.

Following the previous line of reasoning, a conservative method for estimating the instability load for a specific crack in a structural component of the same material and plate thickness is as follows. It is assumed first that the increase of K_R with a (effective) found in R-curve testing will apply to the service component crack. Next, a constant load curve of K versus a, appropriate for the crack in the service component, is adjusted for load level so that it provides a tangency to the R-curve as shown by curve (L_3) in Figure 3. The load corresponding to this position of the L curve is the instability load and the K_c instability point is the point at which the two curves touch. This method is applicable in a straight-forward way to materials in which the influences of strain rate can be neglected. It is conservative for two reasons, (a) the leading edge of a natural crack in a service component is frequently irregular and this may delay and reduce the amount of slow-stable crack extension, (b) there is some evidence that, as the K-gradient increases, where the K-gradient is defined as $(1/K)\ (dk/da)$, the steepness of the initial portion of the R-curve increases. Such an alteration of the R-curve would increase the instability load.

For a rate sensitive steel and with conditions of constraint and temperature such that quasi-cleavage separations still influence the flat-tensile portions of the fracture, the beginning portions of crack extension tend to be unstable with a rapid formation of a crescent

shaped flat-tensile fracture at the plate center. This is represented in the R-curve marked (D) of Figure 4 by introducing a region of small slope after point A. Subsequently additional loss of constraint and shear lip development would cause the R-curve to increase more rapidly as indicated in Figure 4 by the region of curve (D) beyond point B. If a constant load curve (L) similar to that of Figure 3 is adjusted to tangency with curve (D), it is seen that instability would be expected to occur at point A.

Curve (D) of Figure 4 is regarded here as applicable to dynamic loading. In the 0.001 second K_c tests conducted on a drop-weight tester at Lehigh, a sudden crack extension may cause enough load drop for crack arrest to occur. Evidence for such arrests have been often found on the fracture surfaces of dynamic K_c test specimens. As will be discussed at a later point, the drop weight height can be reduced to such a point that the arrested crack remains stationary after its initial forward motion. The K_R value pertaining to such an arrest may be quite large in correspondence to the upper regions of curve (D). However, in a service component, the load drop necessary for such behavior may not occur and the instability load would then be the load for the L curve as shown, corresponding to K_c = 80 ksi.

In Figure 4 the R-curve for a static (1 to 10 seconds) loading is represented schematically as curve (S). Lowering of the yield strength with decrease of loading speed would be expected to result in less constraint applicable to the initial crack extension. Thus curve (S) goes above curve (D) and the effect of initial flat-tensile "pop-in" is shown as greatly reduced. For materials like A441 steel in 1 inch

thickness, it is questionable whether any significant amount of crack extension can occur without causing locally high strain rates equivalent to dynamic loading. Thus, in a bend test, a run-arrest segment of fracturing might develop as indicated by the caption of Figure 4. It was anticipated that occurrences of this type would be observed during the project studies of R-curves. The R-curves examined during Phase 1 appeared to lie at the two extremes. The R-curves measured for a high yield strength material, A514, have small instabilities but mainly resemble curve (S) of Figure 3. The R-curves for A36 steel in 1/2 inch thickness showed no actual crack extension up to the point of plastic hinging of the specimens.

It is desirable to have more information about R-curves for the bridge steels of interest in order to better understand how to use fracture toughness information from various tests in the prediction of bridge steel fracture behavior. For example, the methods commonly employed in DT (dynamic-tear) testing provide only the total energy loss for specimen fracture and the results are dominated by a lowest constraint portion of the dynamic R-curve.

Measurements of bridge steel R-curves with features similar to those indicated by Figure 4 may be primarily a matter of temperature adjustment in the case of static testing. Dynamic R-curves cannot be measured directly. However, the general features of dynamic R-curves may be similar to those of R-curves for the same material at a lower temperature. In addition it is possible to obtain rough estimates of points on the dynamic R-curve after substantial crack extension by use of thickness reduction and crack-arrest bend-angle measurements described later in this chapter.

It was noted above that the initial portion of an R-curve might be influenced by irregularity of the leading edge of a crack in a manner similar to introduction of notch blunting. During the development of the present Lehigh method for dynamic K_c testing, this aspect was given consideration in relation to fatigue pre-cracking of test specimens. Reference (5) requires that the maximum K used in the final segment of fatigue precracking should be 0.6 or less times the critical K value measured during testing. Examinations of the Lehigh experience with dynamic K_c testing of A441 steel showed no correlation between the K_{max} during precracking and the test result. In some cases the pre-crack K_{max} was 10 ksi $\sqrt{in}$ above the measured value of K_c. In addition the relevance of low K_{max} fatigue cracks to crack-like flaws in steel bridge structures was not clear. For these reasons the K_{max} level used in the final segment of fatigue pre-cracking of specimens was placed in the range of 40 to 50 ksi $\sqrt{in}$. This resulted in da/dN values somewhat below 10^{-6} inches per cycle and the specimen preparation time was then not excessive.

2.6 K_c Testing

The specimens used for K_c testing are 3" x 12" x plate thickness, precracked to a depth of approximately 1 inch and broken in 3-point bending across a span of 10 inches. These are shown in Figure 5. Other conventions used in the Lehigh K_c measurements are as follows. Slow stable cracking prior to onset of rapid fracturing is not measured or allowed for in K value computations. The load used for such calculations is the maximum load shown on the oscilloscope load-time record

from the instrumented tup. The loading time is in the range of 0.5 to 2 milliseconds. An r_{YS} plasticity adjustment is added to the initial crack size, where

$$r_{YS} = \frac{1}{2\pi} \left(\frac{K}{\sigma_{YS}}\right)^2 \tag{6}$$

The adjustment of the uni-axial tensile yield point, σ_{YS}, for temperature and loading rate is computed using the method suggested in Ref. (14). For purposes of deriving values of dynamic plane strain fracture toughness K_{Ic} from the dynamic K_c measurements, it is believed satisfactory approximations are provided by the relationship (14),

$$\beta_c = \beta_{Ic} \left(1 + 1.4\, \beta_{Ic}^2\right) \tag{7}$$

With regard to static (one second) K_c measurements, the original plan was to extend these measurements beyond general yielding of the specimen by use of the J-integral method recently discussed by Begley and Landes (8). However, as the work proceeded this plan was dropped and such tests in the region of general yielding of the specimen were not conducted.

2.7 Thickness Reduction and Crack-Arrest Bend-Angle Measurement

Two methods have been given trial which provide interesting supplementary information to the K_c values derived using the drop-weight test method. The intent of each method was to provide a measure of the resistance to crack propagation for a running crack in the 3" x 12" bend specimens which could be measured at testing temperatures above as well as somewhat below the temperature point for general yielding of

the specimen prior to onset of rapid fracturing. From the nature of the analysis basic to the stress intensity factor, K, the validity of K as a characterization factor is limited to conditions such that at the crack tip the plastic zone size is negligible. Use of the plasticity adjustment, r_Y, extends the validity of characterization in terms of K primarily because the plasticity adjusted K value correlates closely with two plasticity type characterizations, the crack opening stretch, δ, and the J-integral. The relationships are

$$K = \sqrt{E\ \sigma_Y\ \delta} \tag{8}$$

and

$$K = \sqrt{E\ J} \tag{9}$$

δ is normally defined as the crack opening measured, a distance r_y behind the crack tip as shown in Figure 6.

Correlations of thickness reduction near the leading edge of a crack with the crack opening stretch, δ, have been under study during the past six years at various laboratories (9, 10). For such studies δ was most often estimated from equation (8) rather than directly measured. Studies were made at Lehigh of thickness reduction adjacent to the fracture surface produced in dynamic fracture tests. After comparing thickness reduction measurements with estimates of δ derived using equation (8), it was concluded that the maximum thickness reduction was somewhat too large to be equated directly to δ. It was also noted that a thickness reduction measurement position spaced away from the flat-tensile portion of the fracture by a distance, s, which was an increasing function of δ could be justified and would be

advantageous. It was then assumed that the thickness reduction could be equated to δ if measured at the spacing position, s, given by an equation of the form

$$s = B\, f(\delta/B) \qquad (10)$$

Only limited guides were at hand for selection of a specific function, f. However, this handicap was greatly reduced by the tolerances for variations of the f function which is obtained from the self-consistency approach. Given any plausible specific choice of the f function, and assuming the thickness reduction at s equals δ, the measurement point can always be adjusted toward the particular measurement position, s, where the results are consistent with equation (10). Improvements in the f function were assisted by comparisons to dynamic K_c results in a testing range where only a moderate elevation of K_R with crack extension was expected. A detailed discussion of the development and application of this method is given in Reference (11).

At the time of writing of Reference (11), work on Phase 1 of this project had started and exploratory trials were being made of crack-arrest bend-angle measurements as an alternative or as a check against K values derived from thickness reduction. This method and the methods based upon thickness reduction were both suggested by ideas introduced by Wells (12). Wells' studies centered attention upon abrupt initiation of crack propagation from saw-cut notches in bend specimens of structural steel. In the temperature range of principal interest, the plastic bend angle prior to fracture could be computed from displacement measurements with an allowance for the elastic bend angle contribution.

When the fracture surfaces were mainly flat-tensile, a less precise estimate could be made by fitting together the broken parts. In either case δ was calculated from the equation,

$$\delta = 0.45\ L_N\ A \tag{11}$$

where A is the plastic bend angle and L_N is the net ligament under the notch. Figure 7 shows some of the bend angle details. In the Lehigh studies it was assumed that the contributions to plastic bending prior to fracture initiation and during initial portions of the run of the cracks were small in comparison to the plastic bending which occurs with the crack at or close to the crack arrest position. Calculations of δ were made using the equation

$$\delta = 0.5\ L_N\ A \tag{12}$$

The plastic bend angle, A, was measured directly after the test. Subsequently the specimen was chilled and broken completely. An estimate was then made of the net ligament, L_N. inserting equation (12) into equation (8) thus gives K as

$$K = \sqrt{0.5\ E\ \sigma_Y\ L_N\ A} \tag{13}$$

The original goal of the above two methods was to obtain an estimate of K_R near the plateau value of maximum resistance to crack extension of an R-curve. However, 3" x 12" specimen dimensions may be inadequate for that purpose, particularly for the 2 inch thickness. In addition the assumptions basic to these methods are questionable. However, the assumptions have enough plausibility so that approximate correlations are not unlikely in comparisons to R-curve results (with

a temperature shift) and in comparison to estimates of the energy loss related to fracture from dynamic-tear measurements. The thickness reduction method is of special interest because it can be applied to fractures produced in service. The crack-arrest bend-angle method is of interest because of its simplicity. The degree of agreement of the two methods with one another from existing data comparisons is quite satisfactory. In the present study thickness reduction and bend-angle estimates of K_c were limited to the A36, A441 and A514 materials.

2.8 Transition Temperature Measurements and Criteria for Adequate Fracture Toughness

From investigations of fracture of welded ships following World War II, it was concluded that satisfactory fracture control could be achieved if V-notch Charpy tests indicated an energy loss of 15 ft.-lbs. or more at the lowest service temperature. Improvements of design and inspection, of course, also contributed to the degree of success achieved in this effort at fracture control. At the Naval Research Laboratory, across the same time period, methods were developed for measurement of a fracture transition point termed the NDT (Nil-Ductility Transition) temperature. The ASTM testing standard for NDT measurements (13) patterned on this work, is of the drop-weight 3-point-bend-specimen type. The crack starting flaw is a strip of brittle weld bead on the tensile face of the specimen. The crack propagates first through the plate thickness and then laterally across the width of the specimen which parallels the axis of bending.

For ship plates having σ_{YS} in the range of 35 to 40 ksi, the temperatures corresponding to CVN = 15 ft.-lbs. and to NDT, on average, were not far apart. However, extension of these comparisons to other steels indicated a trend for the comparison point to shift upward on the V-notch Charpy curve of energy loss versus temperature as the yield strength of the material increased. In the case of A441 steel, CVN = 30 ft.-lbs. would be approximately at the same temperature as NDT. The best known use of NDT measurements for fracture control was in relation to nuclear reactor containment vessels during the period in which the wall thicknesses of these vessels were in the range of 3 to 8 inches. For this application it was decided that fracture safety could be guaranteed if significant pressure loads on the walls of the containment vessel were avoided at temperatures below NDT plus 60^{o} F. As in the case of the welded ships, there were other fracture control elements including careful inspection and proof testing.

One advantage of specifying the fracture toughness requirements in terms of the drop-weight NDT test is that the required fracture toughness increases with the yield strength of the material. Reference (14) provides a fracture mechanics analysis of the drop-weight NDT test and suggested that a fixed proportionality existed between the dynamic plane-strain fracture toughness, K_{Id}, and the dynamic yield point, σ_{Yd}, at the NDT transition temperature. The equation had the form

$$K_{Id} = C\,\sigma_{Yd} \qquad (14)$$

where C = 0.78 $\sqrt{\text{in.}}$ to 0.7 $\sqrt{\text{in.}}$ However, the values suggested for C

have depended to some extent on the choice of σ_{Yd} which is usually estimated rather than directly measured. The equation

$$K_{Id} = 0.7 \sqrt{in.} \ (\sigma_{YS} + 23 \text{ ksi}) \qquad (15)$$

where σ_{YS} is the uni-axial tensile yield point, appears to be in satisfactory agreement with existing data for steels with σ_{YS} less than 100 ksi. Since the use of higher strength steels normally implies proportionately higher stresses in the structure, enhanced danger of fracture from a prior crack of given size can be avoided only if the fracture toughness is increased to an equivalent degree.

In part because of the insensitivity of the drop-weight NDT to directionality introduced by rolling or extrusion, Pellini, Puzak, Lange and co-workers at Naval Research Laboratory have given considerable study to methods of dynamic tear (DT) testing using both drop-weight-tear and double pendulum machines. At Battelle-Columbus, an adaption of DT testing was developed in a form suitable for use as a toughness specification test for gas transmission line-pipe steel. Adequate toughness for prevention of long running cracks in pipe lines was assumed to be present if the test specimen fracture surface showed 85 percent shear fracture at the lowest temperature expected in service. Bridge structure fracture problems are quite different from those encountered with gas transmission pipe-lines. However, the versatility of dynamic-tear testing methods is noteworthy. The likelihood that a test method of the DT type may be most appropriate for bridge steels became apparent at the start of Phase II of this project.

2.9 Estimates of Critical K Values from CVN and NDT Test Methods

Among the various methods of fracture toughness evaluation potentially suitable for bridge steels, ASTM testing standards have been developed only for the Charpy V-notch and DWTT-NDT methods. The relationship of drop-weight NDT results to values of the dynamic plane-strain fracture toughness, K_{Id}, were previously discussed. This was the first relationship between tests of the fracture mechanics type and of the transition temperature type to receive study. Subsequently the relationships of static and dynamic K_{Ic} values to results from Charpy V-notch testing were examined by Barsom and Rolfe (15) and quite recently by Corten and Sailors (16).

Barsom and Rolfe proposed two methods for deriving K_{Ic} values from CVN tests. The first method used CVN energy loss measurements from the transition temperature region of the CVN-Temperature curve. The equation suggested for this region was

$$K_{Ic}^2 = 2E\ (CVN)^{3/2} \qquad (16)$$

where CVN is the energy loss in ft.-lbs., E has the dimensions of lbs. per square inch and K_{Ic} has the dimensions ksi $\sqrt{in}$.

The second method proposed by Barsom and Rolfe applied to the initial region of the "shelf" portion of the CVN curve. The equation suggested for this region was

$$K_{Ic}^2 = 5\left(\frac{CVN}{\sigma_{YS}} - 0.05\right) \qquad (17)$$

where CVN is in ft.-lbs., σ_{YS} is in units of ksi and K_{Ic} is in units

of ksi $\sqrt{in}$. The data scatter shown in comparison to the preceding equations was considerably less for equation (17) than for equation (16).

Suggestions were also furnished by Barsom and Rolfe on derivation of K_{Id} estimates from estimates of static K_{Ic} values. It was proposed that a temperature shift could be estimated from knowledge of σ_{YS} for the steel material of interest. Thus if a value of K_{Ic} (static) is estimated at the temperature, T, this same value can be used as the value of K_{Id} at the temperature, $T + T_s$. Barsom (28) presently gives T_s as

$$T_s = 215 \text{ ksi} - 1.5\ \sigma_{YS} . \qquad (18)$$

Above σ_{YS} = 140 ksi, T_s is assumed to be zero.

The report by Corten and Sailors (16) derived considerable help from the work by Barsom and Rolfe, covered a somewhat larger data collection, and suggested alternative equations and methods. Considerable study was given to sources of scatter in correlation of K_{Ic} with CVN in the transition range for which equation (16) is applicable. For purposes of establishing a reliable correlation, Corten and Sailors eliminated values of CVN less than 5 ft.-lbs. and gave preference to the lowest CVN test results in determining CVN at a given temperature. Attention was also given to relevance of the CVN tests as representative of the region sampled by the K_{Ic} test. In place of equation (16), Corten and Sailors proposed the relationship

$$K_{Ic}^2 = 8\ E\ (CVN) \qquad (19)$$

where the units employed are the same as those for equation (16). The equation is an empirical, not a basic, relationship. Barsom (28) has recently proposed that equation (16) be written in the form

$$K_{Ic}^{2} = A\ E\ CVN \qquad \text{where } A \simeq 5. \tag{20}$$

From the preceding comments, it can be seen that estimates of critical values of K for onset of rapid fracturing can be made using estimates either from Charpy V-notch tests or from drop-weight NDT results. Use of the CVN results appears more versatile. However, care must be taken with regard to the selection and treatment of the CVN data. The specimen is quite small and the scatter in test data can occur for a variety of reasons. In the case of drop-weight NDT testing, it should be noted that the NDT test is not sensitive to rolling direction in the steel. For this reason, in part, measurements of energy loss using dynamic-tear methods are currently favored at the Naval Research Laboratory. Empirical correlations between dynamic-tear measurements of energy loss and K_{Id} values have been discussed by Freed and Goode (17). A good understanding of dynamic-tear results in terms of fracture mechanics seems to be within reach through use of the dynamic R-curve concept coupled with improvements in the testing method.

3. TEST PROGRAM

3.1 Test Program - Phase 1

As already stated, Phase 1 was concerned with the establishment of meaningful measures and tests for fracture toughness. For this purpose a series of preliminary tests were planned for ASTM grades of steel A36, A441 and A514 in thicknesses of 1/2", 1" and 2". The basic test program called for the collection of V-notch Charpy data, K_c data and R-curve data. Details relating to the use and meaning of these data and methods for their collection can be found in Chapter 2 and Appendices J, K, and L.

Specifically Phase 1 consisted of:

1. Design and fabrication of fixtures and instrumentation for R-curve testing.
2. Obtaining a limited number of selected R-curve measurements.
3. A literature study to collect already available V-notch Charpy and K_c measurements for bridge steels.
4. A comparative study of R-curve, K_c, and Charpy measurements and a recommendation for the testing in Phase 2.

3.2 Test Program - Phase 2

As a result of the findings of Phase 1 the following Phase 2 test program was carried out:

1. Standard and precracked V-notch Charpy tests were conducted over a broad range of temperatures for most materials and thicknesses. The tests were generally conducted at three loading rates, impact, very slow and intermediate. The actual testing details can be found in Appendix L.
2. Dynamic and Slow Bend K_c values were measured for most materials and thicknesses over a wide range of temperature. The energy absorbed in the dynamic tests was also measured where possible, thus giving a dynamic tear measurement (DT) for the materials. The test details are discussed in Appendices J and L.
3. R-curve measurements were carried out on the 1/2" and 1" thick materials at various temperatures. The testing details and R-curve concepts are discussed in Chapter 2 and Appendix K.
4. Fracture tests were conducted on four precracked A36 rolled, 14 X 30 beams at approximately -50° F. The testing details are presented in Appendix M.

4. EXPERIMENTAL RESULTS

4.1 V-notch Charpy Testing

The specific Charpy results can be found in Appendices A through H. In general it was found for a given material and thickness that the standard V-notch Charpy or precracked Charpy data took the form shown in Figure 8. Figure 8 schematically shows that as the testing speed is increased the transition temperature and the upper shelf energy tend to increase. At the lower temperature ranges the curves merge to a low energy level usually below 5 ft.-lbs. Some of the more important values relative to the Charpy data are summarized in Table 1. It can also be stated in general that the precracked Charpy results for a given material, thickness and testing speed fall to the right of the standard Charpy results. This is schematically shown in Figure 9. The upper shelf energy levels were lower for the precracked specimens. The effect of material thickness for a given test type, precracked or standard and testing speed are shown in Figure 10.

Figures 8 through 10 as already pointed out represent general trends. In support of Figure 8 the data for the 1/2" A440 and A441 materials can be examined. Figures 11 through 13 present these data. Exceptions to the results indicated in Figure 8 can also be found. Figures 14 and 15 which give the 1" A588 and 2" SAE 1035 notched Charpy data show quite a different result. For the SAE 1035 material the

three loading rates produced what appears to be identical results. The A588 results point to a large amount of scatter in the slow data and again the total picture seems to show no apparent difference between the slow and dynamic results. One other type of behavior quite different from Figure 8 was found for the A242 material. This material showed a double shelf behavior for the slow loading rate. Figure 16 for the 1" material indicates this. The A242 material is the only one tested in this program which showed such a behavior. Similar double shelf behavior has been seen and discussed by Barsom (28).

The general behavior shown in Figure 9 is best illustrated by the data for the A441 1/2" material shown in Figure 17. As with the other results already mentioned exceptions to Figure 9 were noted. Figure 18 for the 2" A36 material shows a case where the precracked dynamic data can be viewed as forming a lower bound for the standard data. However, this behavior was rarely detected as summarized in Table 1 by the T_{15} and T_{15}^{P} which are an indication of this separation of the two data sets. It is also interesting to note that while the dynamic 2" A36 standard and precracked results fall together, the slow data does not as shown in Figure 18.

With regard to the behavior indicated in Figure 10, Figure 19 presents similar results for the A441 material. This type of result is only valid in a general sense when the material is all from the same heat as is the case for the A441 thicknesses. For the other material tested in this program the various thicknesses of a given grade were not from the same heat. Such a comparison for these materials would not yield results as shown in Figure 10 and 19.

4.2 R-curve Results

The R-curve results as obtained in this study are presented in Appendices A through H. A detailed discussion of the R-curve and its use can be found in Chapter 2.

It was expected, based on preliminary room temperature tests run in Phase 1, that R-curves of the types shown in Figures 3 or 4 would be obtained. However, the actual results for the materials tested in Phase 2 gave results that were quite surprising. In an actual test at reduced temperature no stable crack growth was observed. The failure occurred at a given stress intensity level and proceeded to essentially fracture the entire plate. In many cases crack velocities became great enough to produce crack branching. Thus a typical R-curve from the Phase 2 results would be as shown in Figure 20 by the dotted line. Due to the nature of the R-curve results only the parameters at fracture are reported.

4.3 K_c Measurements

The specific results of the K_c tests are presented in Appendices A through H. In general it was found that the results for a given material and thickness took the form shown in Figure 21. Here it is seen that the dynamic K_c curve falls to the right of the static curve. It should also be noted on the plots of static K_c in Appendices A through H that the R-curve data was added to the static plot where possible. This helped extend the data to higher K levels. A procedure such as this is quite acceptable since the form that the R-curve data

took represented a single K_c point. It should also be noted, in the overall test program, that greater attention was paid to dynamic K_c measurements than the static K_c measurements. Furthermore the provisional techniques which were tried in Phase 1 for determining K_c when the specimen is fully plastic were essentially dropped in Phase 2. These techniques were limited primarily to the A36, A441 and A514 materials and are denoted as K_m in the appropriate appendices.

Figures 22 through 25 present the K_c data for the 1/2" and 1" tests of the A440 and A588 materials. These results are typical of the behavior of the other material in the program. In all of these figures it is clear that the R-curve K estimates prove to be very useful in extending the static K_c results to higher temperatures. Various levels of K are given in summary form in Table 1. These values give an excellent overview of how the various materials perform relative to each other. As an example of this consider the T_{15} and K_{Id}^{15} levels for the 1/2" A440 and A588 materials. The A440 has 0^o F and 90 ksi $\sqrt{in}$ respectively for T_{15} and K_{Id}^{15}. The A588 has 50^o F and 80 ksi $\sqrt{in}$. This indicates that for a given temperature above say 0^o F the 1/2" A440 will prove to be tougher.

4.4 Dynamic Tear Measurements

As with the other test data the specific results of the DT tests are given in Appendices A through H. In general the results took the form shown in Figure 26. Since the D.T. measurements were obtained simultaneously with the dynamic K_c measurement, tests were not run at high enough temperatures to obtain the upper shelf energy levels for

the DT curves. At these higher temperatures it would not have been possible to obtain valid dynamic K_c measurements. Also there was concern over destroying the instrumented tup at the higher energy levels. Figures 27 through 29 indicates results typical of all D.T. testing in this program.

4.5 Beam Fracture Tests

Fracture tests of four precracked coverplated 14 X 30 A36 beams were performed at approximately -50° F. For these four tests, two beams failed due to brittle fracture, one failed due to plastic yielding and one failed due to buckling at a loading point. The details of the test results are given in Appendix M. A discussion of these test results and their relation to the program is given in Chapter 5.

5. DISCUSSION, CONCLUSIONS AND RECOMMENDATIONS

5.1 Discussion - General

Chapters 1, 2, 3 and 4 discuss the need for an understanding of the fracture characteristics of structural grade steels, a proposed test program to obtain this understanding and a description of the test results obtained from the test program. In this chapter, Chapter 5, a discussion of salient features of the test results and test program will be undertaken. Where justified conclusions will be drawn and recommendations made.

The main objective of Phase 1 and 2 of this program to measure the fracture toughness of various grades of structural steels found in bridge construction has been met as evidenced by the data collection in Appendices A through H. It should be clearly recognized that these data are only valid for the particular pieces of steel from which the tests were made. Also the results are influenced by the relative position of the specimens with respect to the test piece. The statistical nature of Charpy testing and similar but somewhat less variability in K_c measurements demand that the data be viewed with caution. Wide variations in Charpy and K_c results have been known to occur in steels of like composition but different heats.

Ideally it would be very desirable to have available a simple and inexpensive test with which the fracture resistance of a total

heat or an individual piece of steel could be assessed. The standard ASTM method for plane strain fracture toughness testing as described in Reference (5) does not meet these objectives. The method is quite complex and can prove to be very costly as well as inappropriate for application to materials of the structural steel variety. The method proposed by Barsom (28) for correlating Charpy results and plane strain fracture toughness will be discussed in this chapter. Also the correlation procedure proposed by Pellini and Co-workers (29) for relating dynamic tear energies (DT) to fracture toughness will be discussed. Both of these procedures offer the potential of simple estimates of fracture toughness for structural grade steels.

5.2 K_{Ic} Estimates from Charpy and Dynamic Tear Energies

In a study of the relationship of Charpy testing to plane strain fracture toughness testing, Barsom and Rolfe (15) observed that there seemed to be a definite tie between the temperature transition region of precracked Charpy specimens and dynamic plane strain fracture toughness values. A similar observation was made with regard to the static plane strain fracture toughness and Charpy energies obtained from precracked Charpy specimens tested at very slow loading rates. For these tests the Charpy energy was calculated from the load deflection data. This is shown schematically in Figure 30. These observations lent hope to the possibility of correlations between Charpy tests and plane strain fracture toughness tests. Barsom and Rolfe also noticed that the separation between the slow loading rate

data curve and the dynamic test data curve seemed to be a direct function of yield strength. Barsom (28, presently quantifies these two observations by the relationships

$$K_{Ic} = \sqrt{A\ E\ CVN} \tag{21}$$

and

$$T = 215 - 1.5\ \sigma_y \tag{22}$$

In Equation (21) to estimate a static K_{Ic} level a slow load Charpy energy is used while to estimate a dynamic K_c value, a dynamic Charpy energy is used. E is Young's Modulus and A is suggested as being taken at a value of 5. Equation (22) measures the temperature separation or shift between the static and dynamic curves. σ_y corresponds to the room temperature yield strength. The observed values of the temperature shift measured at the 15 ft.-lb. Charpy energy level for the precracked and standard Charpy tests are tabulated in Table 1. The results for Equation (22) are also noted.

In order to examine the effectiveness of equation (21), values of K_{Ic} as predicted by Equation (21) are plotted in Appendices A through H on the curves of K_c versus temperature. The CVN values chosen for this test were dynamic standard specimen results. In almost all cases such a comparison gives a reasonable and conservative estimate of K_c. Also the upturn in the K_c curve is about in the same place as indicated by the standard dynamic Charpy results. Barsom (28) has claimed that precracked Charpy results should represent a lower bound for all Charpy data at a given testing speed. It can be seen

if the energy values from the dynamic precracked Charpy specimens were to be used, very poor results would be obtained since in general the precracked data is much further to the right of the standard data. An examination of T_{15} and T_{15}^{P} in Table 1 shows this.

In Table 1 values of the dynamic fracture toughness, K_{Id}^{15}, are indicated at the temperature corresponding to the 15 ft.-lb. level in a standard CVN test. Using Equation (21), an A value of 5 and E as 30×10^6 psi, K_{Id}^{15} should be

$$K_{Id}^{15} = 47.4 \text{ ksi } \sqrt{\text{in.}}$$

according to Barsom (28). Comparing this K_{Id}^{15} level with the values reported in Table 1 show that 8 of the 22 data sets are in good agreement with K_{Id}^{15} between 40 and 50 ksi $\sqrt{\text{in}}$. Five show K_{Id}^{15} at 60 ksi $\sqrt{\text{in}}$ and three show K_{Id}^{15} at 70 ksi $\sqrt{\text{in}}$. Only three show levels above 80 ksi $\sqrt{\text{in}}$. Thus using an average value of A of about 8 rather than 5 gives

$$K_{Id}^{15} = 60 \text{ ksi } \sqrt{\text{in}}$$

which with A = 8, E = 30×10^6 psi and CVN = 15 ft.-lb. represents a fair average of all the K_{Id}^{15} data between 40 and 70 ksi $\sqrt{\text{in}}$. It should be recognized that using a value of A above the level proposed by Barsom (28), A = 5, will produce some unconservative results according th the data in this program. The level proposed by Barsom (28), A = 5, serves as a good lower bound for all of the current data.

Pellini and Co-workers (29) have proposed a relationship between the energy absorbed in a standard dynamic tear test and plane strain fracture toughness. This can be most easily thought of as a plot of β_{DT} versus β_{K_c} where

$$\beta_{DT} = \frac{1}{B}\left(\frac{E \cdot DT}{\sigma_{YS}^2}\right) \tag{23}$$

and

$$\beta_{K_c} = \frac{1}{B}\left(\frac{K_c}{\sigma_{YD}}\right)^2$$

where B is the specimen thickness, E is Young's Modulus. DT is the energy absorbed in the dynamic tear test, K_c is the stress intensity factor and σ_{YD} is the dynamic yield strength at a given temperature. To date this correlation has been used primarily at values of β_{K_c} below approximately 1. In the current study β_{K_c} values as high as 3 are encountered. In each appendix where DT values were measured, plots of β_{DT} versus β_{K_c} are provided. It can be seen from these plots that there definitely appears to be a relationship between the two quantities.

It should be understood that although only two possible methods of estimating K_c are discussed here other correlations are certainly possible. It is the philosophy adopted in this final report of Phase 1 and 2 not to try to introduce any new empirical correlations. The extensive data tabulations in Appendices A through H are offered to any one who so desires to search for a new correlation. To this end complete tabulations of all measured quanitites with respect to Charpy

testing (i.e., lateral expansion, maximum load and deflection in a precracked or standard slow bend test, etc.) are provided.

5.3 Discussion - Charpy Testing

In this test program there are two examples, A588 1" standard and SAE 1035 2" standard, for which the plotted data indicate no definite temperature shift.

With regard to A588 1" standard, the scatter of the slow bend data is large and corresponds very well to the scatter suggested by fracture appearance. The fact that a similar degree of scatter does not occur in the dynamic data is surprising. One is led to think about the factors influencing progressive crack extension which might be time dependent to various degrees: formation of arrays of voids on slip planes, de-cohesion of inclusions from the matrix, strain aging, abrupt separations. Studies across many years have indicated that plastic stress-strain relations can be adjusted for strain rate (in bcc metals) using a temperature shift computed from log strain rate ratio. We have only empirical grounds for expecting that fracture toughness values at different strain rates can be superimposed using a temperature shift. On the basis of this fact plus our data, the following attitude toward use of temperature shift seems appropriate. It can be agreed that demonstration of a general temperature shift trend, based upon trials with certain available plates of various compositions, provides helpful information. However, exceptions to this trend are evidently quite possible. Although our most numerous comparisons are in terms of fracture energy rather than K_c values,

there is reason to question whether the lowest static K_c values applicable to natural cracks are significantly higher than dynamic K_c values. This must be demonstrated using adequate sampling of the materials of interest.

With regard to SAE 1035 2" standard, comparisons of Charpy bar fractures having similar appearance suggest a slow bend to dynamic temperature shift of about 70° F. The fracture energy comparisons show no clear difference between slow bend and dynamic results. While the fracture appearance examination does show a shift, this shift is still less than the predicted (28).

Returning to A588 1" Charpy bar tests, the precracked results, slow bend and fast bend, show much less scatter than was the case using standard specimens. Using fracture appearance and ignoring the testing speed difference between slow and fast bend tests, a small temperature shift of about 50° F is indicated between these and the dynamic tests.

In making estimates of temperature shift using fracture appearance, selection of specimens which show similar crack arrest markings is helpful. In the case of standard specimens, one can look also for growth of a fringe of fibrous fracture at the notch root. The following temperature shifts based upon fracture appearance were observed (slow bend to dynamic)

A440	2"	Standard	160° F

A441	Standard	Precracked
1/2"	25° F	120° F
1"	80° F	140° F
2"	85° F	100° F

Within the uncertainties involved in estimating a temperature shift from fracture energy results, the above values seem reasonable. Evidently the magnitude of a temperature shift in the case of a fracture test performed slow and fast depends on the nature of the fracture test.

If data scatter was the only consideration, use of dynamic CVN tests seems preferable to use of slow bend Charpy tests. Use of precracked specimens in place of standard specimens seems to reduce scatter of results although the degree of this is variable. There is no evident reason why precracked results should provide a lower-bound indication for results from standard specimens as discussed by Barsom (28) except the supposition that natural flaws in the material, interacting with the notch, will sometimes produce degrees of notch severity equivalent to the fatigue precrack. If this supposition is accepted, one must also consider whether the flaw-notch interaction may introduce locally high strain rates (from abrupt separations) and thus reduce or eliminate the slow-dynamic temperature shift. This seems to be the simplest way of explaining the variable and sometimes zero temperature shifts observed. However, other rate dependent processes deserve consideration and a satisfactory understanding of slow

bend dynamic test result differences is not available at the present time.

5.4 K_c and R-curve Testing

As already indicated primary emphasis was placed in Phase 1 and Phase 2 on dynamic K_c testing. In these tests loading times to failure of the order of 0.001 seconds were maintained. For the slow or static K_c measurements a loading time to failure of one second was maintained.

For all of the materials tested in this program it was generally possible to obtain valid test results for the dynamic K_c measurements over a range of temperatures of interest to bridge designers. It is indicated in Chapter 2 that as the temperature increases, toughness increases. This means that the r_y value is increasing since K_c is going up while σ_y is going down. Thus as testing temperature is raised for a fixed size specimen, the constraint decreases and the ability of linear elastic fracture mechanics to calculate stress intensity levels decreases. Stated somewhat differently, the zone of plastic material behavior in the specimen is getting large relative to the specimen and thus linear stress analysis does not apply. All of this means that for a fixed size specimen there is an upper limit on the K_c level which can be measured by the specimen. The primary specimen used in this program, a 12" by 3" three-point bend specimen, has an effective upper limit, ignoring thickness effects of about 100 to 120 ksi $\sqrt{in}$. This limit and the basic material response encountered in this study gave results which generally showed a lower dynamic K_c

shelf in the range of 40 ksi $\sqrt{in}$ and an effective upper temperature for K_c measurements (i.e., K_c still valid) in the range of 0^o to 50^o F. If it is necessary to measure K_c dynamic above these temperatues a larger specimen is needed.

The static K_c measurements were all made at temperatures well below those of interest to bridge design. This is due to the temperature shift phenomena already discussed. Since it is important to be able to estimate material response over an effective temperature range of say -75^o F to $+75^o$ F, it is necessary to devise or use other techniques than those normally employed with the 12" x 3" specimens when K_c levels exeed 100 to 120 ksi $\sqrt{in}$. This was the intent of the thickness reduction and bend angle measurements. However, due to the complexities involved and the tentative nature of these methods, they were dropped in Phase 2.

It is interesting to note that the R-curve results in Phase 2 showed no stable crack growth up to the point of final instability. This is a great benefit to a designer since the critical K level turns out to be a single point rather than a curve. Thus the calculation of failure loads is greatly simplified. Rather than trying to find a point of tangency between two curves, it is only necessary to calculate the load to give a specific K level. Another important aspect of the R-curve results is that they were tested at a loading rate similar to the static 12" x 3" K_c tests. This means that the R-curve results can be used to supplement the static K_c results for K_c levels over 100 ksi $\sqrt{in}$. The 23" x 23" R-curve specimens can be used to K_c levels of approximately 300 ksi $\sqrt{in}$. The various figures of K_c versus

temperature quite clearly indicate the usefulness of the R-curve results in extending the static K_c results to higher temperatures.

As noted in the various appendices, there was a definite temperature shift between the static and dynamic K_c test. These shifts tended to agree with the trend reported by Barsom (28). Also these shifts were present in many cases where it was not obvious that a shift existed when just viewing the Charpy results.

5.5 Discussion - Beam Tests

Four A36 14 x 30 coverplated precracked beams were tested in an attempt to evaluate the ability of fracture mechanics concepts to predict failure loads of bridge components. In two tests the beams failed in what might be termed a rapid or catastrophic failure. These failures were due to rapid propagation of the precrack through the beam. In the other two tests failure did not occur due to fracture. In one test web buckling was encountered while in the other test the beam failed due to the formation of a plastic hinge.

The analysis and discussion of the four beam tests in Appendix M demonstrates the role and interaction of stress analysis and material characterization in fracture control. In order to properly understand the test results it was first necessary to analyze the cracks in the beams in order to calculate the relationship between the applied load and the stress intensity factor. For some of the beams this meant comparing the stress intensity values at different locations in the beam to see where the crack would first be expected to go unstable. After completion of the stress analysis it was necessary to chose

a value of K_c for the material. This procedure was complicated by typical problems such as a lack of clear knowledge as to what loading rate was present at the crack tip. With this in mind the K_c data obtained from one flange of one of the test beams was examined and compared to CVN results from the same region of the beam and also to K_c data obtained for the A36 material in this program. From other considerations a K_c value was then chosen for completing the analysis. This produced for each beam a relationship between the applied load and K_c.

As pointed out in Appendix M a rather simple method of analysis was adopted to study the failure of the precracked beams. In spite of this fairly reasonable results were obtained with regard to the maximum load the precracked beams could sustain. This type of limited success generates a certain degree of optimism that fracture mechanics, within its present linear framework as discussed in this report, can be used a a design tool to eliminate the possibility of high speed or catastrophic fractures in bridge structures. However, such optimism should still be viewed with caution until more extensive tests on full size sections can be carried out.

5.6 Data Comparison

The most effective way to examine the total result of this program and the relative performance of the various materials is through Table 1. This table coupled with Figures 8, 9, 10 and 30 give all of the necessary information to rank the material performance.

To illustrate the usefulness of Table 1 first consider the first two columns T_{15} and T_{15}^{P}. These two values give the temperature of the 15 ft.-lb. energy level for the dynamic standard and precracked tests of the Charpy specimens. Since the K_c levels for all materials, except for a few cases, fall within the range of 40 to 70 ksi $\sqrt{in}$ for the 15 ft.-lb. temperature it is possible to see which material will be tougher at a given temperature. Scanning down the first column shows that the materials get tougher in the order of the listing or in this particular case as the yield strength is increasing. By this it is meant that the T_{15} for the A7 material is higher than the A242, A514 etc. This means that for the A242 or the A514 material the temperature transition behavior is occurring at a lower temperature. Also by scanning across between the first two columns it is possible to see the difference between the standard and precracked Charpy tests. For the A36 1" tests the T_{15}^{P} was greater than the T_{15} by 40^{o} F. It was greater by 75^{o} F for the A441 1/2" material and these typical results very quickly show that in this program the precracked results are well displaced from the standard tests and are not a lower bound for the standard tests.

The next three columns ΔT, ΔT^{P} and ΔT_{B} give the temperature shift for the standard specimens, the precracked specimens and Barsom's prediction (28) respectively. A scan of these three columns quickly show a generally good agreement with Barsom's prediction and ΔT. It also shows a much smaller ΔT^{P} than ΔT or ΔT_{B}. Thus it is clear that the standard test results show better agreement with ΔT_{B} than ΔT^{P} does.

The column T_{15-5} is just an indication of how fast the standard Charpy curve is rising in the region between the 5 and 15 ft.-lb. energy levels. This is useful in judging the steepness of the Charpy transition region. The columns CVN_{SH}, K_{Id}^{15} and K_{Id}^{*} quickly present the upper shelf Charpy energy, the dynamic K_c at the T_{15} temperature and the lower shelf dynamic K_c. This format allows easy comparative analysis of the data. The remaining columns also allow for quick comparisons to be made among the data.

5.7 AASHTO Charpy Requirements

At the request of the Federal Highway Administration, the American Iron and Steel Institute investigated the possibility of using Charpy testing as a means of guaranteeing minimum toughness in structural grade steels. As a result of this investigation, it was proposed to the American Association of State Highway and Transportation Officials, that they adopt a set of requirements which call for the various grades of steel to meet specified Charpy energies at a certain temperature. The Charpy levels which are presently being used are given in Table 3. In the present specifications there are three groups which depend on the operating service temperature. To compare how the materials tested in this program would be rated, Table 4 was prepared. From Table 4 it can be seen that 11 of the 22 steels tested would be suitable down to -60° F, 14 to -30° F and 21 to 0° F. Only the A7 material proved to not meet any of the service groups.

It would appear on the surface that most materials used in bridge construction would easily meet the ASSHTO requirements for CVN since the materials used in this program can be regarded as a random selection of the particular type of steel. However, although this is a critical aspect of the question to a steel producer, it is not the critical question to a user. What is required is an answer to just how much toughness is guaranteed by these CVN levels. Recalling the concept of a temperature shift, it will be recognized that for the proposed CVN levels there is more than adequate fracture toughness for static loading rates. This can be seen in any of the K_c curves either in the body of this report or in the appendices. Thus if static loading rates are postulated as governing in a bridge, the proposed CVN levels will guarantee adequate fracture toughness.

It is the view of the writers of this report that the present requirements are very adequate for normal redundant design. However, in cases where a single element or member can control complete collapse of the structure, it is felt that designing for static K_c levels is not sufficient. It is felt that situations can arise where dynamic loading rates can be applied either to the member or local to a fatigue crack. This would then require design based on dynamic K_c levels and the ASSHTO CVN values will not provide adequate toughness for this case.

5.8 Conclusions

1. Within the composition and tensile properties specified for a given type of steel (A36, A441, A514, etc.) toughness can vary widely

and plates unsatisfactory for use in tensile load bearing members of bridges are possible.

2. It was observed during the R-curve tests that actual slow-stable crack extension during a fracture toughness test is negligible for the bridge steels studied. This simplifies the problem of estimating the critical stress conditions for onset of rapid fracturing at the leading edge of a crack of given size in a bridge structure.

3. Relative to the idea that the fracture toughness observed in a dynamic fracture test corresponds to a similar fracture toughess using slow (one second) loading at a lower testing temperature, a large variability was observed in the slow speed-dynamic temperature shift, particularly for slow and dynamic bend tests of standard V-notch Charpy bars. For purposes of conservative, rather than "on-average" toughness estimates, toughness values measured at loading rates which approximate minimum dynamic values would seem to be most reliable at the present time.

4. Estimates of dynamic K_c values using CVN correlations suggested by Barsom (28) were usually conservative when compared to measured dynamic K_c values.

5. Considering the uncertainties which underly empirical estimates of K_c and K_{Ic} based upon CVN testing, there is a definite need for the development and standardization of a fracture toughness test which is more appropriate than currently available standard tests for application to bridge steels. For this purpose, it appears

a modified version of dynamic-tear testing would hold best promise in terms of simplicity and enhanced capability for fracture mechanics interpretation.

5.9 Recommendations

There appear to be two major roles for fracture toughness evaluations of bridge steels: (a) elimination of very brittle steels which cause unnecessary expense during fabrication and produce potentially hazardous conditions if used for tensile load bearing members of a bridge, (b) careful assessment of the fracture reliability of non-redundant tensile load bearing bridge components.

1. Standard CVN tests appear to be as suitable for role (a) above as are fatigue precracked CVN tests or their slow-bend counterparts.

2. Development of modified dynamic-tear test as a future replacement for standard CVN tests in routine toughness evaluations of bridge steels is desirable.

3. In the case of bridge steels used in non-redundant components, careful evaluation of the steel toughness is needed. Unless employed with very conservative interpretations, CVN tests are not recommended for this purpose. Even an improved version of dynamic-tear testing may turn out to lack adequate precision. Thus it is recommended that some attention be given to instrumented fracture tests with specimen sizes large enough to permit K_c or K_{Ic} determinations for critical

members. The actual extent of the testing needed will have be determined from studies of the statistics associated with K_c testing. The current program did not evaluate this question. It should be recognized that although K_c testing is much more costly than qualifying a material by CVN results, the amount of such testing should be small since most of the structural members will not be critical non-redundant members. Thus the total cost of a job should not be effected.

TABLE 1 DATA SUMMARY

Material	Thickness	T_{15} (°F)	T_{15}^P (°F)	ΔT (°F)	ΔT^P (°F)	ΔT_B (°F)	$T_{15}-T_5$ (°F)	CVN_{SH} (ft-lb)	K_{ID}^{15} (ksi√in)	K_{ID}^* (ksi√in)	σ_y (ksi)	σ_u (ksi)	Elongation (%)
A7	1/2	100	--	125	--	162	60	73	> 80	35	35.5	63.0	27.5
A36	1/2	50	70	160	100	158	60	> 85	70	50	37.5	62.0	30.0
A36	1	60	100	150	80	152	60	62	60	50	42.5	65.0	31.0
A36	2	60	50	175	60	148	60	> 100	60	50	45.0	76.0	--
SAE 1035	1/2	70	--	175	--	147	70	55	70	50	45.3	80.7	23.0
SAE 1035	1	55	--	135	--	155	70	52	70	30	39.7	76.2	25.0
SAE 1035	2	50	--	0	--	148	125	> 60	60	50	44.3	89.7	--
A242	1/2	- 65	--	200	--	134	50	> 120	50	40	53.9	73.5	26.0
A242	1	25	--	200	--	138	50	> 90	50	30	50.9	74.8	23.0
A242	2	35	--	150	--	148	60	88	50	40	45.0	72.0	--
A440	1/2	- 25	0	125	100	121	50	65	90	50	62.6	83.2	23.0
A440	1	0	50	135	60	137	60	> 80	50	40	51.8	78.8	28.0
A440	2	70	30	210	130	121	120	> 60	62	40	62.5	82.0	--
A441	1/2	- 15	60	115	45	130	40	100	60	40	56.7	82.3	27.2
A441	1	- 10	65	60	40	130	70	> 100	40	40	55.9	87.0	--
A441	2	40	80	65	40	130	90	> 80	40	40	55.0	94.0	29.0
A588-B	1/2	- 10	50	160	70	112	90	80	80	40	68.5	94.0	20.0
A588-B	1	- 75	100	--	75	111	75	95	45	30	69.1	80.5	20.0
A588-B	2	- 15	115	85	135	121	60	90	43	30	62.5	87.0	--
A514-M	1/2	-150	--	110	0	24	50	35	--	--	127.0	131.5	--
A514-P	1	-100	-145	200	0	52	125	33	--	--	108.0	121.8	--
A514-M	2	-125	- 50	95	105	55	75	58	--	--	106.0	117.0	--

T_{15} - Temperature corresponding to the 15 ft.-lb. energy level from a test of standard CVN specimens.

T_{15}^{P} - Temperature corresponding to the 15 ft.-lb. energy level from a test of pre-cracked CVN specimens.

ΔT - Temperature shift at 15 ft.-lb. level between dynamic and slow bend (.02 in./min. crosshead speed) standard CVN specimens.

ΔT^{P} - Temperature shift at 15 ft.-lb. level between dynamic and slow bend (.02 in./min. crosshead speed) pre-cracked CVN specimens.

ΔT_{B} - $(215 - 1.5\ \sigma_y)$ where σ_y is the room temperature yield strength.

$T_{15}-T_{5}$ - Difference in temperature going from 5 to the 15 ft.-lb. energy level in a standard CVN test.

CVN_{SH} - Upper shelf Charpy energy

K_{ID}^{15} - K_{ID} at the temperature corresponding to the 15 ft.-lb. level in a standard CVN test.

K_{ID}^{*} - Apparent K_{ID} lower shelf.

σ_y - Yield strength.

σ_u - Ultimate strength

TABLE 2 CHEMISTRY SUMMARY OF PLATE

Plate Grade	Plate Thickness	C	Mn	P	S	Si	Cu	V	Ni	Cr	Mo	B	Heat No.
A7	1/2	0.22	0.44	0.014	0.038	0.02	0.01	< 0.002	0.045	0.01	< 0.02	< 0.001	
A36	1/2	0.21	0.54	0.008	0.021	0.05							490B5631
	1	0.18	0.95	0.009	0.015	0.05							490C0461
	2	0.20	1.00	0.011	0.018	0.24							422B3861
A242	1/2	0.10	0.75	0.07	0.023	0.30	0.29		0.33	0.58			401C6101
	1	0.10	0.73	0.08	0.030	0.31	0.27		0.37	0.53			481B1981
	2	0.10	0.85	0.056	0.024	0.28	0.28		0.34	0.53			481C0061
A440	1/2	0.18	1.14	0.009	0.025	0.15	0.26						487C0381
	1	0.18	1.14	0.009	0.025	0.15	0.26						487C0381
	2	0.16	1.13	0.012	0.021	0.23	0.23						412C5233
A441	1/2	0.20	1.08	0.017	0.025	0.21	0.23	0.051	0.02	0.03	0.002		482T0241
		0.20	1.08	0.017	0.025	0.21	0.23	0.051	0.02	0.03	0.002		482T0241
	2	0.20	1.08	0.017	0.025	0.21	0.23	0.051	0.02	0.03	0.002		482T0241
A514M	1/2	0.19	0.65	0.008	0.026	0.27			1.38		0.59	0.002	533Z0023
A514P	1	0.10	0.58	0.009	0.023	0.30			1.40	0.91	0.56	0.005	521X0027
A514M	2	0.18	0.65	0.010	0.032	0.27			1.39		0.59	0.005	532Z0265
A558B	1/2	0.15	1.15	0.014	0.026	0.23	0.30	0.027	0.30	0.56			432B2371
	1	0.13	1.05	0.013	0.030	0.26	0.31	0.029	0.31	0.52			401C2251
	2	0.15	1.15	0.014	0.026	0.23	0.30	0.027	0.30	0.56			432B2371
SAE 1035	1/2	0.38	0.61	0.008	0.021	0.17							422B5674
	1	0.38	0.61	0.008	0.021	0.17							422B5674
	2	0.38	0.74	0.016	0.019	0.21							402C2991

TABLE 3 AASHTO SPECIFICATIONS FOR BRIDGE STEELS

ASTM Designation	Originally Proposed by FHWA Based on Minimum Service Temperature of -30°		CVN Recommendations of AISI Bridge Steel Specifications Group (6/28/73)		
	Thickness (in.)	CVN ft.-lbs.	Group 1 See Footnote	Group 2 See Footnote	Group 3 See Footnote
A36		15 @ 40° F	15 @ 70° F	15 @ 40° F	15 @ 10° F
A572*	Up to 4" mechanically fastened	"	"	"	"
	Up to 2" welded	"	"	"	"
A440		"	"	"	"
A441		"	"	"	"
A242		"	"	"	"
A588*	Up to 4" mechanically fastened	"	"	"	"
	Up to 2" welded	"	"	"	"
	Over 2" welded	20 @ 40° F	20 @ 70° F	20 @ 40° F	20 @ 10° F
A514	Up to 4" mechanically fastened	25 @ 0° F	25 @ 30° F	25 @ 0° F	25 @-30° F
	Up to 2-1/2" welded	25 @ 0° F	25 @ 30° F	25 @ 0° F	25 @-30° F
	Over 2-1/2" to 4" welded	35 @ 0° F	35 @ 30° F	35 @ 0° F	35 @-30° F

Footnotes: Group 1: Minimum Service Temperature 0° F and above.
Group 2: Minimum Service Temperature from -1° to -30° F.
Group 3: Minimum Service Temperature from -31° to -60° F.

*If the yield point of the material exceeds 65 ksi, the temperature for the CVN value for acceptability shall be reduced by 15° F for each increment of 10 ksi above 65 ksi.

TABLE 4 MATERIAL PROGRAM COMPLIANCE WITH AASHTO FOR CVN SPECIFICATIONS

Material	Thickness (in.)	ASSHTO Group
A7	1/2	-*
A36	1/2	1
A36	1	1
A36	2	1
SAE 1035	1/2	1*
SAE 1035	1	1*
SAE 1035	2	1*
A242	1/2	1, 2, 3
A242	1	1, 2
A242	2	1, 2
A440	1/2	1, 2, 3
A440	1	1, 2, 3
A440	2	1
A441	1/2	1, 2, 3
A441	1	1, 2, 3
A441	2	1, 2
A588	1/2	1, 2, 3
A588	1	1, 2, 3
A588	2	1, 2, 3
A514	1/2	1, 2, 3
A514	1	1, 2, 3
A514	2	1, 2, 3

*Although these materials were not listed in Table 3 they would be similar to A36.

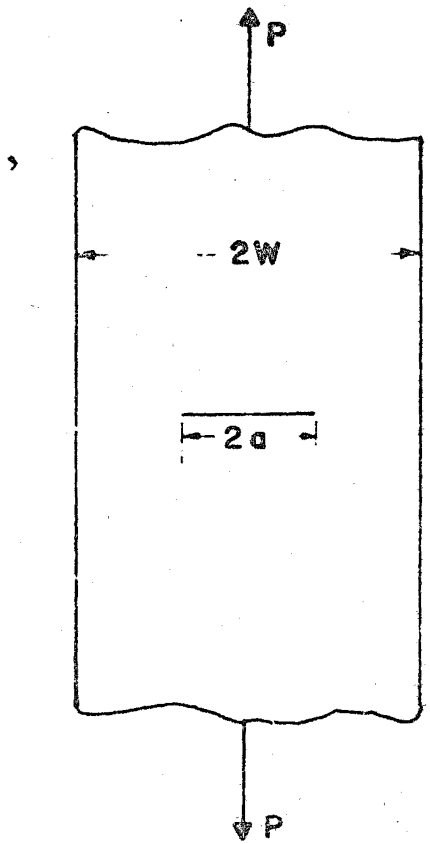

$$Y = 1.77(1 - 0.1(2a/W) + (2a/W)^2)$$

FIGURE 1a

$$K = Y\frac{P a^{1/2}}{BW}$$

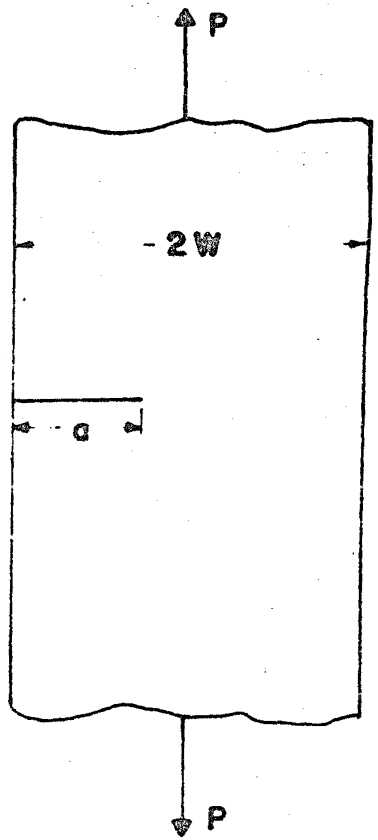

$$Y = 1.99 - 0.41(a/W) + 18.70(a/W)^2 - 38.48(a/W)^3 + 53.85(a/W)^4$$

FIGURE 1b

Fig. 1 Two Fracture Mechanics Specimens

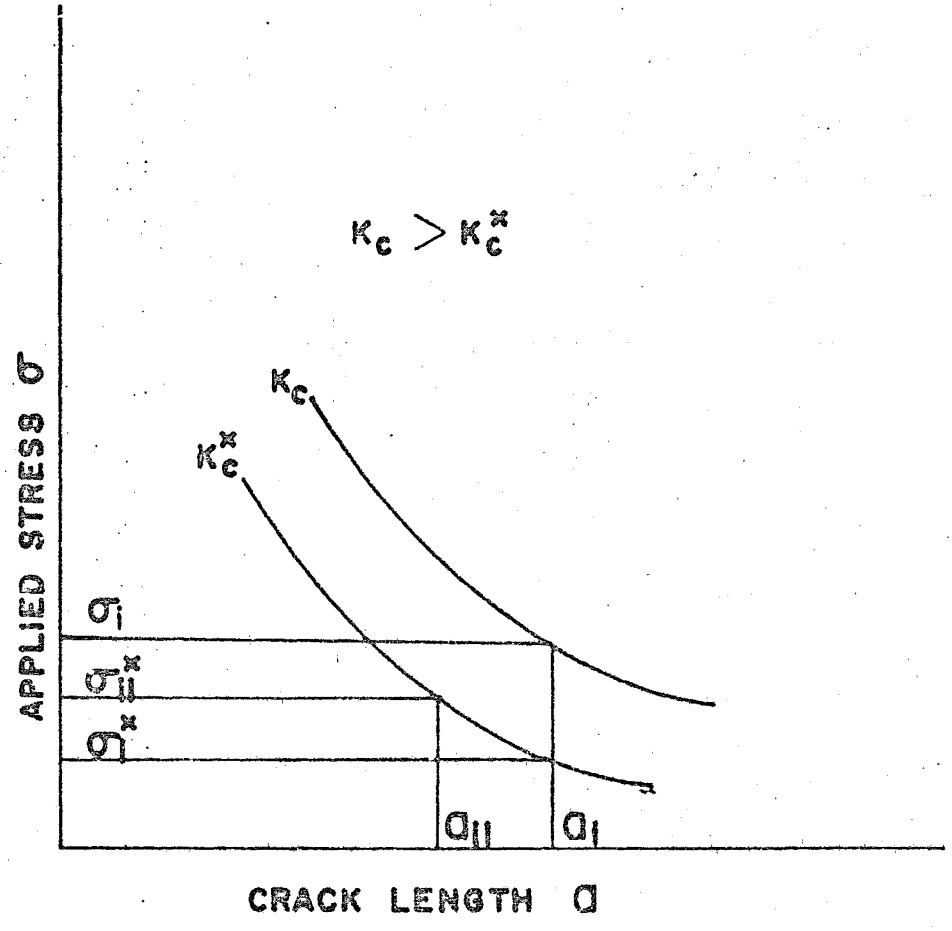

Fig. 2 Stress versus Crack Length for a Fixed K_c Value.
$\sigma_i > \sigma_i^*$ Represents going to a Higher K_c at a Fixed Crack Length.
$\sigma_{ii}^* > \sigma_i^*$ Represents going to a Smaller Crack Size at a Fixed K_c Level.

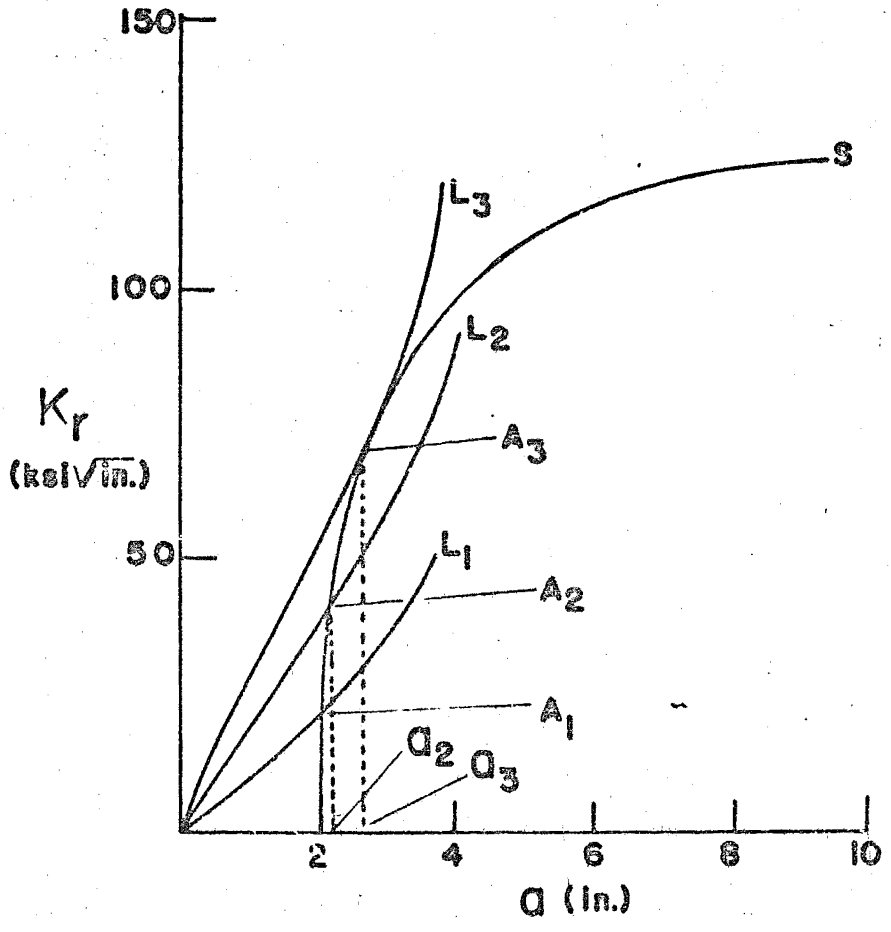

Fig. 3 A Schematic Representation of K_R versus a (effective) for a material such as High Purity 2024-T3 Aluminum in 1/8" Thickness is shown as Curve (S). Curves (L) show Constant Load Curves of K versus a ($L_3 > L_2 > L_1$). Point A_3 indicates an Instability Point Corresponding to a K_c of about 75 ksi √in.

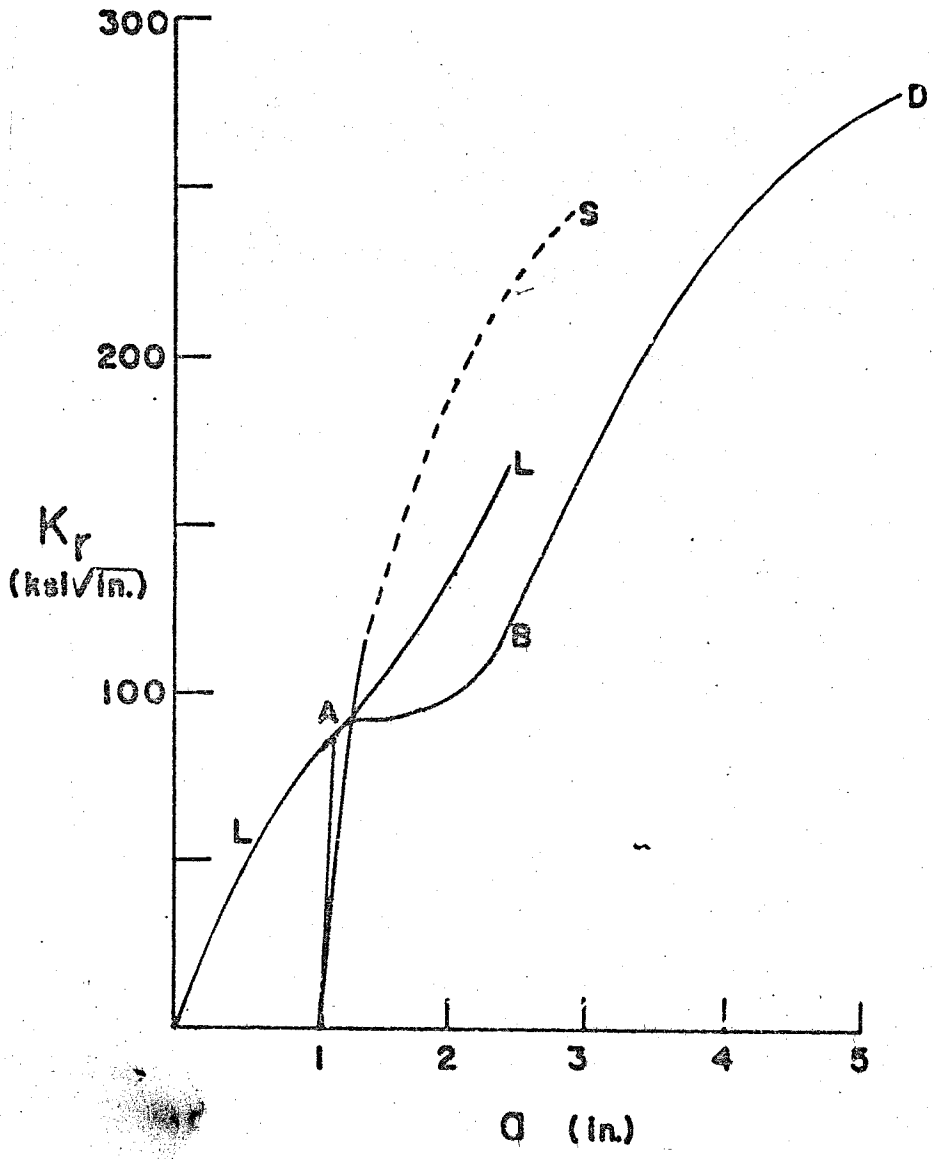

Fig. 4 A Schematic Representation of K_R versus a (effective), believed to be appropriate for A441 steel in 1" Thickness under Dynamic Loading at 60° F, as shown as Curve (D). Curve (L) is a Load-constant Curve of K versus a indicating a Dynamic Instability Point, A, corresponding to K_c = 80 ksi √in. Curve (S) represents K_R versus a (effective) for Static (one second) Loading. Instability might occur at the Solid Line End of Curve (S) at a Load somewhat above that of Curve (L). A short run of the Crack accompanied by a Load Drop might then result in Crack Arrest at Point B.

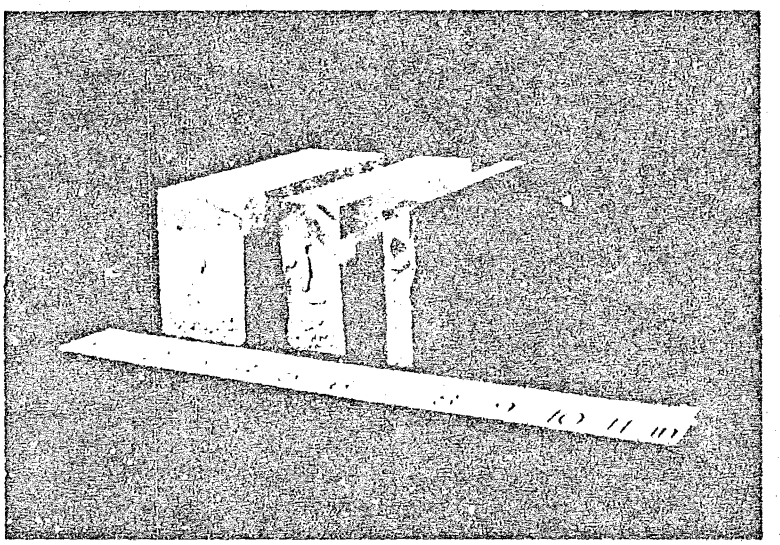

Photo of 1/2", 1" and 2" - 3" x 12" K_c Specimen

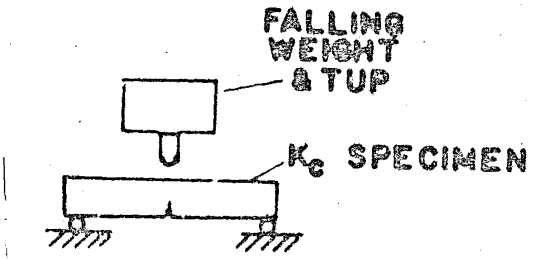

Drawing of Loading of 3" x 12" Specimen

Fig. 5 K_c Specimens - Loading Arrangement

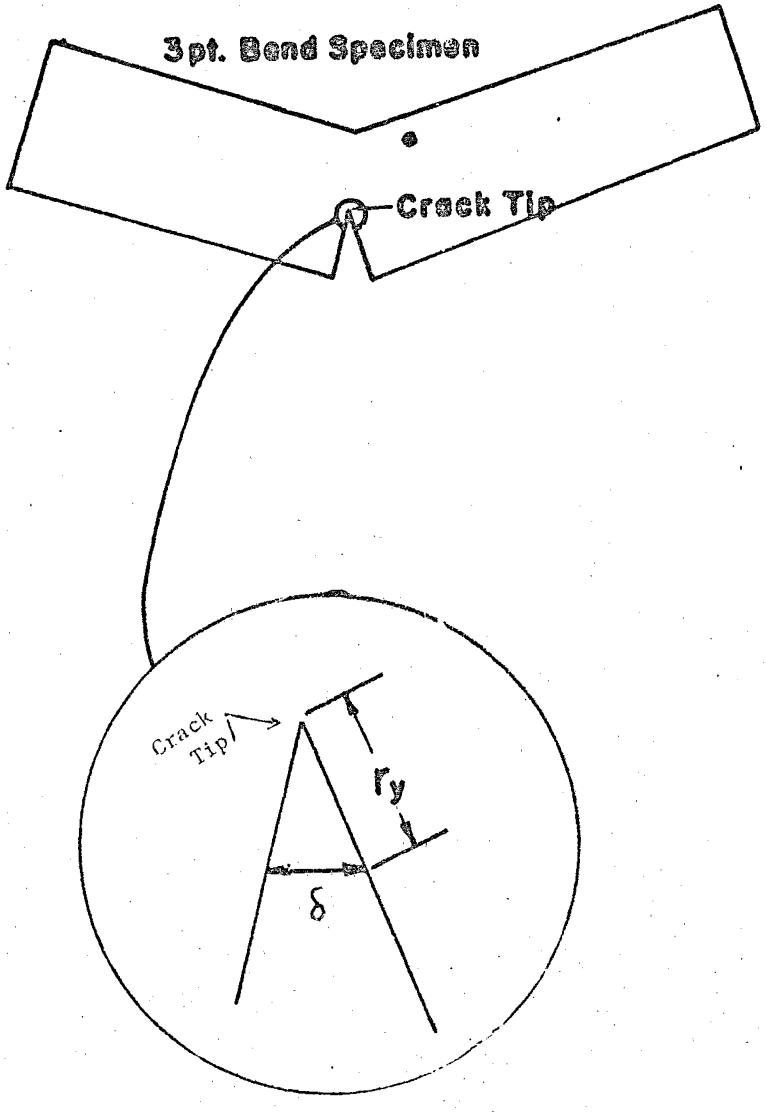

Fig. 6 Crack Opening Stretch Measurement Position

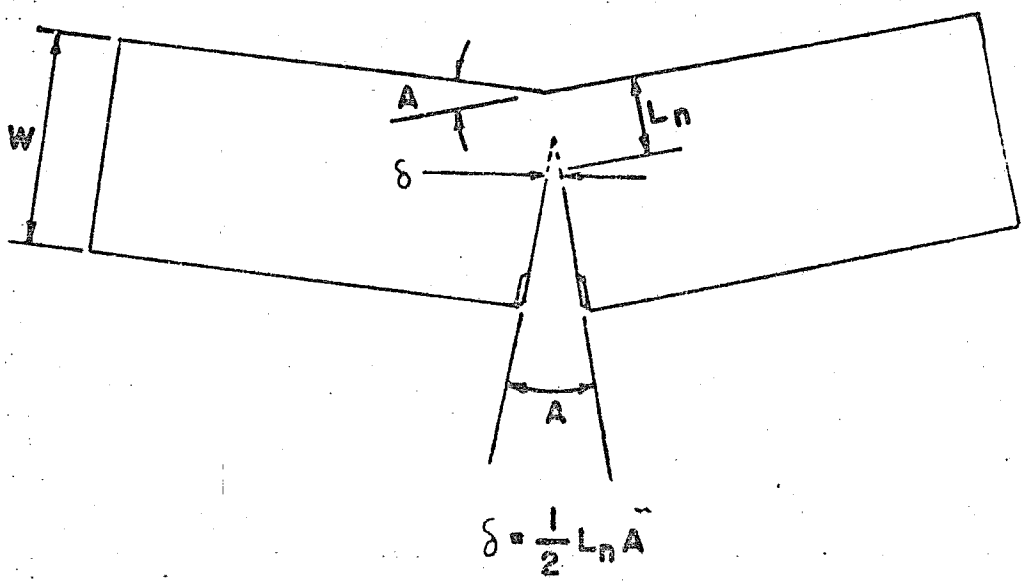

Fig. 7 Typical Partially Fractured Test Specimen Used in Bend Angle Procedure

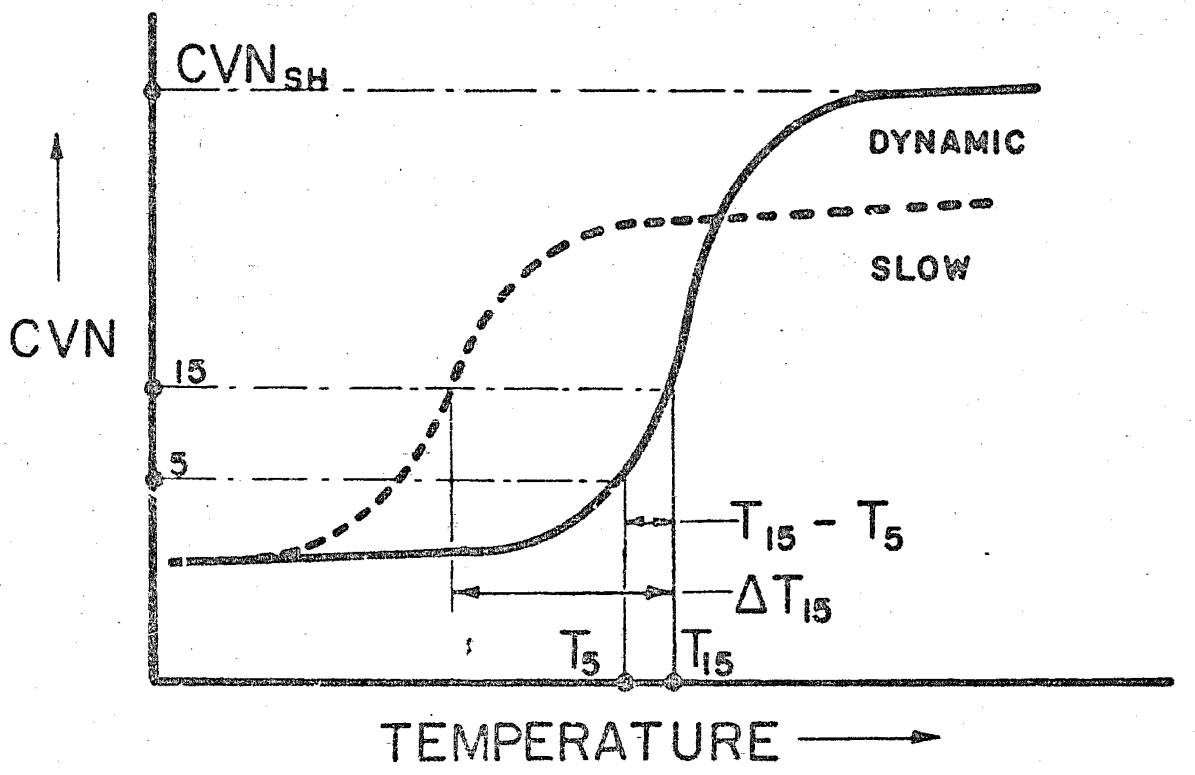

Fig. 8 Typical CVN Curve for Slow and Dynamic Loading

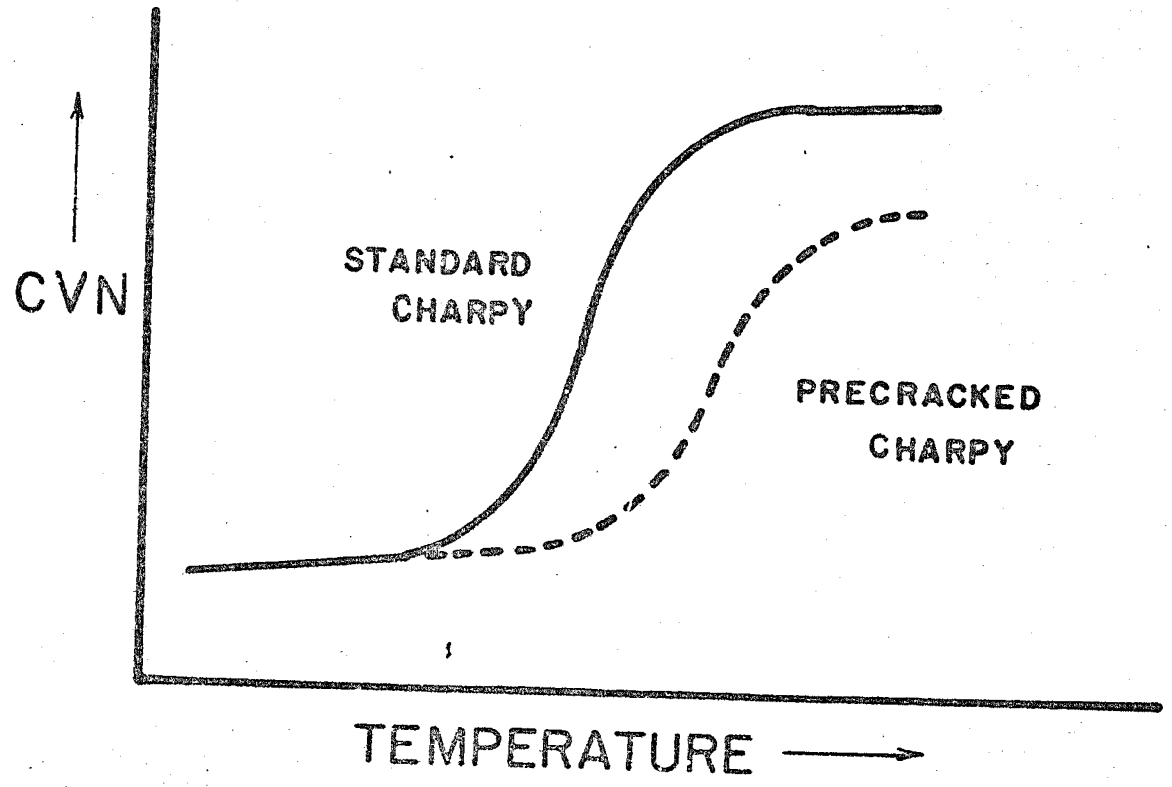

Fig. 9 Typical Results for Standard and Precracked, Charpy Specimens

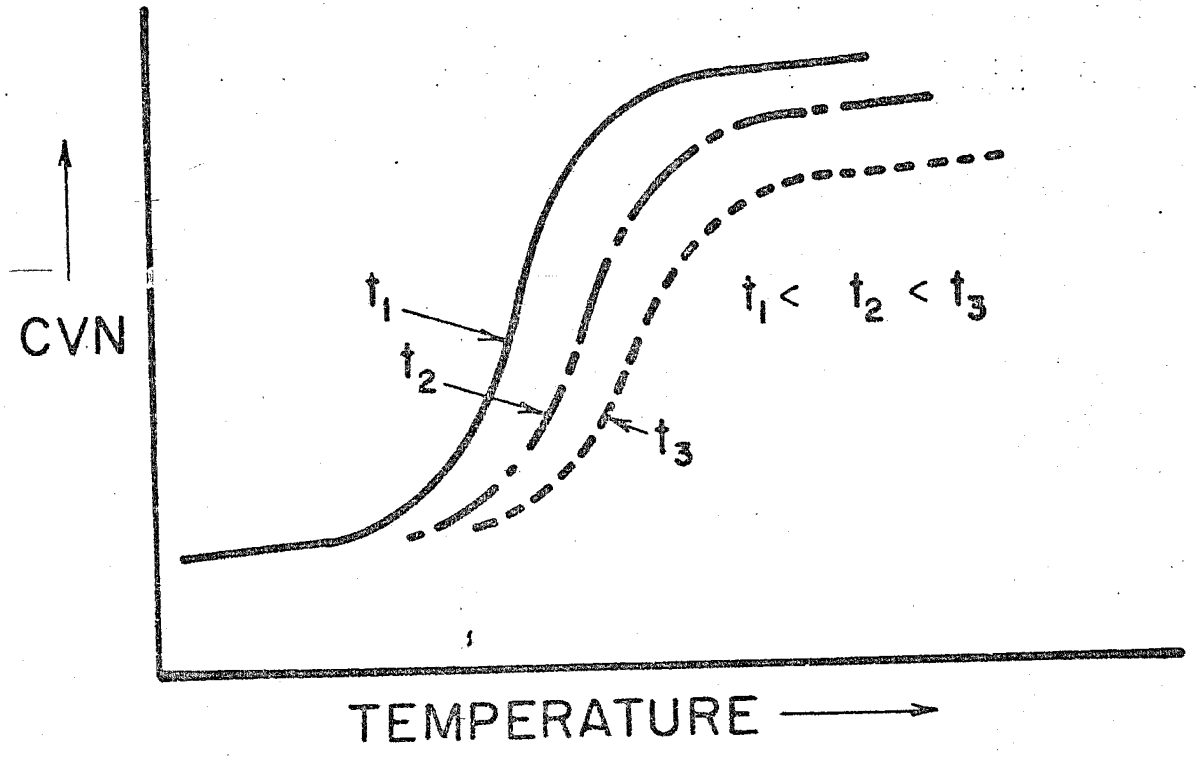

Fig. 10 Typical Thickness Effect on Charpy Results

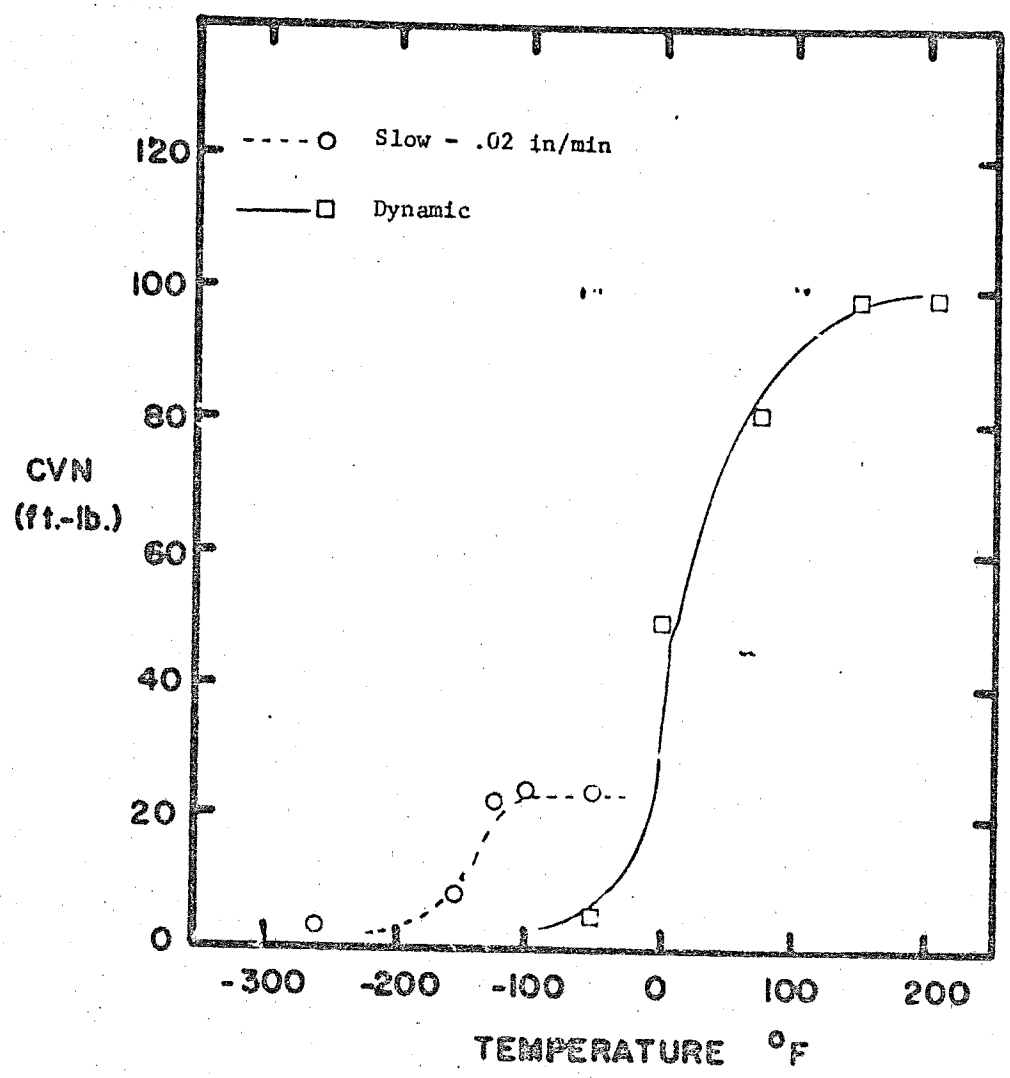

Fig. 11 A441 1/2" Notched Charpy Data for Two Rates of Loading

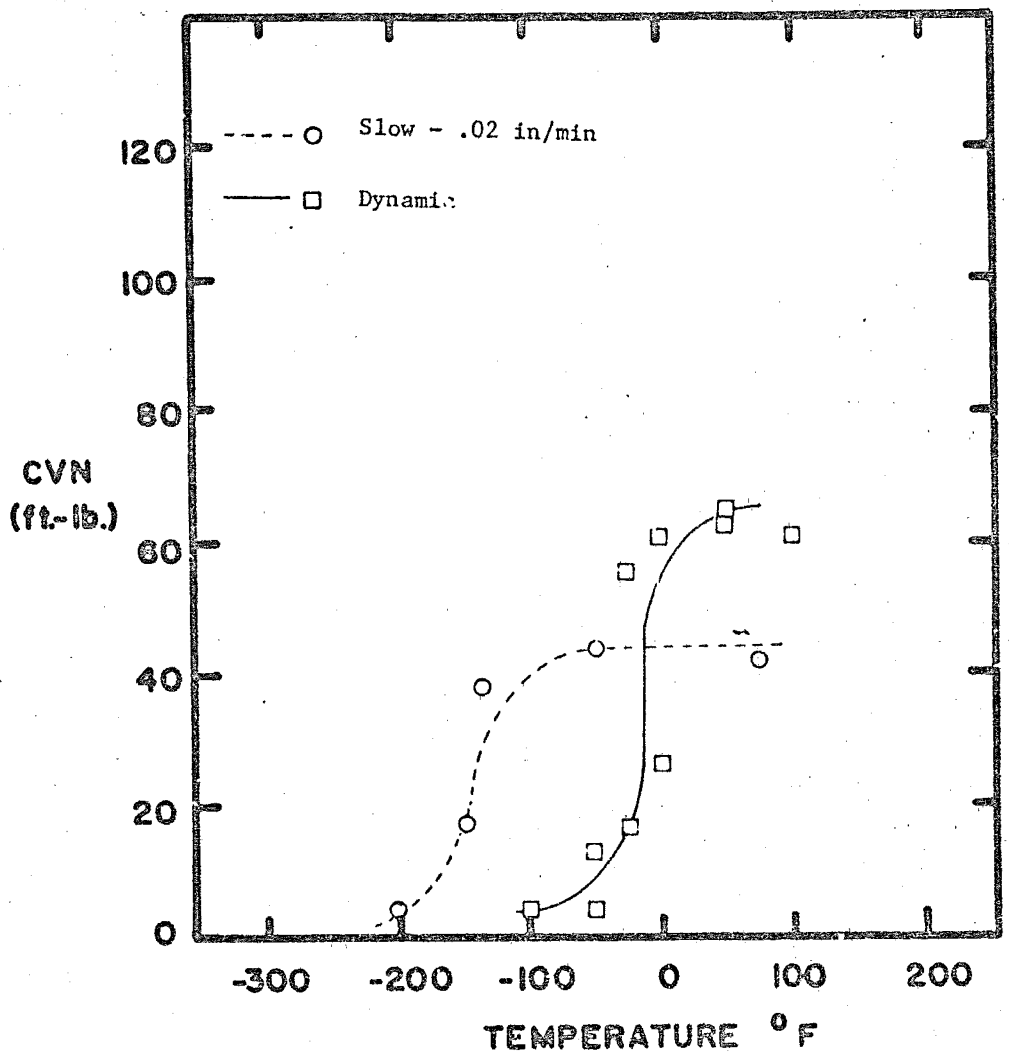

Fig. 12 A440 1/2" Notched Charpy Data for Two Rates of Loading

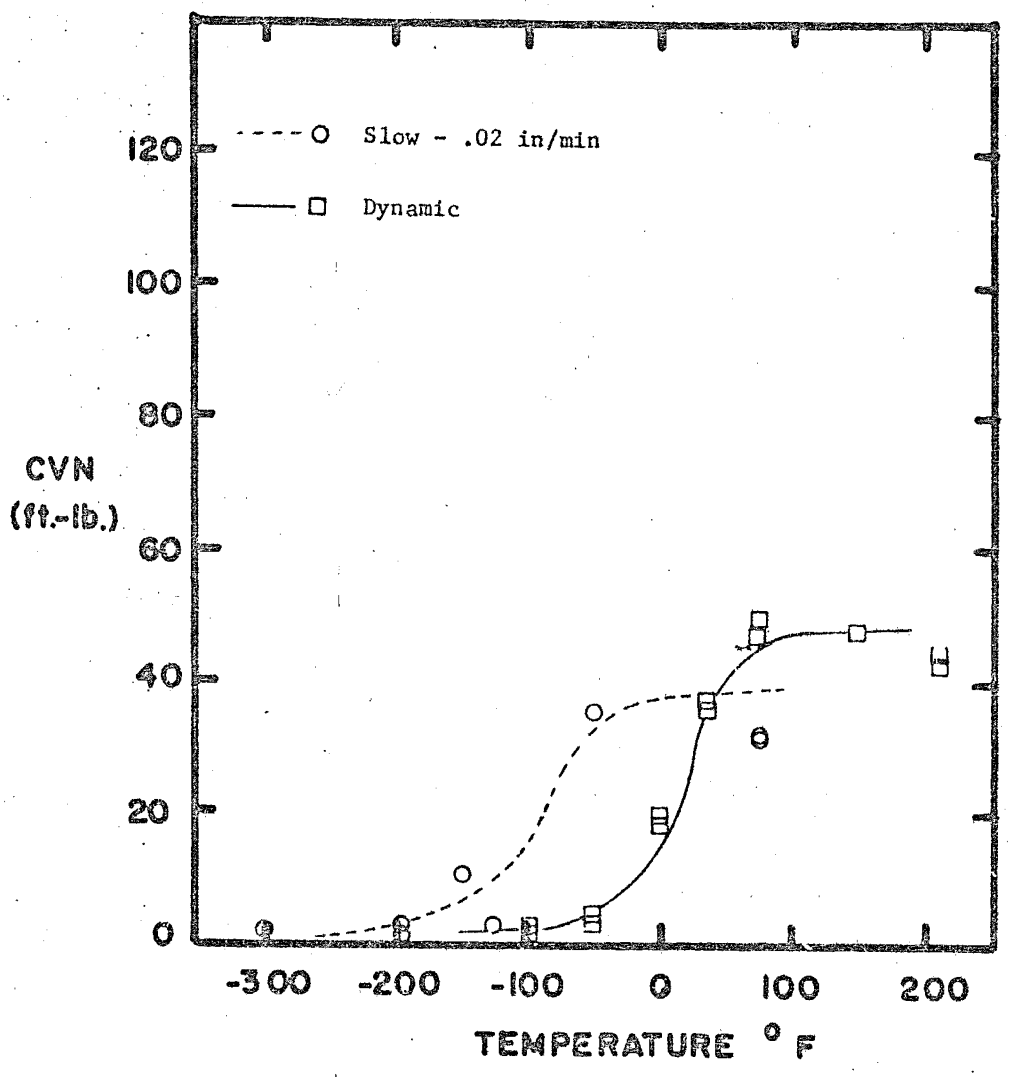

Fig. 13 A440 1/2" Precracked Data

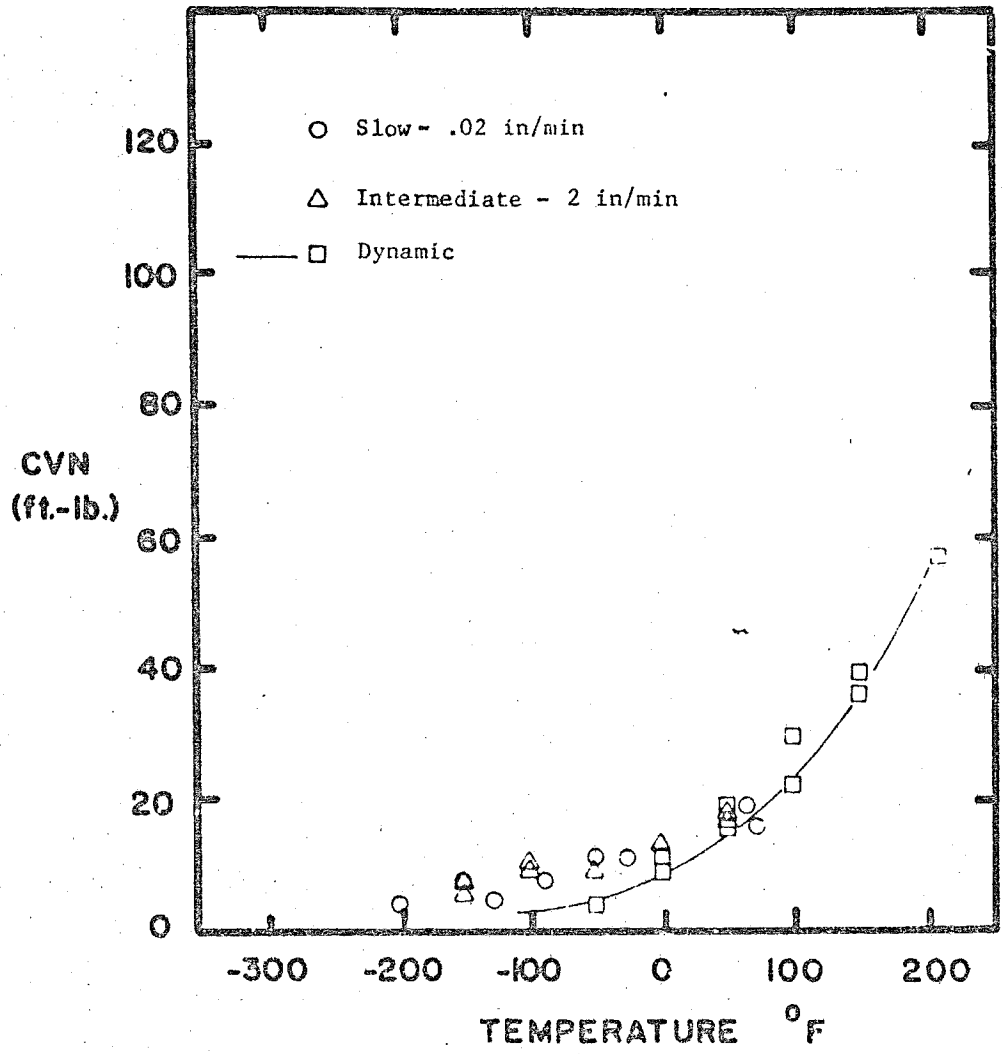

Fig. 14 SAE 1035 2" Notched Charpy Data for Three Rates of Loading

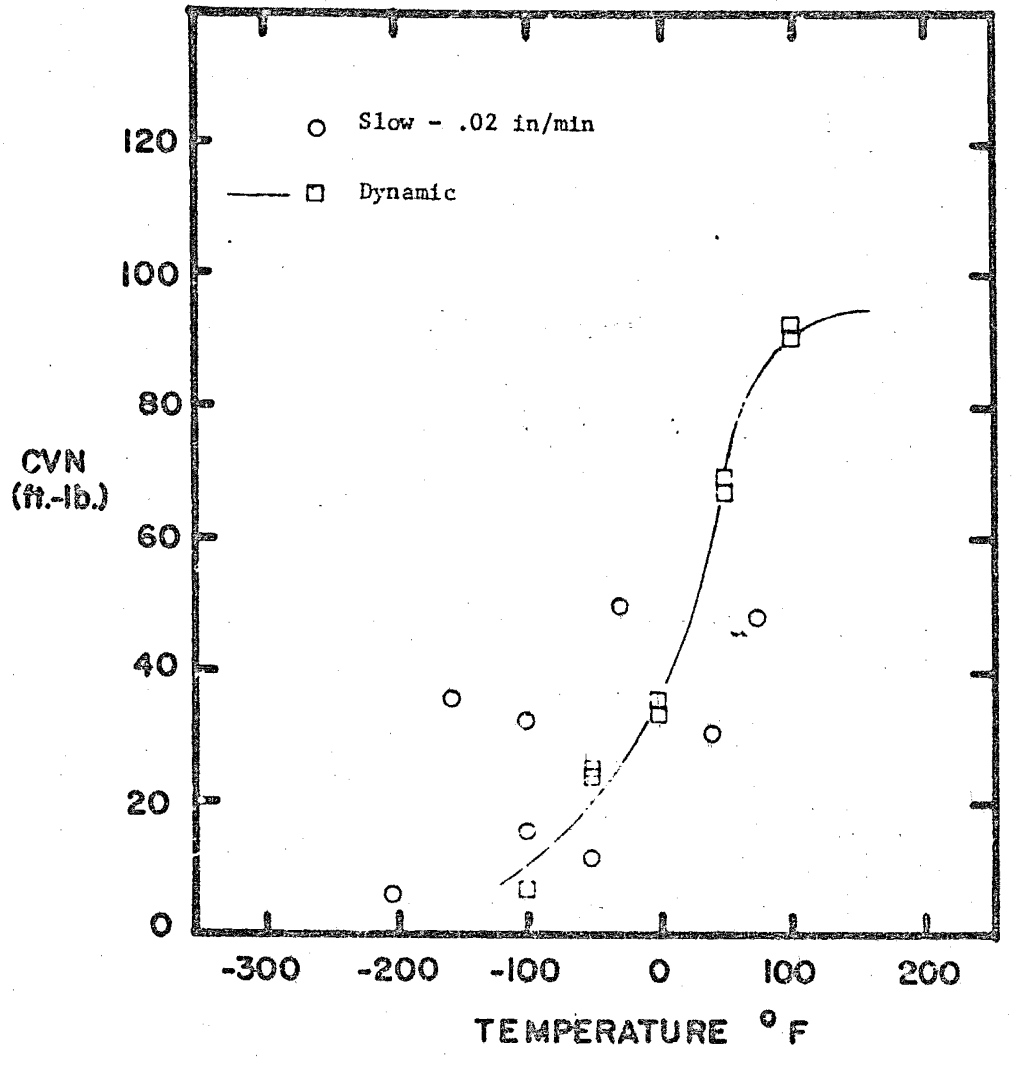

Fig. 15 A588 1" Notched Charpy Data for Two Rates of Loading

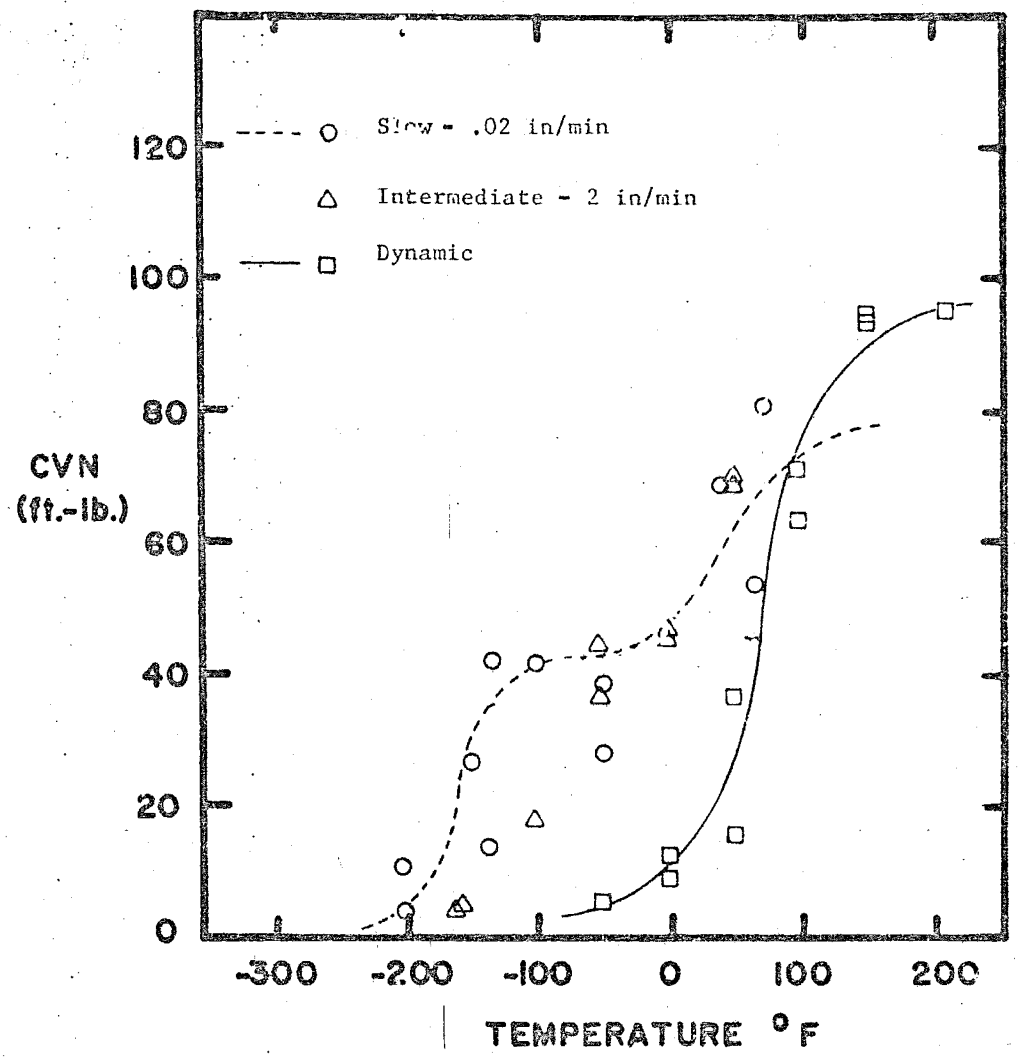

Fig. 16 A242 1" Notched Charpy Data for Three Rates of Loading

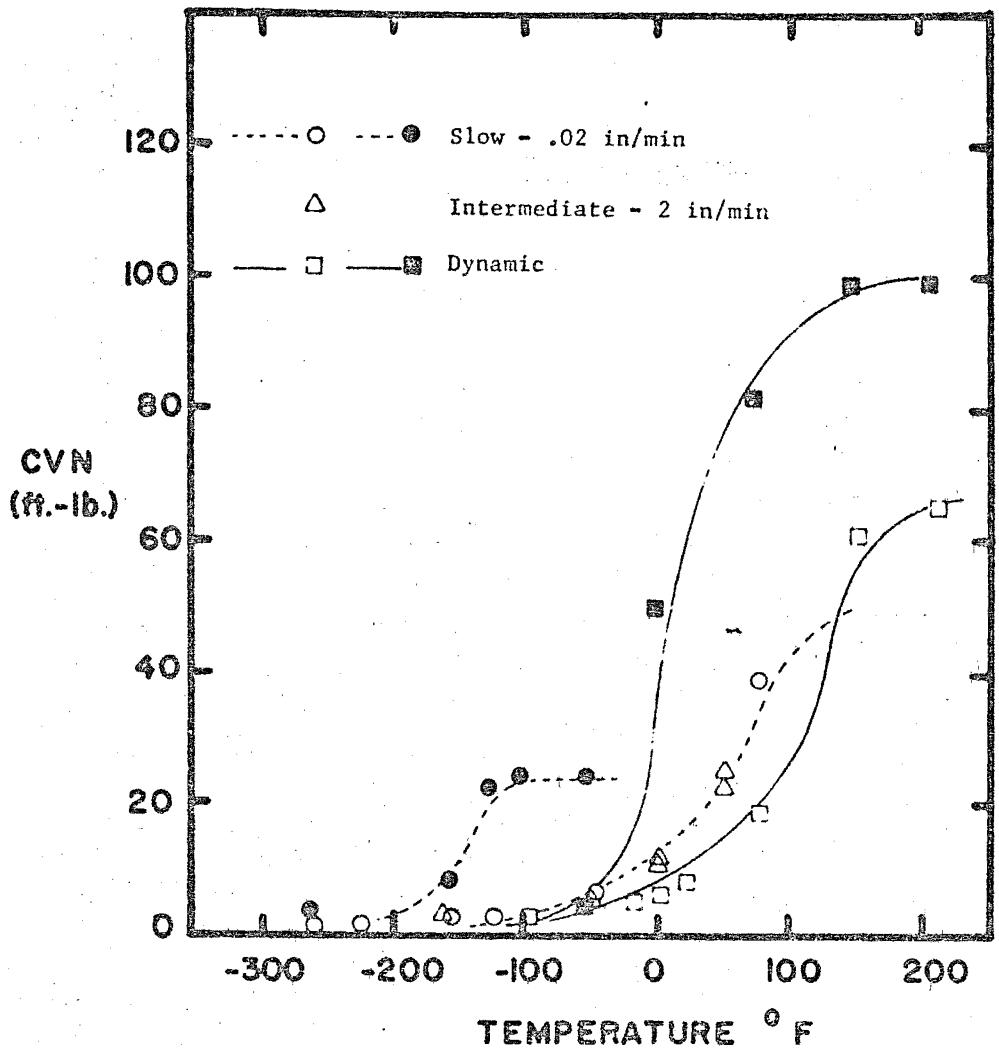

Fig. 17 A441 1/2" Precracked Data and Notched Charpy Data for Three Rates of Loading

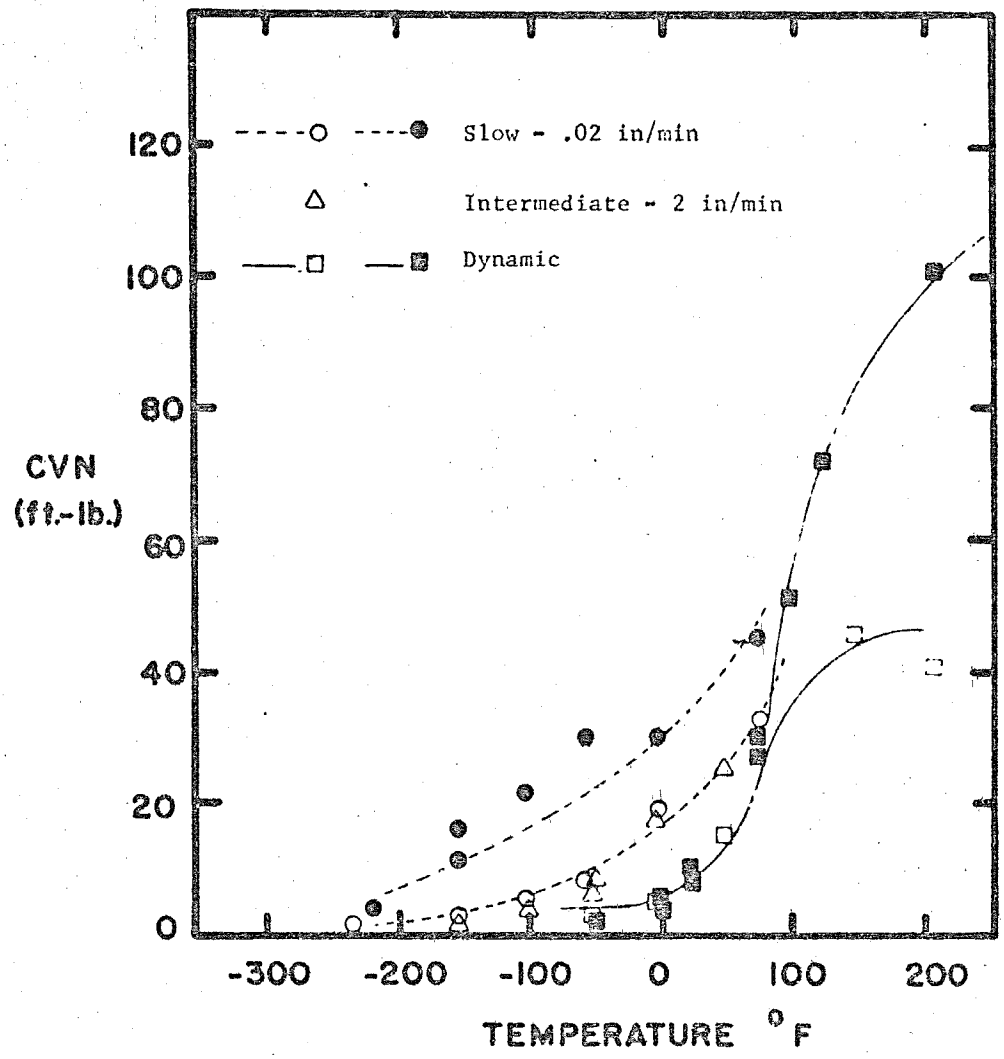

Fig. 18 A36 2" Precracked Data and Notched Charpy Data for Three Rates of Loading

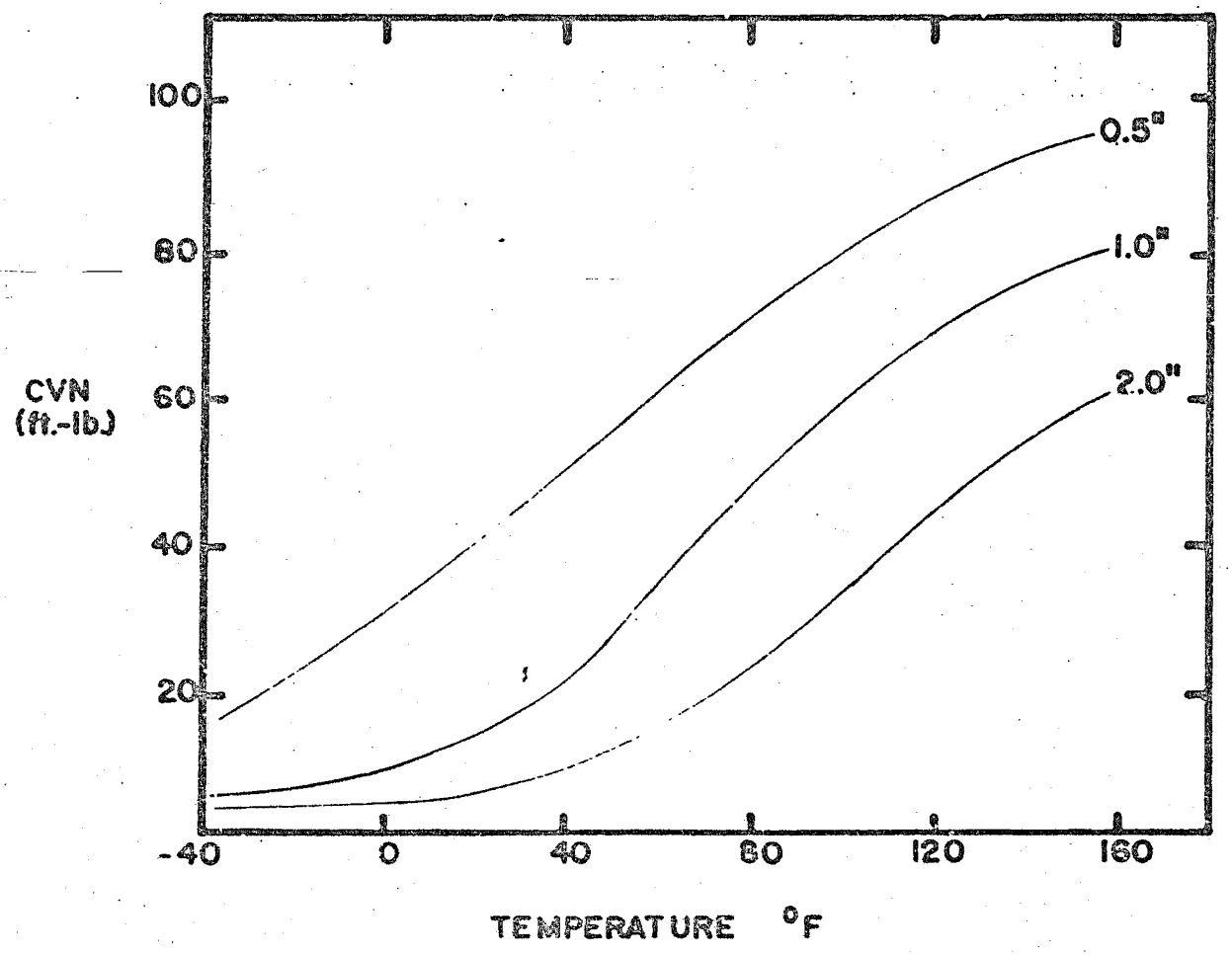

Fig. 19 CVN Values for A441 Material

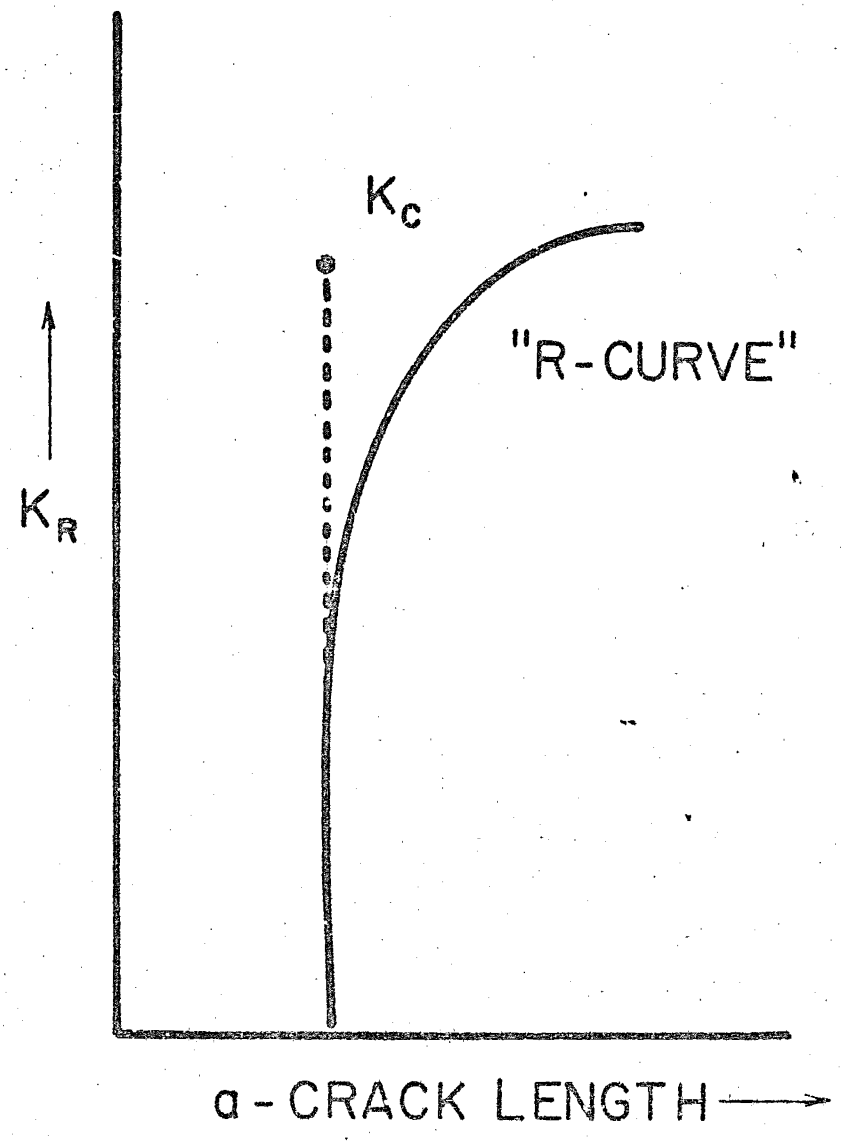

Fig. 20 R-Curve

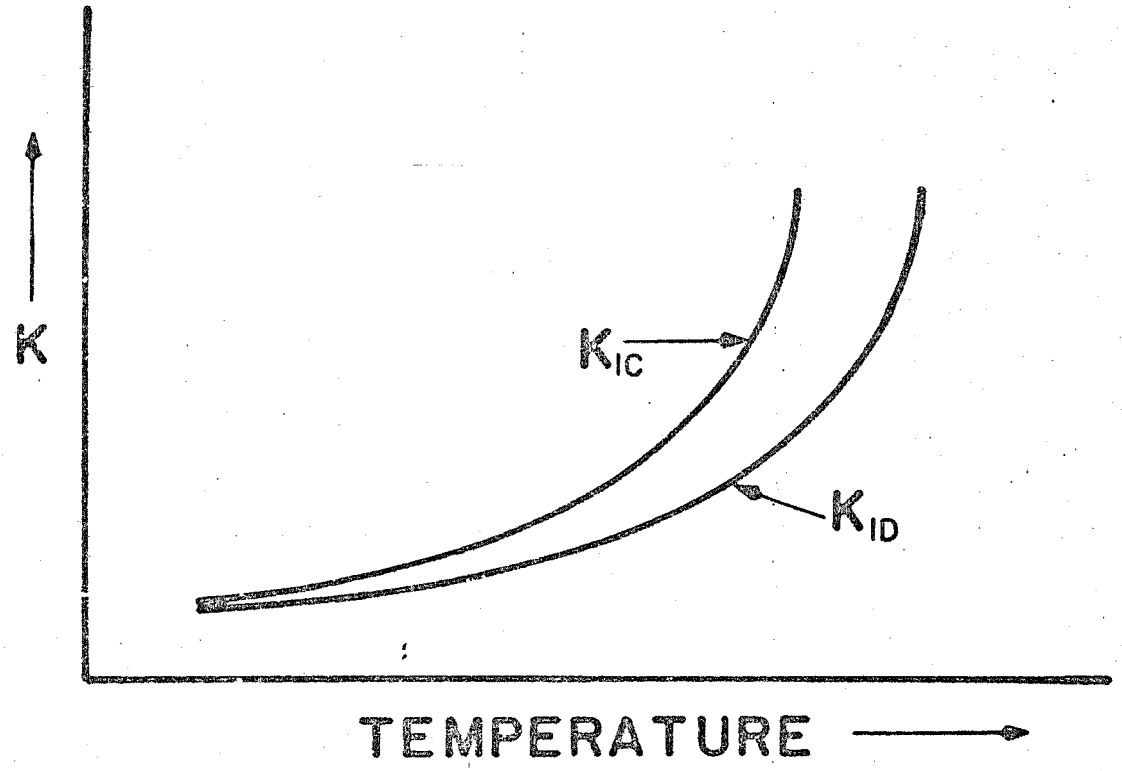

Fig. 21 Temperature Shift for K_c Tests

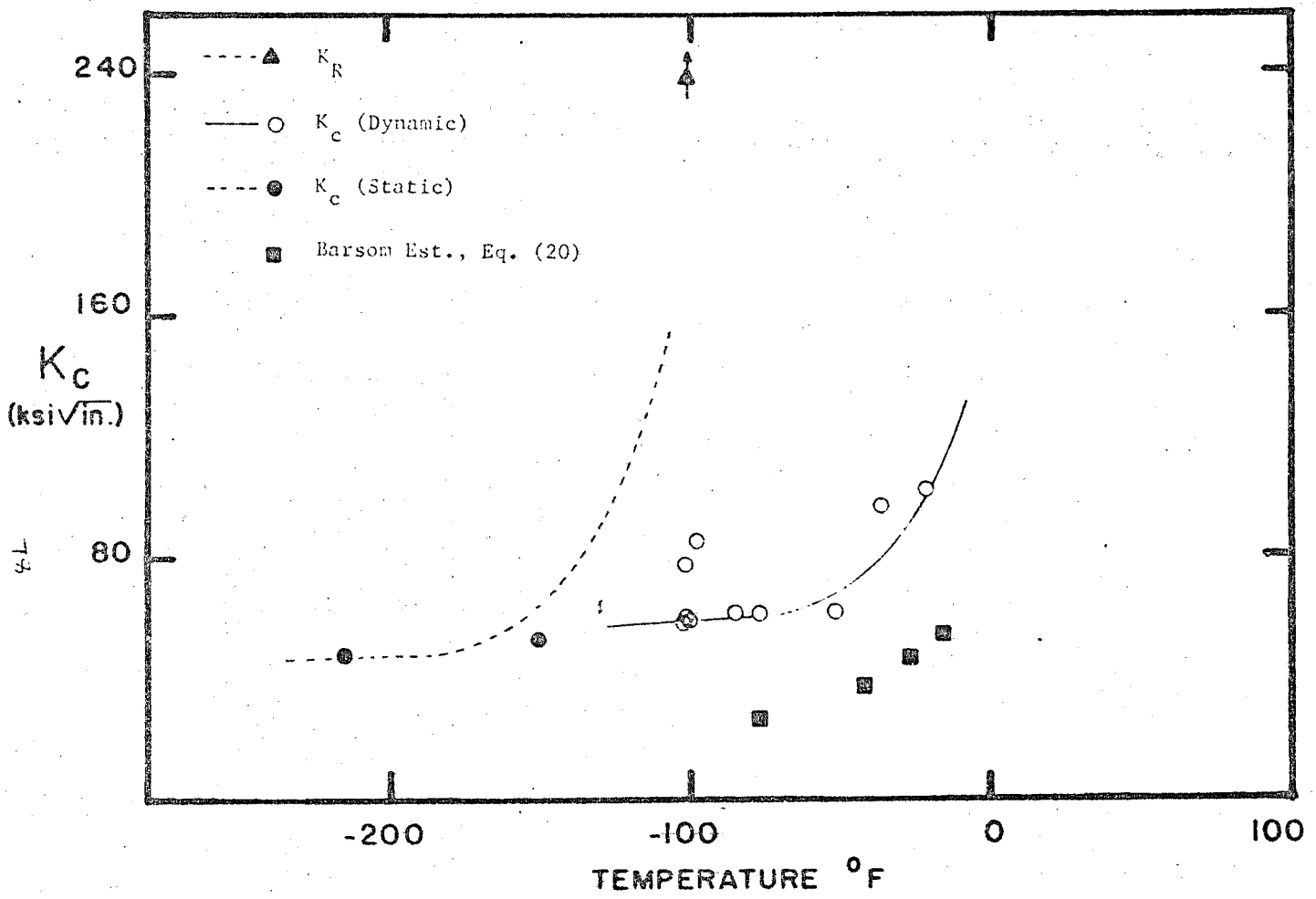

Fig. 22 K_c Data for A440 1/2" Material

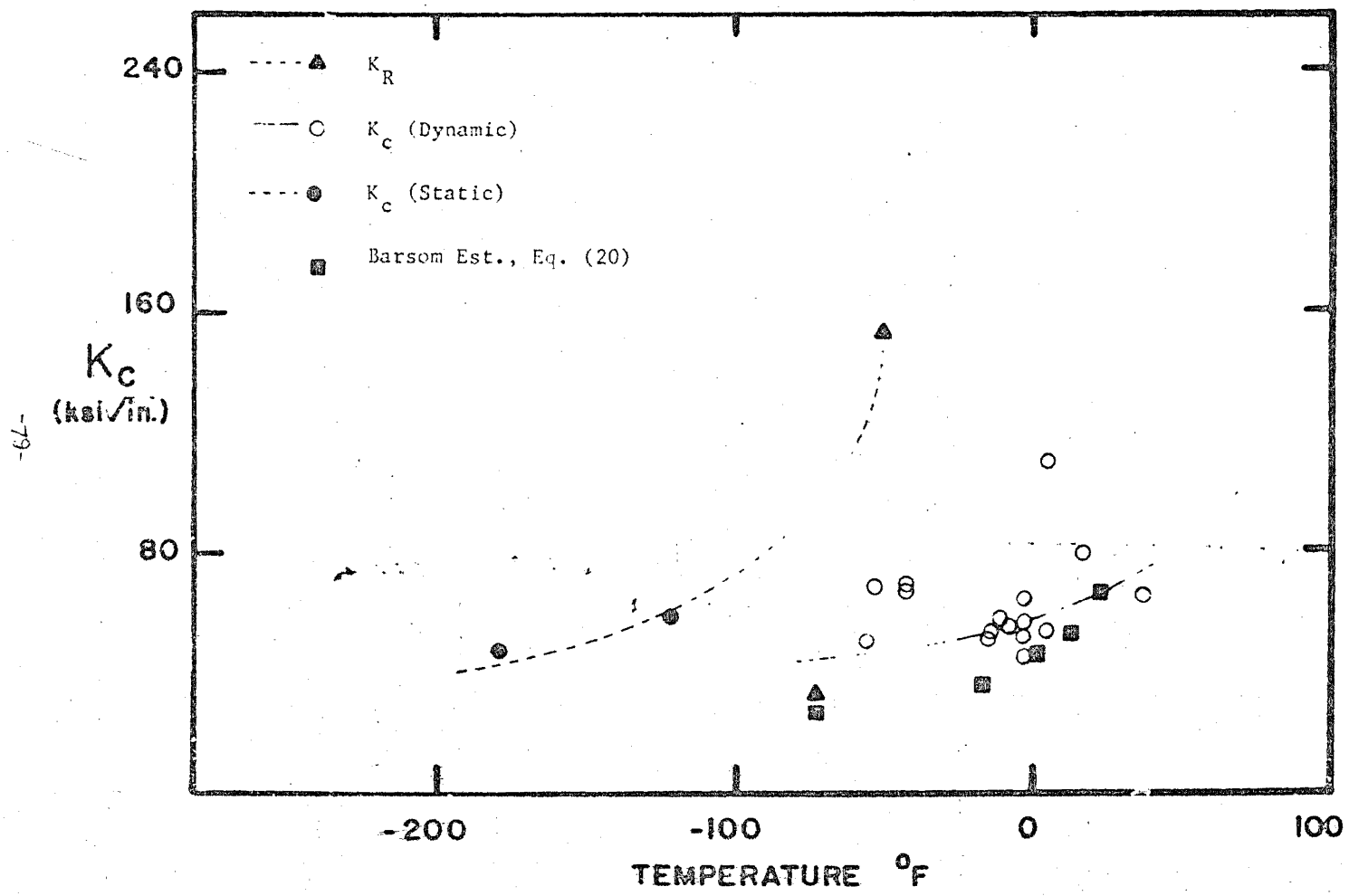

Fig. 23 K_c Data for A440 1" Material

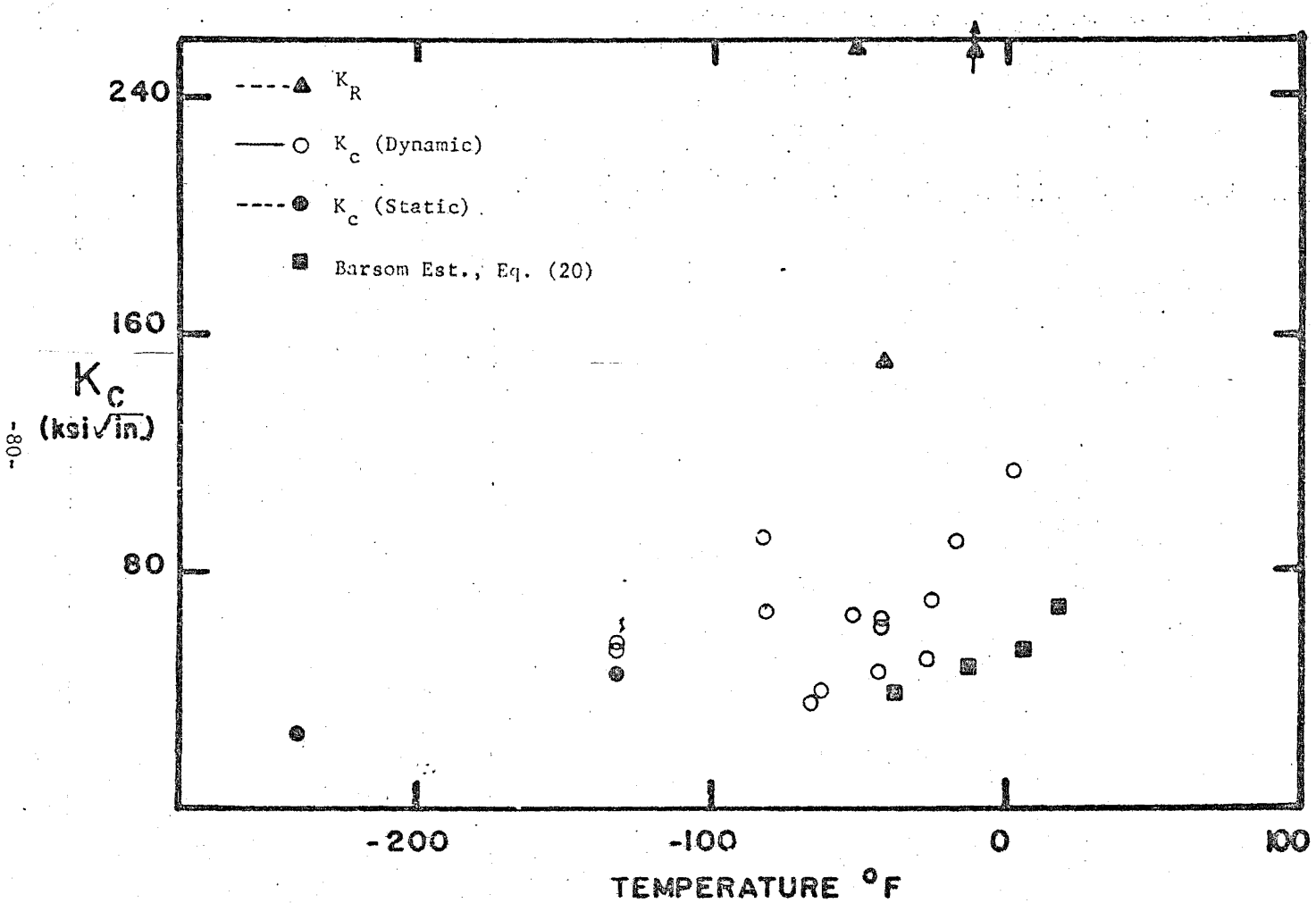

Fig. 24 K_c Data for A588B 1/2" Material

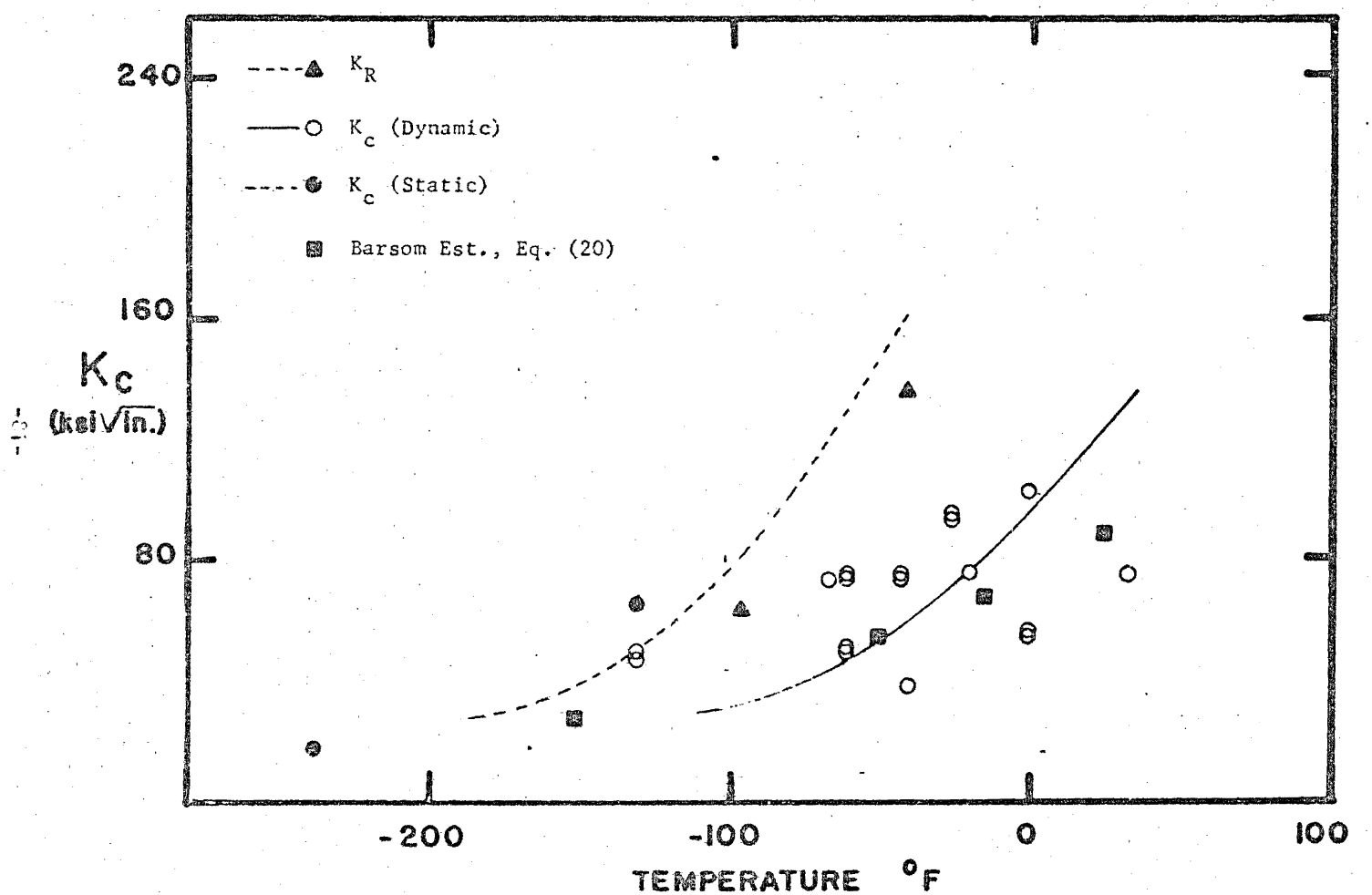

Fig. 25 K_c Data for A588B 1" Material

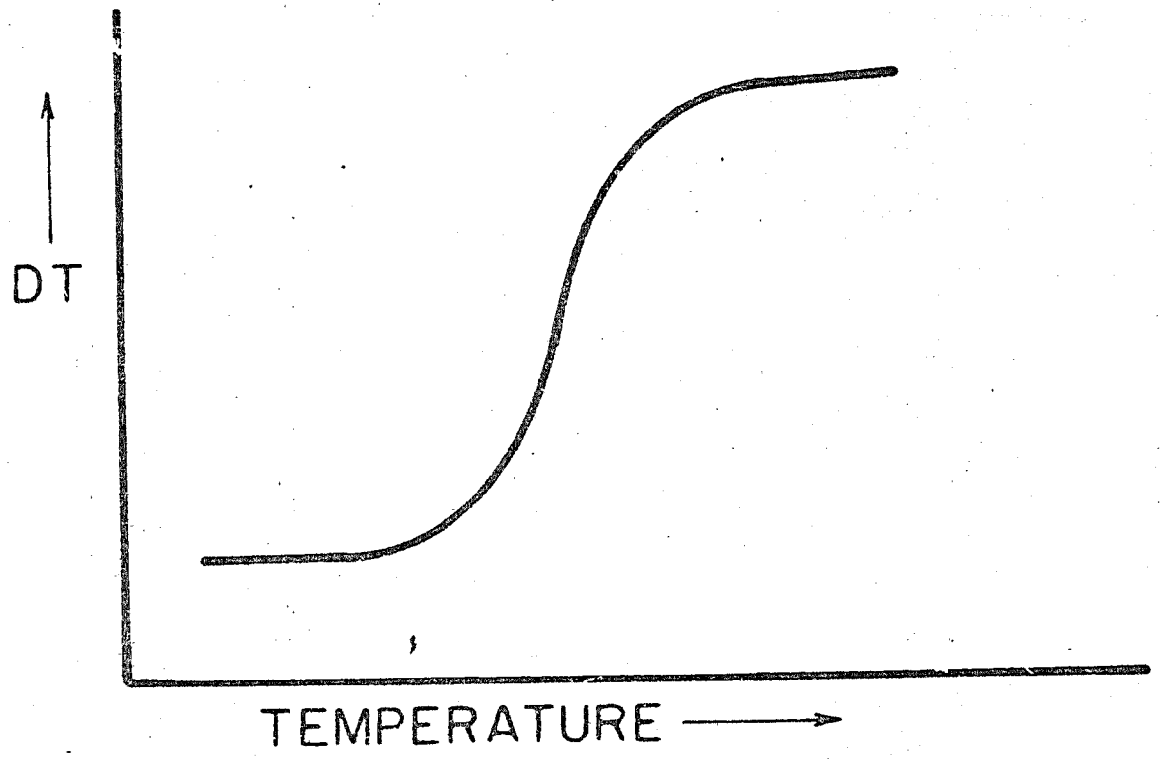

Fig. 26 Typical DT versus Temperature

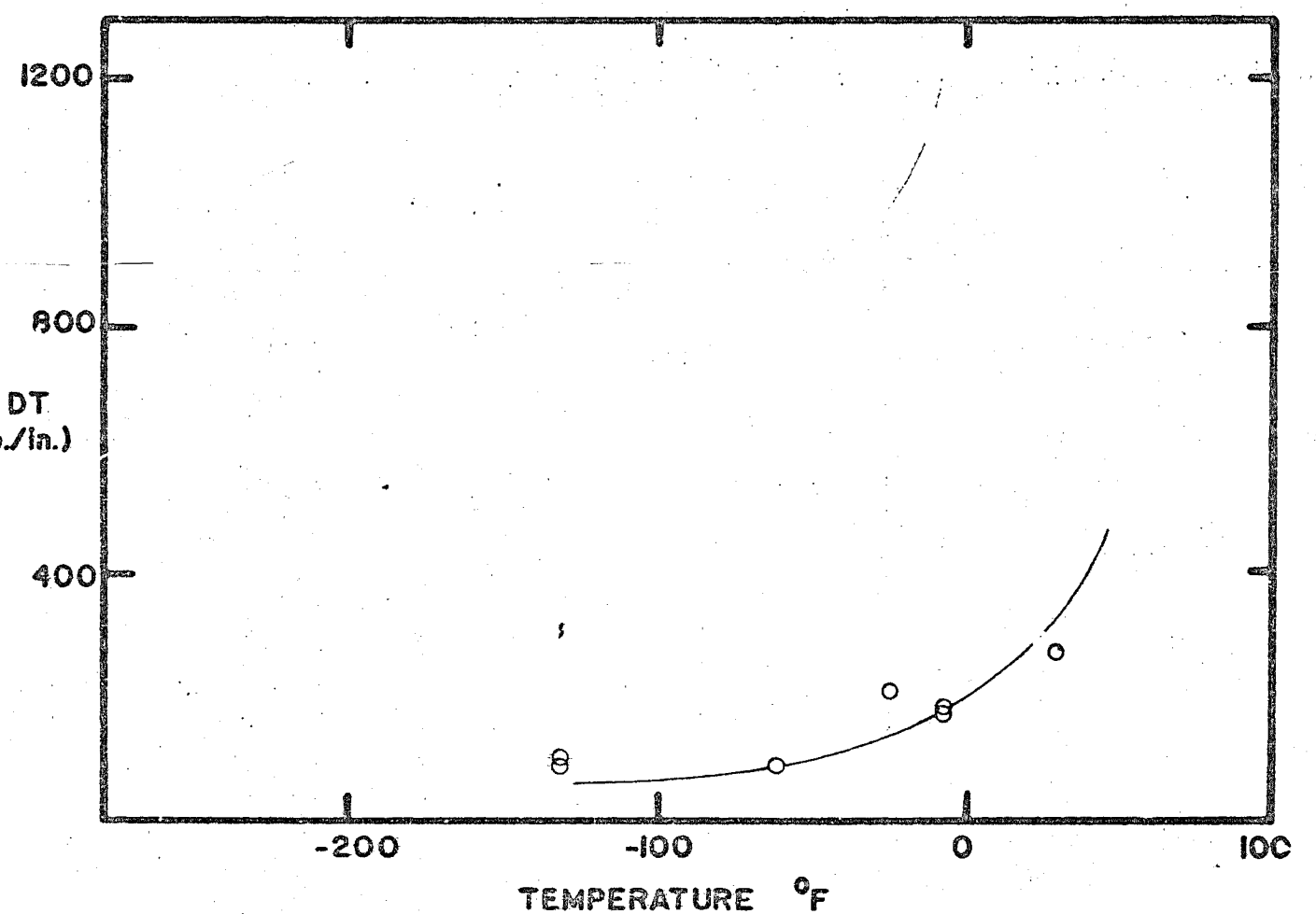

Fig. 27 Dynamic Tear Data for A588B 2" Material

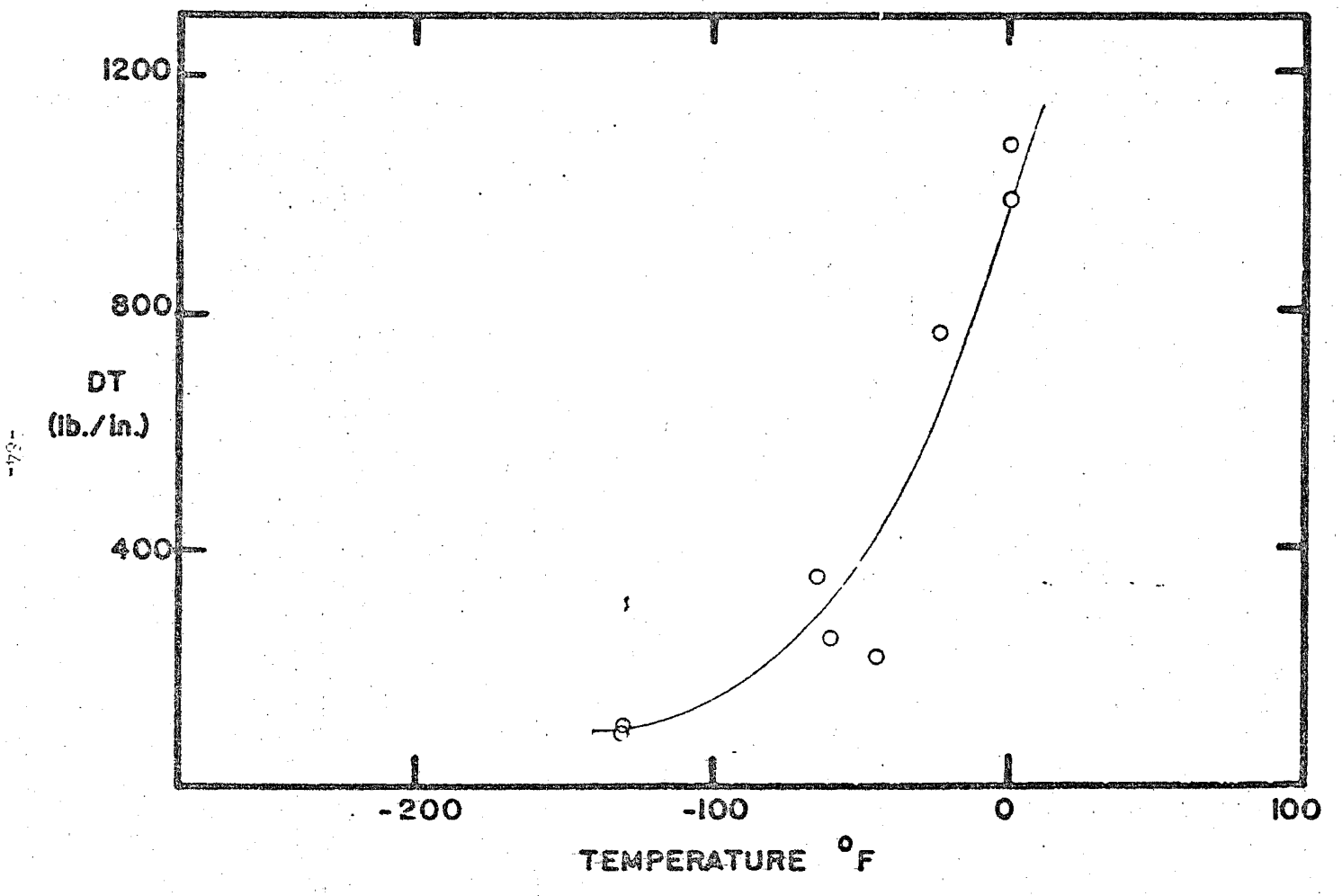

Fig. 28 Dynamic Tear Data for A588B 1" Material

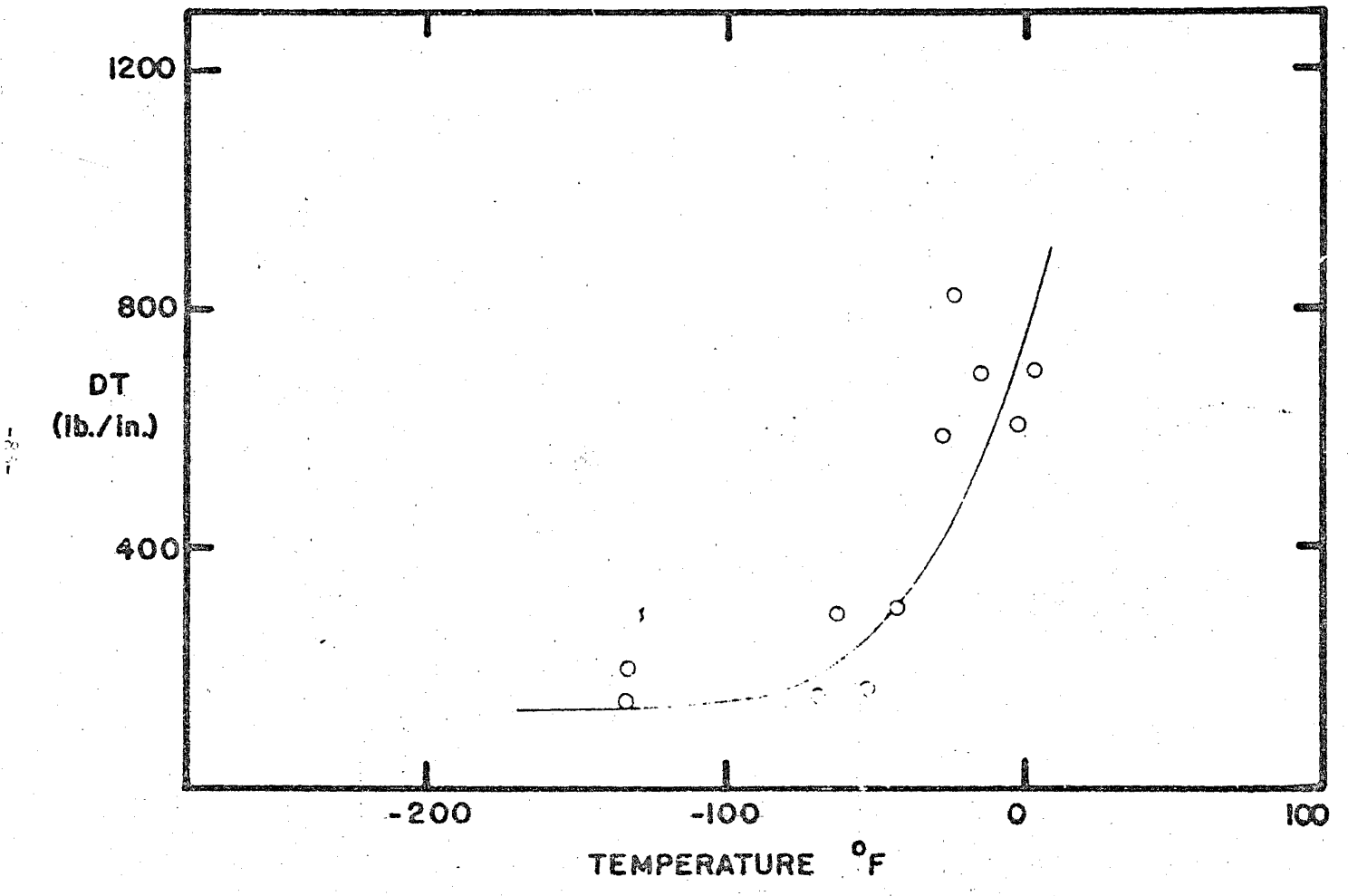

Fig. 29 Dynamic Tear Data for A588B 1/2" Material

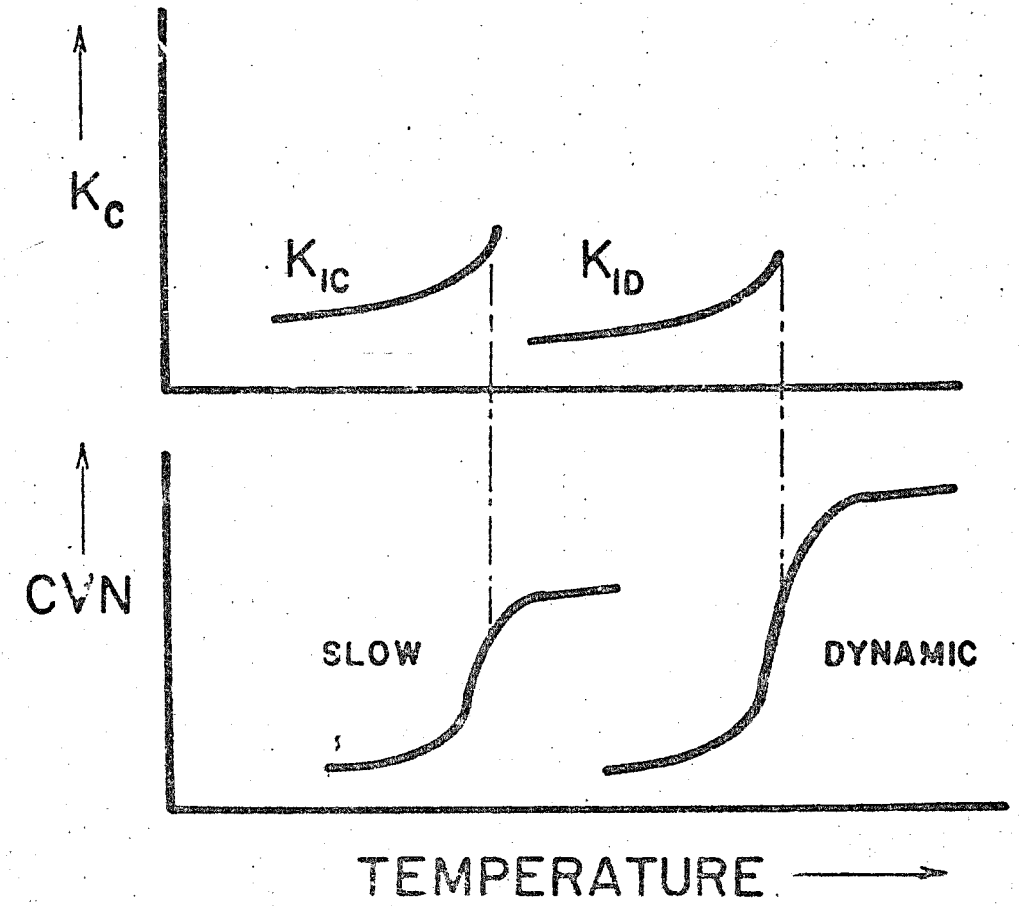

Fig. 30 K - CVN Correlation Regions and Temperature Shifts

APPENDIX A - A7 DATA

The 1/2 inch A7 material tested in Phase 2 of this project was supplied to Lehigh University from a bottom chord section of the Congress Street Bridge over the Hudson River at Troy, New York. The material was obtained through the cooperation of the FHWA and the State of New York. The bridge was constructed in 1915. The physical properties of the material are given in Tables 1 and 2 of the text.

The Charpy test results are shown in Figure A-1. For these particular tests and this material there was no apparent difference between the slow and fast Charpy results. The slow and dynamic tests of the standard Charpy specimens did show a shift in temperature of 125^{o} F as opposed to a shift of 162^{o} F predicted by Barsom (28). The results of the standard Charpy testing showed a 15 ft.-lbs. temperature of 100^{o} F. The individual Charpy test results are given in Table A-2. Some of the salient Charpy data are tabulated in Table A-1.

The K_c and D.T. results are presented in Table A-3 and Figures A-2 and A-3. As can be seen in Figures A-2 and A-3 the transition in the K_c and D.T. data occur in approximately the same temperature range, 50 - 100^{o} F. The estimate of K_c using Barsom's (28) equation and the Charpy data (Figure A-1) do not show good correlation. For this type of correlation a value of the constant A should be 35 rather than 5.

For the A7 material the two R-curve tests did not show any stable crack growth. The cracks when they did start to grow were not stable and the plates fractured completely. As in many of the other R-curve tests in this program the crack velocity was great enough to cause branching. The individual R-curve data are given in Figure A-2 and Table A-4. The R-curve data plotted in Figure A-2 does not show the general trend observed for most of the other steels. In these tests the data fell almost on top of the dynamic K_c results. For the other materials the R-curve data tended to follow the static K_c values. At this time there is no apparent explanation for the anomalous results.

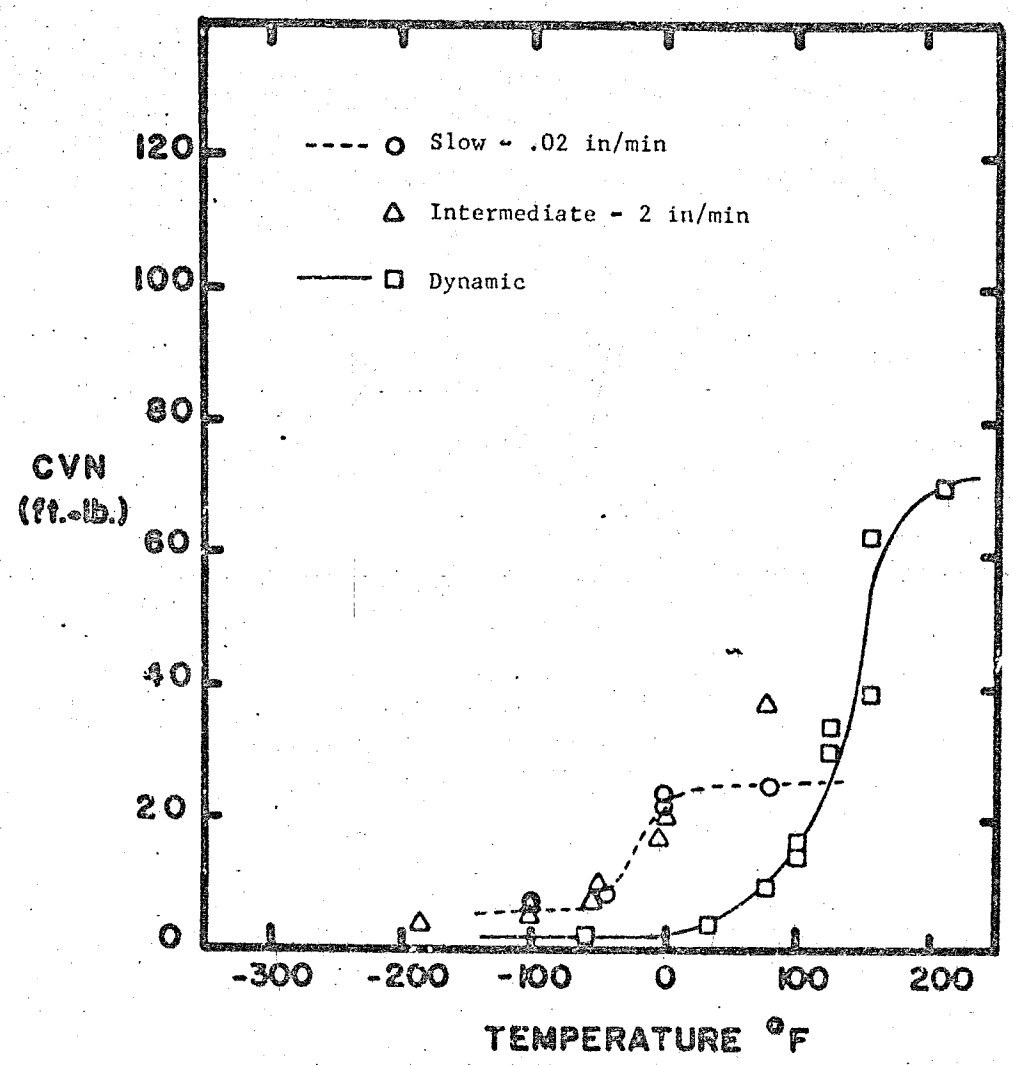

Fig. A-1 A7 1/2" Notched Charpy Data at Three Rates of Loading

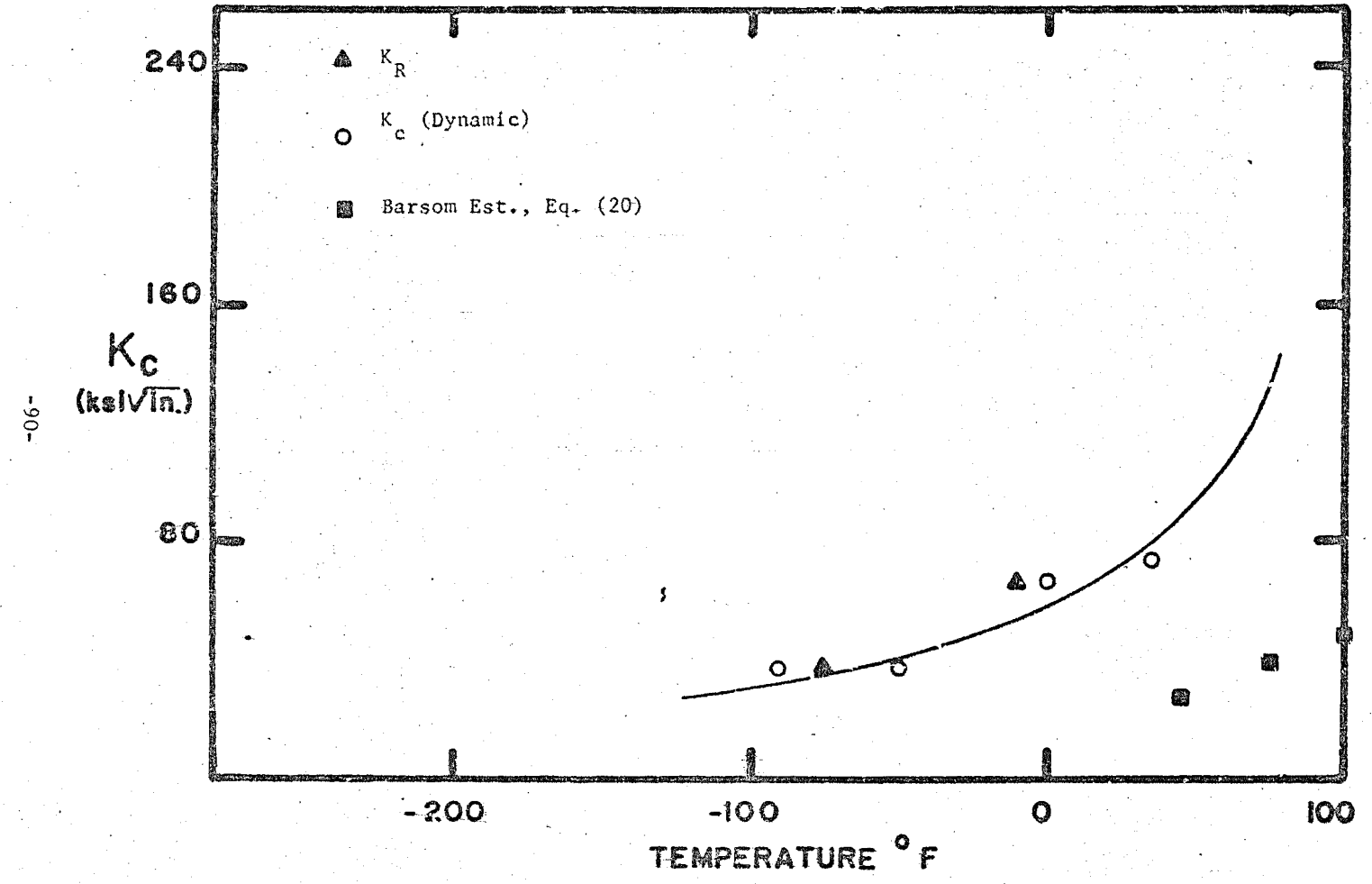

Fig. A-2 K_c Data for A7 Material

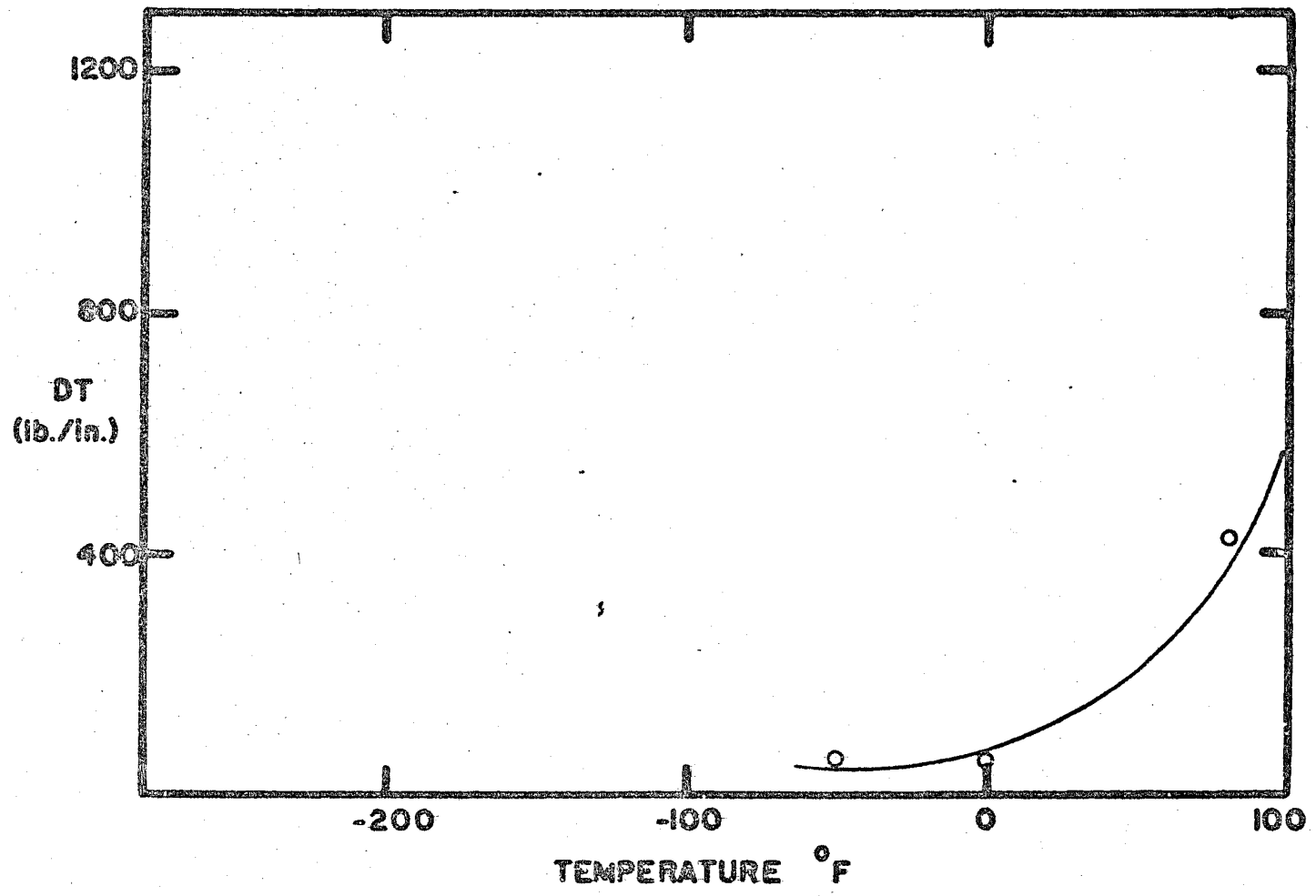

Fig. A-3 Dynamic Tear Data for A7 Material

TABLE A1.1* - A7 CHARPY DATA SUMMARY

Test	Material Thickness (in.)	T_{15} (°F)	T_{30} (°F)	T_{SH} (°F)	CVN_{SH} (ft.-lb.)
DS	0.5	100	135	200	73
SS	0.5	- 25	---	25	25

TABLE A1.2

Test	T	ΔT (°F)	ΔT_B (°F)
S	0.5	125	162

*
- DS - Dynamic Standard Charpy Test
- DP - Dynamic Pre-cracked Charpy Test
- SS - Slow Standard Charpy Test
- SP - Slow Pre-cracked Charpy Test
- S - Standard Charpy Test
- P - Pre-cracked Charpy Test
- T_{15} - Temperature corresponding to 15 ft.-lb. energy level
- T_{30} - Temperature corresponding to 30 ft.-lb. energy level
- T_{SH} - Temperature at which upper shelf energy level is fully developed
- CVN_{SH} - Upper Shelf Charpy energy
- ΔT - Temperature shift between dynamic and slow bend Charpy curve at 15 ft.-lb. energy level
- ΔT_B - $[215 - 1.5\ \sigma_y]$ where σ_y is room temperature yield strength

TABLE A2 - CHARPY TEST DATA

A7 1/2" (Notched) Dynamic

Specimen No.	Temp. (° F)	Maximum Load (lb.)	Deflection at Maximum Load (in.)	Crack-Depth (in.)	Energy Absorbed		Shear (%)	Lateral Expansion (mils)
					Actual (ft.-lb.)	Normalized (ft.-lb.)		
	- 58			0.079	2.0	2.0	0	4
	- 58			0.079	2.0	2.0	0	4
	+ 32			0.079	4.0	4.0	0	4
	+ 32			0.079	4.0	4.0	0	6
	+ 75			0.079	9.5	9.5	< 5	9
	+ 75			0.079	9.5	9.5	< 5	13
	+ 100			0.079	16.0	16.0	< 10	23
	+ 100			0.079	14.0	14.0	< 10	19
	+ 125			0.079	30.0	30.0	< 15	35
	+ 125			0.079	34.0	34.0	< 15	40
	+ 155			0.079	39.0	39.0	30	39
	+ 155			0.079	63.0	63.0	30	60
	+ 212			0.079	71.0	71.0	85	65

TABLE A2 - CHARPY TEST DATA

A7 1/2" (Notched) Fast Bend

Specimen No.	Temp. (° F)	Maximum Load (lb.)	Deflection at Maximum Load (in.)	Crack-Depth (in.)	Energy Absorbed		Shear (%)	Lateral Expansion (mils)
					Actual (ft.-lb.)	Normalized (ft.-lb.)		
434	- 185	2150	0.024	0.079	3.6	3.6	0	2
433	- 100	2600	0.032	0.079	5.3	5.3	0	5
432	- 100	2660	0.036	0.079	6.9	6.9	0	5
431	- 55	2550	0.048	0.079	7.1	7.1	0	10
430	- 50	2660	0.052	0.079	9.2	9.2	0	11
429	- 5	2950	0.089	0.079	16.5	16.5	0	24
428	0	2910	0.099	0.079	20.4	20.4	< 10	24
427	+ 74	2900	0.144	0.079	37.3	37.3	15	47

TABLE A2 - CHARPY TEST DATA

A7 1/2" (Notched) Slow Bend

Specimen No.	Temp. (° F)	Maximum Load (lb.)	Deflection at Maximum Load (in.)	Crack-Depth (in.)	Energy Absorbed		Shear (%)	Lateral Expansion (mils)
					Actual (ft.-lb.)	Normalized (ft.-lb.)		
239	- 100	2450	0.066	0.079	7.12	7.12	0	10
237	- 45	2350	0.061	0.079	8.10	8.10	0	13
453	0	2575	0.122	0.079	21.80	21.80	< 5	32
236	0	2680	0.132	0.079	23.60	23.60	< 5	32
235	+ 77	2500	0.120	0.079	24.30	24.30	40	50

TABLE A3* - A7 K_c DATA

A7 1/2"

Nominal Yield Strength YS = 37.0 ksi

Specimen No.	B (in.)	Temp. (°F)	A_o (in.)	F.A. ($in.^2$)	$P_{max.}$ (kips)	Time (sec)	K_c ksi/in.	G (lb/in)	DTE (lb/in)	β_{K_c}	β_{DT}	σ_{YD} (ksi)
8.004	0.5	- 90	0.800	1.100	7.0	5.0E-04	38.46	50.0	0.0	0.490	0.0	77.7
8.003	0.5	- 50	0.775	1.112	6.9	5.0E-04	37.36	47.2	64.7	0.554	0.761	71.0
8.002	0.5	0	1.400	0.800	6.0	6.0E-04	66.00	147.2	60.0	2.153	0.878	63.6
8.005	0.5	35	0.860	1.070	10.5	7.5E-04	72.69	178.5	0.0	3.027	0.0	59.1
8.001	0.5	75	0.765	1.117	13.3	9.0E-04	0.0	0.0	424.2	0.0	8.346	54.9

*B - Specimen thickness
Temp. - Test temperature
A_o - Initial crack length
F.A. - Fracture Area
P_{max} - Maximum load at fracture
Time - Load time to P_{max}
K_c - Stress Intensity Factor
G - Strain Energy Release Rate
DTE - Dynamic Tear Energy

$$\beta_{K_c} - = \frac{1}{B}\left(\frac{K_c}{\sigma_{YS}}\right)^2$$

$$\beta_{DT} - = \frac{1}{B}\left(\frac{E \times DTE}{\sigma_{YD}^2}\right)$$ where E is Young's Modulus 30×10^6 psi.

σ_{YD} - Yield strength at temperature and loading rate

TABLE A4 - A7 R-CURVE INSTABILITY SUMMARY

Thickness (in.)	Test Temperature (^{o}F)	Fatigue Crack Length (in.)	K_c at Instability (psi)	Apparent Crack Length at Instability (in.)
0.5*	- 75	6.05	30,700	6.56
0.5**	- 10	6.30	66,700	7.95

*Crack branching occurred at 12.9"

**Crack branching occurred at 12.35"

APPENDIX B - A36

This appendix contains the data collected for the 1/2", 1" and 2" thicknesses of the A36 material. This steel was supplied to the program by the Bethlehem Steel Corporation. The chemical analysis, physical properties and heat designations appear in Tables 1 and 2.

The data in this appendix is presented in the form of a Charpy summary, a detailed Charpy tabulation, a K_c tabulation, an R-curve summary and appropriate figures which best illustrate the data trends. Details of the test procedures and terminology can be found in appendices J, K and L and Chapter 2.

Standard and precracked Charpy specimens were tested for the three thicknesses of the A36 at three testing speeds. For both the standard and precracked Chapry specimens the slow and fast data tended to overlap and did not show any temperature shift. A temperature shift was observed between the slow and dynamic tests with the standard specimens showing a greater similarity with the trends reported by Barsom (28). For the standard specimens the shift was of the order of 150° F for the three thicknesses. For the precracked specimens the shift was much less. Also with regard to the precracked Charpy specimens, they showed a much higher transition temperature than the standard specimens. The precracked specimens did not appear to be a set of lower bound values for the standard Charpy tests as reported by Barsom in Reference (28).

Figures B-1 through B-6 present the individual Charpy data while data tabulations are given in Table B-2. Table B-1 presents some of the more important features of the Charpy data while Table 1 of the tests gives a comparative listing of all Charpy data.

Figures B-7 through B-10 present the dynamic K_c data collected for the A36 material. The individual data are tabulated in Table B-3. Since the A36 material was part of Phase 1 primary emphasis was placed on dynamic K_c testing. D.T. testing was not undertaken until Phase 2 at which time there were no A36 specimens remaining. Thickness reduction and bend angle measurements were also used for the A36 material to supplement the data. The data from these tests point to an up swing in the trends which was not apparent from just the dynamic K_c results. With regard to estimates of K_c from Charpy data it appears that for the A36 material in the 1/2", 1" and 2" thickness the equation proposed by Barsom (28)

$$K_{Ic} = \sqrt{A\ E\ CVN}$$

would be acceptable if A is taken as 8 and the standard Charpy data is used.

R-curve testing was performed on the A36 material in both Phase 1 and Phase 2. The tests in Phase 1 did not show any real crack growth as already reported in the Phase 1 report. The specimens just plastically deformed. The results obtained in Phase 2 exhibited rapid unstable crack growth. Once the crack started it ran completely through the specimen. In one of the 1/2 inch tests, high velocities and crack

branching occurred. The R-curve data appear to be consistent with what would be expected for slow K_c values.

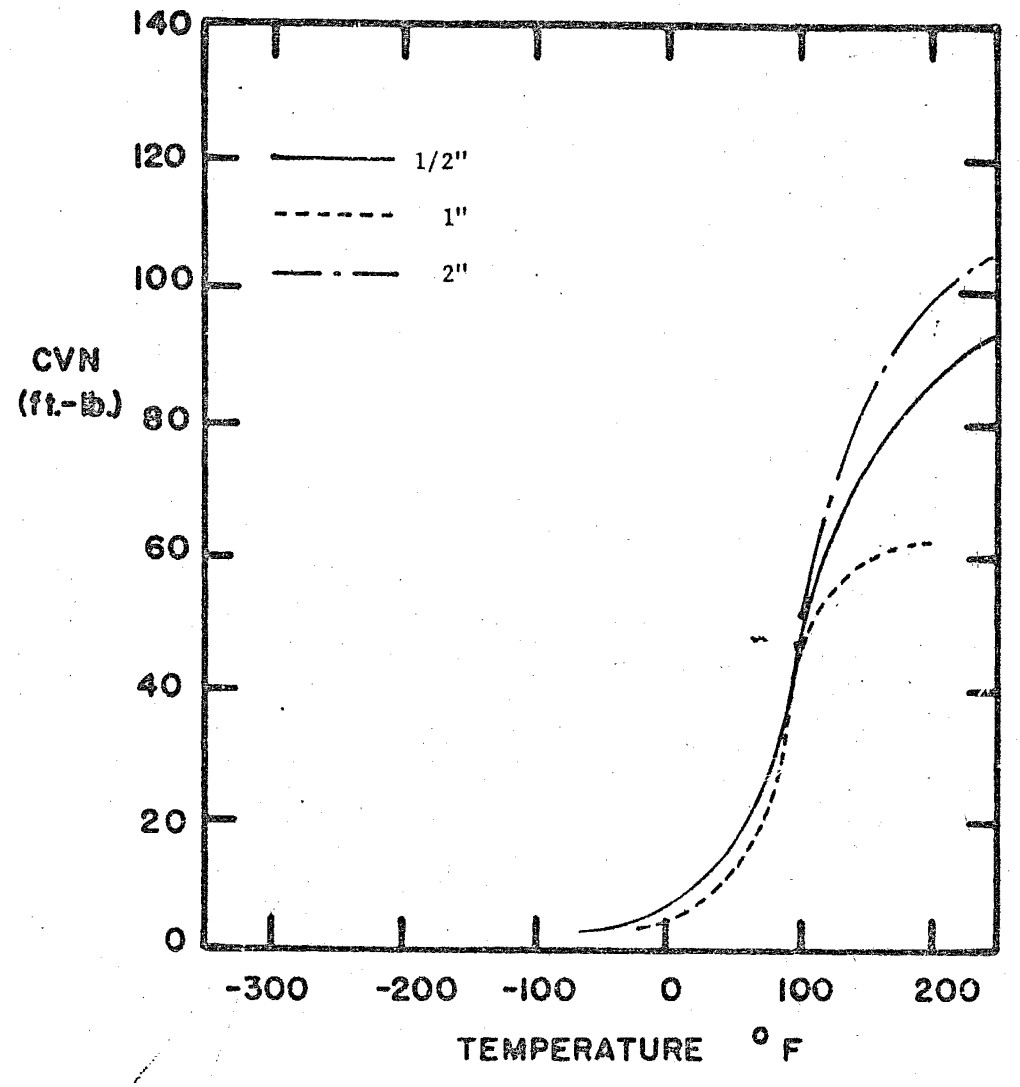

Fig. B-1a Composite Charpy Curves for A36 Material

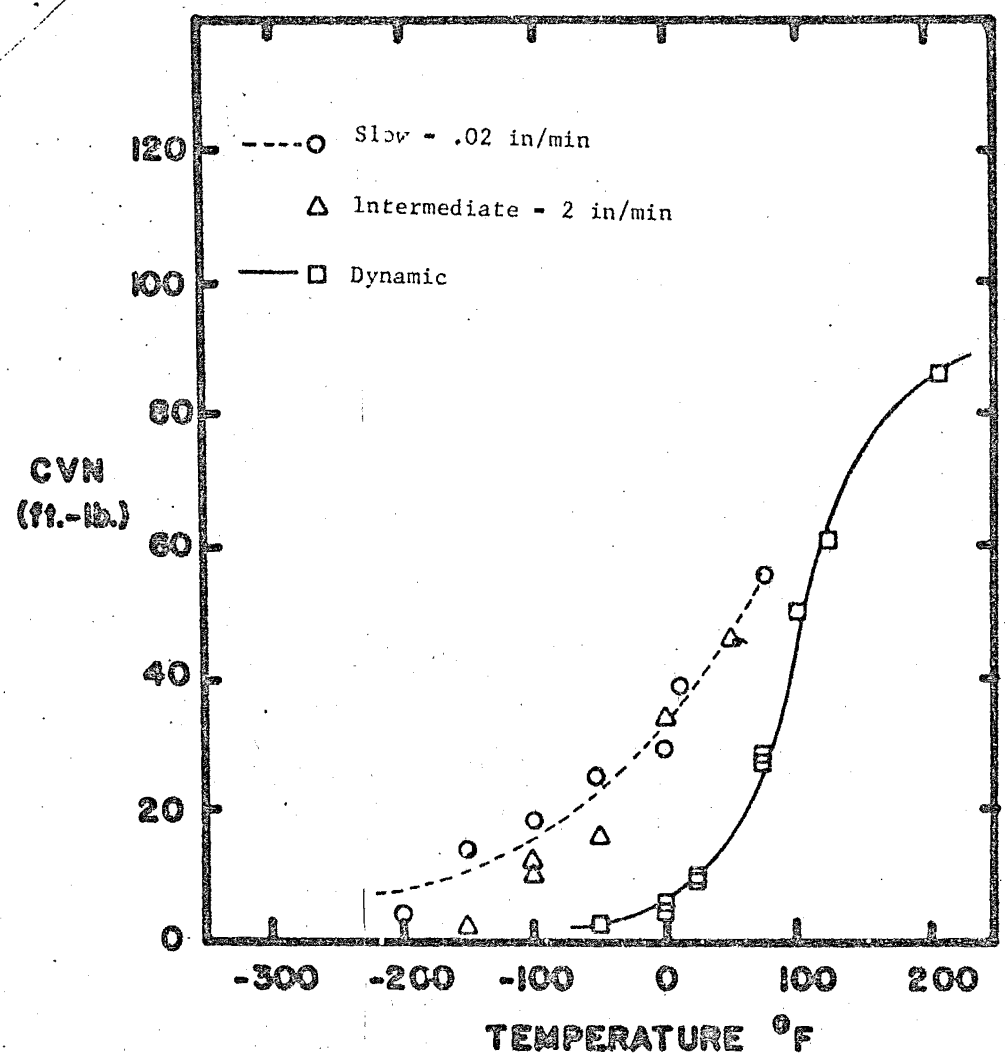

Fig. B-1 A36 1/2" Notched Charpy Data for Three Loading Rates

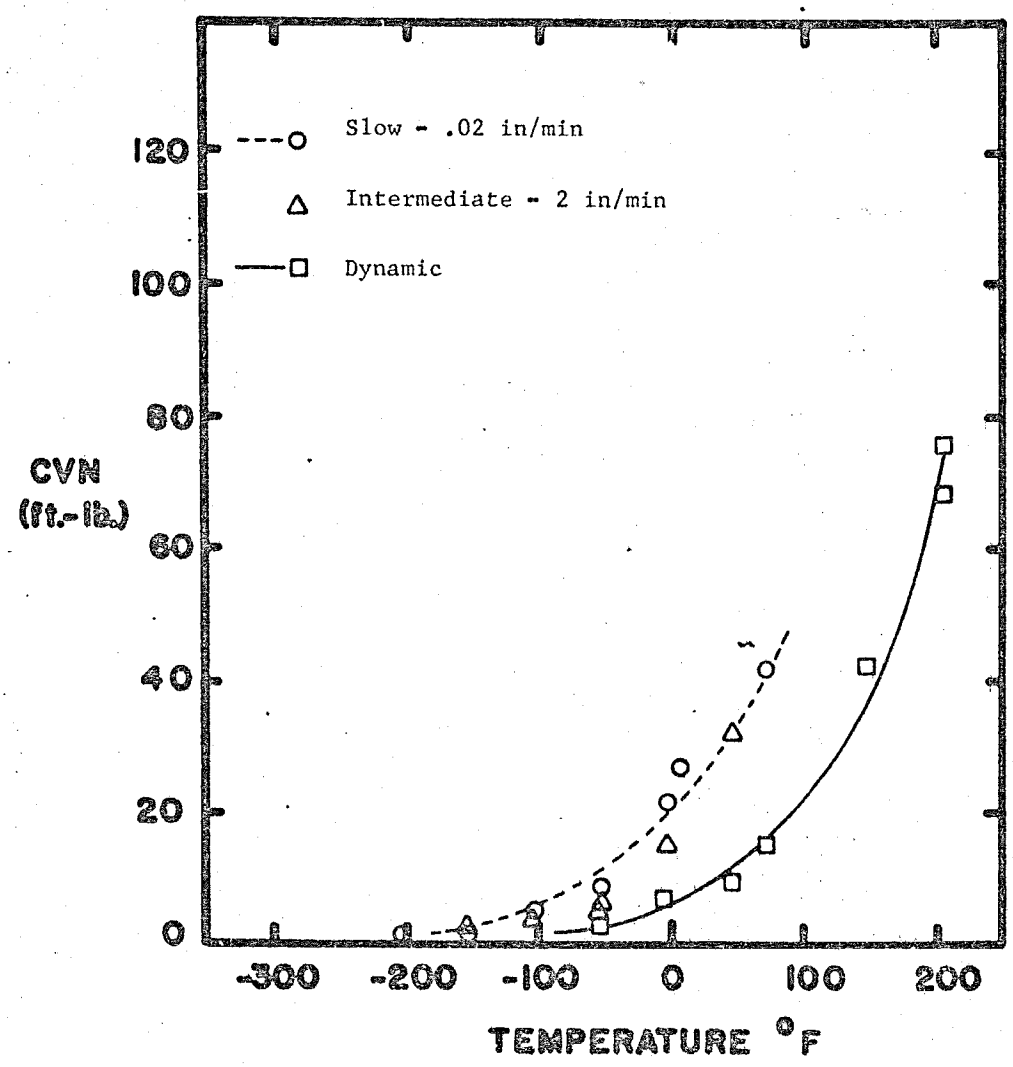

Fig. B-2 A36 1/2" Precracked Data for Three Loading Rates

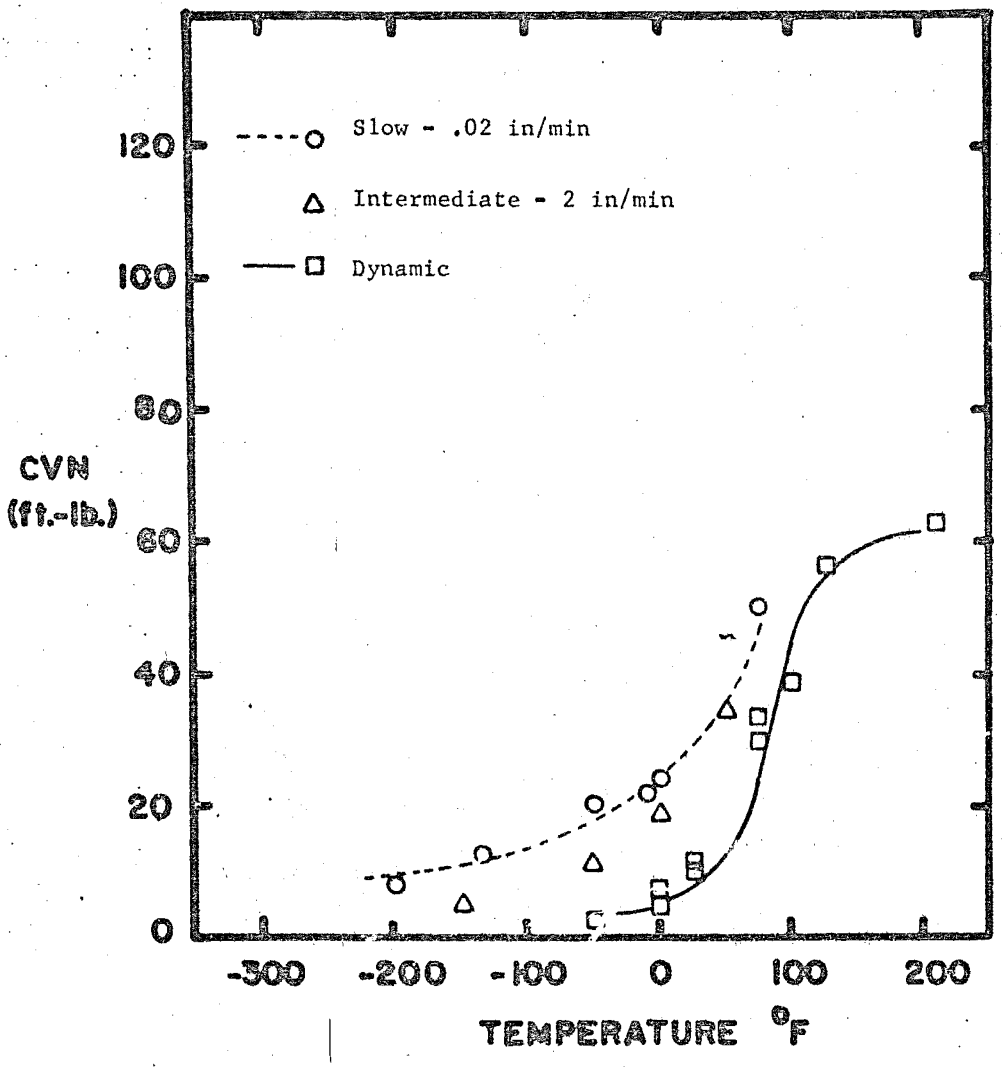

Fig. B-3 A36 1" Notched Charpy Data for Three Loading Rates

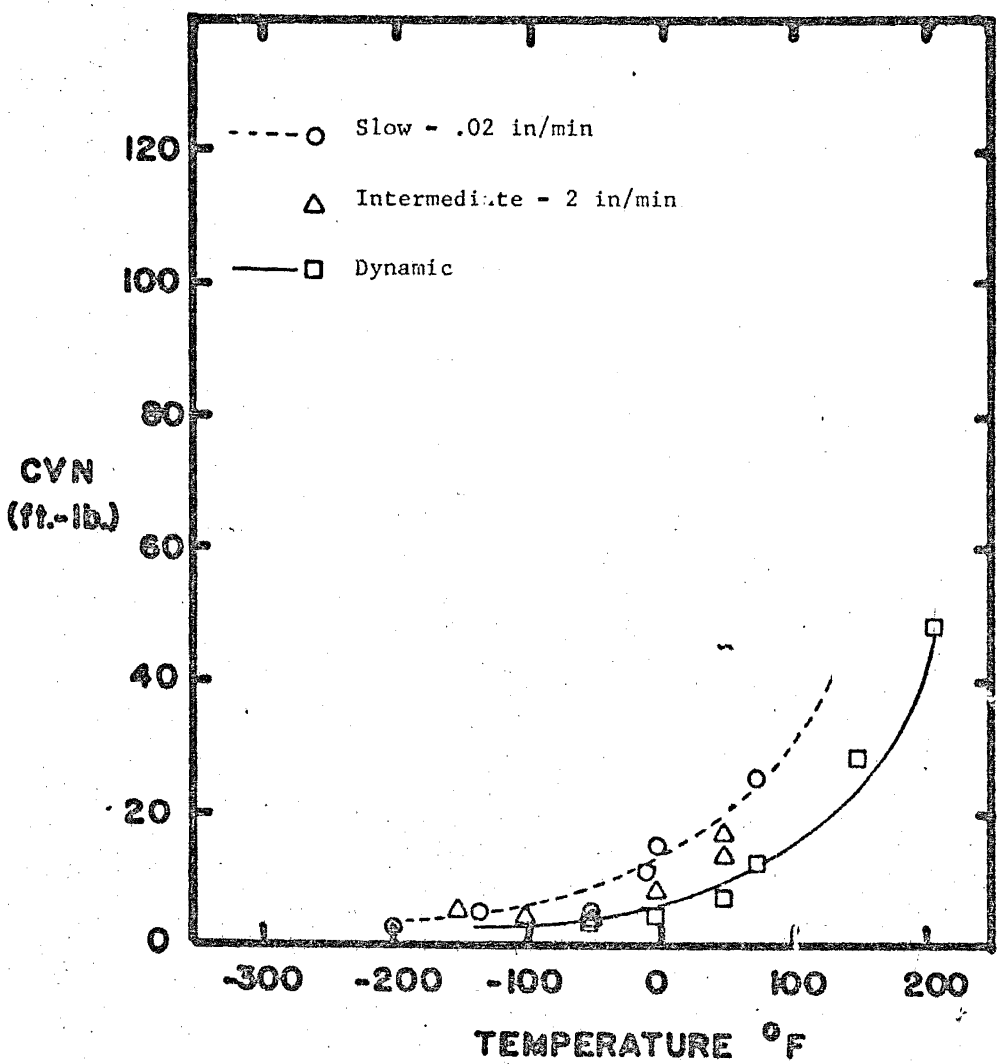

Fig. B-4 A36 1" Precracked Data for Three Loading Rates

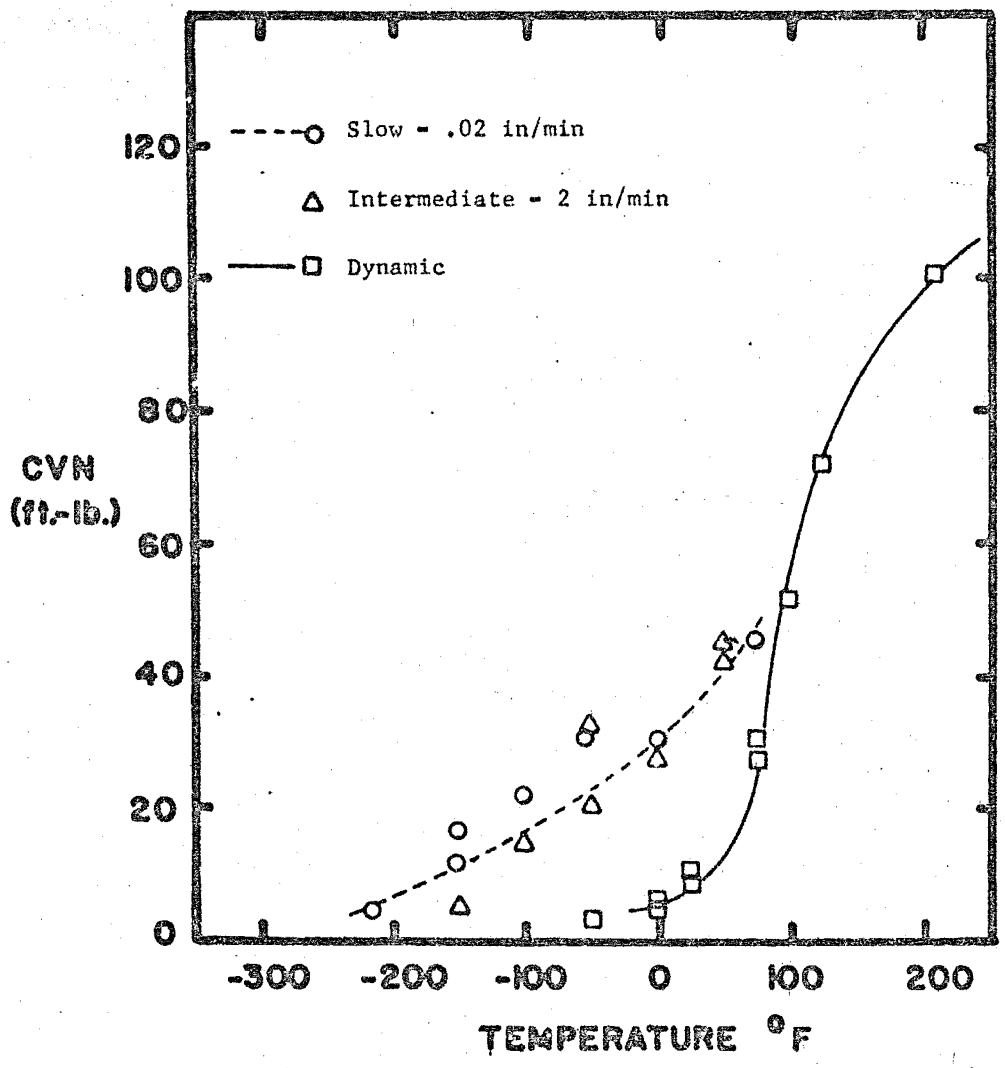

Fig. B-5 A36 2" Notched Charpy Data for Three Loading Rates

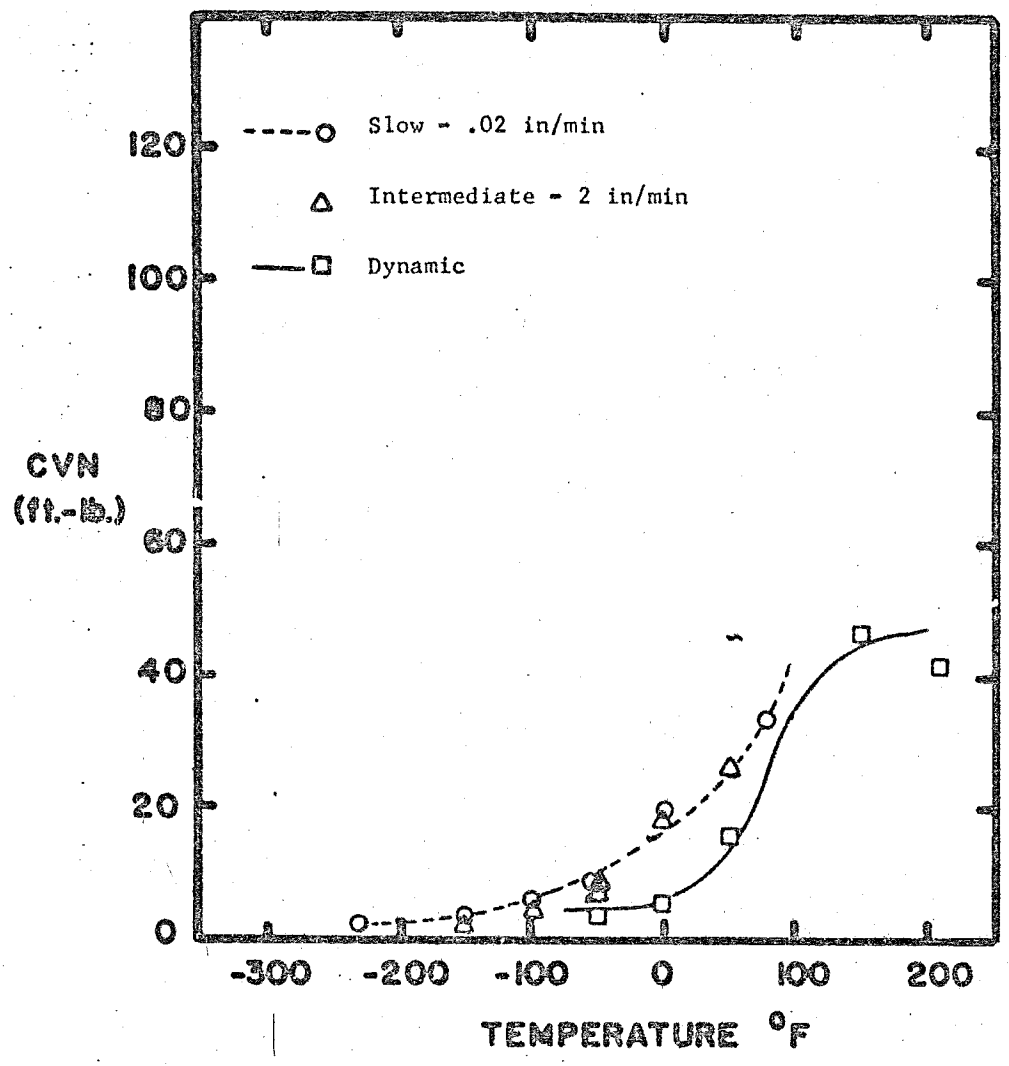

Fig. B-6 A36 2" Precracked Data for Three Loading Rates

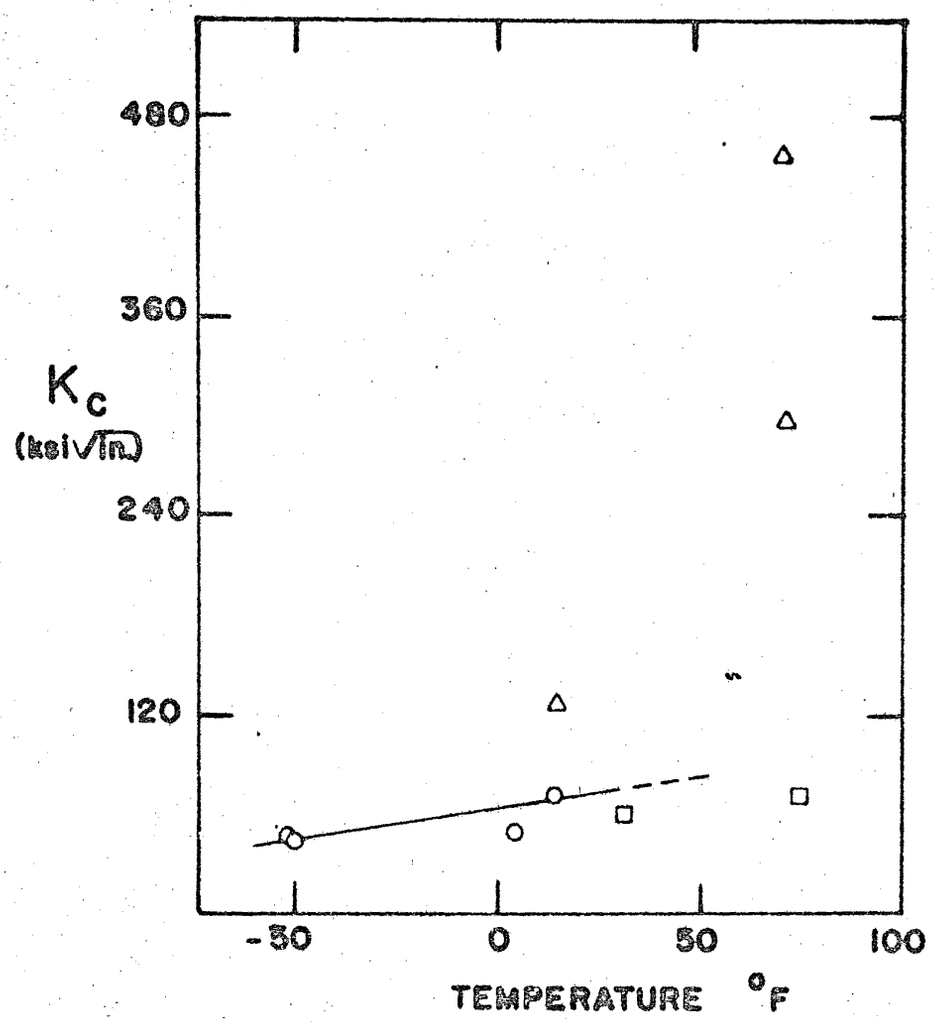

Fig. B-7 Circles Show Dynamic K_c Values for 1/2" A36 Plate. Triangles Show Estimates of Dynamic K_M from the Crack-Arrest Bend-Angle Method. Squares Show Estimates of Dynamic K_c from Eqs. (20) and (7) from Phase I Report.

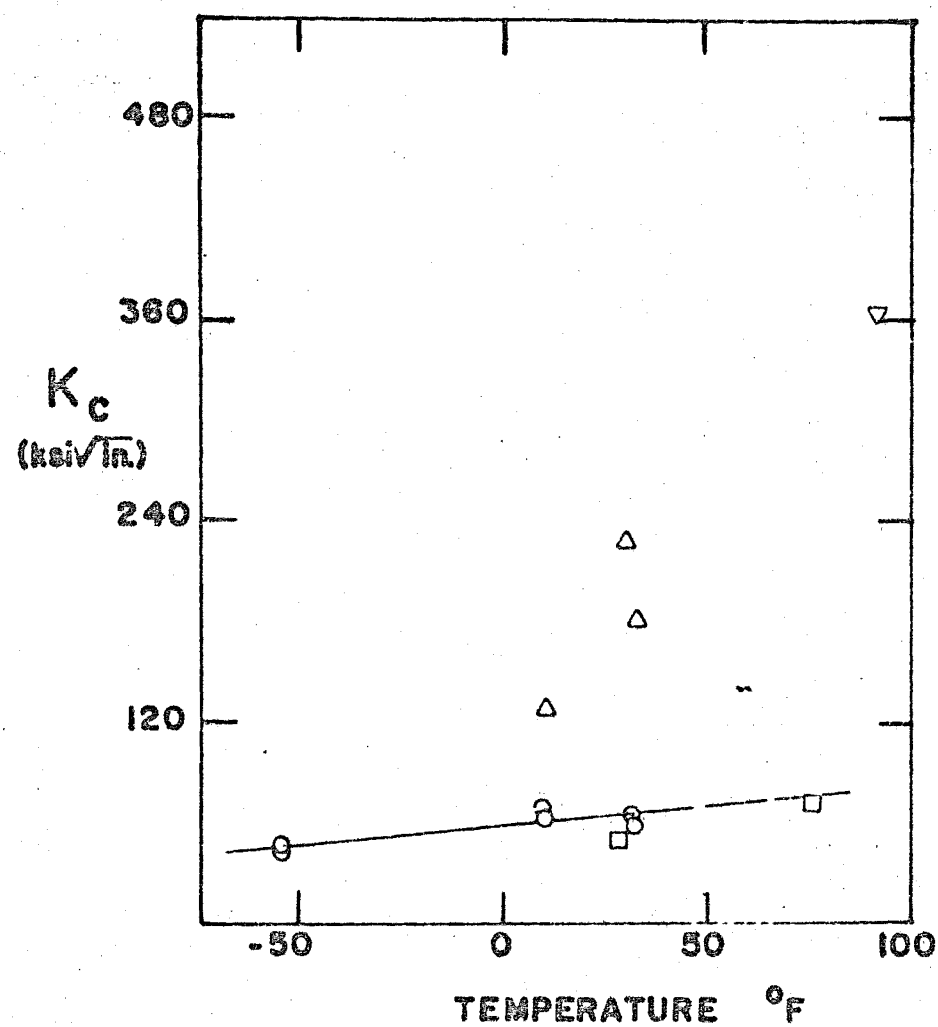

Fig. B-8 Circles Show Dynamic K_c Values for 1" A36 Plate.
Triangles show Estimates of Dynamic K_M from the Crack-Arrest Bend-Angle Method.
Squares show Estimates of Dynamic K_c from Eqs (20) and (7) from Phase I Report.
Inverted Triangle shows the K_M Values obtained from Thickness Reduction Measurements.

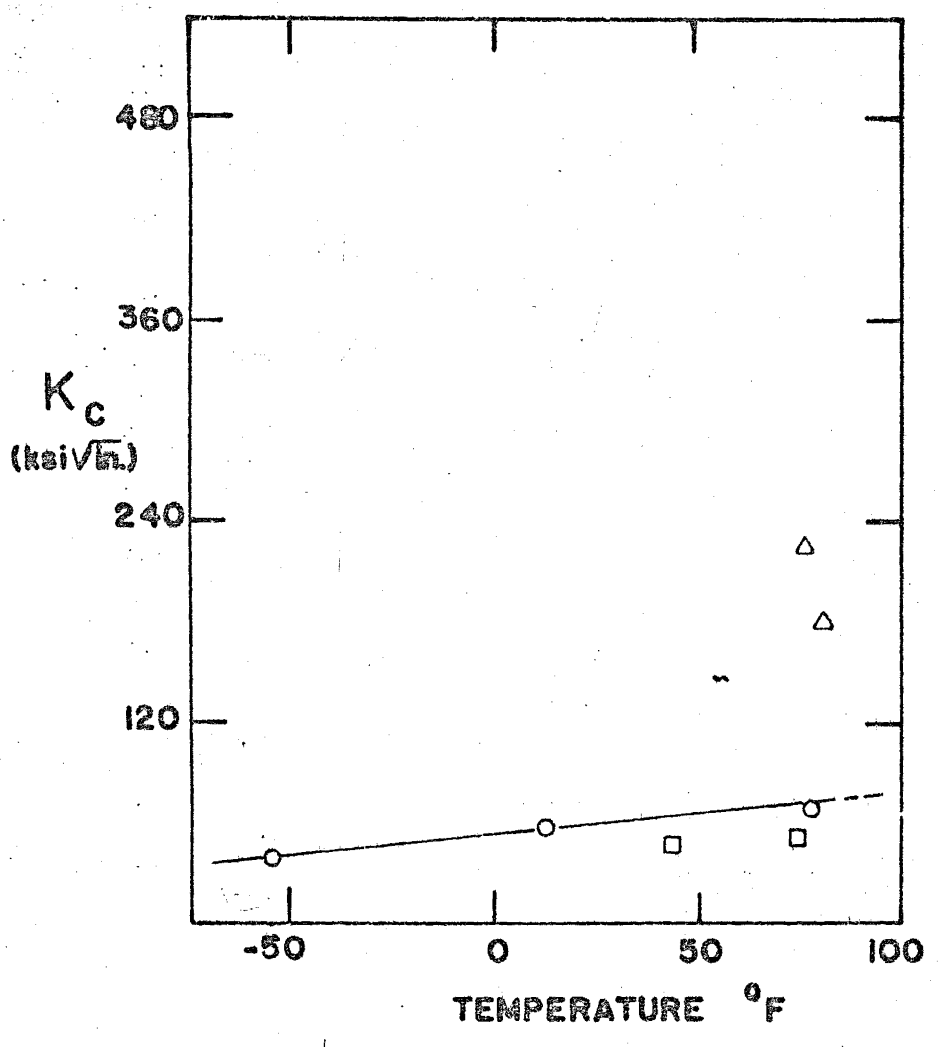

Fig. B-9 Circles show Dynamic K_c Values for 2" A36 Plate.
Triangles show Estimates of Dynamic K_M from the Crack-Arrest Bend-Angle Method.
Squares show Estimates of Dynamic K_c from Eqs. (20) and (7) from Phase I Report.

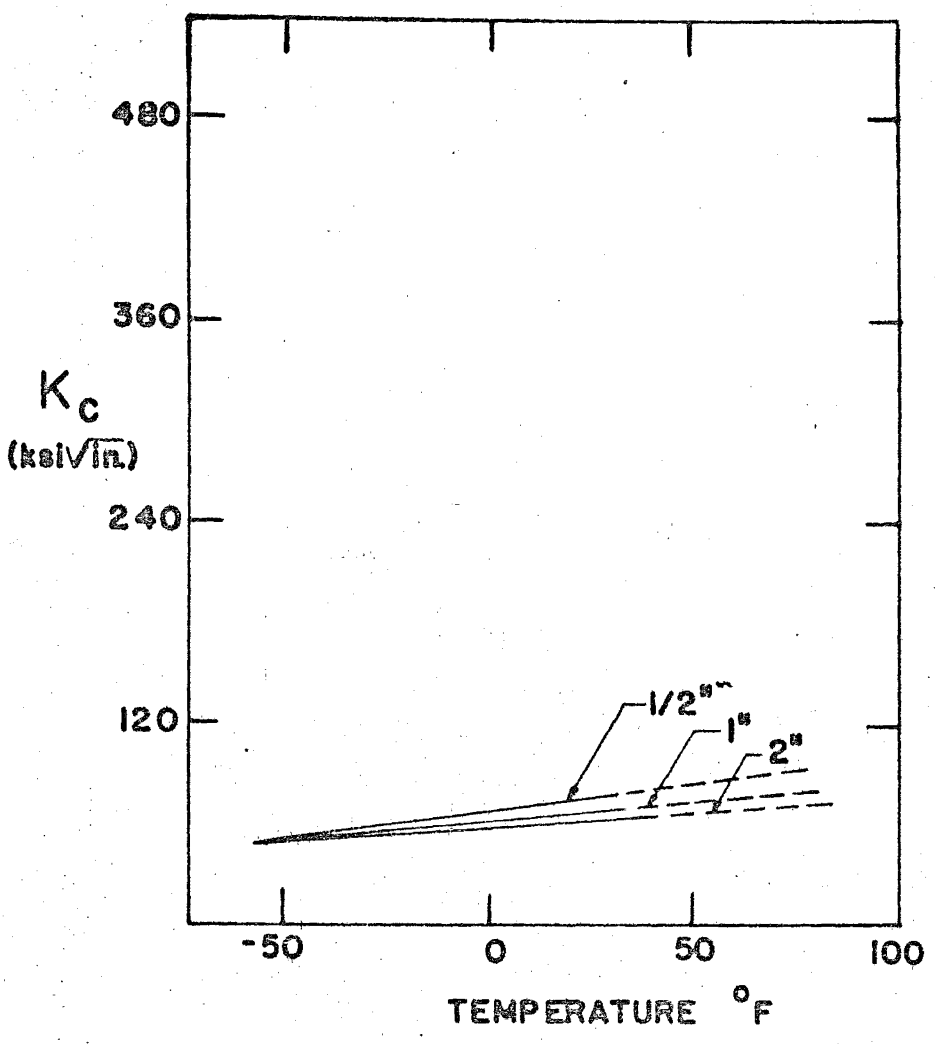

Fig. B-10 Collection is Shown for the Dynamic K_c Trend Lines of the Previous Figures

TABLE B1.1* - A36 CHARPY DATA SUMMARY

Test	Material Thickness (in.)	T_{15} (°F)	T_{30} (°F)	T_{SH} (°F)	CVN_{SH} (ft.-lb.)
DS	0.5	50	80	> 200	> 85
DP	0.5	70	130	> 200	> 70
SS	0.5	- 105	- 15	--	> 60
SP	0.5	- 25	40	> 75	> 40
DS	1.0	60	80	175	62
DP	1.0	100	175	> 200	> 40
SS	1.0	- 75	35	> 75	> 40
SP	1.0	25	100	> 100	> 30
DS	2.0	60	75	> 200	> 100
DP	2.0	50	90	150	45
SS	2.0	- 100	0	> 75	> 45
SP	2.0	- 10	70	> 75	> 30

TABLE B1.2

Test	t (in.)	ΔT (°F)	ΔT_B (°F)
S	0.5	150	158
P	0.5	100	
S	1.0	150	
P	1.0	80	
S	2.0	175	148
P	2.0	60	

*See Table A1.1 for designations

TABLE B2 - CHARPY TEST DATA

A36 1/2" (Notched) Slow Bend

Specimen No.	Temp. (° F)	Maximum Load (lb.)	Deflection at Maximum Load (in.)	Crack-Depth (in.)	Energy Absorbed		Shear (%)	Lateral Expansion (mils)
					Actual (ft.-lb.)	Normalized (ft.-lb.)		
124-SP	- 200	2325	0.041	0.079	4.0	4.0	0	5
105-SN	- 150	2625	0.094	0.079	14.0	14.0	0	20
76-SN	- 100	2500		0.079	17.9	17.9		26
166-SN	- 50	2600	0.151	0.079	24.75	24.75	< 5	30
8-SN	0	2500	0.214	0.079	29.20	29.20	< 10	31
44-SN	+ 10	2500	0.170	0.079	38.60	38.60	20	56
136-SN	+ 75	2255	0.160	0.079	55.83	55.83	100	66

TABLE B2 - CHARPY TEST DATA

A36 1/2" (Notched) Fast Bend

Specimen No.	Temp. (° F)	Maximum Load (lb.)	Deflection at Maximum Load (in.)	Crack-Depth (in.)	Energy Absorbed		Shear (%)	Lateral Expansion (mils)
					Actual (ft.-lb.)	Normalized (ft.-lb.)		
440	- 160	2700	0.034	0.079	5.5	5.5	0	3
386	- 100	2450	0.056	0.079	9.75	9.75	0	10
385	- 100	2515	0.068	0.079	12.30	12.30	0	12
350	- 50	2530	0.098	0.079	15.92	15.92	< 5	20
306	0	2770	0.180	0.079	34.00	34.00	10	47
266	+ 50	2600	0.176	0.079	46.32	46.32	25	55

TABLE B2 - CHARPY TEST DATA

A36 1/2" (Notched) Dynamic

Specimen No.	Temp. (°F)	Maximum Load (lb.)	Deflection at Maximum Load (in.)	Crack-Depth (in.)	Actual (ft.-lb.)	Normalized (ft.-lb.)	Shear (%)	Lateral Expansion (mils)
	- 50			0.079	2.5	2.5	0	5
	0			0.079	4.5	4.5	0	6
	0			0.079	5.0	5.0	0	7
	+ 25			0.079	10.0	10.0	< 5	11
	+ 25			0.079	9.5	9.5	< 5	13
	+ 75			0.079	27.0	27.0	15	32
	+ 75			0.079	28.0	28.0	15	33
	+ 100			0.079	50.0	50.0	40	47
	+ 125			0.079	61.0	61.0	75	56
	+ 212			0.079	86.0	86.0	100	71

TABLE B2 - CHARPY TEST DATA

A36 1/2" (Pre-cracked) Slow Bend

Specimen No.	Temp. (° F)	Maximum Load (lb.)	Deflection at Maximum Load (in.)	Crack-Depth (in.)	Energy Absorbed		Shear (%)	Lateral Expansion (mils)
					Actual (ft.-lb.)	Normalized (ft.-lb.)		
123-SP	- 200	1458	0.030	0.130	1.15	1.37		4
104-SP	- 150	1450	0.028	0.135	1.20	1.45		4
75-SP	- 100	1200		0.150	3.30	5.10		11
165-SP	- 50	1450	0.046	0.125	7.45	8.73	0	17
7-SP	0	1500	0.074	0.140	17.20	21.4	30	28
43-SP	+ 10	1325	0.095	0.125	22.60	26.5	40	35
135-SP	+ 75	1450	0.095	0.155	31.75	41.66	100	43

TABLE B2 - CHARPY TEST DATA

A36 1/2" (Pre-cracked) Fast Bend

Specimen No.	Temp. (°F)	Maximum Load (lb.)	Deflection at Maximum Load (in.)	Crack-Depth (in.)	Energy Absorbed		Shear (%)	Lateral Expansion (mils)
					Actual (ft.-lb.)	Normalized (ft.-lb.)		
439	- 150	1000	0.034	0.145	2.1	2.6	0	4
384	- 100	1500	0.024	0.115	3.43	4.03	0	3
348	- 50	1500	0.030	0.120	5.93	6.85	< 5	14
349	- 50	1250	0.020	0.135	5.20	6.34	< 5	11
305	0	1350	0.044	0.135	12.53	15.32	10	24
264	+ 50	1880	0.112	0.105	31.41	31.41	30	37

TABLE B2 - CHARPY TEST DATA

A36 1/2" (Pre-Cracked) Dynamic

Specimen No.	Temp. (° F)	Maximum Load (lb.)	Deflection at Maximum Load (in.)	Crack-Depth (in.)	Energy Absorbed		Shear (%)	Lateral Expansion (mils)
					Actual (ft.-lb.)	Normalized (ft.-lb.)		
	- 50			0.140	2.0	2.48	0	3
	0			0.156	4.8	6.30	0	4
	+ 50			0.125	7.8	9.10	< 5	8
	+ 75			0.130	12.5	14.90	10	15
	+ 150			0.135	34.0	41.50	60	45
	+ 212			0.156	54.0	75.30	100	44
	+ 212			0.148	52.0	68.0	100	54

TABLE B2 - CHARPY TEST DATA

A36 1" (Notched) Slow Bend

Specimen No.	Temp. (° F)	Maximum Load (lb.)	Deflection at Maximum Load (in.)	Crack-Depth (in.)	Energy Absorbed		Shear (%)	Lateral Expansion (mils)
					Actual (ft.-lb.)	Normalized (ft.-lb.)		
126-SN	- 200	2700	0.055	0.079	7.40	7.40	0	10
93-SN	- 135	2750	0.092	0.079	12.30	12.30	0	14
20-SN	- 50	2950	0.121	0.079	20.00	20.00	0	22
48-SN	- 10	2950	0.134	0.079	21.20	21.20	0	25
10-SN	0	3000	0.130	0.079	23.80	23.80	0	24
151-SN	+ 75	2850	0.126	0.079	50.40	50.40	100	52

TABLE B2 - CHARPY TEST DATA

A36 1" (Notched) Fast Bend

Specimen No.	Temp. (°F)	Maximum Load (lb.)	Deflection at Maximum Load (in.)	Crack-Depth (in.)	Energy Absorbed		Shear (%)	Lateral Expansion (mils)
					Actual (ft.-lb.)	Normalized (ft.-lb.)		
443	- 150	1820	0.034	0.079	5.46	5.46	0	3
352	- 50	2610	0.064	0.079	11.27	11.27	0	12
308	0	2760	0.100	0.079	18.61	18.61	0	23
269	+ 50	3050	0.144	0.079	34.30	34.30	15	36

TABLE B2 - CHARPY TEST DATA

A36 1" (Notched) Dynamic

Specimen No.	Temp. (° F)	Maximum Load (lb.)	Deflection at Maximum Load (in.)	Crack-Depth (in.)	Energy Absorbed		Shear (%)	Lateral Expansion (mils)
					Actual (ft.-lb.)	Normalized (ft.-lb.)		
	- 50			0.079	2.5	2.5	0	3
	0			0.079	5.0	5.0	0	13
	0			0.079	7.0	7.0	0	12
	+ 25			0.079	10.0	10.0	< 5	15
	+ 25			0.079	10.5	10.5	5	17
	+ 75			0.079	29.5	29.5	20	36
	+ 75			0.079	33.0	33.0	40	37
	+ 100			0.079	38.0	38.0	60	45
	+ 125			0.079	56.0	56.0	85	63
	+ 212			0.079	62.5	62.5	100	66

TABLE B2 - CHARPY TEST DATA

A36 1" (Pre-cracked) Slow Bend

Specimen No.	Temp. (°F)	Maximum Load (lb.)	Deflection at Maximum Load (in.)	Crack-Depth (in.)	Energy Absorbed		Shear (%)	Lateral Expansion (mils)
					Actual (ft.-lb.)	Normalized (ft.-lb.)		
127-SP	- 200	1575	0.031	0.155	1.83	2.40	0	4
125-SP	- 200	900		0.170			0	4
92-SP	- 135	1250	0.038	0.150	3.20	4.14	0	4
19-SP	- 50	1400	0.038	0.156	4.06	5.35	0	7
47-SP	- 10	1750	0.058	0.125	9.29	10.90	0	16
9-SP	0	1500	0.056	0.156	11.20	14.70	0	19
152-SP	+ 75	1050	0.086	0.195	15.60	25.20	30	27

TABLE B2 - CHARPY TEST DATA

A36 1" (Pre-cracked) Fast Bend

Specimen No.	Temp. (° F)	Maximum Load (lb.)	Deflection at Maximum Load (in.)	Crack-Depth (in.)	Energy Absorbed		Shear (%)	Lateral Expansion (mils)
					Actual (ft.-lb.)	Normalized (ft.-lb.)		
387	- 100	1660	0.044	0.115	3.00	3.50	0	4
351	- 50	1400	0.022	0.125	2.86	3.37	0	6
307	0	1200	0.032	0.175	5.58	8.10	< 5	13
267	+ 50	1625	0.044	0.130	10.96	13.07	10	22
268	+ 50	1750	0.066	0.135	13.82	16.66	10	22

TABLE B2 - CHARPY TEST DATA

A36 1" (Pre-cracked) Dynamic

Specimen No.	Temp. (° F)	Maximum Load (lb.)	Deflection at Maximum Load (in.)	Crack-Depth (in.)	Energy Absorbed		Shear (%)	Lateral Expansion (mils)
					Actual (ft.-lb.)	Normalized (ft.-lb.)		
	- 50			0.130	2.2	2.62	0	4
	0			0.130	3.0	3.58	0	5
	+ 50			0.125	5.5	6.45	< 5	10
	+ 75			0.120	10.30	11.80	10	10
	+ 150			0.187	18.50	28.10	15	23
	+ 212			0.132	42.00	48.00	85	42

TABLE B2 - CHARPY TEST DATA

A36 2" (Notched) Slow Bend

Specimen No.	Temp. (° F)	Maximum Load (lb.)	Deflection at Maximum Load (in.)	Crack-Depth (in.)	Energy Absorbed		Shear (%)	Lateral Expansion (mils)
					Actual (ft.-lb.)	Normalized (ft.-lb.)		
187-SN	- 215	3020	0.049	0.079	4.5	4.5	0	6
177-SN	- 138	3430	0.105	0.079	16.6	16.6	0	19
178-SN	- 150	2620	0.087	0.079	11.0	11.0	0	14
168-SN	- 100	2650	0.132	0.079	20.8	20.8	0	29
164-SN	- 55	2600	0.140	0.079	30.2	30.2	0	45
154-SN	0	2550	0.136	0.079	29.6	29.6	40	38
150-SN	+ 75	2550	0.176	0.079	45.3	45.3	85	64

TABLE B2 - CHARPY TEST DATA

A36 2" (Notched) Fast Bend

Specimen No.	Temp. (° F)	Maximum Load (lb.)	Deflection at Maximum Load (in.)	Crack-Depth (in.)	Energy Absorbed		Shear (%)	Lateral Expansion (mils)
					Actual (ft.-lb.)	Normalized (ft.-lb.)		
491	- 150	2650	0.024	0.079	4.31	4.31	0	9
391	- 100	2850	0.092	0.079	14.45	14.45	0	18
390	- 100	3000	0.097	0.079	22.80	22.80	0	12
355	- 50	2750	0.104	0.079	19.91	19.91	0	12
356	- 50	2900	0.144	0.079	32.28	32.28	< 5	31
310	0	2800	0.132	0.079	27.20	27.20	20	33
272	+ 50	2730	0.148	0.079	41.30	41.30	60	50
271	+ 50	2780	0.116	0.079	43.50	43.50	60	58

TABLE B2 - CHARPY TEST DATA

A36 2" (Notched) Dynamic

Specimen No.	Temp. (° F)	Maximum Load (lb.)	Deflection at Maximum Load (in.)	Crack-Depth (in.)	Energy Absorbed		Shear (%)	Lateral Expansion (mils)
					Actual (ft.-lb.)	Normalized (ft.-lb.)		
	- 50			0.079	2.5	2.5	0	4
	0			0.079	4.5	4.5	0	8
	0			0.079	5.0	5.0	0	10
	+ 25			0.079	9.5	9.5	< 5	15
	+ 25			0.079	7.0	7.0	< 5	12
	+ 75			0.079	30.0	30.0	15	37
	+ 75			0.079	26.5	26.5	15	31
	+ 100			0.079	51.0	51.0	20	53
	+ 125			0.079	71.5	71.5	50	62
	+ 212			0.079	100.0	100.0	100	71

TABLE B2 - CHARPY TEST DATA

A36 2" (Pre-cracked) Slow Bend

Specimen No.	Temp. (° F)	Maximum Load (lb.)	Deflection at Maximum Load (in.)	Crack-Depth (in.)	Energy Absorbed		Shear (%)	Lateral Expansion (mils)
					Actual (ft.-lb.)	Normalized (ft.-lb.)		
188-SP	- 230	1560	0.030	0.109	1.47	1.61	0	
176-SP	- 150	1975	0.030	0.130	2.52	3.08	0	7
167-SP	- 100	1250	0.046	0.153	4.16	5.45	0	15
163-SP	- 55	1250	0.042	0.120	7.03	8.09	10	14
153-SP	0	800	0.050	0.190	12.50	19.30	60	24
149-SP	+ 75	1820	0.097	0.109	29.08	32.90	95	47

TABLE B2 - CHARPY TEST DATA

A36 2" (Pre-cracked) Fast Bend

Specimen No.	Temp. (° F)	Maximum Load (lb.)	Deflection at Maximum Load (in.)	Crack-Depth (in.)	Energy Absorbed		Shear (%)	Lateral Expansion (mils)
					Actual (ft.-lb.)	Normalized (ft.-lb.)		
442	- 155	930	0.020	0.150	2.20	2.75	0	4
441	- 155	880	0.021	0.160	1.93	2.50	0	3
389	- 100	1145	0.024	0.125	3.31	3.90	0	6
388	- 100	875	0.020	0.170	2.62	3.90	0	8
353	- 50	1000	0.028	0.185	5.55	8.26	< 10	12
354	- 50	1520	0.020	0.145	5.13	6.51	< 10	16
309	0		0.066	0.125	15.55	18.27	20	24
270	+ 50	1300	0.064	0.155	17.80	25.45	40	31

TABLE B2 - CHARPY TEST DATA

A36 2" (Pre-cracked) Dynamic

Specimen No.	Temp. (° F)	Maximum Load (lb.)	Deflection at Maximum Load (in.)	Crack-Depth (in.)	Energy Absorbed		Shear (%)	Lateral Expansion (mils)
					Actual (ft.-lb.)	Normalized (ft.-lb.)		
	- 50			0.125	2.50	2.92	0	4
	0			0.150	4.00	5.15	0	4
	+ 50			0.150	11.50	14.90	< 15	19
	+ 150			0.145	36.00	45.40	90	45
	+ 212			0.180	28.50	41.40	100	37

TABLE B3.1 - DYNAMIC K_c AND K_M VALUES FOR 1/2 INCH A36 PLATE

Specimen Number	Initial Crack Length a (inches)	Test Temperature T (^oF)	Dynamic Yield Stress σ_{Yd} (ksi)	Net Ligament (inches)	Bend Angle (radians)	Max. Load P (kips)	Dynamic K_c (ksi$\sqrt{in}$)	K_M (ksi$\sqrt{in}$)
01	0.769	- 49	69.60	--	--	9.0	51.3	--
02	0.786	- 52	70.00	--	--	9.8	55.8	--
03	0.955	+ 12	61.00	--	--	10.1	78.5	--
04	0.812	+ 5	61.80	--	--	9.3	56.8	--
06	0.882	+ 13	58.60	0.420	0.049	16.3	> 76.0	132
05	0.767	+ 73	61.70	1.780	0.074	11.5	> 76.0	323
010	0.852	+ 73	62.90	1.580	0.172	16.8	> 76.0	467

K_M - K_c estimated from bend angle or thickness reduction.

TABLE B3.2 - DYNAMIC K_c AND K_M VALUES FOR 1 INCH A36 PLATE

Specimen Number	Initial Crack Length a (inches)	Test Temperature T (^{o}F)	Dynamic Yield Stress σ_{Yd} (ksi)	Net Ligament (inches)	Bend Angle A (radians)	Max. Load P (kips)	Dynamic K_c (ksi/in)	K_M (ksi/in)
11	0.777	- 55	75.66	--	--	16.0	45.3	--
12	0.788	- 55	74.78	--	--	15.5	53.8	--
13	0.802	+ 09	66.69	--	--	22.5	72.9	--
14	0.784	+ 11	66.47	1.48	0.013	20.7	63.3	132
16	0.785	+ 30	63.46	0.53	0.113	20.0	61.6	234
19	0.782	+ 31	62.68	0.51	0.078	20.6	65.4	190
15	0.791	+ 78	58.70	1.63	0.036	28.8		222
110	0.798	+ 73	60.50	--	--	31.6		--

K_M - K_c estimated from bend angle or thickness reduction.

TABLE B3.2 - DYNAMIC K_c AND K_M VALUES FOR 2 INCH A36 PLATE

Specimen Number	Initial Crack Length a (inches)	Test Temperature T (^{o}F)	Dynamic Yield Stress σ_{Yd} (ksi)	Net Ligament (inches)	Bend Angle A (radians)	Max. Load P (kips)	Dynamic K_c (ksi/in)	K_M (ksi/in)
23	0.850	- 56	76.0	--	--	27.90	38.9	--
24	0.826	- 56	76.0	--	--	28.40	38.8	--
21	1.025	+ 12	68.0	--	--	37.50	60.9	--
22	0.953	+ 12	68.0	--	--	38.50	58.8	--
25	--	+ 78	61.0	0.480	0.117	46.30	70.8	225
26	--	+ 78	61.0	0.560	0.068	67.90	> 76.0	183

$K_M - K_c$ estimated from bend angle or thickness reduction.

TABLE B4 - A36 R-CURVE INSTABILITY SUMMARY

Thickness (in.)	Test Temperature (^{o} F)	Fatigue Crack Length (in.)	K_c at Instability (psi)	Apparent Crack Length at Instability (in.)
1	- 44	6.20	169,897	7.33
0.5	- 47	6.25	116,652	7.09
0.5*	- 100	6.25	46,359	6.71

*Crack branching occurred at crack length of 8.85"

APPENDIX C - SAE 1035 DATA

This appendix contains the data collected for the 1/2", 1" and 2" thicknesses of the SAE 1035 material. This steel was supplied to the program by the Bethlehem Steel Corporation. The chemical analysis, physical properties and heat designations appear in Tables 1 and 2.

The data in this appendix is presented in the form of a Charpy summary, a detailed Charpy tabulation, a K_c tabulation, an R-curve summary and appropriate figures which best illustrate the data trends. Details of the test procedures and terminology can be found in appendices J, K and L and Chapter 2.

The SAE 1035 CVN curves are given in Figures C-1 through C-3. Charpy data is tabulated in Tables C-1 and C-2. Standard Charpy specimens were tested at three testing speeds for the three thicknesses of SAE 1035. As with most of the tests in this program the slow and fast results were similar and showed no temperature shift. The slow and dynamic results did show a temperature shift and the shift for the 1/2" and 1" materials was consistent with Barsom's results (28). For the 2" material there was no apparent shift. However, this can be misleading since the results of a shift can be masked or hidden by the very low values of the slow and fast results for the 2" tests. It is conceivable that a trend can be justified in the data which

would show a shift. However, it is the choice of the authors not to attempt this.

Slow and dynamic K_c results were collected for the three thicknesses of SAE 1035 material. These results are shown in Figures C-4 through C-6. D.T. results were also collected and are shown in Figures C-7 through C-9. K_c and D.T. data are tabulated in Table C-3. First it should be noted that upturns in the dynamic K_c and D.T. curves occur over similar temperature ranges. The standard CVN results also show similar upswings for the same temperature zones. It is further interesting to note that the temperature shift is present in the K_c data for all of the thicknesses. The level of the shift is also consistent with Barsom (28). The fact that the shift is present tends to reinforce agreements for claiming a shift in the 2" CVN data. If one is to use the equation

$$K_{Ic} = \sqrt{A\ E\ CVN}$$

for estimating K_{Ic} from CVN results, the average value of A should be 9 for the SAE 1035 material. Another method for estimating K_c results is shown in Figure C-10. Here β_{DT} is plotted against β_{K_c}. From this figure it appears that it is more than reasonable to attempt correlation between D.T. and K_{Ic}. In fact for β_{K_c} less than one the curve shows an excellent agreement.

R-curve tests were run on the 1/2" and 1" SAE 1035 material. The data are tabulated in Table C-4. Figures C-4 and C-5 show the data plotted along with the K_c data. For all of these tests there was no apparent stable crack growth. The cracking was unstable and proceeded

to fracture the complete specimen. In one of the 1/2" tests the crack velocity was great enough to cause crack branching. As seen in Figures C-4 and C-5 the R-curve data is an excellent supplement to the static K_c data.

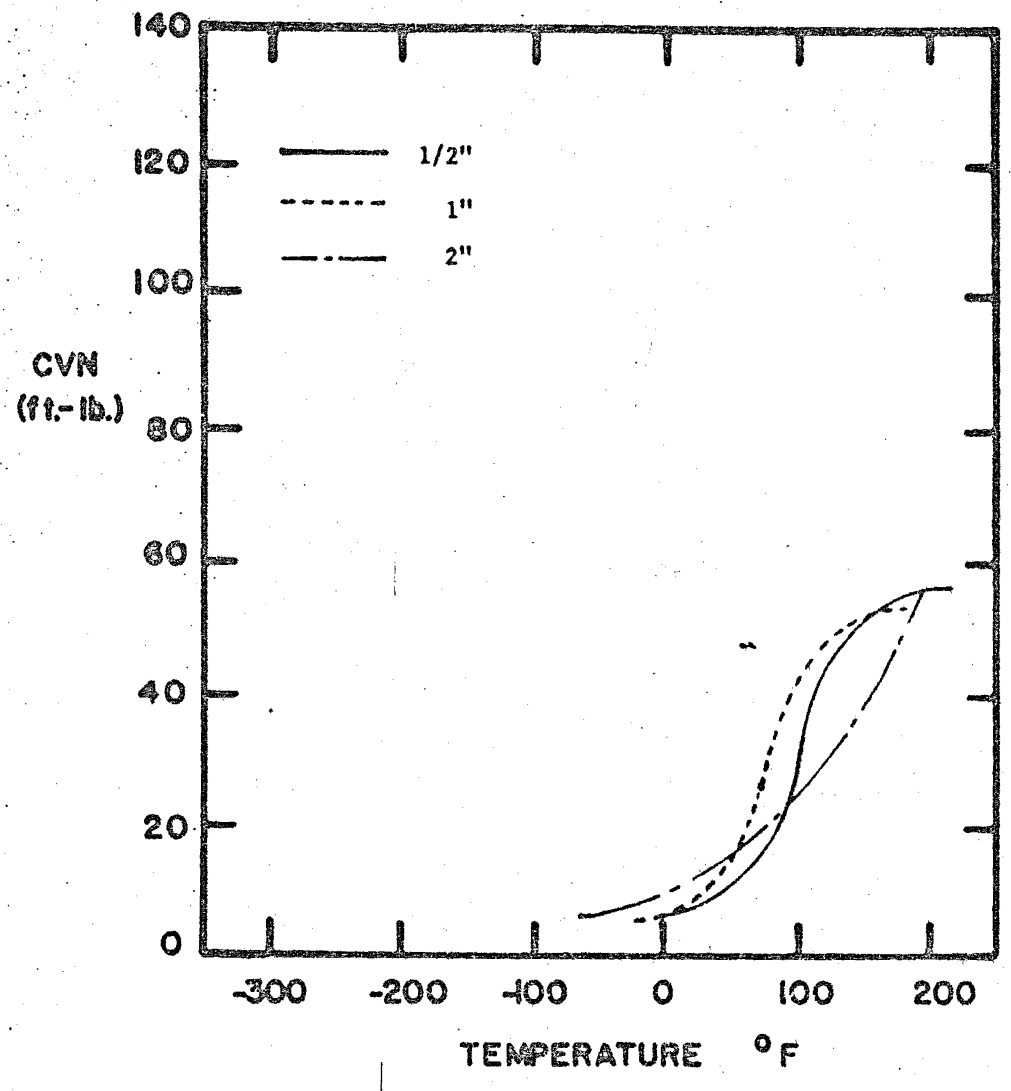

Fig. C-1a Composite Charpy Curves for SAE 1035 Material

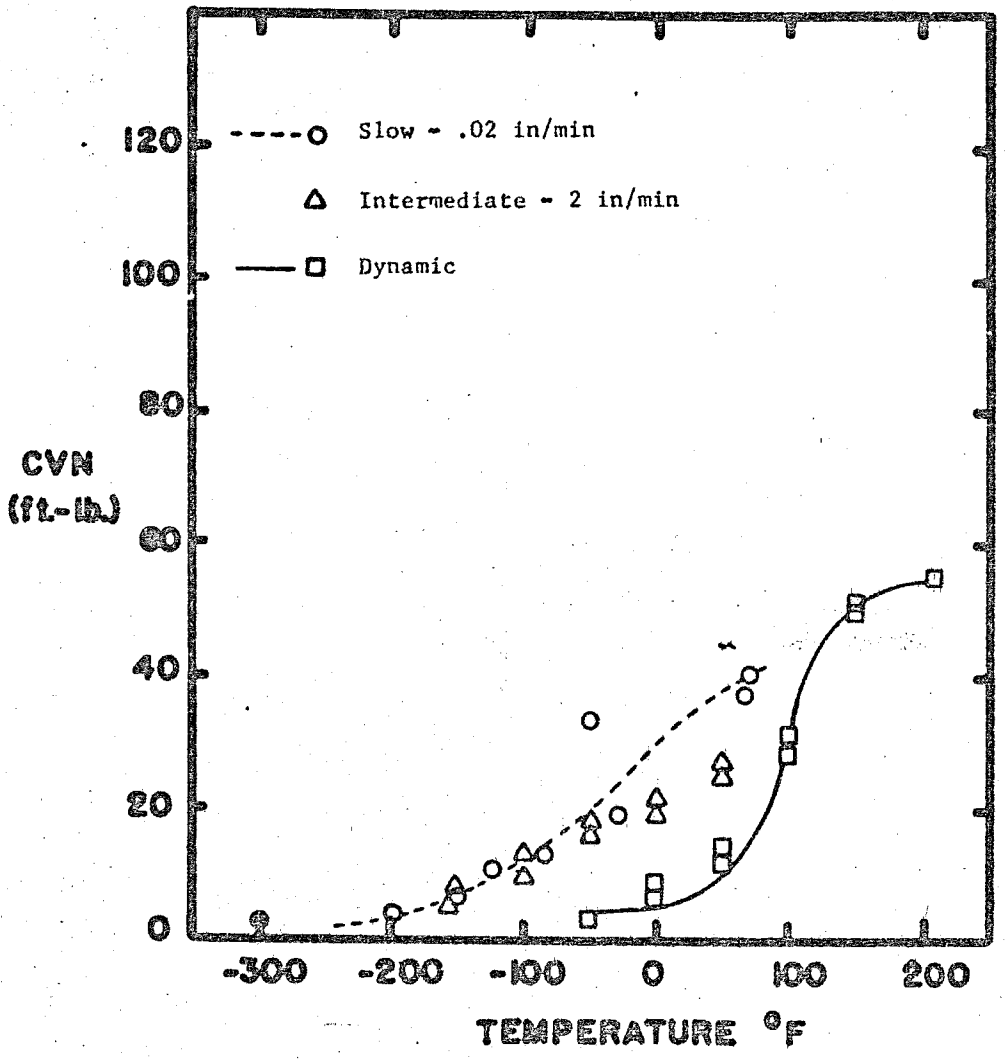

Fig. C-1 SAE 1035 1/2" Notched Charpy Data for Three Loading Rates

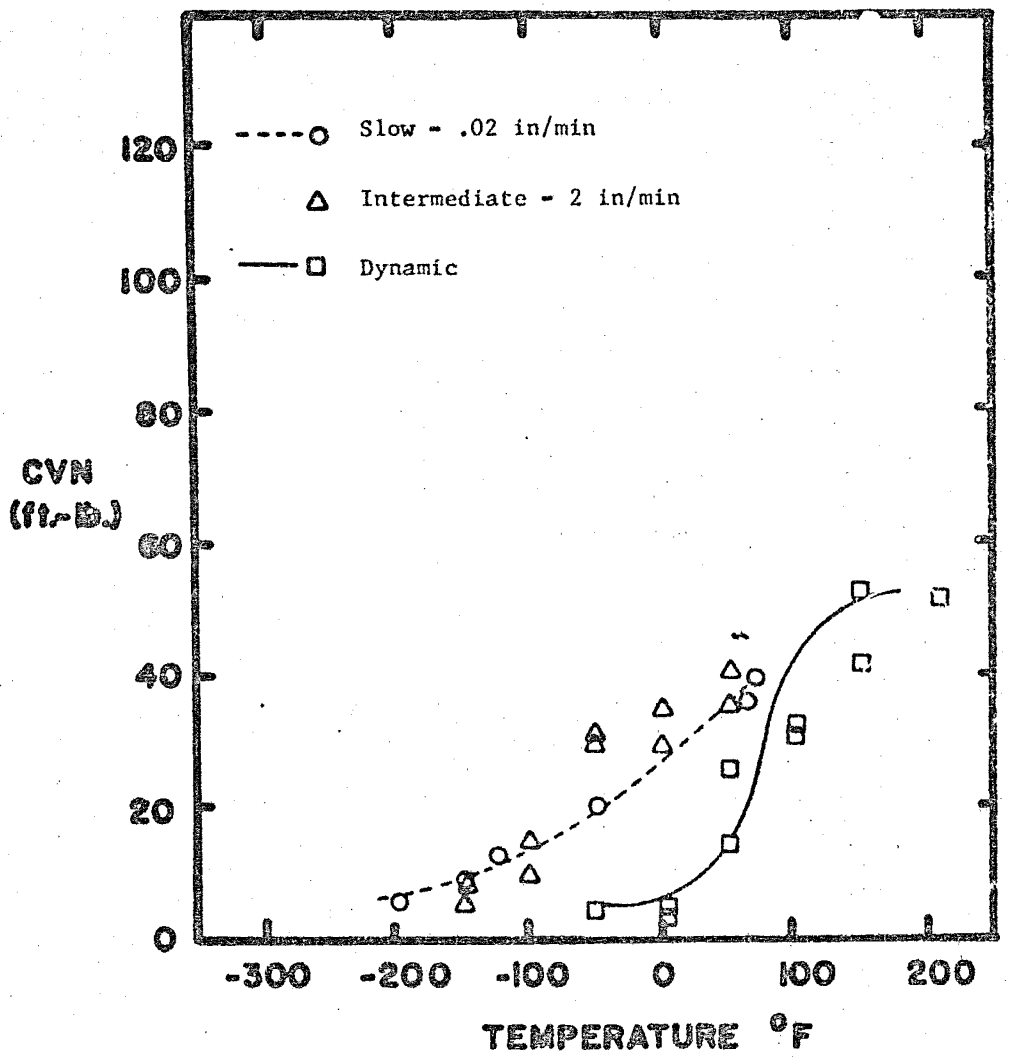

Fig. C-2 SAE 1035 1" Notched Charpy Data for Three Loading Rates

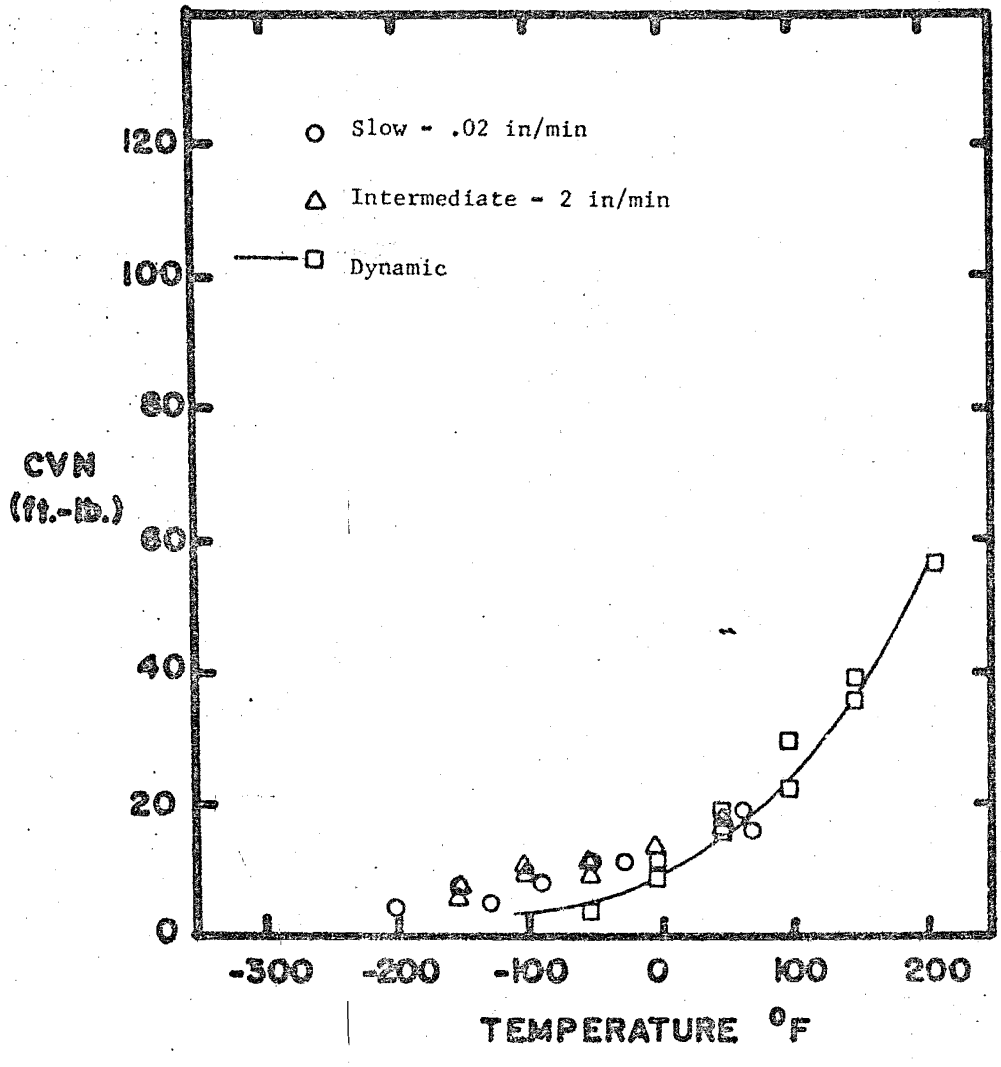

Fig. C-3 SAE 1035 2" Notched Charpy Data for Three Loading Rates

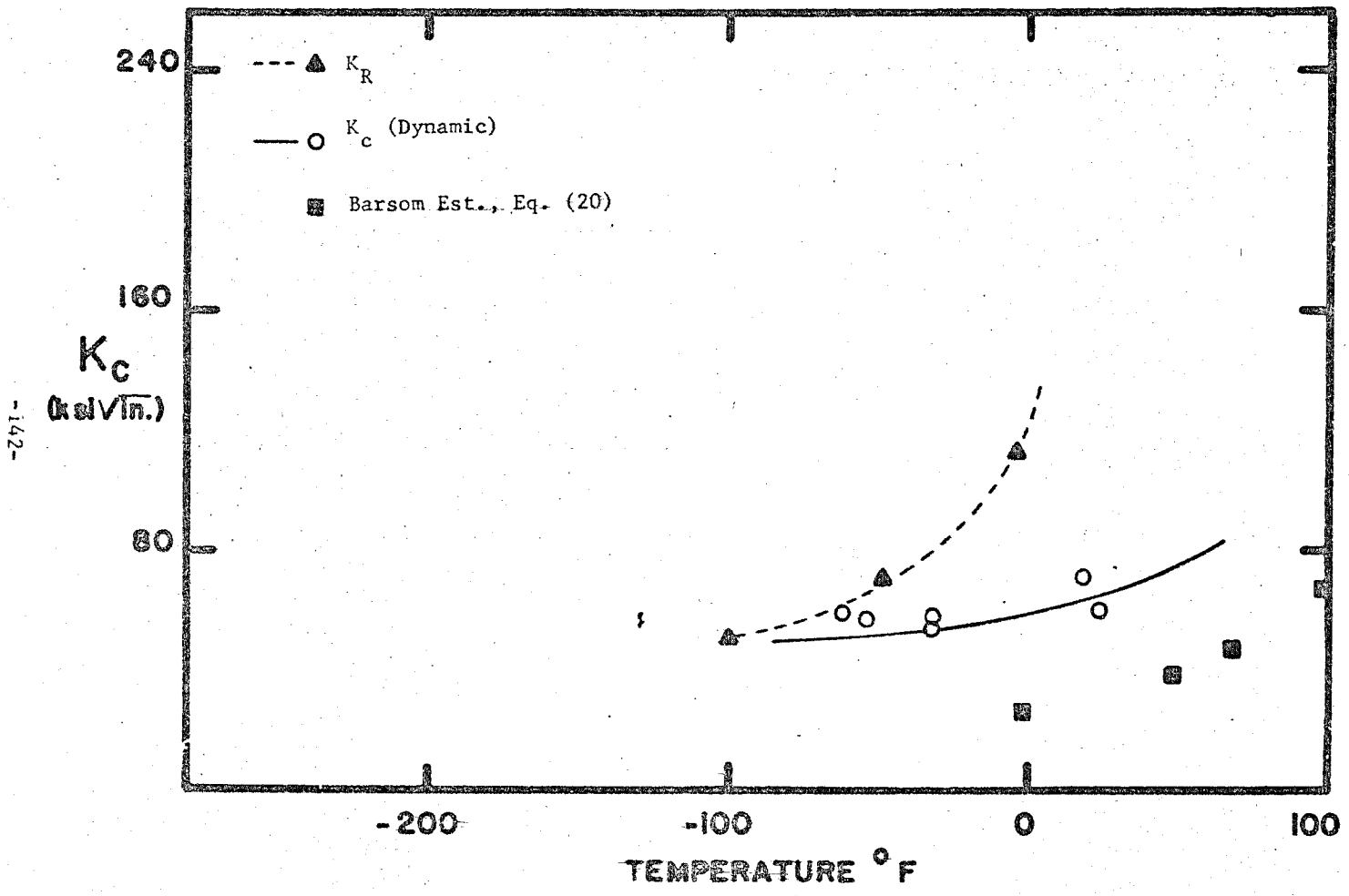

Fig. C-4 K_c Data for SAE 1035 1/2" Material

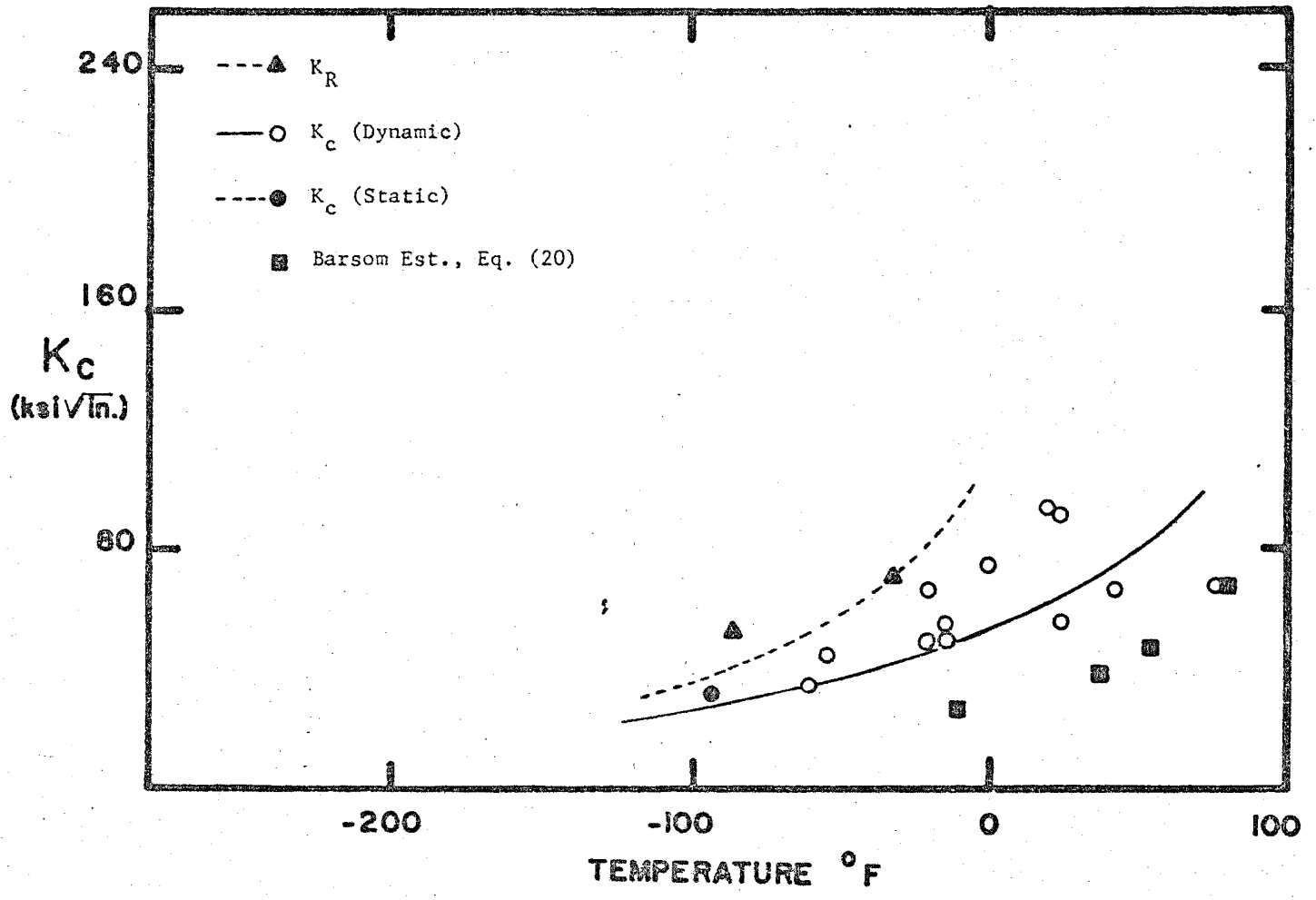

Fig. C-5 K_c Data for SAE 1035 1" Material

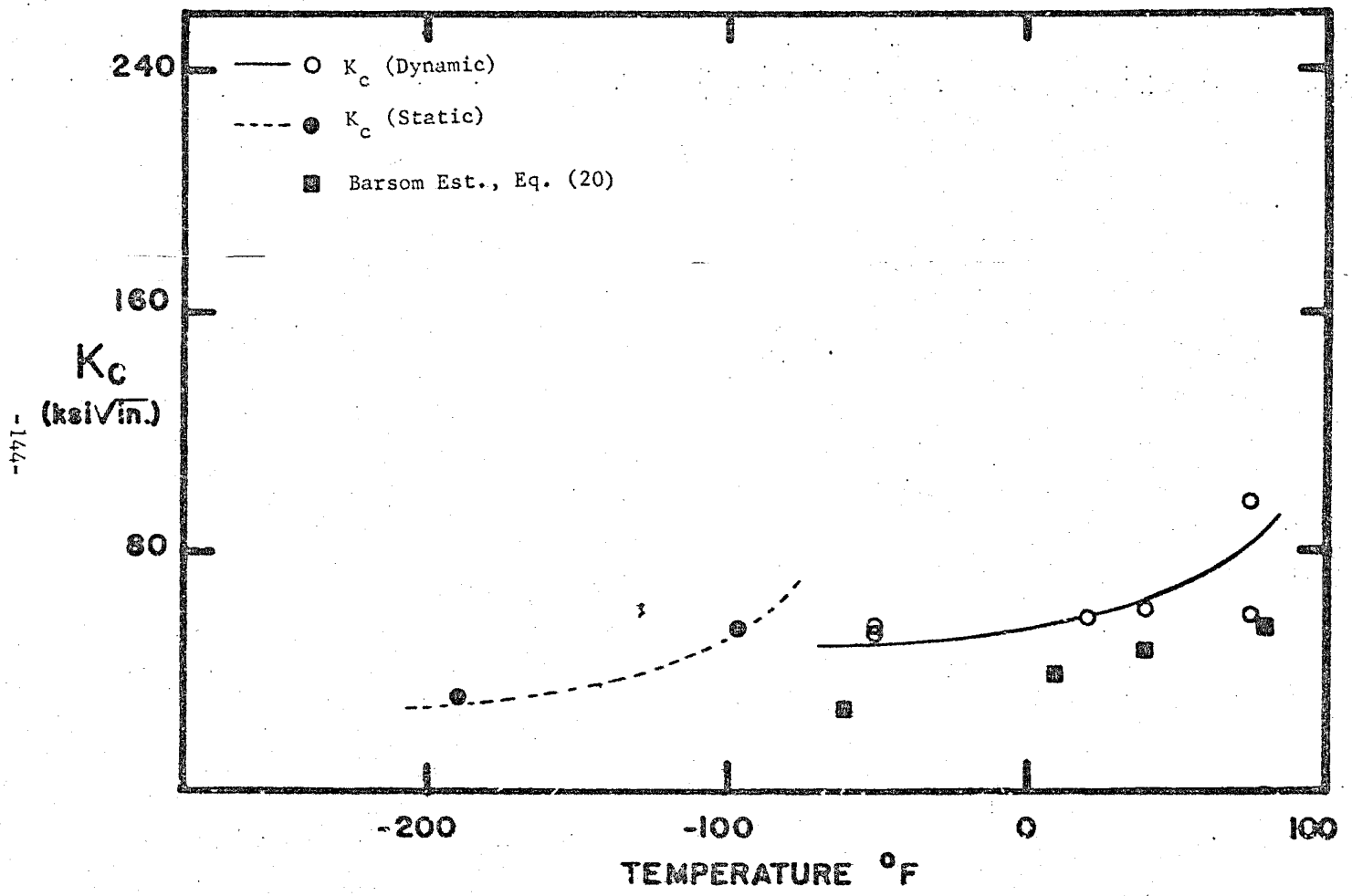

Fig. C-6 K_c Data for SAE 1035 2" Material

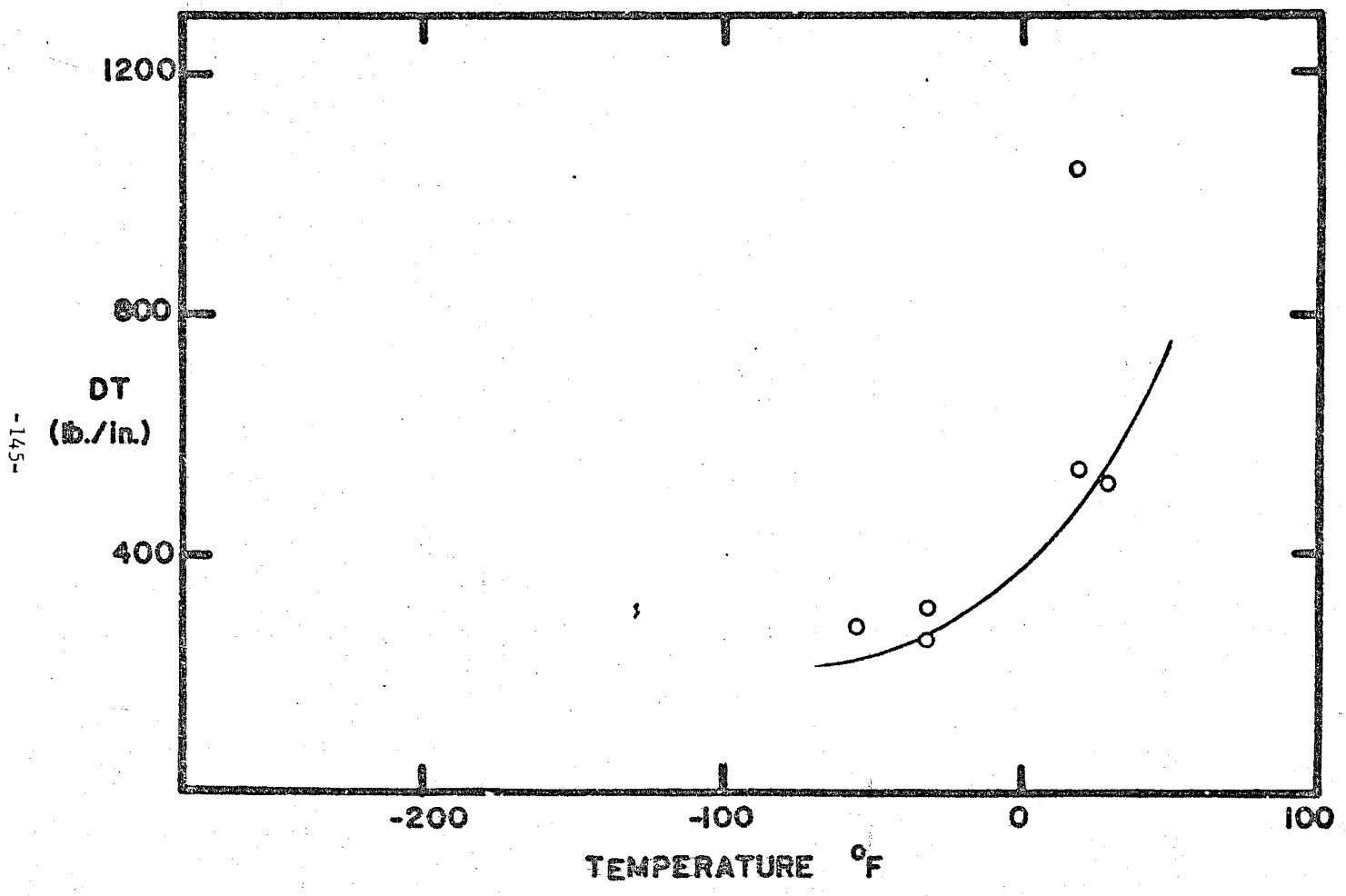

Fig. C-7 Dynamic Tear Data for SAE 1035 1/2" Material

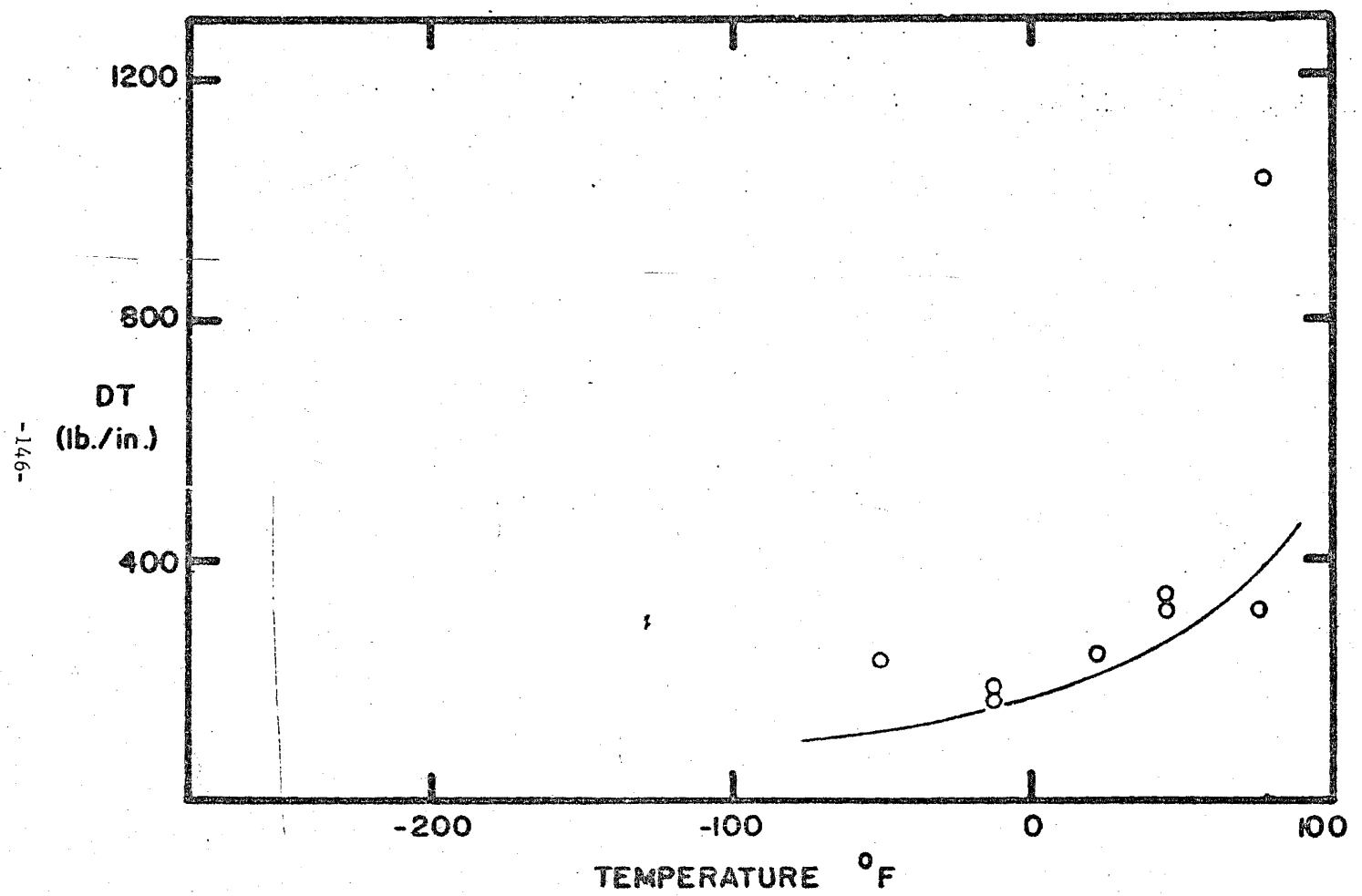

Fig. C-8 Dynamic Tear Data for SAE 1035 1" Material

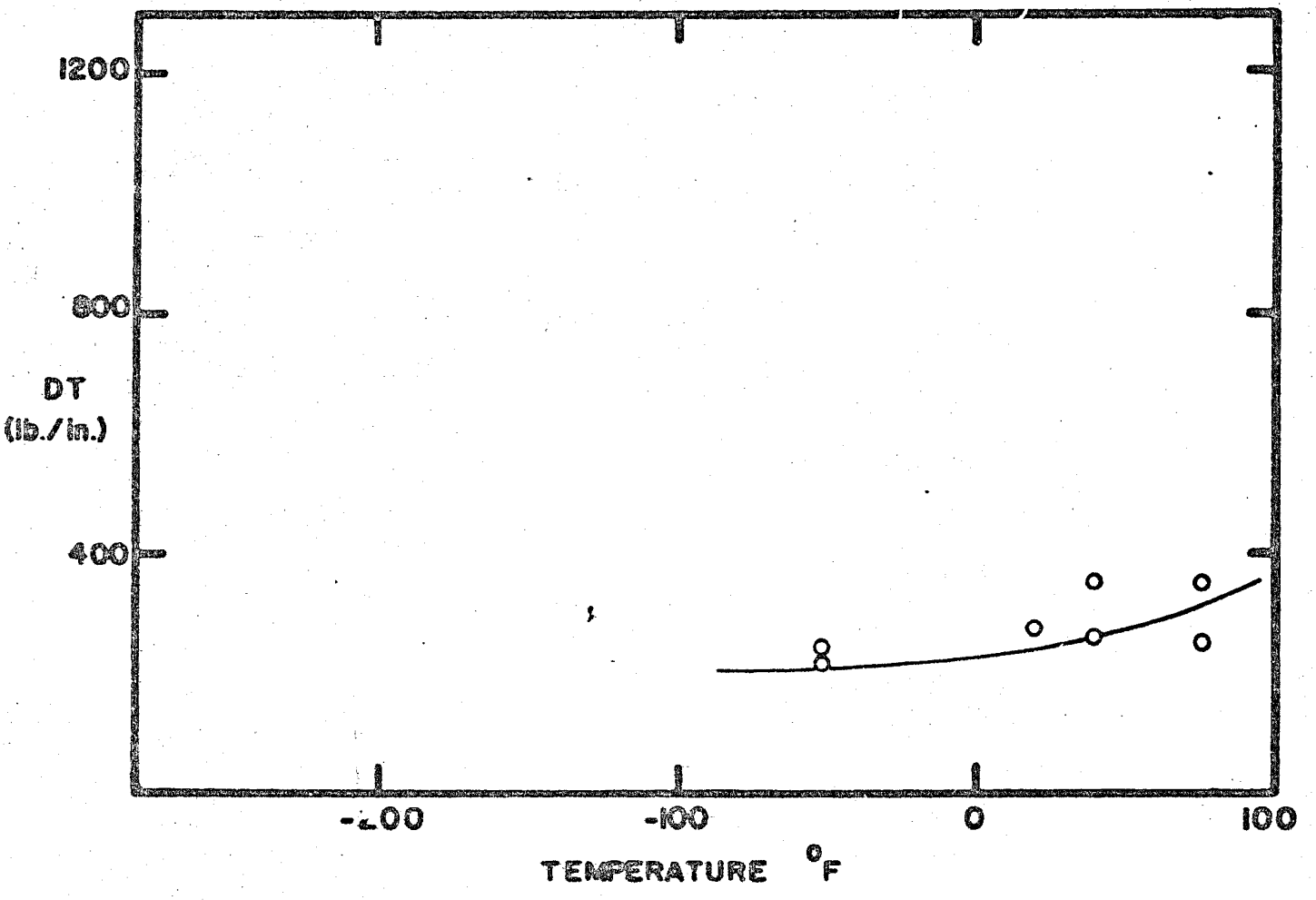

Fig. C-9 Dynamic Tear Data for SAE 1035 2" Material

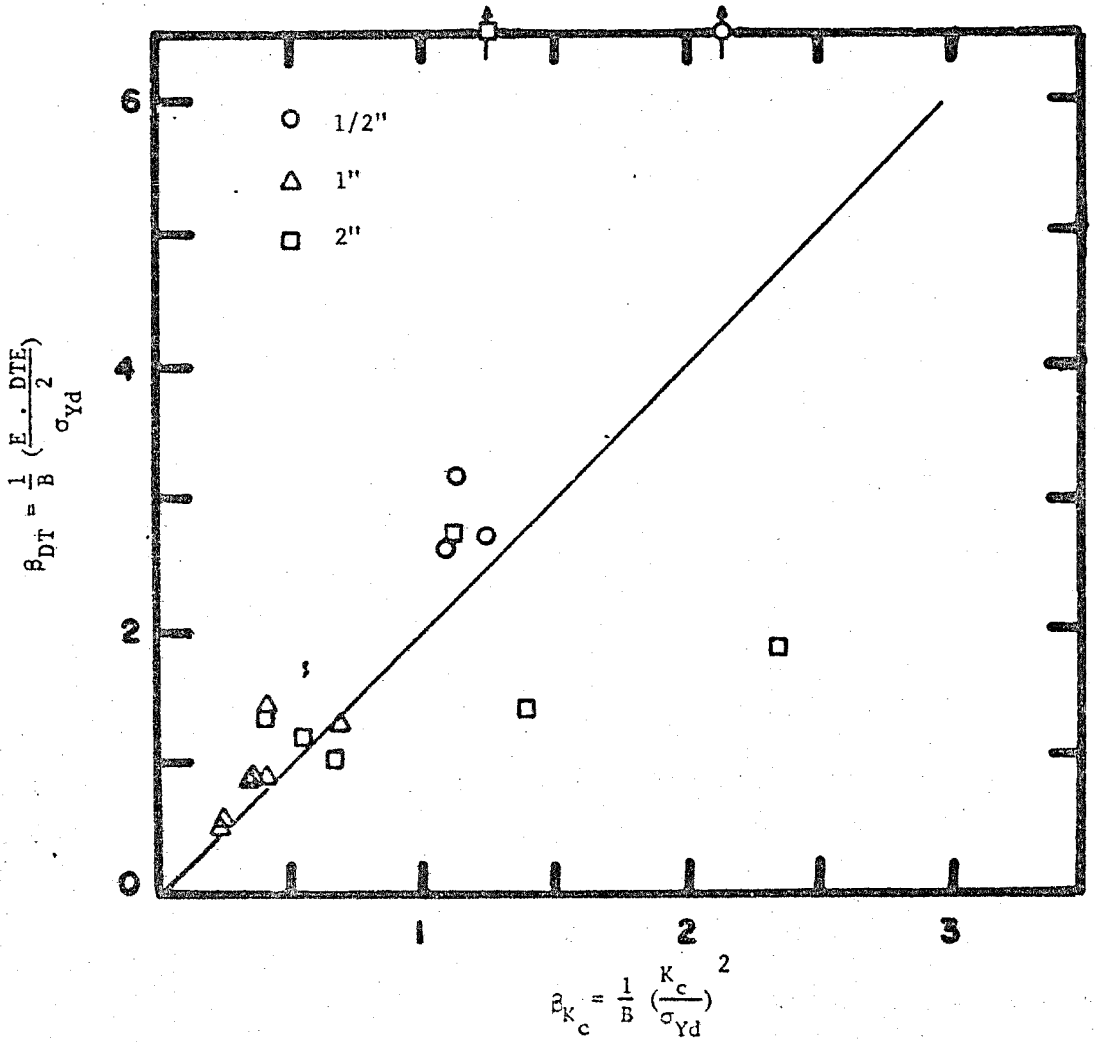

Fig. C-10 SAE 1035 β Data

TABLE C1.1* - SAE 1035 CHARPY DATA SUMMARY

Test	Material Thickness (in.)	T_{15} (°F)	T_{30} (°F)	T_{SH} (°F)	CVN_{SH} (ft.-lb.)
DS	0.5	70	100	200	55
SS	0.5	- 80	0	75	40
DS	1.0	55	80	150	52
SS	1.0	- 75	25	---	> 35
DS	2.0	50	125	---	> 60
SS	2.0	50	---	---	> 20

TABLE C1.2

Test	T	ΔT (°F)	ΔT_B (°F)
S	0.5	175	147
S	1.0	135	155
S	2.0	0	148

*See Table A1.1 for designations

TABLE C2 - CHARPY TEST DATA

SAE1035 1/2" (Notched) Slow Bend

Specimen No.	Temp. (° F)	Maximum Load (lb.)	Deflection at Maximum Load (in.)	Crack-Depth (in.)	Energy Absorbed		Shear (%)	Lateral Expansion (mils)
					Actual (ft.-lb.)	Normalized (ft.-lb.)		
198-SN	- 320	2585	0.033	0.079	2.45	2.45	0	4
181-SN	- 200	2730	0.044	0.079	4.52	4.52	0	5
86-SN	- 125	2675	0.086	0.079	11.54	11.54	0	14
60-SN	- 85	2750	0.089	0.079	12.54	12.54	0	15
50-SN	- 30	2675	0.104	0.079	18.65	18.65	< 15	25
27-SN	+ 63	2625	0.110	0.079	36.88	36.88	100	42
478	- 150	2775	0.050	0.079	6.93	6.93	0	8
421	- 92	2900	0.091	0.079	14.58	14.58	< 5	16
454	- 50	2940	0.200	0.079	33.03	33.03	< 5	21
447	- 5	3000	0.136	0.079	22.00	22.00	< 5	21
492	+ 68	2900	0.098	0.079	40.00	40.00	95	42

TABLE C2 - CHARPY TEST DATA

SAE1035 1/2" (Notched) Fast Bend

Specimen No.	Temp. (°F)	Maximum Load (lb.)	Deflection at Maximum Load (in.)	Crack-Depth (in.)	Energy Absorbed		Shear (%)	Lateral Expansion (mils)
					Actual (ft.-lb.)	Normalized (ft.-lb.)		
400	156	2485	0.040	0.079	4.97	4.97	0	2
401	- 152	2730	0.036	0.079	7.91	7.91	0	5
363	- 100	2920	0.068	0.079	13.65	13.65	0	12
364	- 100	2960	0.052	0.079	9.11	9.11	0	8
325	- 50	3000	0.092	0.079	18.06	18.06	0	14
324	- 50	2850	0.090	0.079	15.33	15.33	0	14
279	0	2950	0.098	0.079	18.42	18.42	0	19
280	0	2900	0.100	0.079	20.96	20.96	< 5	20
245	+ 50	2840	0.118	0.079	24.37	24.37	40	28
244	+ 50	2950	0.120	0.079	26.72	26.72	40	39

TABLE C2 - CHARPY TEST DATA

SAE1035 1/2" (Notched) Dynamic

Specimen No.	Temp. (° F)	Maximum load (lb.)	Deflection at Maximum Load (in.)	Crack-Depth (in.)	Energy Absorbed		Shear (%)	Lateral Expansion (mils)
					Actual (ft.-lb.)	Normalized (ft.-lb.)		
	- 50			0.079	3.0	3.0	0	4
	0			0.079	6.0	6.0	0	7
	0			0.079	8.5	8.5	0	16
	+ 50			0.079	11.0	11.0	0	16
	+ 50			0.079	13.0	13.0	< 5	19
	+ 100			0.079	31.0	31.0	20	35
	+ 100			0.079	27.5	27.5	20	33
	+ 150			0.079	49.5	49.5	80	54
	+ 150			0.079	51.0	51.0	75	52
	+212			0.079	54.5	54.5	100	59

TABLE C2 - CHARPY TEST DATA

SAE1035 1" (Notched) Slow Bend

Specimen No.	Temp. (° F)	Maximum Load (lb.)	Deflection at Maximum Load (in.)	Crack-Depth (in.)	Energy Absorbed		Shear (%)	Lateral Expansion (mils)
					Actual (ft.-lb.)	Normalized (ft.-lb.)		
178A-SN	- 200	2650	0.056	0.079	4.80	4.80	--	7
85-SN	- 125	2550	0.088	0.079	12.24	12.24	0	17
61-SN	- 85	2650	0.108				0	22
58-SN	- 50	2600	0.118	0.079	19.50	19.50	< 10	24
54-SN	- 50	2675	0.125	0.079	19.60	19.60	< 5	24
28-SN	+ 63	2625	0.114	0.079	35.45	35.45	100	43
479	- 150	2660	0.056	0.079	8.46	8.46	0	10
422	- 95	2560	0.086	0.079	12.29	12.29	< 5	20
455	- 50	2675	0.236	0.079	40.00	40.00	10	24
493	+ 68	2700	0.090	0.079	39.10	39.10	100	49
448	0	2830	0.135	0.079	32.70	32.70	15	38

TABLE C2 - CHARPY TEST DATA

SAE1035 1" (Notched) Fast Bend

Specimen No.	Temp. (° F)	Maximum Load (lb.)	Deflection at Maximum Load (in.)	Crack-Depth (in.)	Energy Absorbed		Shear (%)	Lateral Expansion (mils)
					Actual (ft.-lb.)	Normalized (ft.-lb.)		
402	- 150	2600	0.044	0.079	7.79	7.79	0	5
403	- 150	2630	0.042	0.079	5.70	5.70	0	5
365	- 100	3000	0.072	0.079	14.58	14.58	0	13
366	- 100	2650	0.052	0.079	9.08	9.08	0	9
328	- 50	2610	0.076	0.079	20.45	20.45	< 5	26
329	- 50	2715	0.115	0.079	18.30	18.30	< 5	25
281	0	2800	0.097	0.079	19.22	19.22	10	32
282	0	2630	0.112	0.079	24.65	24.65	15	23
246	+ 50	2600	0.128	0.079	34.93	34.93	60	44
247	+ 50	2565	0.116	0.079	40.65	40.65	85	45

TABLE C2 - CHARPY TEST DATA

SAE1035 1" (Notched) Dynamic

Specimen No.	Temp. (°F)	Maximum Load (lb.)	Deflection at Maximum Load (in.)	Crack-Depth (in.)	Energy Absorbed		Shear (%)	Lateral Expansion (mils)
					Actual (ft.-lb.)	Normalized (ft.-lb.)		
	- 50			0.079	4.0	4.0	0	5
	0			0.079	3.0	3.0	0	5
	0			0.079	4.0	4.0	0	7
	+ 50			0.079	25.0	25.0	< 5	35
	+ 50			0.079	14.0	14.0	< 5	30
	+ 100			0.079	32.0	32.0	30	42
	+ 100			0.079	31.0	31.0	30	44
	+ 150			0.079	52.0	52.0	90	54
	+ 150			0.079	41.0	41.0	85	56
	+ 212			0.079	51.0	51.0	100	58

TABLE C2 - CHARPY TEST DATA

SAE1035 2" (Notched) Slow Bend

Specimen No.	Temp. (° F)	Maximum Load (lb.)	Deflection at Maximum Load (in.)	Crack-Depth (in.)	Energy Absorbed		Shear (%)	Lateral Expansion (mils)
					Actual (ft.-lb.)	Normalized (ft.-lb.)		
185-SN	- 200	2950	0.046	0.079	4.34	4.34	0	6
87-SN	- 125	2325	0.048	0.079	5.12	5.12	0	10
62-SN	- 85	2575	0.061	0.079	7.93	7.93	< 10	8
51-SN	- 30	2650	0.074	0.079	10.86	10.86	20	13
29-SN	- 50	2700	0.083	0.079	15.28	15.28	50	16
33-SN	+ 63	2650	0.082	0.079	19.94	19.94	60	24
480	- 150	2950	0.042	0.079	6.20	6.20	0	6
423	- 95	2750	0.059	0.079	8.46	8.46	0	11
501	- 50	2600	0.072	0.079	10.60	10.60		16
449	0	3000	0.082	0.079	13.90	13.90	10	16
494	+ 68	2830	0.082	0.079	18.50	18.50	20	28
495	+ 68	2850	0.080	0.079	16.50	16.50		27

TABLE C2 - CHARPY TEST DATA

SAE1035 2" (Notched) Fast Bend

Specimen No.	Temp. (°F)	Maximum Load (lb.)	Deflection at Maximum Load (in.)	Crack-Depth (in.)	Energy Absorbed		Shear (%)	Lateral Expansion (mils)
					Actual (ft.-lb.)	Normalized (ft.-lb.)		
405	- 150	2850	0.040	0.079	7.20	7.20	0	6
404	- 150	2875	0.040	0.079	8.30	8.30	0	6
368	- 100	2820	0.052	0.079	9.71	9.71	0	8
367	- 100	2900	0.052	0.079	10.40	10.40	0	7
327	- 50	2820	0.058	0.079	12.52	12.52	0	10
326	- 50	2750	0.064	0.079	10.00	10.00	0	12
283	0	2650	0.078	0.079	14.55	14.55	0	19
249	+ 50	2760	0.072	0.079	17.94	17.94	20	21
248	+ 50	2945	0.088	0.079	18.20	18.20	20	16

TABLE C2 - CHARPY TEST DATA

SAE1035 2" (Notched) Dynamic

Specimen No.	Temp. (° F)	Maximum Load (lb.)	Deflection at Maximum Load (in.)	Crack-Depth (in.)	Energy Absorbed		Shear (%)	Lateral Expansion (mils)
					Actual (ft.-lb.)	Normalized (ft.-lb.)		
	- 50			0.079	3.0	3.0	0	4
	0			0.079	11.0	11.0	0	11
	0			0.079	8.0	8.0	0	9
	+ 50			0.079	18.0	18.0	< 5	19
	+ 50			0.079	15.0	15.0	< 5	19
	+ 100			0.079	29.0	29.0	15	32
	+ 100			0.079	22.0	22.0	15	26
	+ 150			0.079	35.0	35.0	45	40
	+ 150			0.079	38.0	38.0	60	39
	+ 212			0.079	56.0	56.0	95	56

TABLE C3.1* - SAE 1035 K_c DATA

SAE 1035 1/2"

Nominal Yield Strength YS = 45.3 ksi

Specimen No.	B (in.)	Temp. (^{o}F)	A_o (in.)	F.A. (in.^{2})	P_{max} (kips)	Time (sec)	K_c (ksi/in.)	G (lb/in)	DTE (lb/in)	β_{K_c}	β_{DT}	σ_{YD} (ksi)
2.009	0.5	- 60	0.795	1.102	10.5	7.0E-04	60.31	122.9	0.0	1.150	0.000	79.5
2.001	0.5	- 54	0.715	1.142	10.9	7.5E-04	58.24	114.6	273.1	1.105	2.632	78.4
2.005	0.5	- 30	0.665	1.167	11.5	7.0E-04	59.48	119.5	257.0	1.252	2.691	75.2
2.003	0.5	- 30	0.615	1.192	11.5	7.0E-04	56.45	107.7	301.9	1.127	3.161	75.2
2.011	0.5	- 40	1.690	0.655	8.8	6.0E-04	0.00	0.0	0.0	0.0	0.0	77.1
2.004	0.5	20	0.605	1.197	13.8	7.5E-04	72.09	175.6	1042.2	2.187	12.979	68.9
2.007	0.5	20	1.100	0.950	11.5	8.0E-04	0.00	0.0	543.2	0.0	6.803	68.7
2.018	0.5	25	0.710	1.145	11.1	7.5E-04	61.16	126.4	0.0	1.598	0.000	68.4
2.012	0.5	30	1.095	0.953	12.0	9.0E-04	0.00	0.0	516.5	0.0	6.742	67.3
2.017	0.5	40	0.725	1.137	16.6	7.2E-04	0.00	0.0	0.0	0.0	0.000	67.0
Slow Bend Tests												
2.006	0.5	-165	0.740	1.130	31.2	3.0E-01	0.00	0.0	0.0	0.0	0.000	79.3
2.013	0.5	- 72	0.700	1.150	57.9	5.0E-01	0.00	0.0	0.0	0.0	0.000	63.3

*See Table A3 for designation

TABLE C3.2* - SAE 1035 K_c DATA

SAE 1035 1"

Nominal Yield Strength YS = 39.7 ksi

Specimen No.	B (in.)	Temp. (°F)	A_o (in.)	F.A. ($in.^2$)	P_{max} (kips)	Time (sec)	K_c (ksi/in)	G (lb/in)	DTE (lb/in)	β_{K_c}	β_{DT}	σ_{YD} (ksi)
2.111	1.0	- 60	0.915	2.085	11.3	6.0E-04	34.09	39.3	0.0	0.209	0.000	74.5
2.101	1.0	- 53	0.815	2.185	15.9	1.0E-03	45.46	69.8	225.2	0.403	1.301	71.6
2.116	1.0	- 20	0.900	2.100	20.0	8.0E-04	66.30	148.5	0.0	0.956	0.000	67.8
2.114	1.0	- 20	0.900	2.100	15.0	5.8E-04	49.89	84.1	0.0	0.524	0.000	68.9
2.102	1.0	- 15	1.060	1.940	15.1	8.0E-04	55.66	104.7	154.6	0.686	1.014	67.2
2.103	1.0	- 15	0.900	2.100	15.7	1.0E-03	49.31	82.1	177.1	0.550	1.187	66.5
2.113	1.0	0	0.910	2.090	21.3	9.0E-04	75.15	190.8	0.0	1.336	0.000	65.0
2.106	1.0	20	0.905	2.095	23.3	1.2E-03	94.92	304.4	234.8	2.349	1.812	61.9
2.109	1.0	25	0.900	2.100	18.0	6.0E-04	58.88	117.1	0.0	0.860	0.000	63.5
2.117	1.0	25	0.920	2.080	28.0	7.8E-04	92.79	290.9	0.0	2.190	0.000	62.7
2.107	1.0	43	0.900	2.100	28.3	7.2E-04	0.00	0.0	308.6	0.000	2.446	61.1
2.105	1.0	43	0.880	2.120	19.5	1.0E-03	65.66	145.6	334.0	1.191	2.732	60.2
2.112	1.0	75	0.925	2.075	18.7	5.0E-04	66.23	148.2	1029.4	1.252	8.694	59.2
2.118	1.0	75	0.900	2.100	28.8	7.5E+00	0.00	0.0	308.6	0.000	5.259	41.7
Slow Bend Tests												
2.108	1.0	-156	0.830	2.170	11.0	3.3E-01	30.76	32.0	0.0	0.185	0.000	71.6
2.110	1.0	- 93	0.920	2.080	30.0	1.2E+00	0.00	0.0	0.0	0.000	0.000	58.6

*See Table A3 for designation

TABLE C3.3* - SAE 1035 K_c DATA

SAE 1035 2"

Nominal Yield Strength YS = 44.3 ksi

Specimen No.	B (in.)	Temp. (°F)	A_o (in.)	F.A. ($in.^2$)	P_{max} (kips)	Time (sec)	K_c (ksi/in)	G (lb/in)	DTE (lb/in)	β_{K_c}	β_{DT}	σ_{YD} (ksi)
2.203	2.0	- 50	0.980	4.040	32.3	8.5E-04	53.71	97.5	216.8	0.243	0.541	77.0
2.204	2.0	- 50	1.020	3.960	31.6	8.0E-04	54.48	100.3	248.5	0.249	0.616	77.2
2.206	2.0	20	0.750	4.500	40.0	1.2E-03	56.23	106.8	274.7	0.350	0.899	67.2
2.201	2.0	40	1.015	3.970	33.1	1.0E-03	59.53	119.7	272.0	0.410	0.931	65.7
2.202	2.0	40	0.795	4.410	57.6	1.5E-03	0.00	0.0	351.0	0.000	1.244	64.6
2.207	2.0	75	0.900	4.200	42.5	7.5E-04	75.02	190.1	345.7	0.701	1.275	63.3
2.208	2.0	75	0.950	4.100	34.4	7.5E-04	58.73	116.5	242.9	0.430	0.896	63.3
Slow Bend Tests												
2.209	2.0	-187	0.830	4.340	22.0	3.8E-01	30.48	31.4	0.0	0.067	0.000	83.3
2.205	2.0	- 97	0.925	4.150	33.0	1.4E+00	53.98	98.5	0.0	0.354	0.000	64.7

*See Table A3 for designation.

TABLE C4 - SAE 1035 R-CURVE INSTABILITY SUMMARY

Thickness (in.)	Test Temperature (°F)	Fatigue Crack Length (in.)	K_c at Instability (psi)	Apparent Crack Length at Instability (in.)
1	- 85	6.07	54,150	6.42
1	- 32	6.35	71,400	6.52
0.5	- 47	6.25	71,400	6.52
0.5*	- 3	6.30	114,000	7.14
0.5	- 98	6.25	51,700	6.23

*Crack branching occurred at crack length of 9.65"

APPENDIX D - A242 DATA

This appendix contains the data collected for the 1/2", 1" and 2" thicknesses of the A242 material. This steel was supplied to the program by the Bethlehem Steel Corporation. The chemical analysis, physical properties and heat designations appear in Tables 1 and 2.

The data in this appendix is presented in the form of a Charpy summary, a detailed Charpy tabulation, a K_c tabulation, an R-curve summary and appropriate figures which best illustrate the data trends. Details of the test procedures and terminology can be found in appendices J, K and L and Chapter 2.

Standard Charpy specimens were tested at three loading rates for all three thicknesses. The results of these tests are shown in Figures D-1 through D-3. Tabulated results are given in Table D-2. Table D-1 gives a Charpy data reduction summary. As with most of the Charpy data reported in this program there was no discernable difference between the slow and fast rates of loading. There was a clear temperature shift present between the slow and dynamic curves. This shift was consistent with results reported by Barsom (28) for the 2" material and somewhat higher for the 1/2" and 1" materials. However, due to the very limited nature of the present data it is possible to see that through more testing or even a re-evaluation of current tests, the temperature shift for the 1/2" and 1" material might be reduced

and thus agree with Barsom's prediction (28). The 1" and 2" data also suggested the double shelf behvaior suggested by Barsom (28).

K_c and D.T. results were obtained for the 1/2", 1" and 2" A242 material. These results are shown in Figures D-4 through D-9. Table D-3 gives individual data point information. The transition or upward turning portion of the standard CVN, K_c and D.T. curves all occur over the same temperature range for corresponding thicknesses. The temperature shift is also present between the static and dynamic K_c data. The 1" data appears to have a smaller than expected shift. It is interesting to note that the equation for correlating K_{Ic} and CVN data (28)

$$K_{Ic} = \sqrt{A\ E\ CVN}$$

works excellently where A = 5. A plot of β_{DT} versus β_{K_c} is also given in Figure D-10. This shows that there is a reasonable basis for using D.T. values for predicting K_c levels. As with most of the data collected under this program, for β_{K_c} less than one, the agreement is excellent.

R-curve data was collected for the 1/2" and 1" A242 material. These results are presented in Table D-4. As with the other materials tested in this program there was not any noticeable stable crack extension. All crack growth was unstable causing complete failure of the specimens. In the tests crack branching was not observed. The individual data points are plotted in Figures D-4 and D-5. It is clear that the R-curve K estimates are very useful to extend the static three-point bend K_c value to higher levels.

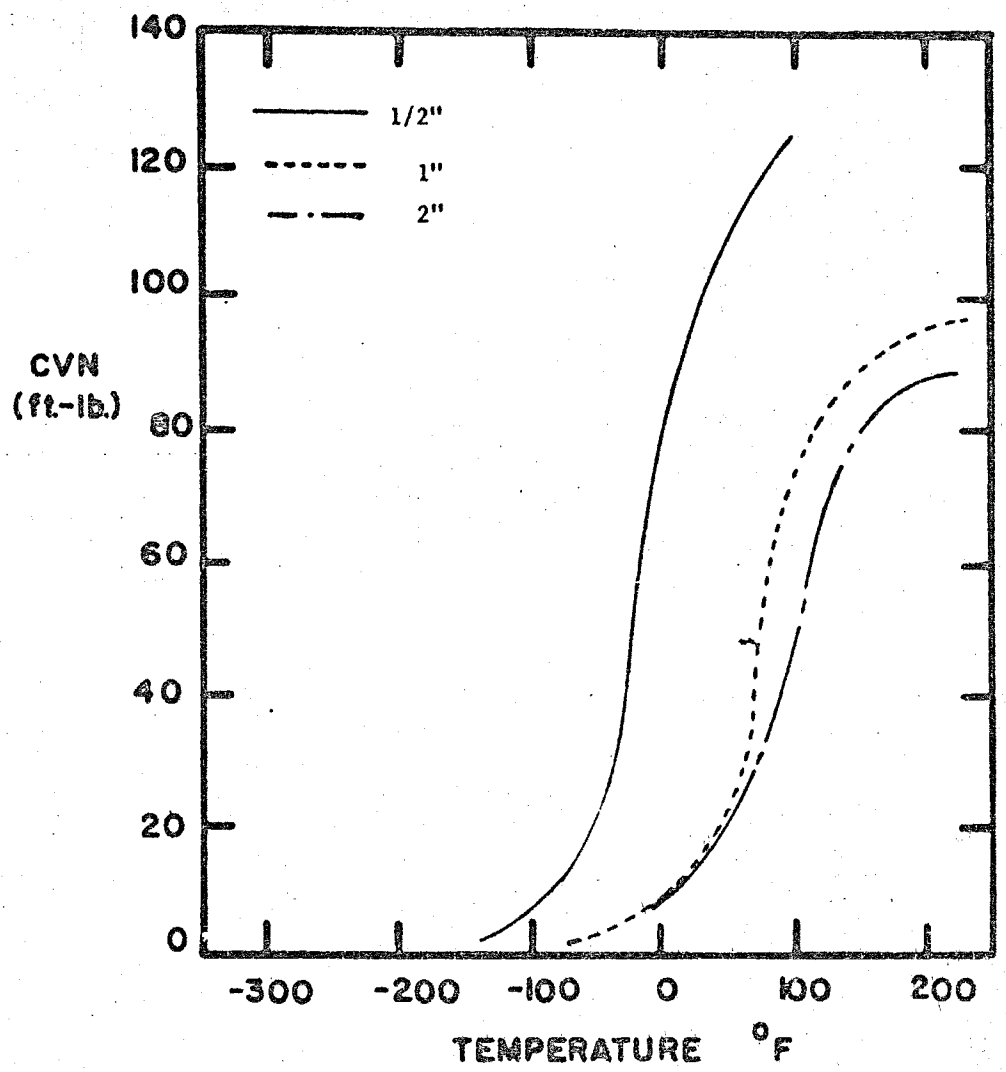

Fig. D-1a Composite Charpy Curves for A242 Material

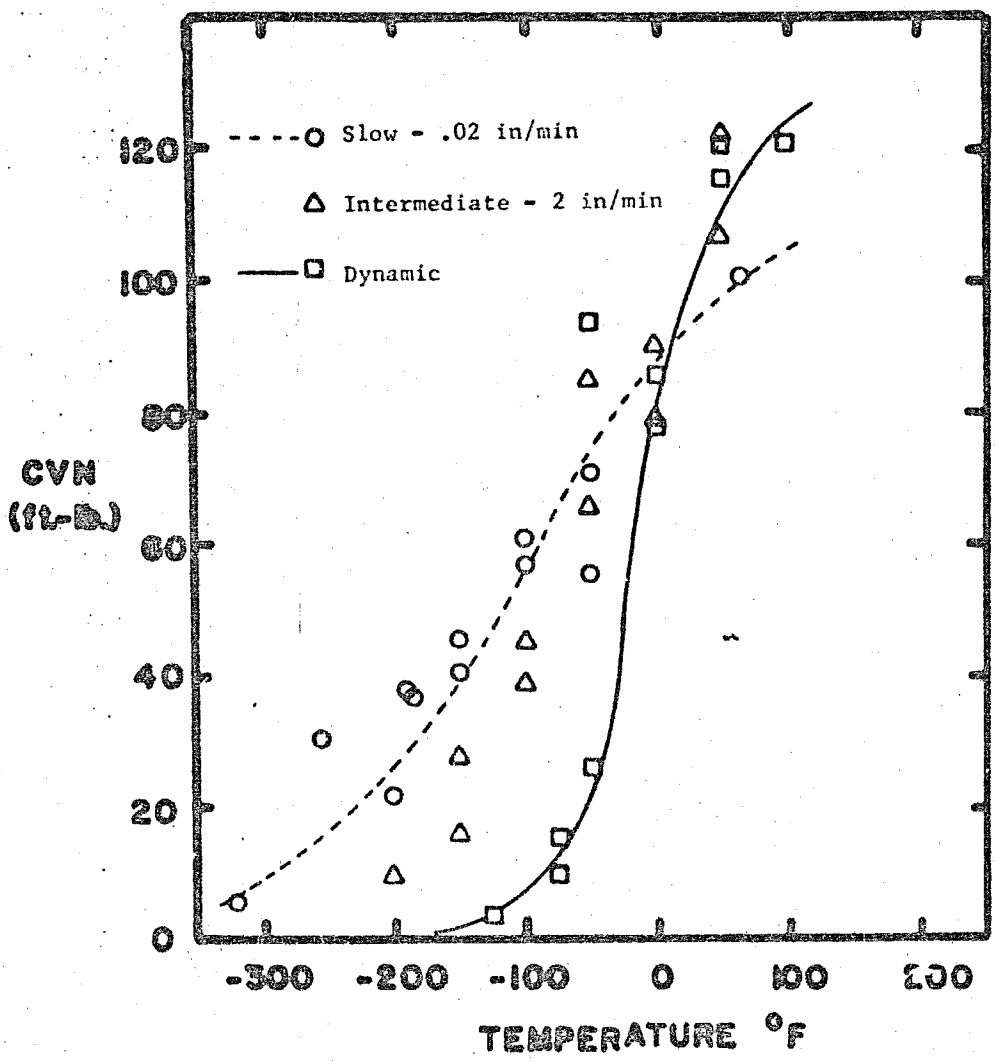

Fig. D-1 A242 1/2" Notched Charpy Data for Three Loading Rates

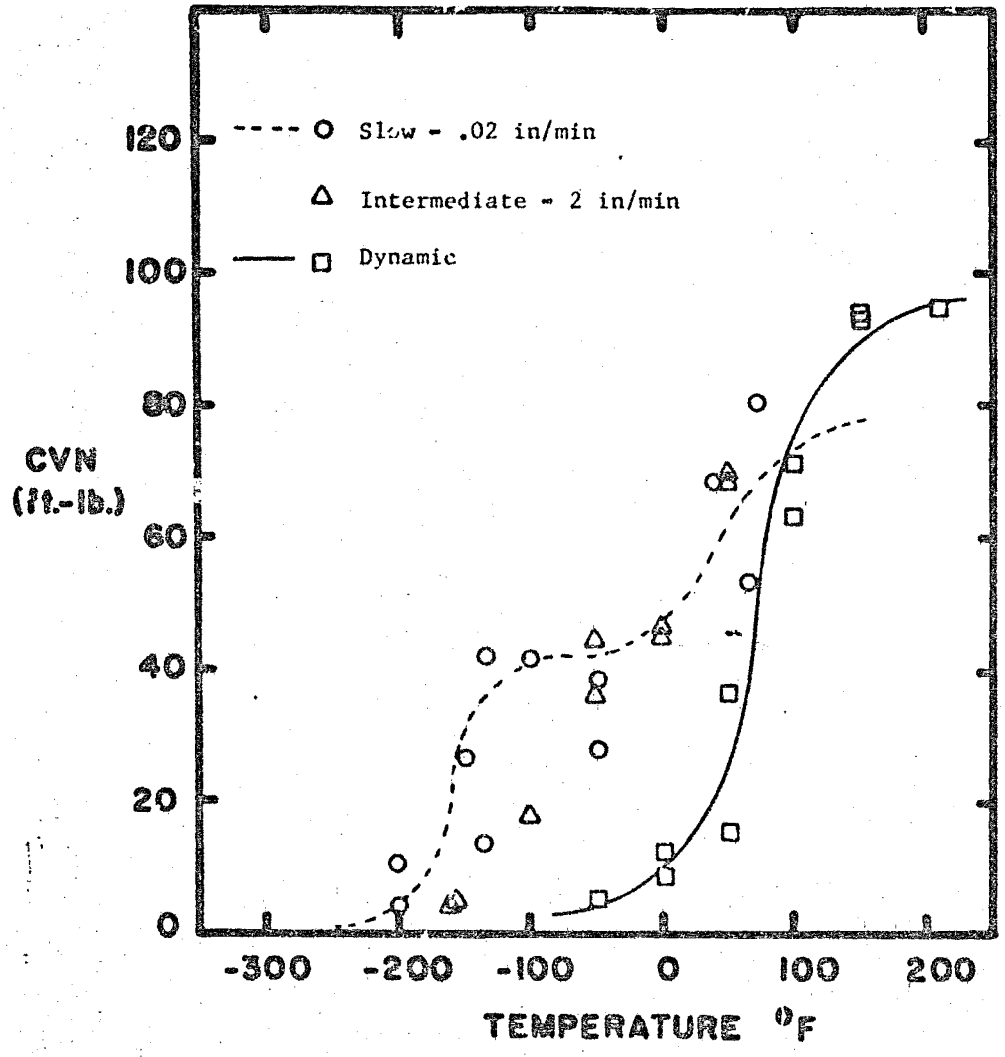

Fig. D-2 A242 1" Notched Charpy Data for Three Loading Rates

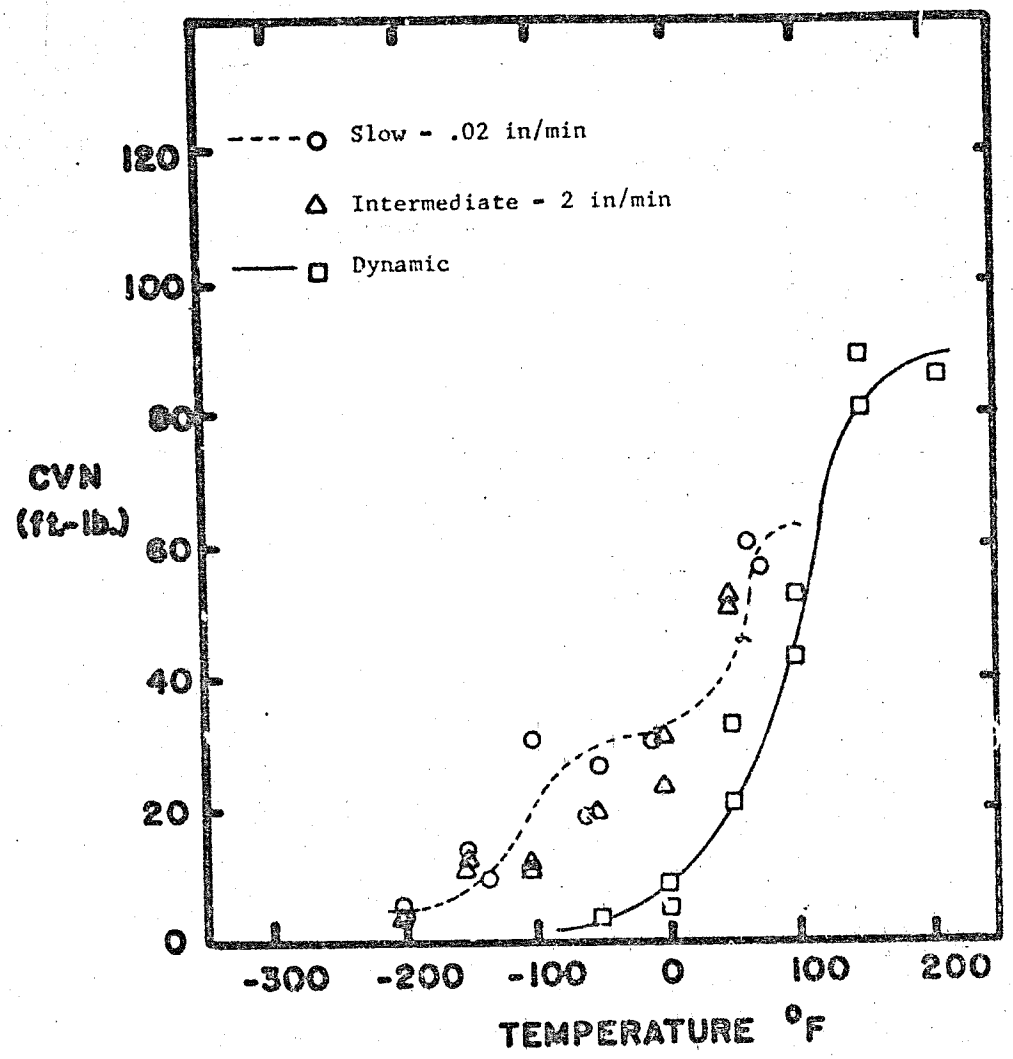

Fig. D-3 A242 2" Notched Charpy Data for Three Loading Rates

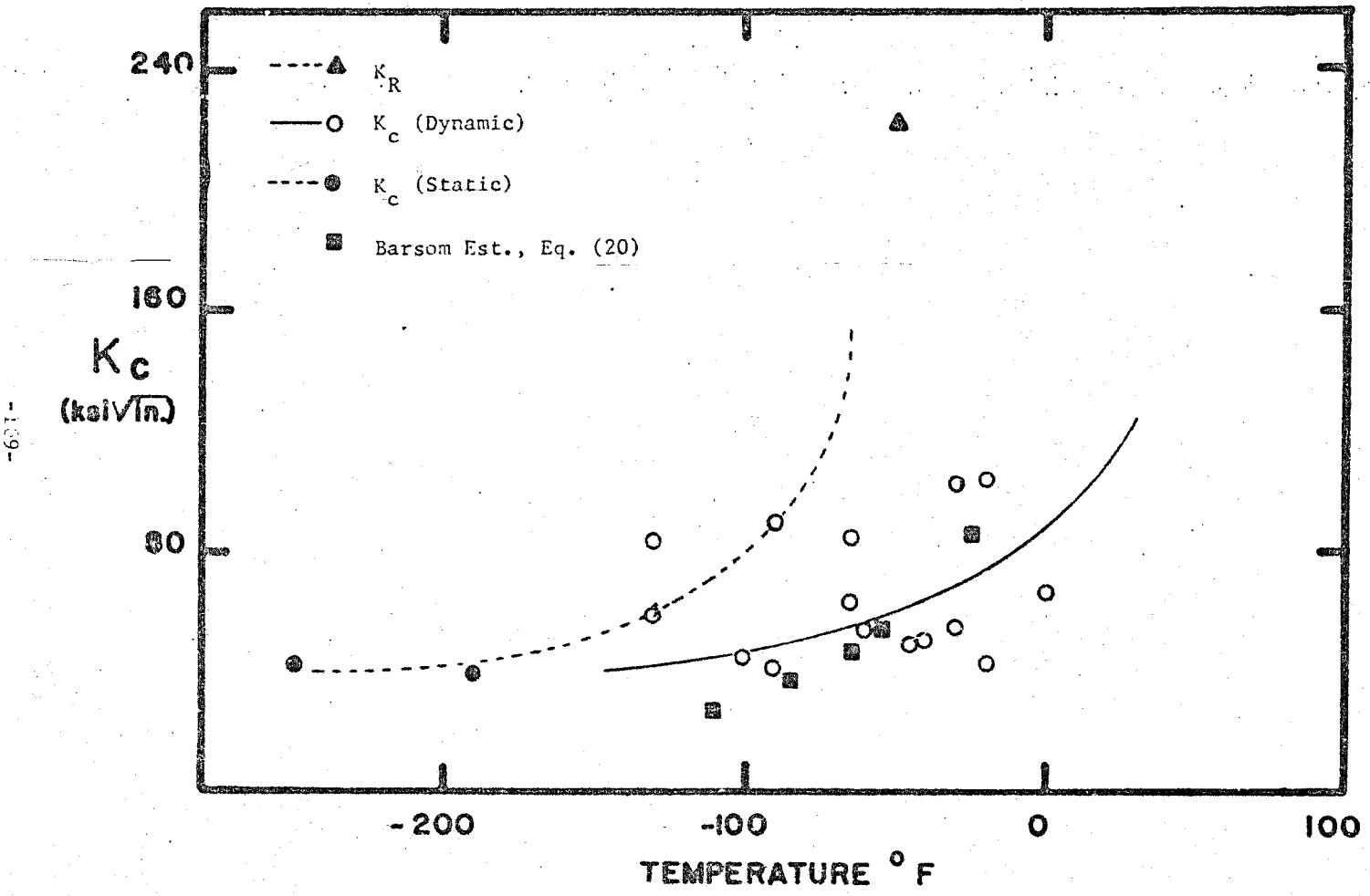

Fig. D-4 K_c Data for A242 1/2" Material

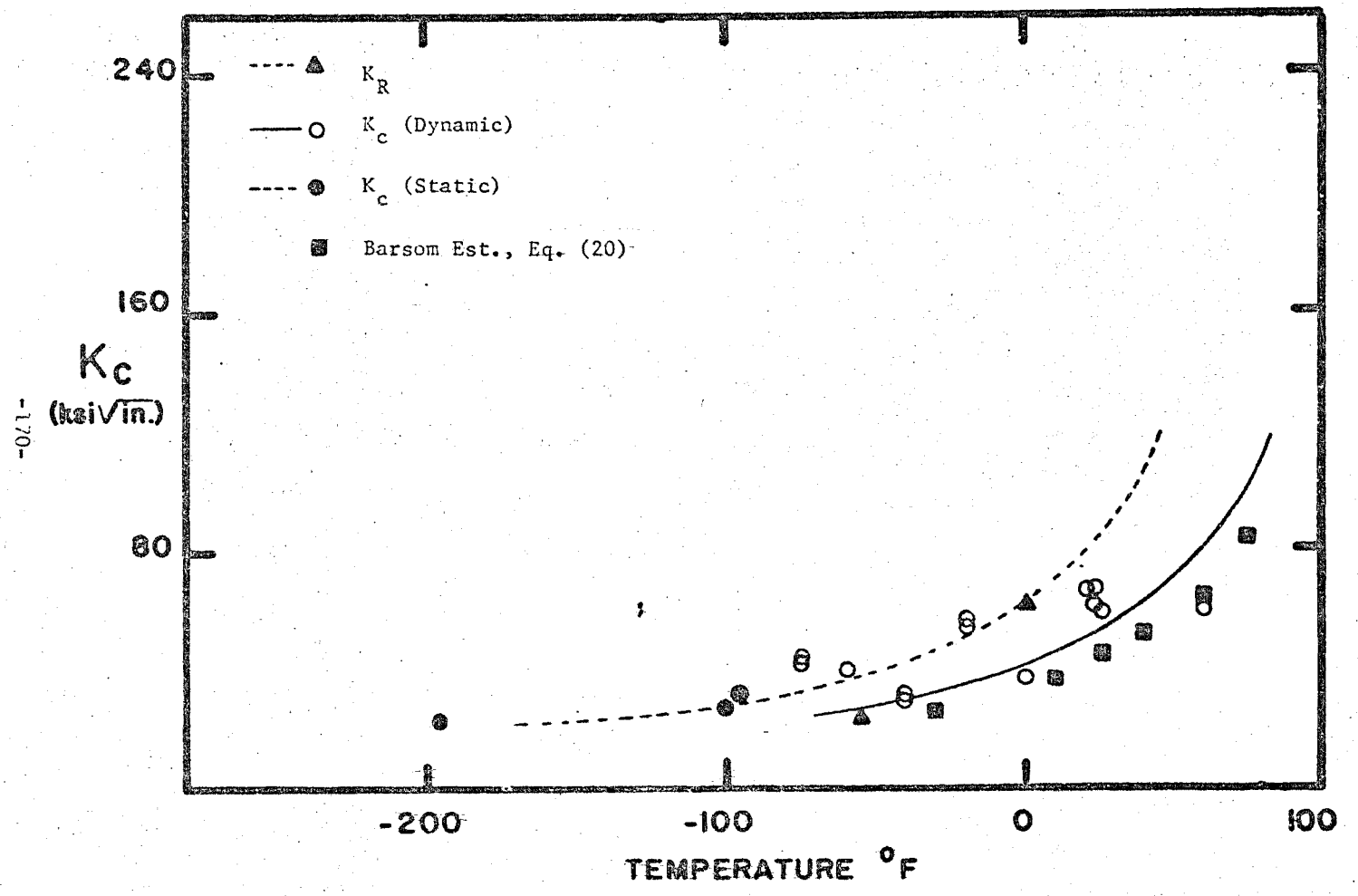

Fig. D-5 K_c Data for A242 1" Material

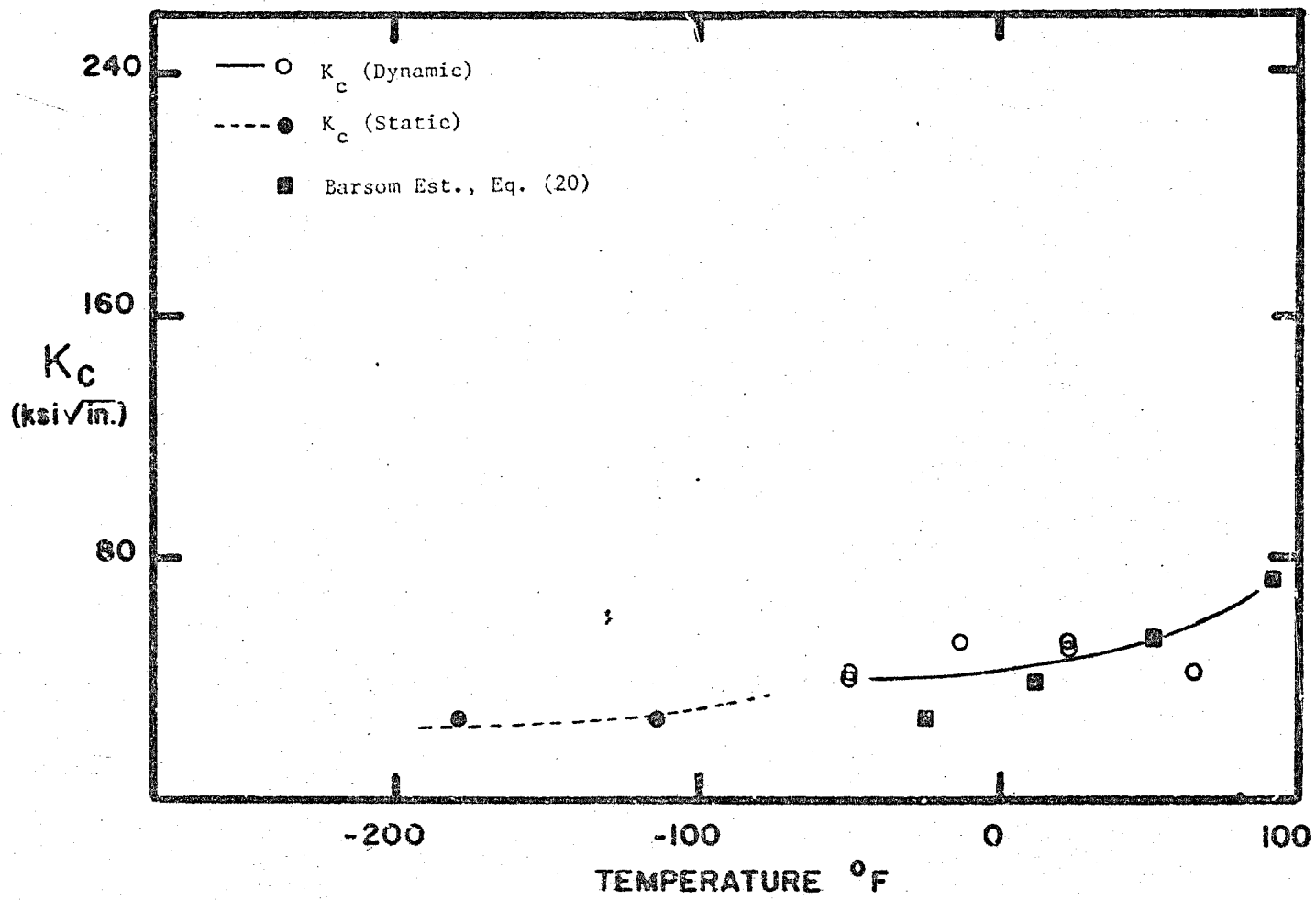

Fig. D-6 K_c Data for A242 2" Material

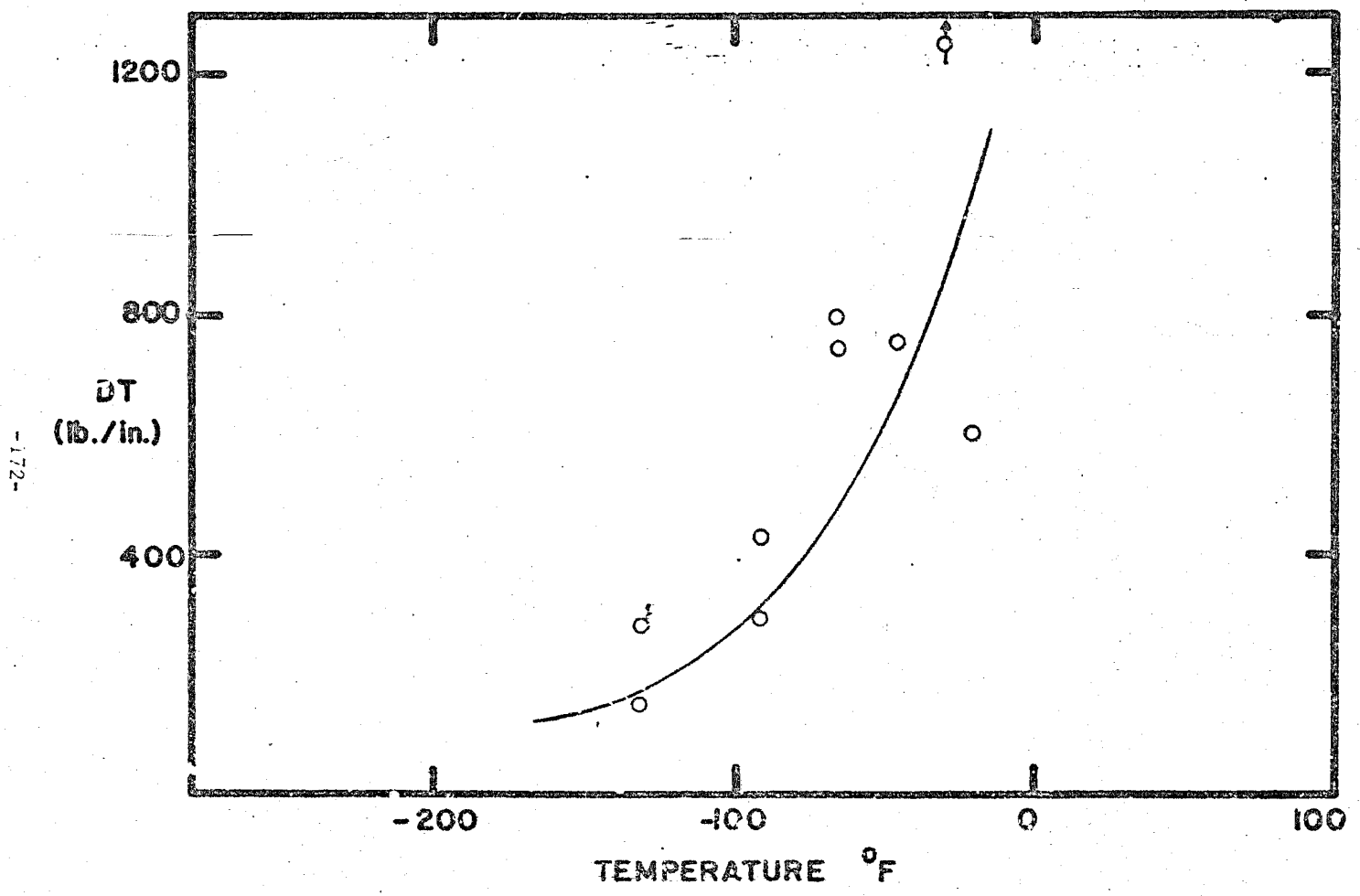

Fig. D-7 Dynamic Tear Data for A242 1/2" Material

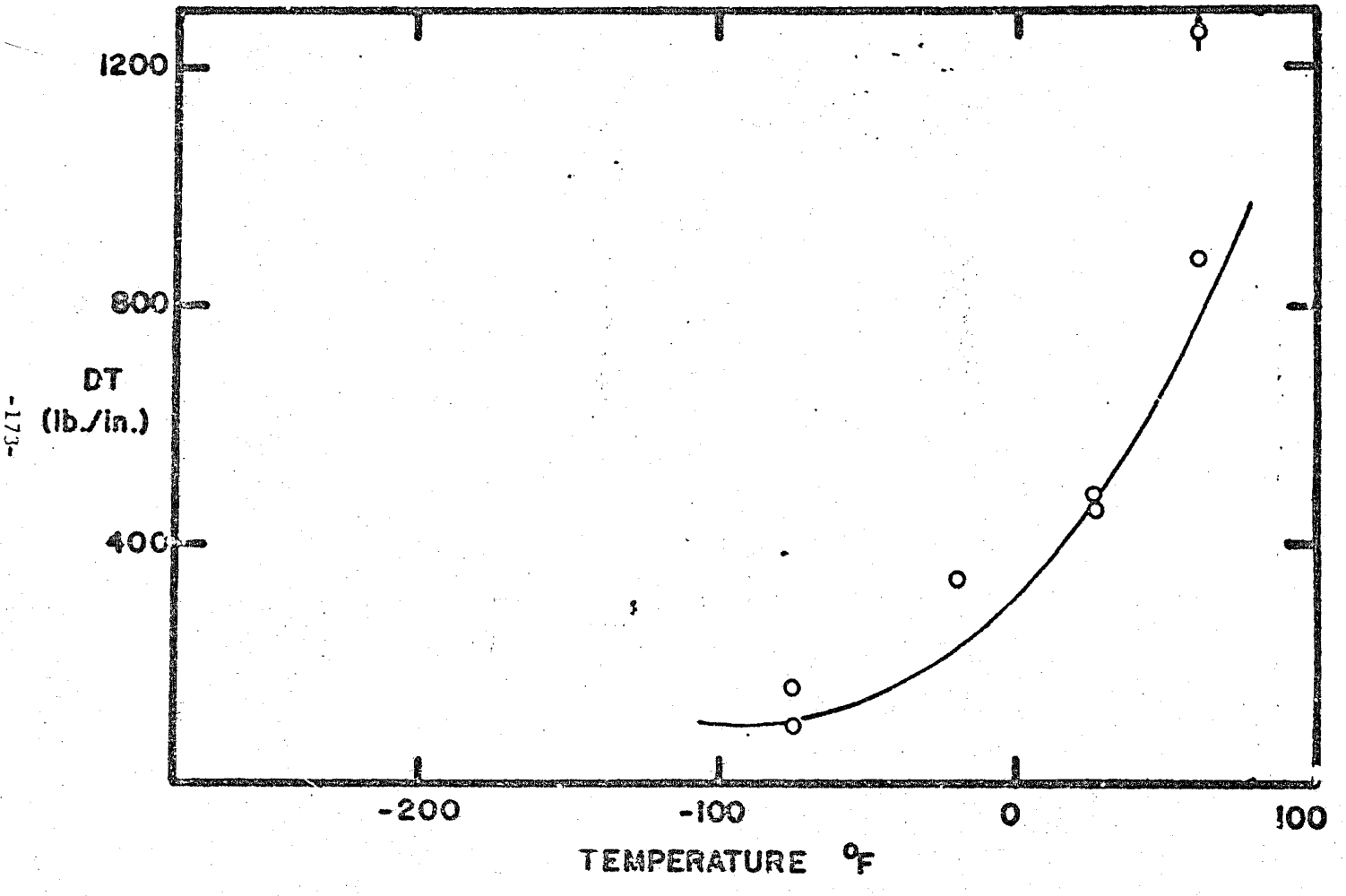

Fig. D-8 Dynamic Tear Data for A242 1" Material

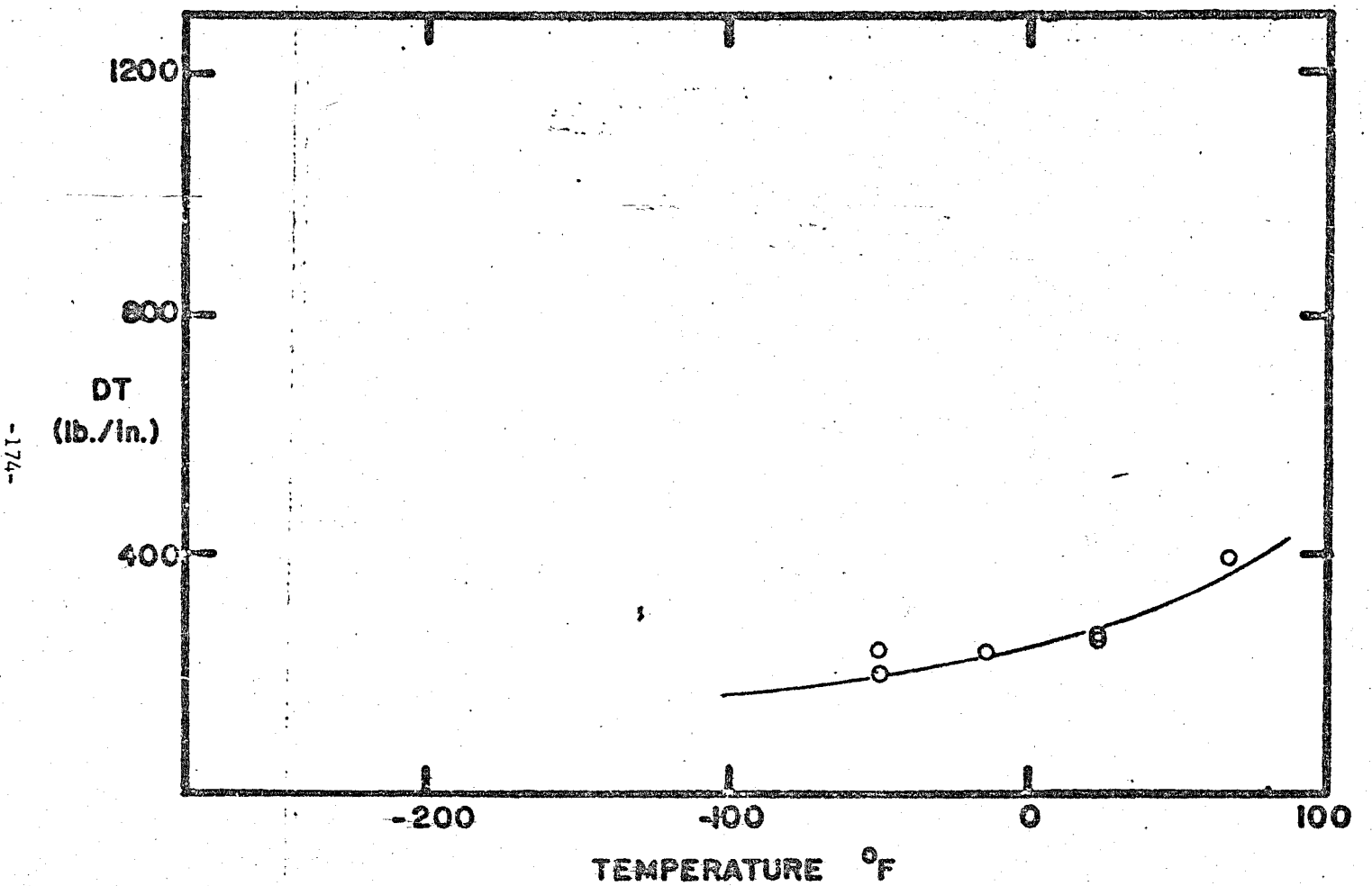

Fig. D-9 Dynamic Tear Data for A242 2" Material

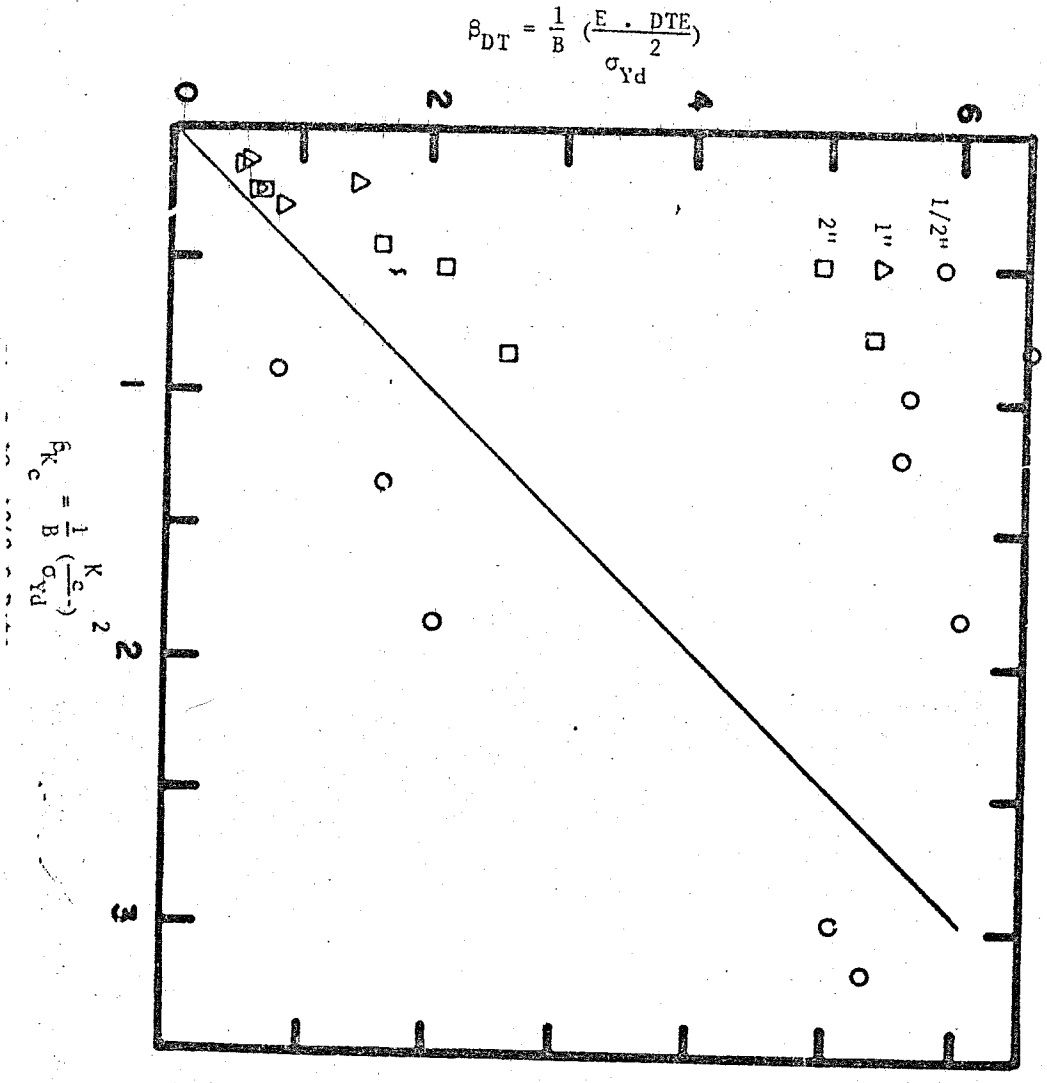
$\beta_{DT} = \frac{1}{B}\left(\frac{E \cdot DTE}{2}\right)$
σ_{Yd}
0
2
4
6
1/2"
1"
2"
1
2
3
$\beta_{K_c} = \frac{1}{B}\left(\frac{K_c}{\sigma_{Yd}}\right)^2$

TABLE D1.1* - A242 CHARPY DATA SUMMARY

Test	Material Thickness (in.)	T_{15} (°F)	T_{30} (°F)	T_{SH} (°F)	CVN_{SH} (ft.-lb.)
DS	0.5	- 365	- 40	> 100	> 120
SS	0.5	- 255	- 185	> 100	> 100
DS	1.0	25	60	> 200	> 90
SS	1.0	- 160	- 150	> 50	> 70
DS	2.0	35	75	200	88
SS	2.0	- 110	- 45	> 75	> 50

TABLE D1.2

Test	T	ΔT (°F)	ΔT_B (°F)
S	0.5	200	134
S	1.0	200	138
S	2.0	150	148

*See Table A1.1 for designations

TABLE D2 - CHARPY TEST DATA

A242 1/2" (Notched) Slow Bend

Specimen No.	Temp. (° F)	Maximum Load (lb.)	Deflection at Maximum Load (in.)	Crack-Depth (in.)	Energy Absorbed		Shear (%)	Lateral Expansion (mils)
					Actual (ft.-lb.)	Normalized (ft.-lb.)		
195-SN	- 320	2380	0.046	0.079	5.04	5.04	0	4
202-SN	- 255	3440	0.152	0.079	29.20	29.20	0	31
111-SN	- 150	3400	0.196	0.079	40.00	40.00	0	44
200-SN	- 185	3430	0.181	0.079	36.20	36.20	< 5	30
169-SN	- 100	3225	0.029	0.079	60.00	60.00	< 20	70
55-SN	- 50	3150	---	0.079	70.10	70.10	25	84
30-SN	+ 63	3000	0.240	0.079	100.80	100.80	100	92
475	- 190	3600	0.176	0.079	37.10	37.10	0	33
472	- 200	3490	0.101	0.079	21.28	21.28	0	22
481	- 150	3575	0.188	0.079	44.80	44.80	0	44
424	- 100	3450	0.260	0.079	54.45	54.45	< 5	56
504	- 100	3580	0.246	0.079	56.40	56.40	< 5	57
502	- 50	3400	0.270	0.079	55.38	55.38	< 5	55
450	0	3350	0.230	0.079	97.75	97.75	40	96
496	+ 70	3230	0.250	0.079	140.00	140.00	80	104

TABLE D2 - CHARPY TEST DATA

A242 1/2" (Notched) Fast Bend

Specimen No.	Temp. (° F)	Maximum Load (lb.)	Deflection at Maximum Load (in.)	Crack-Depth (in.)	Energy Absorbed		Shear (%)	Lateral Expansion (mils)
					Actual (ft.-lb.)	Normalized (ft.-lb.)		
457-FN	- 200	3100	---	0.079	---	---	0	10
456-FN	- 200	3130	0.040	0.079	8.70	8.70	0	6
406-FN	- 150	2900	0.080	0.079	15.55	15.55	0	16
407-FN	- 145	3320	0.120	0.079	27.90	27.90	0	37
369-FN	- 100	3450	0.192	0.079	44.82	44.82	0	36
372-FN	- 100	3700	0.164	0.079	42.41	42.41	< 5	38
370-FN	- 100	3350	0.164	0.079	38.32	38.32	0	48
330-FN	- 50	3460	0.250	0.079	84.00	84.00	< 10	62
331-FN	- 50	3400	0.230	0.079	65.00	65.00	15	82
284-FN	0	3325	0.240	0.079	77.93	77.93	15	78
285-FN	0	3330	0.248	0.079	89.41	89.41	20	86
251-FN	+ 50	3250	0.250	0.079	121.50	121.50	90	87
250-FN	+ 50	3200	0.248	0.079	106.10	106.10	90	92

TABLE D2 - CHARPY TEST DATA

A242 1/2" (Notched) Dynamic

Specimen No.	Temp. (° F)	Maximum Load (lb.)	Deflection at Maximum Load (in.)	Crack-Depth (in.)	Energy Absorbed		Shear (%)	Lateral Expansion (mils)
					Actual (ft.-lb.)	Normalized (ft.-lb.)		
	- 125			0.079	3.0	3.0	0	4
	- 75			0.079	9.0	9.0	0	9
	- 75			0.079	15.0	15.0	0	15
	- 50			0.079	25.5	25.5	< 5	27
	- 50			0.079	93.0	93.0	< 5	24
	0			0.079	77.0	77.0	10	73
	0			0.079	85.0	85.0	20	75
	+ 50			0.079	120.0	120.0	20	83
	+ 50			0.079	115.5	115.5	40	95
	+ 100			0.079	120.0	120.0	40	106

TABLD D2 - CHARPY TEST DATA

A242 1" (Notched) Slow Bend

Specimen No.	Temp. (° F)	Maximum Load (lb.)	Deflection at Maximum Load (in.)	Crack-Depth (in.)	Energy Absorbed		Shear (%)	Lateral Expansion (mils)
					Actual (ft.-lb.)	Normalized (ft.-lb.)		
182-SN	- 200	2470	0.068	0.079	10.18	10.18	0	9
89-SN	- 135	2500	0.094	0.079	13.23	13.23	0	18
56-SN	- 50	2800	0.210	0.079	37.70	37.70	< 10	48
38-SN	+ 40	2750	0.240	0.079	68.20	68.20	100	71
31-SN	+ 63	2650	0.204	0.079	52.71	52.71	65	70
476	- 200	2060	0.026	0.079	2.40	2.40	0	4
473	- 200	2300	0.034	0.079	3.80	3.80	0	5
482	- 150	3150	0.136	0.079	26.61	26.61	< 5	34
484	- 135	3675	0.180	0.079	41.23	41.23	< 5	39
425	- 100	2800	0.143	0.079	23.36	23.36	0	40
505	- 100	3180	0.246	0.079	56.40	56.40	< 5	45
503	- 50	3000	0.200	0.079	27.50	27.50	< 5	42
451	- 5	3000	0.210	0.079	51.16	51.16	< 15	59
497	+ 68	2855	0.140	0.079	56.60	56.60	100	85

TABLE D2 - CHARPY TEST DATA

A242 1" (Notched) Fast Bend

Specimen No.	Temp. (° F)	Maximum Load (lb.)	Deflection at Maximum Load (in.)	Crack-Depth (in.)	Energy Absorbed		Shear (%)	Lateral Expansion (mils)
					Actual (ft.-lb.)	Normalized (ft.-lb.)		
459-FN	- 200	2980	0.036	0.079	7.35	7.35	0	6
458-FN	- 200	2100	0.024	0.079	3.10	3.10	0	3
462-FN	- 200	2050	0.035	0.079	3.66	3.66	0	4
409-FN	- 156	2075	0.035	0.079	4.10	4.10	0	6
408-FN	- 162	2250	0.036	0.079	4.50	4.50	0	6
371-FN	- 100	2670	0.094	0.079	17.55	17.55	0	20
333-FN	- 50	3000	0.190	0.079	44.00	44.00	< 10	48
332-FN	- 50	3050	0.185	0.079	36.15	36.15	< 10	40
286-FN	0	2950	0.220	0.079	44.80	44.80	< 10	50
287-FN	0	2950	0.224	0.079	46.00	46.00	< 10	52
252-FN	+ 50	2860	0.212	0.079	69.80	69.80	100	76
253-FN	+ 50	2820	0.230	0.079	68.20	68.20	100	78

TABLE D2 - CHARPY TEST DATA

A242 1" (Notched) Dynamic

Specimen No.	Temp. (°F)	Maximum Load (lb.)	Deflection at Maximum Load (in.)	Crack-Depth (in.)	Energy Absorbed		Shear (%)	Lateral Expansion (mils)
					Actual (ft.-lb.)	Normalized (ft.-lb.)		
	- 50			0.079	5.0	5.0	0	9
	0			0.079	12.0	12.0	0	18
	0			0.079	8.0	8.0	0	6
	+ 50			0.079	15.0	15.0	< 5	19
	+ 50			0.079	36.0	36.0	0	43
	+ 100			0.079	63.0	63.0	45	45
	+ 100			0.079	71.0	71.0	50	60
	+ 150			0.079	93.0	93.0	95	77
	+ 150			0.079	92.5	92.5	95	71
	+ 212			0.079	94.0	94.0	100	76

TABLE D2 - CHARPY TEST DATA

A242 2" (Notched) Slow Bend

Specimen No.	Temp. (° F)	Maximum Load (lb.)	Deflection at Maximum Load (in.)	Crack-Depth (in.)	Energy Absorbed		Shear (%)	Lateral Expansion (mils)
					Actual (ft.-lb.)	Normalized (ft.-lb.)		
187-SN	- 200	2370	0.037	0.079	2.60	2.60	0	4
90-SN	- 135	2500	0.074	0.079	9.80	9.80	0	17
57-SN	- 50	2425	0.182	0.079	26.80	26.80	0	32
49-SN	- 10	2875	0.172	0.079	30.00	30.00	< 10	39
32-SN	+ 63	2850	0.195	0.079	60.40	60.40	100	73
477	- 200	2750	0.060	0.079	5.40	5.40	0	11
474	- 200	2300	0.027	0.079	2.84	2.84	0	5
483	- 150	2850	0.076	0.079	12.04	12.04	0	16
506	- 100	3350	0.148	0.079	30.00	30.00	0	32
426	- 100	3120	0.162	0.079	25.40	25.40	0	30
507	- 60	2960	0.103	0.079	18.60	18.60	0	24
452	0	3200	0.168	0.079	34.03	34.03	< 10	41
498	+ 68	2980	0.140	0.079	56.60	56.60	80	61

TABLE D2 - CHARPY TEST DATA

A242 2" (Notched) Fast Bend

Specimen No.	Temp. (° F)	Maximum Load (lb.)	Deflection at Maximum Load (in.)	Crack-Depth (in.)	Energy Absorbed		Shear (%)	Lateral Expansion (mils)
					Actual (ft.-lb.)	Normalized (ft.-lb.)		
460	- 200	2600	0.028	0.079	3.90	3.90	0	4
461	- 200	2250	0.027	0.079	3.70	3.70	0	4
410	- 150	2570	0.041	0.079	7.00	7.00	0	10
411	- 150	2420	0.038	0.079	5.60	5.60	0	8
373	- 100	2630	0.070	0.079	11.35	11.35	0	14
374	- 100	2750	0.068	0.079	10.35	10.35	0	14
334	- 50	2900	0.100	0.079	19.30	19.30	0	21
335	- 50	2900	0.105	0.079	19.25	19.25	0	22
288	0	3150	0.144	0.079	30.49	30.49	< 5	35
289	0	3030	0.166	0.079	23.28	23.28	< 5	23
254	+ 50	3150	0.172	0.079	49.39	43.39	20	55
255	+ 50	2900	0.160	0.079	51.24	51.24	70	65

TABLE D2 - CHARPY TEST DATA

A242 2" (Notched) Dynamic

Specimen No.	Temp. (° F)	Maximum Load (lb.)	Deflection at Maximum Load (in.)	Crack-Depth (in.)	Energy Absorbed		Shear (%)	Lateral Expansion (mils)
					Actual (ft.-lb.)	Normalized (ft.-lb.)		
	- 50			0.079	3.0	3.0	0	5
	0			0.079	8.0	8.0	0	13
	0			0.079	4.0	4.0	0	9
	+ 50			0.079	20.0	20.0	0	27
	+ 50			0.079	32.0	32.0	< 5	31
	+ 100			0.079	52.0	52.0	40	69
	+ 100			0.079	42.5	42.5	20	55
	+ 150			0.079	88.0	88.0	95	74
	+ 150			0.079	80.0	80.0	100	70
	+ 212			0.079	85.0	85.0	100	74

TABLE D3.1* - A242 K_c DATA

A242 1/2"

Nominal Yield Strength YS = 53.9 ksi

Specimen No.	B (in.)	Temp. (°F)	A_o (in.)	F.A. ($in.^2$)	$P_{max.}$ (kips)	Time (sec)	K_c (ksi/in.)	G (lb/in)	DTE (lb/in)	β_{K_c}	β_{DT}	σ_{YD} (ksi)
3.001	0.5	- 130	0.965	1.017	10.5	7.5E-04	68.71	159.5	141.5	0.924	0.820	101.1
3.002	0.5	- 130	1.280	0.860	9.2	8.0E-04	83.39	235.0	279.1	1.368	1.625	100.8
3.007	0.5	- 100	0.900	1.050	7.3	7.5E-04	43.36	63.5	0.0	0.418	0.000	94.8
3.010	0.5	- 90	1.140	0.930	5.5	8.0E-04	40.23	54.7	425.8	0.377	2.935	92.7
3.014	0.5	- 90	1.180	0.910	10.5	8.0E-04	89.70	271.8	290.1	1.874	2.000	92.7
3.003	0.5	- 65	1.050	0.975	8.8	8.0E-04	62.38	131.5	738.5	0.995	5 590	88.4
3.004	0.5	- 65	1.120	0.940	10.6	8.0E-04	85.42	246.5	791.5	1.866	5.992	88.4
3.012	0.5	- 45	0.960	1.020	7.6	6.0E-04	48.07	78.1	752.9	0.618	5.964	86.4
3.013	0.5	- 60	0.760	1.120	9.8	8.0E-04	53.00	94.9	0.0	0.731	0.000	87.6
3.018	0.5	- 40	1.010	0.995	7.5	5.5E-04	50.12	84.9	0.0	0.679	0.000	86.0
3.016	0.5	- 40	1.780	0.610	5.0	5.0E-04	0.00	0.0	0.0	0.000	0.000	86.4
3.009	0.5	- 30	1.085	0.957	7.6	6.0E-04	54.55	100.5	1416.2	0.837	11.788	84 3
3.015	0.5	- 20	1.120	0.940	11.6	8.0E-04	103.70	363.3	600.0	3.197	5.280	82.0
3.017	0.5	- 20	0.800	1.100	7.5	4.5E-04	41.11	57.1	0.0	0.479	0 000	84.0
3.005	0.5	0	0.850	1.075	10.8	7.5E 04	66.00	147.2	0.0	1.368	0.000	79.8
Slow Bend Test												
3.011	0.5	- 254	0.870	1.065	7.5	3.0E-01	42.96	62.4	0.0	0.279	0.000	115.0
3.006	0.5	- 190	1.030	0.985	5.9	3.5E-01	39.02	51.4	0.0	0.351	0.000	93.2

*See Table A3 for designations

TABLE D3.2* - A242 K_c DATA

A242 1"

Nominal Yield Strength YS = 50.9 ksi

Specimen No.	B (in.)	Temp. (°F)	A_o (in.)	F.A. ($in.^2$)	P_{max} (kips)	Time (sec)	K_c (ksi$\sqrt{in.}$)	G (lb/in)	DTE (lb/in)	β_{K_c}	β_{DT}	σ_{YD} (ksi)
3.101	1.0	- 75	0.880	2.120	14.7	9.0E-04	43.37	63.5	96.2	0.251	0.380	86.6
3.102	1.0	- 75	0.980	2.020	13.9	9.0E-04	44.65	67.4	154.5	0.266	0.609	86.6
3.113	1.0	- 40	0.980	2.020	10.0	7.5E-04	31.61	33.8	0.0		0.000	81.9
3.116	1.0	- 60	1.360	1.640	8.7	5.5E-04	39.37	52.4	0.0	0.209	0.000	86.1
3.115	1.0	- 40	0.990	2.010	9.5	6.0E-04	30.05	30.5	0.0	0.132	0.000	82.7
3.107	1.0	- 20	0.900	2.100	17.5	7.0E-04	54.12	98.9	337.1	0.464	1.580	79.5
3.114	1.0	- 20	1.000	2.000	16.5	6.0E-04	55.79	105.2	0.0	0.486	0.000	80.0
3.117	1.0	--	0.880	2.120	12.6	5.0E-04	37.00	46.3	0.0	0.224	0.000	78.1
3.111	1.0	--	0.900	2.100	15.0	8.0E-04	0.00	0.0	0.0	0.000	0.000	31.0
3.103	1.0	26	0.960	2.040	18.0	1.0E-03	60.51	123.7	458.8	0.686	2.545	73.0
3.112	1.0	25	0.910	2.090	20.7	6.0E-04	67.96	156.0	0.0	0.827	0.000	74.7
3.110	1.0	25	0.860	2.140	20.0	7.5E-04	61.73	128.7	0.0	0.696	0.000	74.0
3.104	1.0	26	0.930	2.070	20.5	7.5E-04	68.90	160.4	475.4	0.869	2.576	73.9
3.118	1.0	60	0.925	2.075	18.5	1.0E-03	60.97	125.6	873.3	0.763	5.309	69.8
3.106	1.0	60	0.920	2.080	25.0	8.0E-04	96.02	311.5	1603.8	1.860	9.579	70.4
Slow Bend Test												
3.109	1.0	- 195	0.940	2.060	7.5	3.0E-01	22.23	16.7	0.0	0.058	0.000	91.9
3.108	1.0	- 100	0.945	2.055	8.5	4.0E-01	25.94	22.7	0.0	0.126	0.000	73.0
3.105	1.0	- 95	0.925	2.075	11.0	8.0E-01	33.56	38.1	0.0	0.224	0.000	70.9

*See Table A3 for designations

TABLE D3.3* - A242 K_c DATA

A242 2"

Nominal Yield Strength YS = 45.0 ksi

Specimen No.	B (in.)	Temp. (°F)	A_o (in.)	F.A. ($in.^2$)	P_{max} (kips)	Time (sec)	K_c (ksi/in.)	G (lb/in)	DTE (lb/in)	β_{K_c}	β_{DT}	σ_{YD} (ksi)
3.202	2.0	- 50	0.980	4.040	26.2	7.5E-04	42.41	60.8	203.5	0.150	0.502	77.5
3.205	2.0	- 50	0.940	4.120	25.8	7.5E-04	40.08	54.3	238.8	0.134	0.589	77.5
3.207	2.0	- 15	0.960	4.080	31.2	8.0E-04	51.04	88.0	235.3	0.248	0.663	72.5
3.201	2.0	23	0.935	4.130	33.2	9.5E-04	54.29	99.6	252.8	0.322	0.818	67.6
3.208	2.0	23	0.795	4.410	34.7	9.5E-04	49.56	83.0	253.1	0.269	0.819	67.6
3.210	2.0	65	0.900	4.200	27.5	9.5E-04	42.40	60.7	388.6	0.222	1.423	63.6
3.203	2.0	60	2.100	1.800	18.7	3.0E-04	0.00	0.0	000.0	0.000	0.000	67.4
Slow Bend Tests												
3.204	2.0	- 180	1.150	3.700	15.0	3.0E-01	27.21	25.0	0.0	0.055	0.000	82.3
3.206	2.0	- 114	0.990	4.020	17.0	3.0E-01	27.10	24.8	0.0	0.075	0.000	69.8

*See Table A3 for designations

TABLE D4 - A242 R-CURVE INSTABILITY SUMMARY

Thickness (in.)	Test Temperature (^{o} F)	Fatigue Crack Length (in.)	K_c at Instability (psi)	Apparent Crack Length at Instability (in.)
1	0	6.30	62,096	6.30
1	- 55	6.27	24,049	6.28
0.5 *	0			
0.5	- 50	6.30	224,934	7.57
0.5**	80			

*Test record lost

**Plastic failure of specimen - no crack extension

APPENDIX E - A440 DATA

This appendix contains the data collected for the 1/2", 1" and 2" thicknesses of the A440 material. This steel was supplied to the program by the Bethlehem Steel Corporation. The chemical analysis, physical properties and heat designations appear in Tables 1 and 2.

The data in this appendix is presented in the form of a Charpy summary, a detailed Charpy tabulation, a K_c tabulation, an R-curve summary and appropriate figures which best illustrate the data trends. Details of the test procedures and terminology can be found in appendices J, K, and L and Chapter 2.

Standard and precracked Charpy specimens were tested for all three thicknesses of the A440 material. CVN curves are presented in Figures E-1 through E-6. A summary of the Charpy results is given in Table E-1 and the individual data can be found in Table E-2. When tested, there was no apparent difference between slow and fast Charpy results for both standard and precracked specimens. This is typical of the results for the other material tested in this program. There was a definite shift for the slow and dynamic tests of the standard and precracked specimens. The 1/2" and 1" standard results were in line with Barsom's results (28) while the 2" data gave a larger than predicted temperature shift. The results for all of the precracked specimens show a smaller shift than expected. This result was typical for all materials

tested. The dynamic precracked data all fell to the right of the standard dynamic data. The precracked data did not form a lower bound for the standard CVN tests. With regard to the high temperature shift for the standard 2" CVN data there does not appear to be any clear explanation for these results.

K_c and D.T. tests were run on the three thicknesses of the A440 material. These results are shown in Figures E-7 through E-9 and the data as tabulated in Table F-3. For the three thicknesses, the dynamic K_c, the D.T. data and the standard CVN data all showed a temperature transition at about the same temperature for each thickness. There appeared to be a temperature shift between the static K_c and the dynamic K_c curves. This shift for all three thicknesses was approximately what would be expected from Barsom's work (28). This fact is interesting in view of the high shift temperature for the 2" CVN data. The K_c data does not show such a high shift but rather a value typical of expected levels. With regard to K_c predictions from CVN data by using

$$K_{Ic} = \sqrt{A \Sigma CVN}$$

this type of correlation works if A is taken as about 20 for the 1/2" material and 7 for the 1" and 2" data. The A value for the 1" and 2" material is close to Barsom's recommended level of 5. Figure E-10 shows β_{DT} plotted against β_{K_c}. This figure shows a fair correlation for K_c and D.T. for β_{K_c} less than 1. This result is similar to those found for the other materials tested.

R-curves were run for the 1/2" and 1" materials. For two of the 1/2" specimens no crack growth was observed and the specimens failed due to plastic buckling. For the remaining tests there was not any stable crack growth. All growth was unstable and led to complete failure of the specimens. For two of the plates, one 1" and one 1/2", crack velocities were great enough for crack branching. The K levels predicted from the R-curve tests are plotted in Figure E-7 and E-8. These results point to the usefulness of the R-curve specimens in extending the static K_c data to higher temperatures.

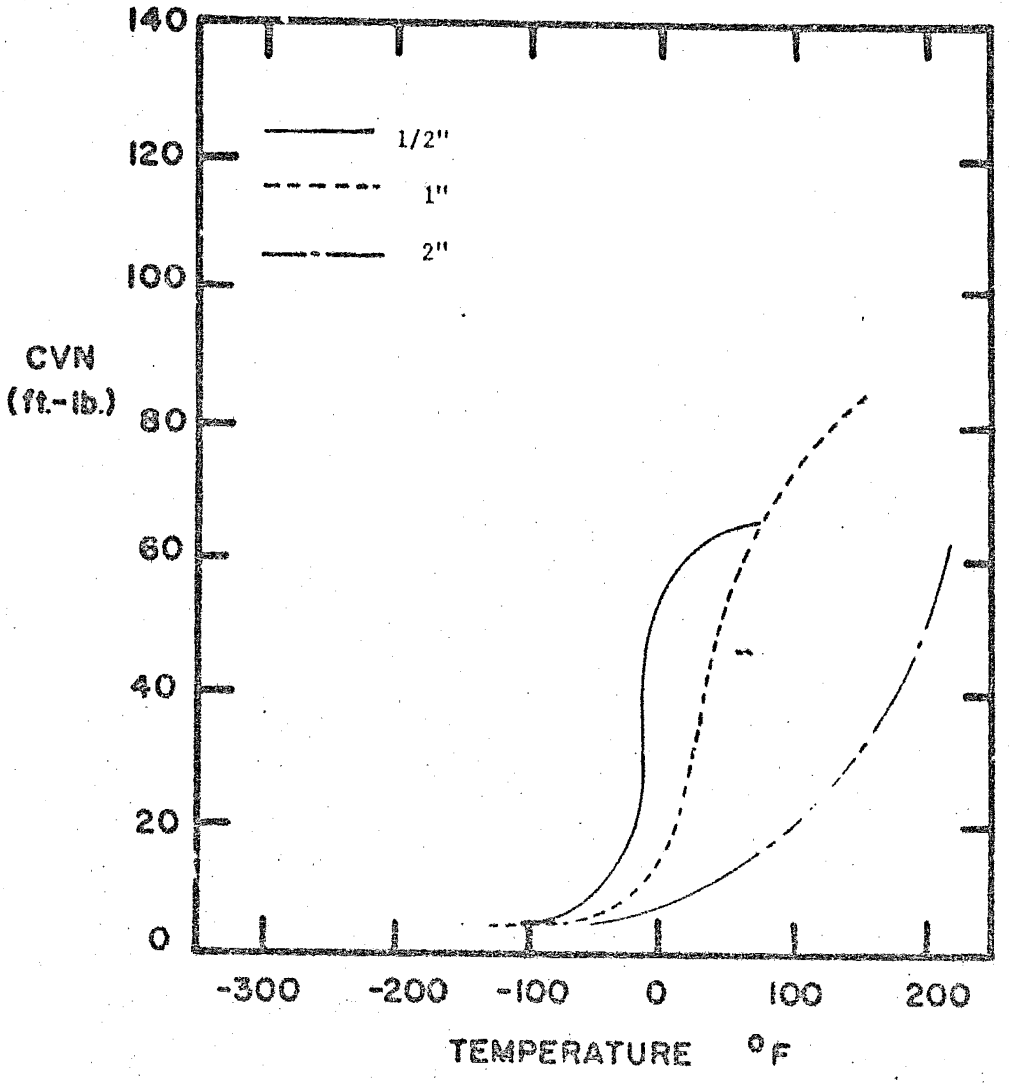

Fig. E-1a Composite Charpy Curves for A440 Material

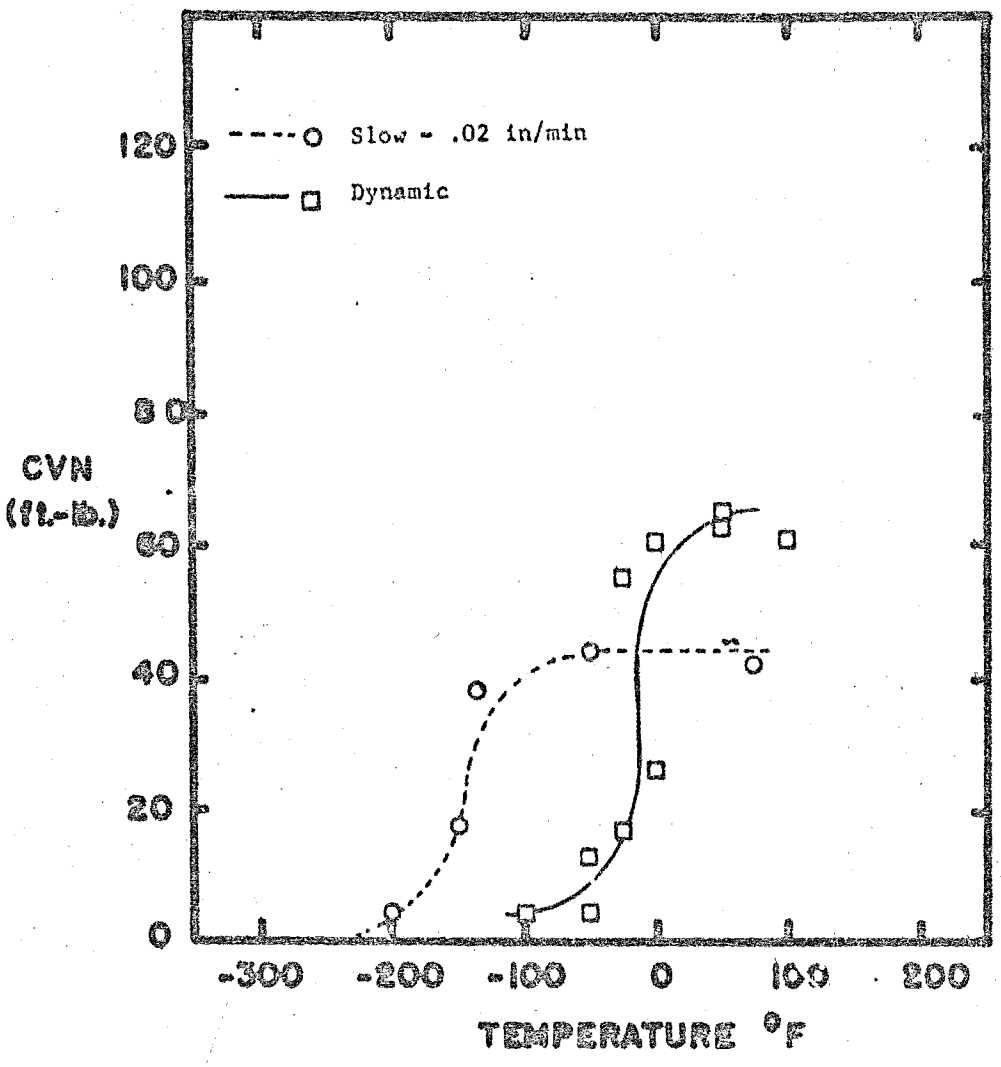

Fig. E-1 A440 1/2" Notched Charpy Data for Two Loading Rates

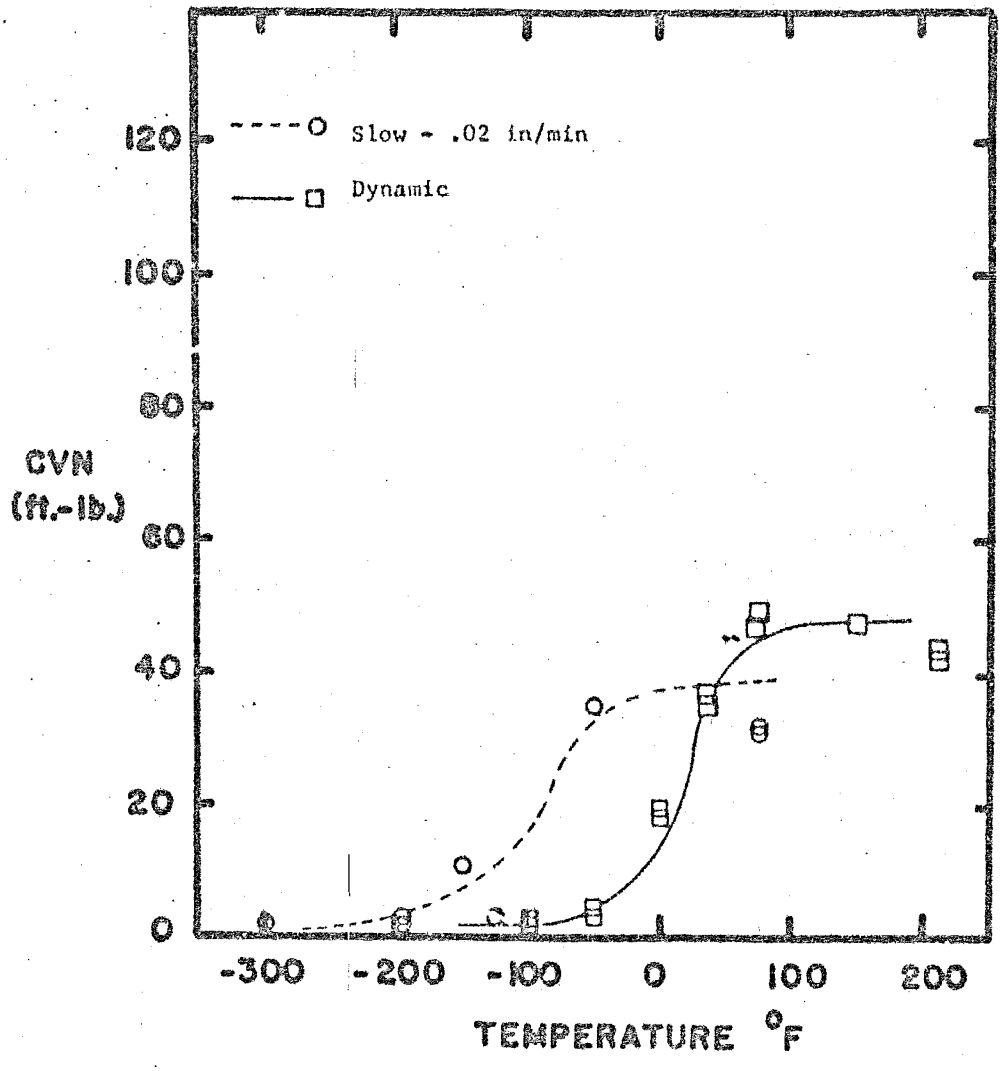

Fig. E-2 A440 1/2" Precracked Charpy Data for Two Loading Rates

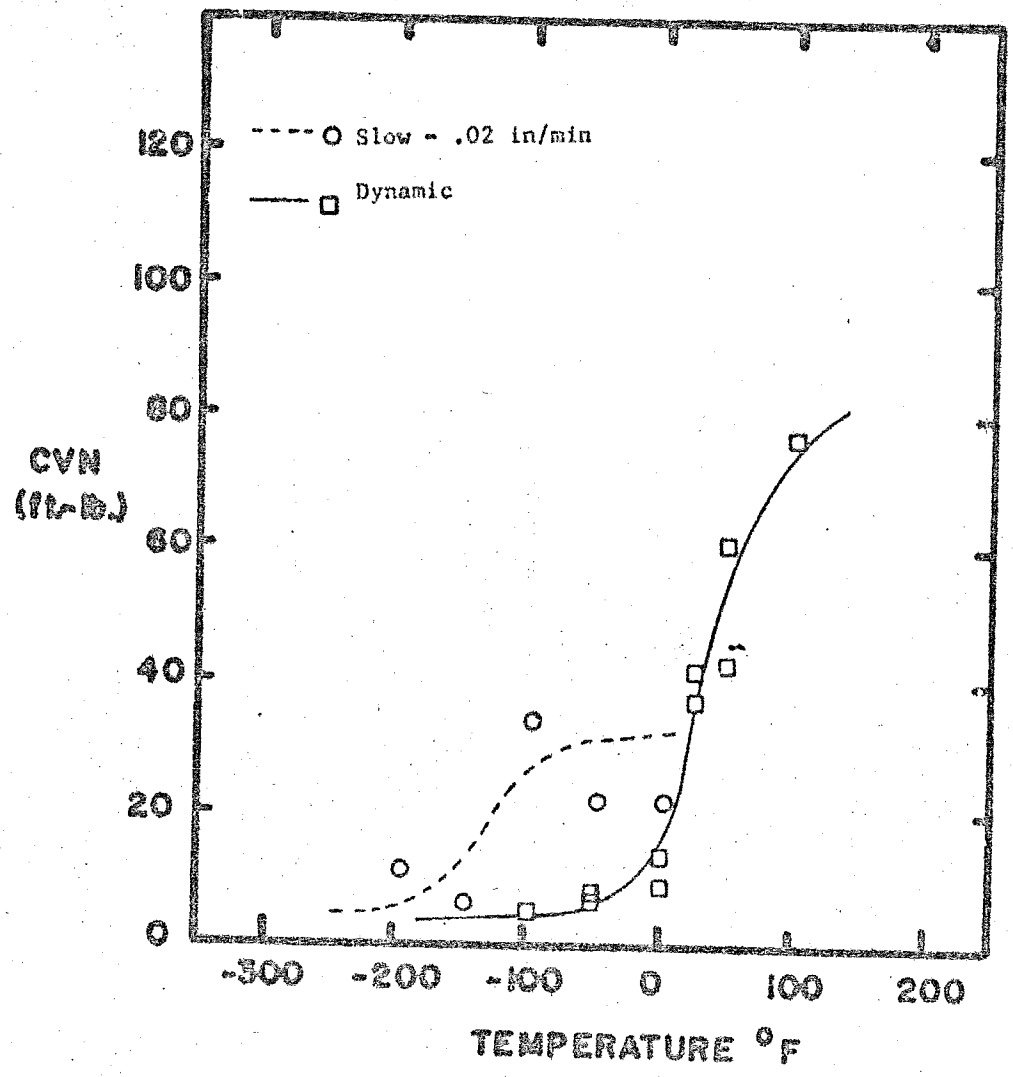

Fig. E-3 A440 1" Notched Charpy Data for Two Loading Rates

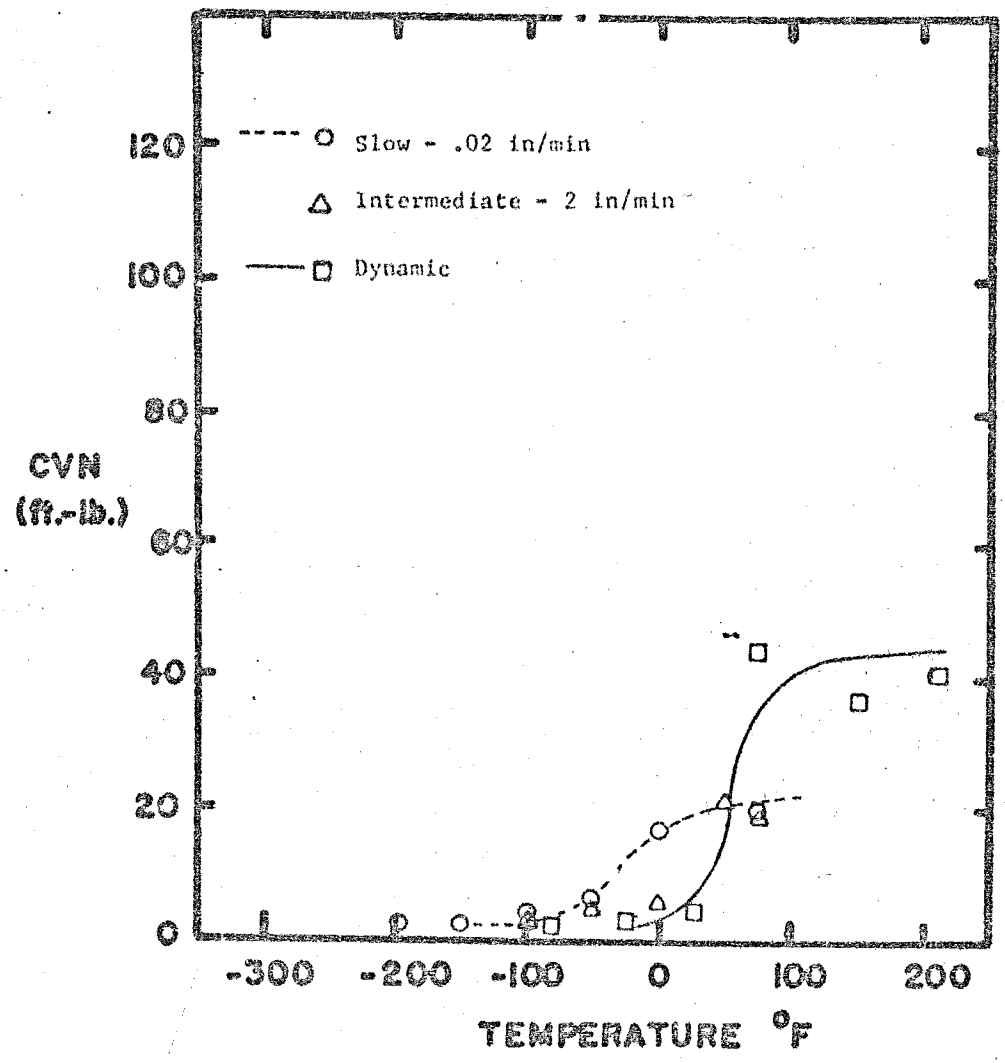

Fig. E-4 A440 1" Precracked Charpy Data for Three Loading Rates

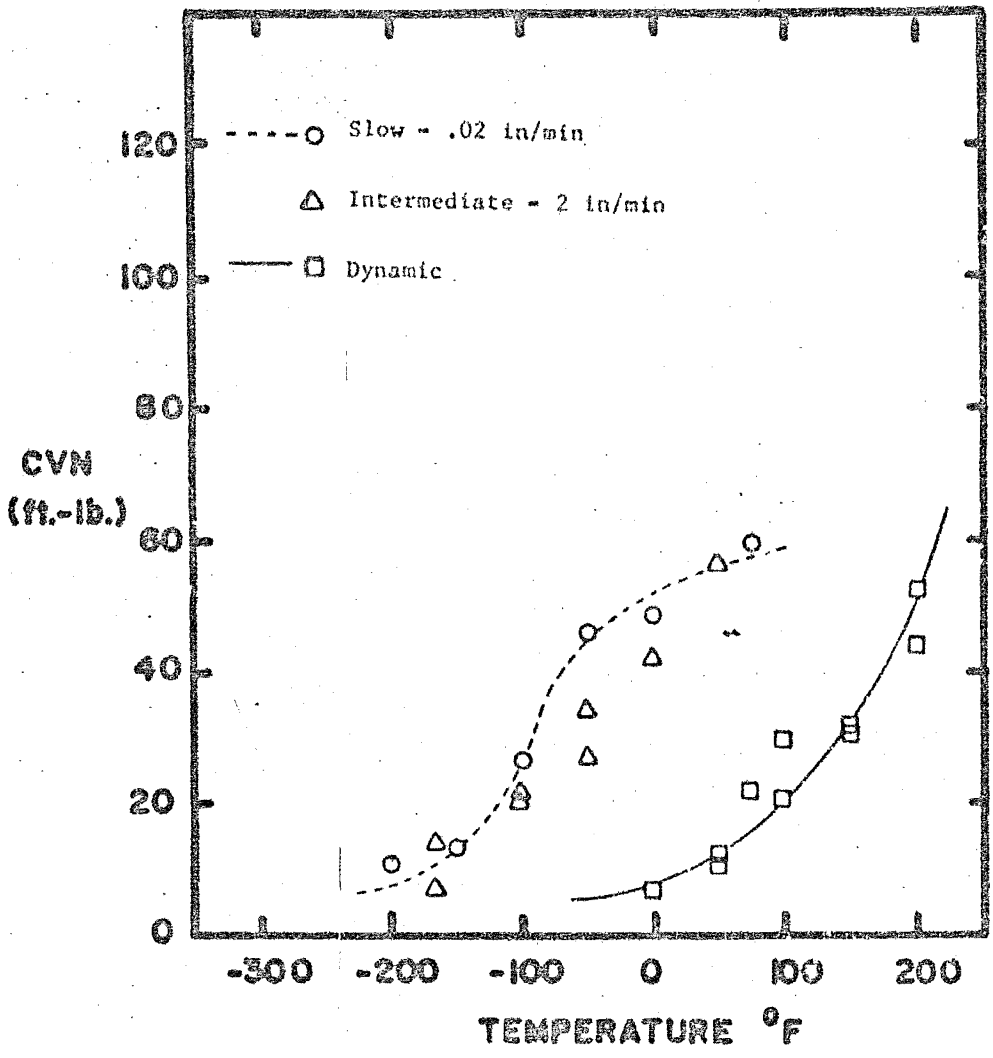

Fig. E-5 A440 2" Notched Charpy Data for Three Loading Rates

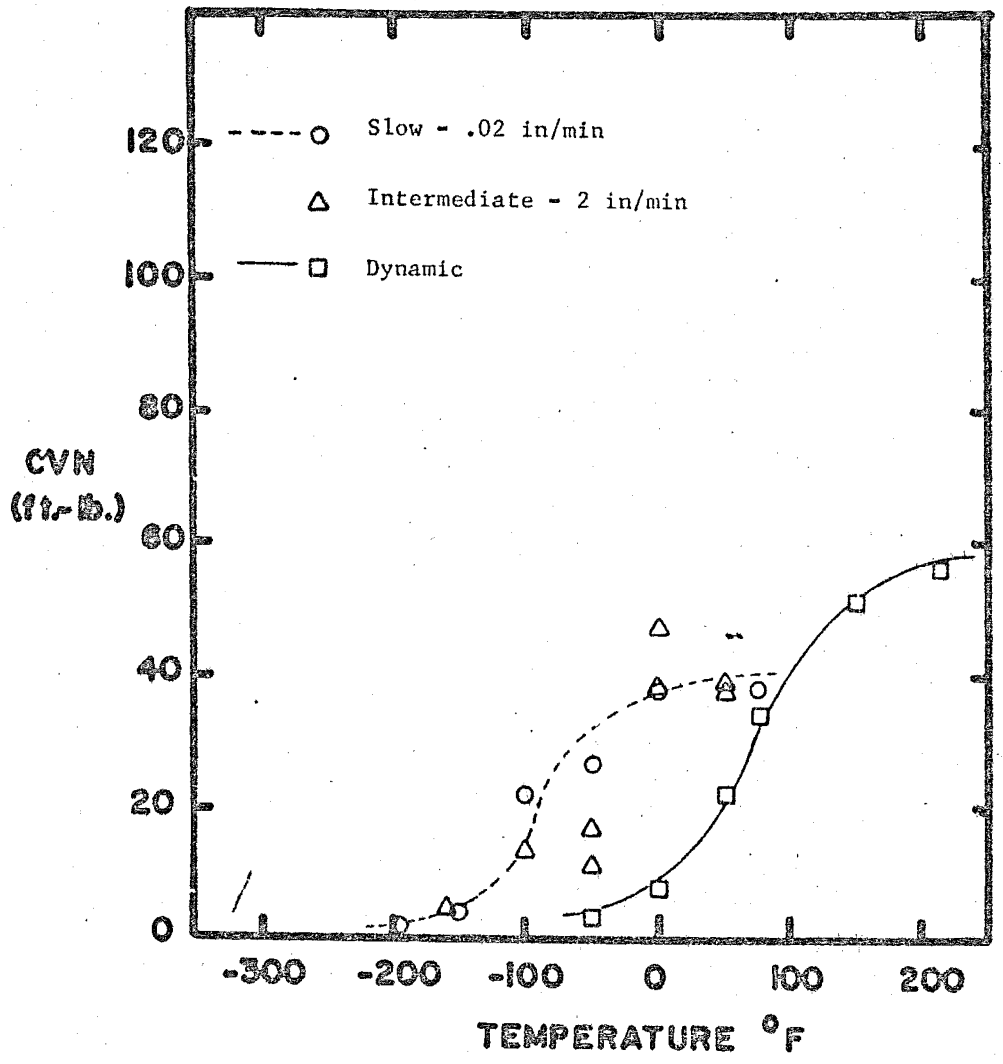

Fig. E-6 A440 2" Precracked Charpy Data for Three Loading Rates

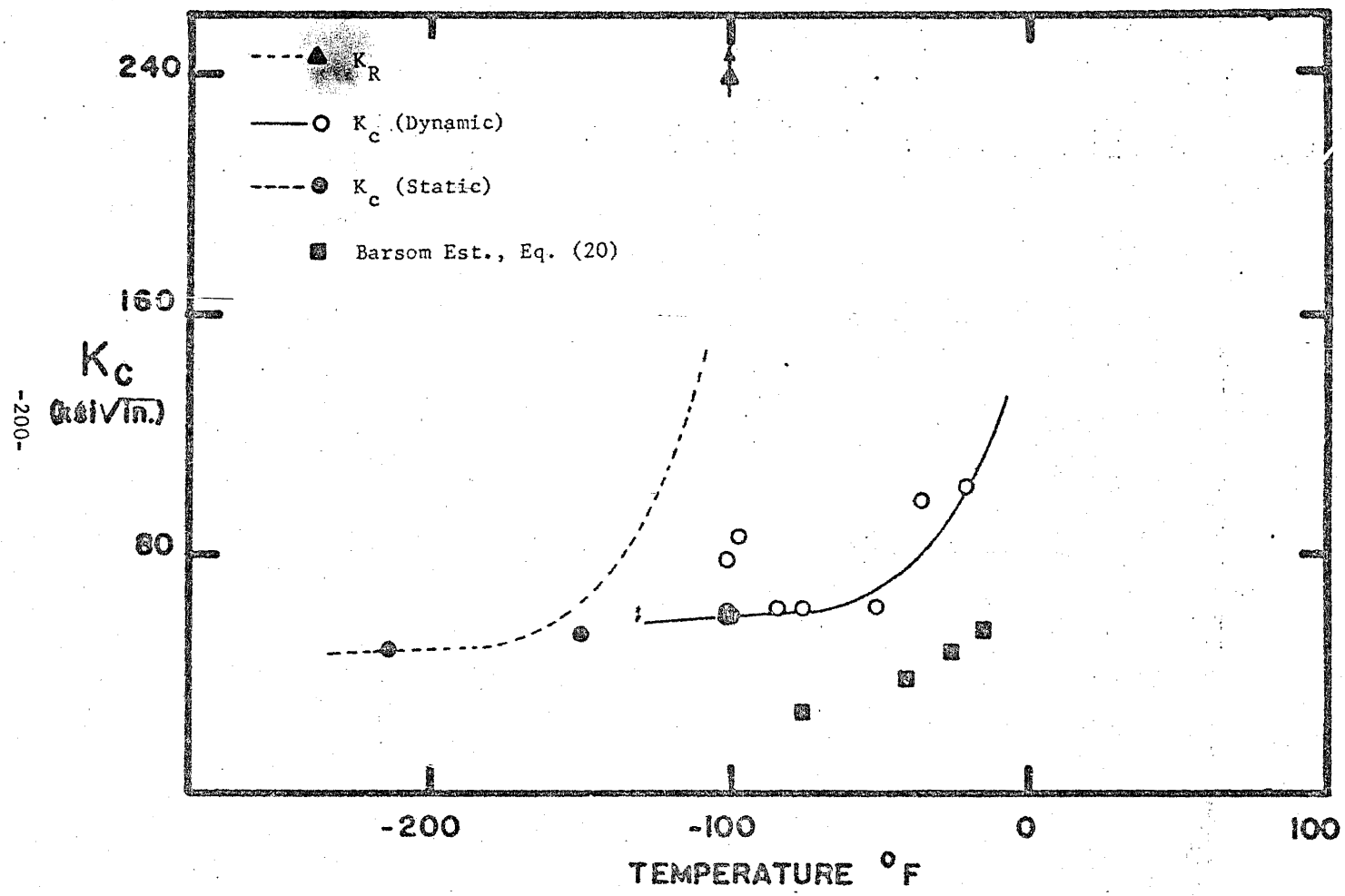

Fig. E-7 K_c Data for A440 1/2" Material

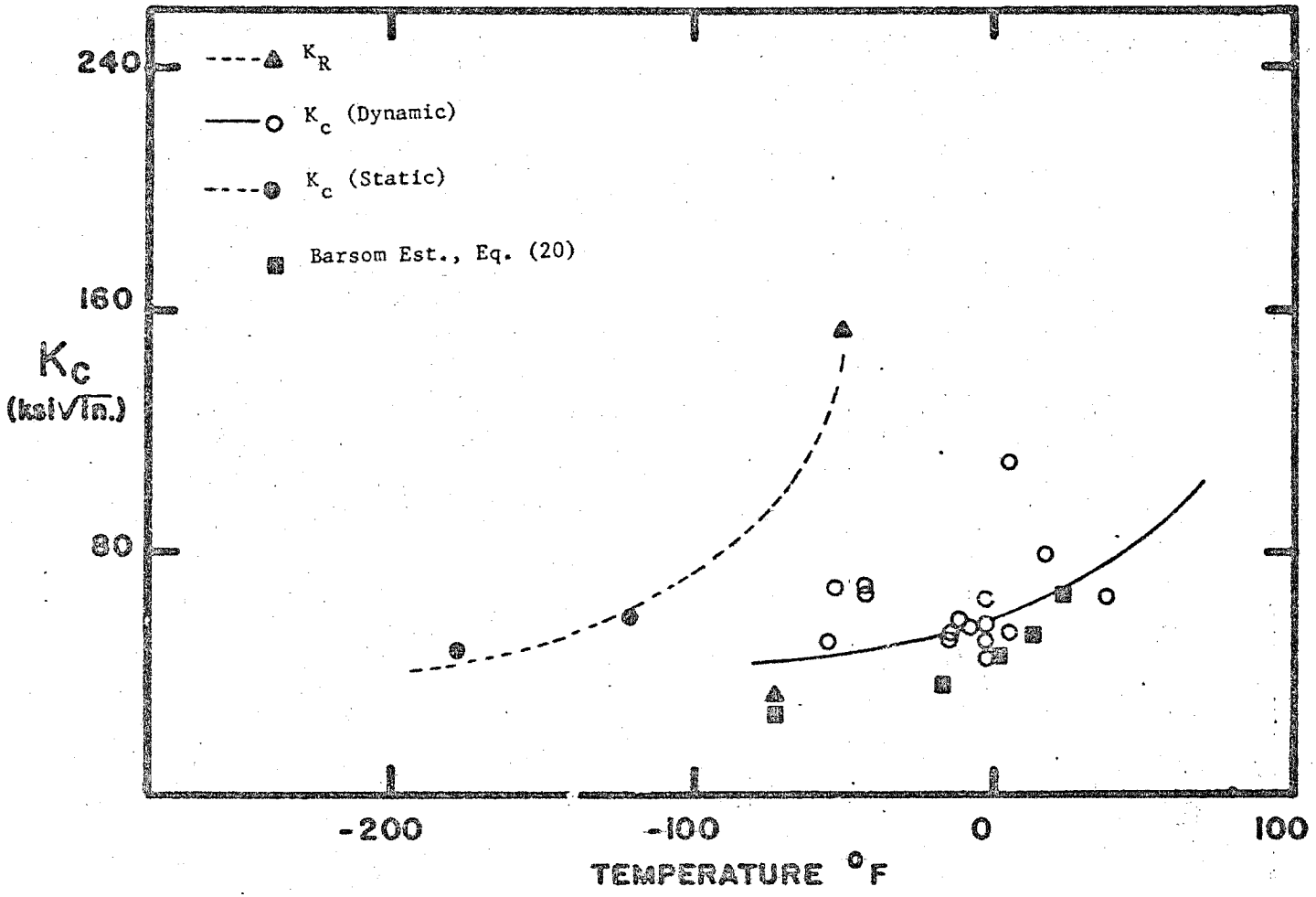

Fig. E-8 K_c Data for A440 1" Material

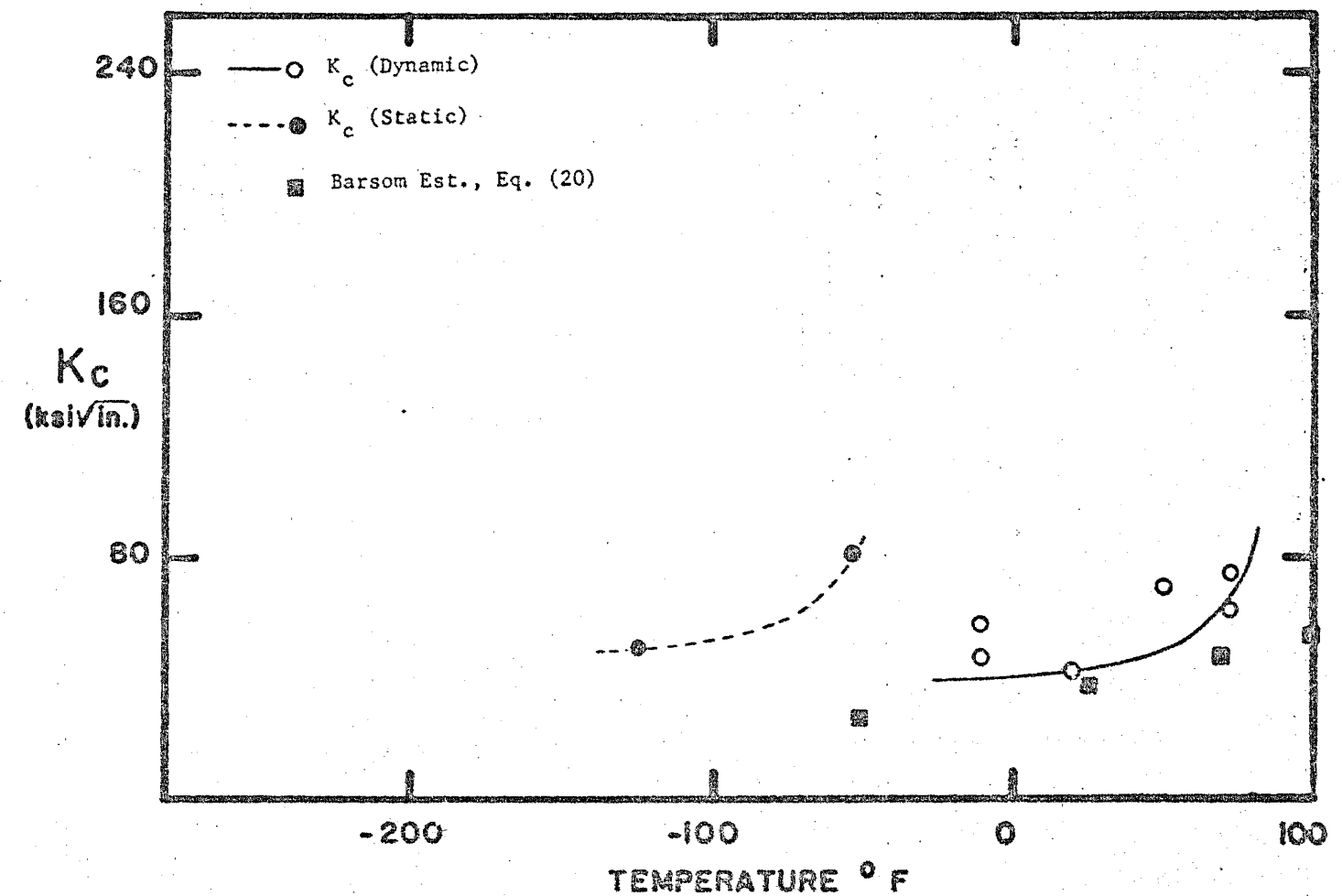

Fig. E-9 K_c Data for A440 2" Material

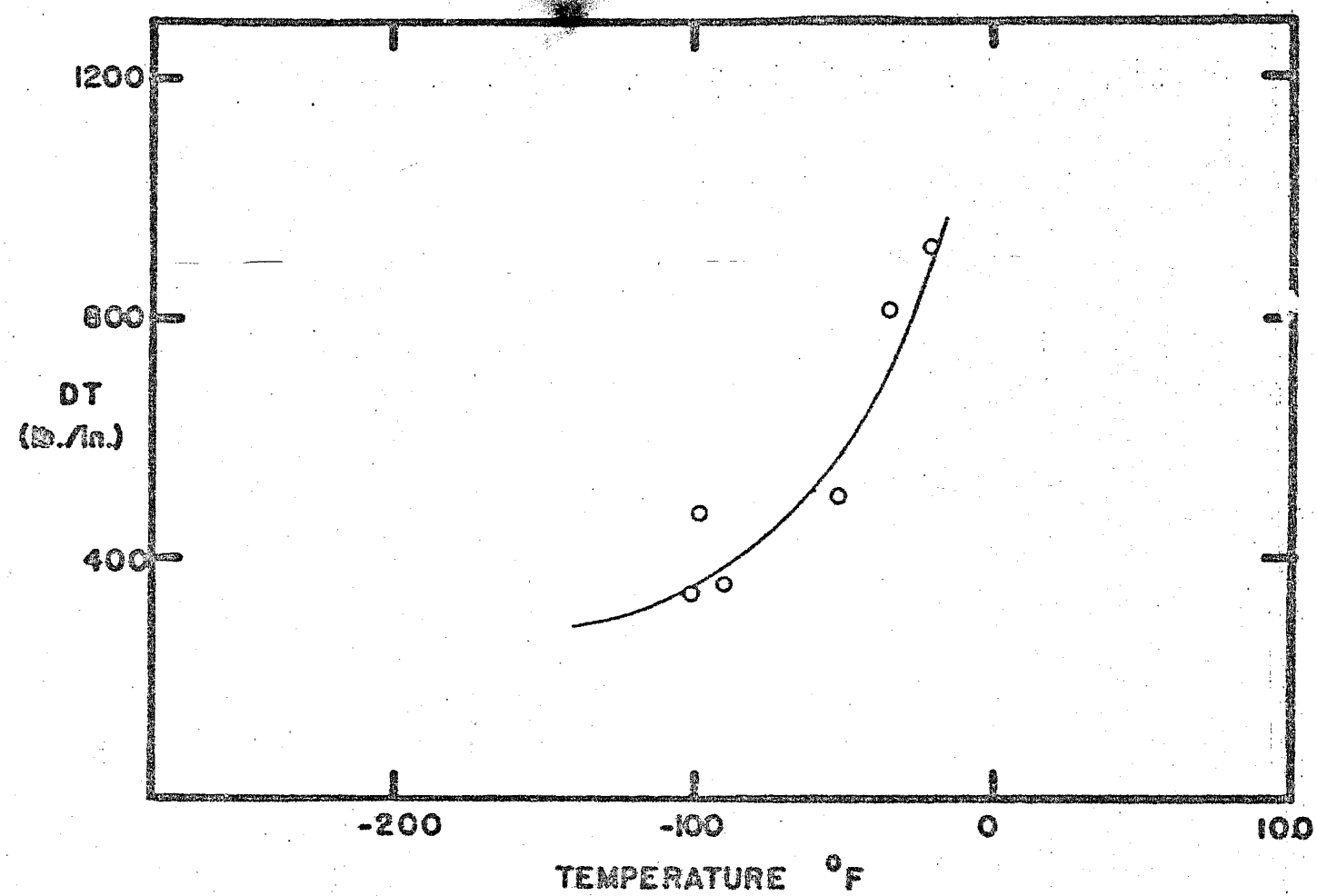

Fig. E-10 Dynamic Tear Data for A440 1/2" Material

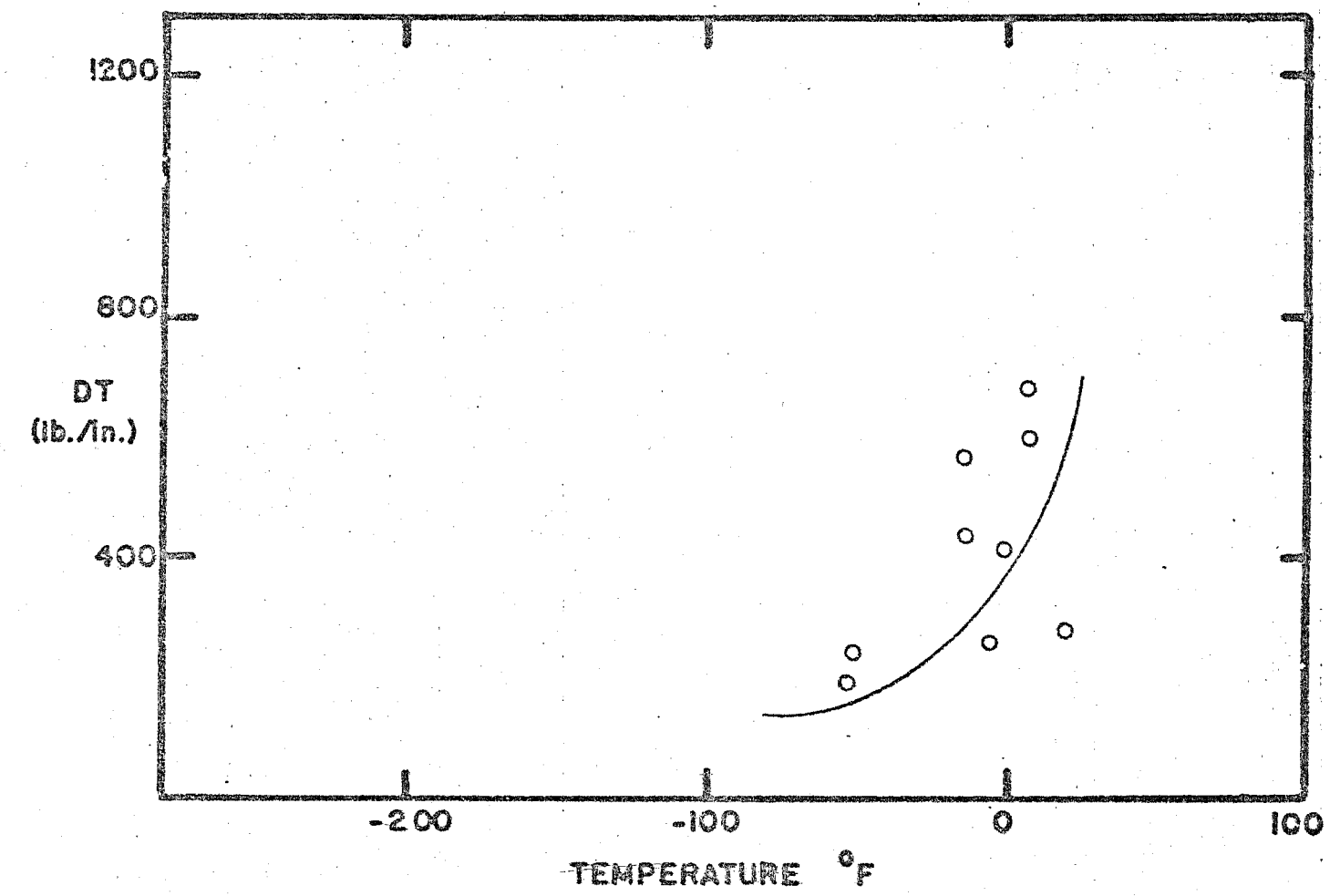

Fig. E-11 Dynamic Tear Data for A440 1" Material

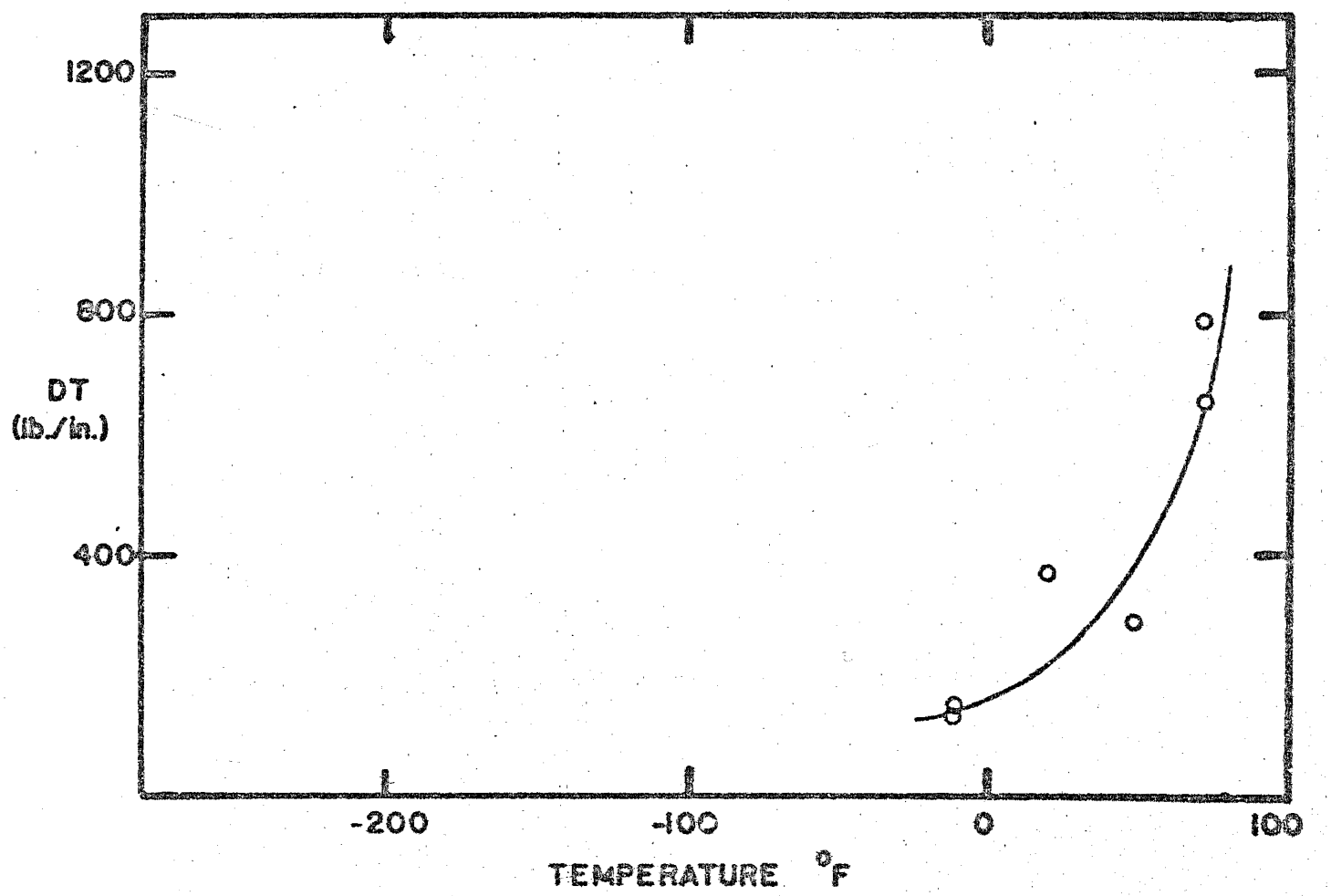

Fig. E-12 Dynamic Tear Data for A440 2" Material

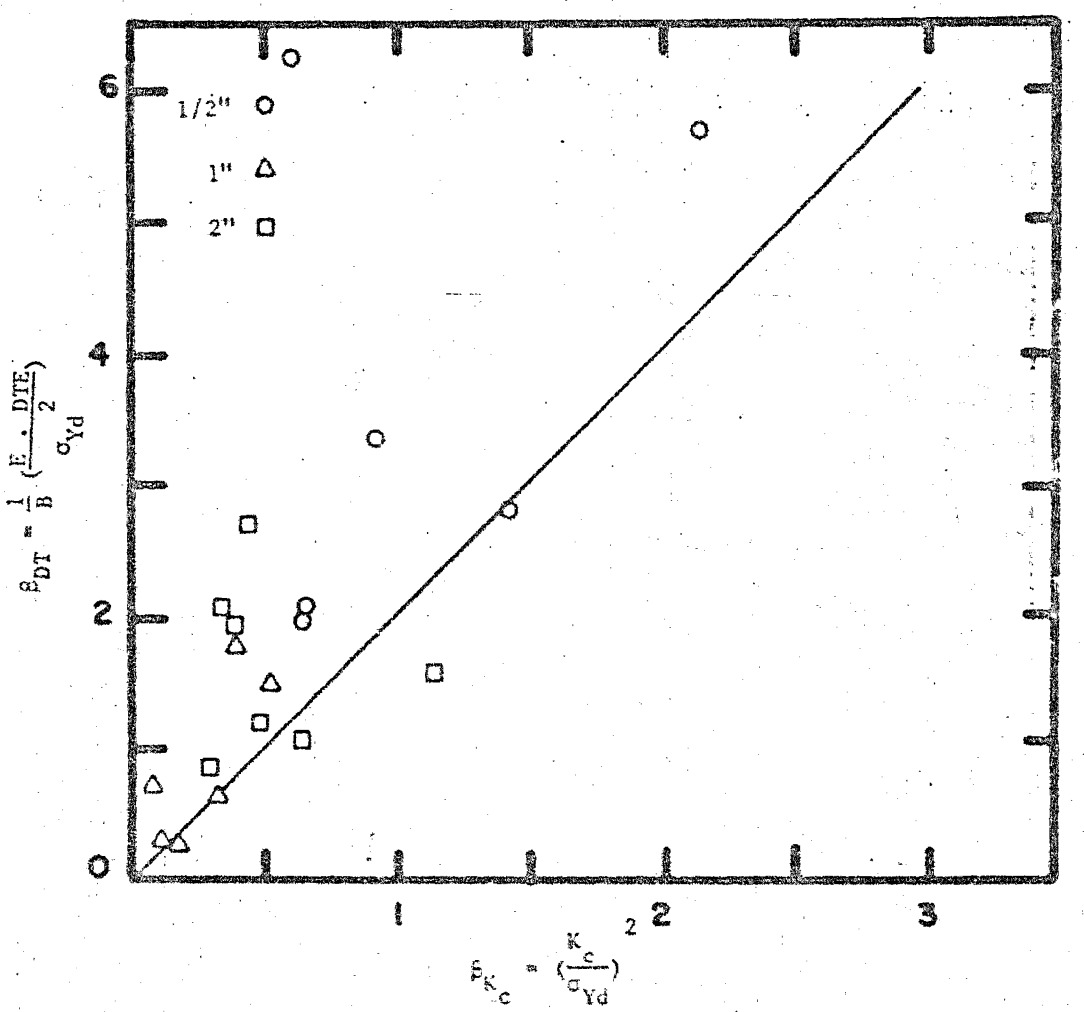

Fig. E-13 A440 β Data

TABLE E1.1* - A440 CHARPY DATA SUMMARY

Test	Material Thickness (in.)	T_{15} (°F)	T_{30} (°F)	T_{SH} (°F)	CVN_{SH} (ft.-lb.)
DS	0.5	- 25	- 10	50	65
DP	0.5	0	25	100	48
SS	0.5	- 150	- 140	- 50	44
SP	0.5	- 105	- 65	0	39
DS	1.0	0	25	0	> 80
DP	1.0	50	65	150	44
SS	1.0	- 135	- 75	- 50	32
SP	1.0	- 5	--	50	20
DS	2.0	70	150	--	> 60
DP	2.0	30	70	200	58
SS	2.0	- 135	- 95	100	58
SP	2.0	- 100	- 60	50	38

TABLE E1.2

Test	T	ΔT (°F)	ΔT_B (°F)
S	0.5	125	121
P	0.5	100	
S	1.0	135	137
P	1.0	50	
S	2.0	210	121
P	2.0	130	

*See Table A1.1 for designations

TABLE E2 - CHARPY TEST DATA

A440 1/2" (Notched) Slow Bend

Specimen No.	Temp. (° F)	Maximum Load (lb.)	Deflection at Maximum Load (in.)	Crack-Depth (in.)	Energy Absorbed		Shear (%)	Lateral Expansion (mils)
					Actual (ft.-lb.)	Normalized (ft.-lb.)		
128-SN	- 200	2575	0.044	0.079	4.7	4.7	0	5
108-SN	- 150	3250	0.096	0.079	17.6	17.6	0	20
94-SN	- 135	3150	0.110	0.079	38.0	38.0	40	36
22-SN	- 50	2950	0.120	0.079	44.0	44.0	95	54
82-SN	+ 74	2775	0.110	0.079	42.2	42.2	95	51

TABLE E2 - CHARPY TEST DATA

A440 1/2" (Notched) Dynamic

Specimen No.	Temp. (° F)	Maximum Load (lb.)	Deflection at Maximum Load (in.)	Crack-Depth (in.)	Energy Absorbed		Shear (%)	Lateral Expansion (mils)
					Actual (ft.-lb.)	Normalized (ft.-lb.)		
	- 100			0.079	4.5	4.5	0	5
	- 50			0.079	4.0	4.0	< 5	15
	- 50			0.079	13.0	13.0	< 5	8
	- 25			0.079	17.0	17.0	30	53
	- 25			0.079	55.0	55.0	85	21
	0			0.079	26.0	26.0	60	31
	0			0.079	60.0	60.0	95	54
	+ 50			0.079	65.0	65.0	100	61
	+ 50			0.079	63.0	63.0	100	58
	+ 100			0.079	60.5	60.5	100	50

TABLE E2 - CHARPY TEST DATA

A440 1/2" (Pre-Cracked) Slow Bend

Specimen No.	Temp. (° F)	Maximum Load (lb.)	Deflection at Maximum Load (in.)	Crack-Depth (in.)	Energy Absorbed		Shear (%)	Lateral Expansion (mils)
					Actual (ft.-lb.)	Normalized (ft.-lb.)		
203-SP	- 300	1850	0.026	0.126	1.52	1.78	0	4
204-SP	- 200	2150	0.031	0.128	2.38	2.81	0	4
205-SP	- 200	2275	0.026	0.131	2.83	3.40	0	4
206-SP	- 150	2200	0.072	0.132	9.47	11.40	< 5	12
207-SP	- 125	2075	0.031	0.114	2.47	2.81	0	4
208-SP	- 50	2175	0.064	0.116	30.50	35.00	100	32
209-SP	+ 75	1700	0.070	0.139	25.00	31.55	100	35
210-SP	+ 75	1675	0.068	0.140	25.00	31.80	100	32

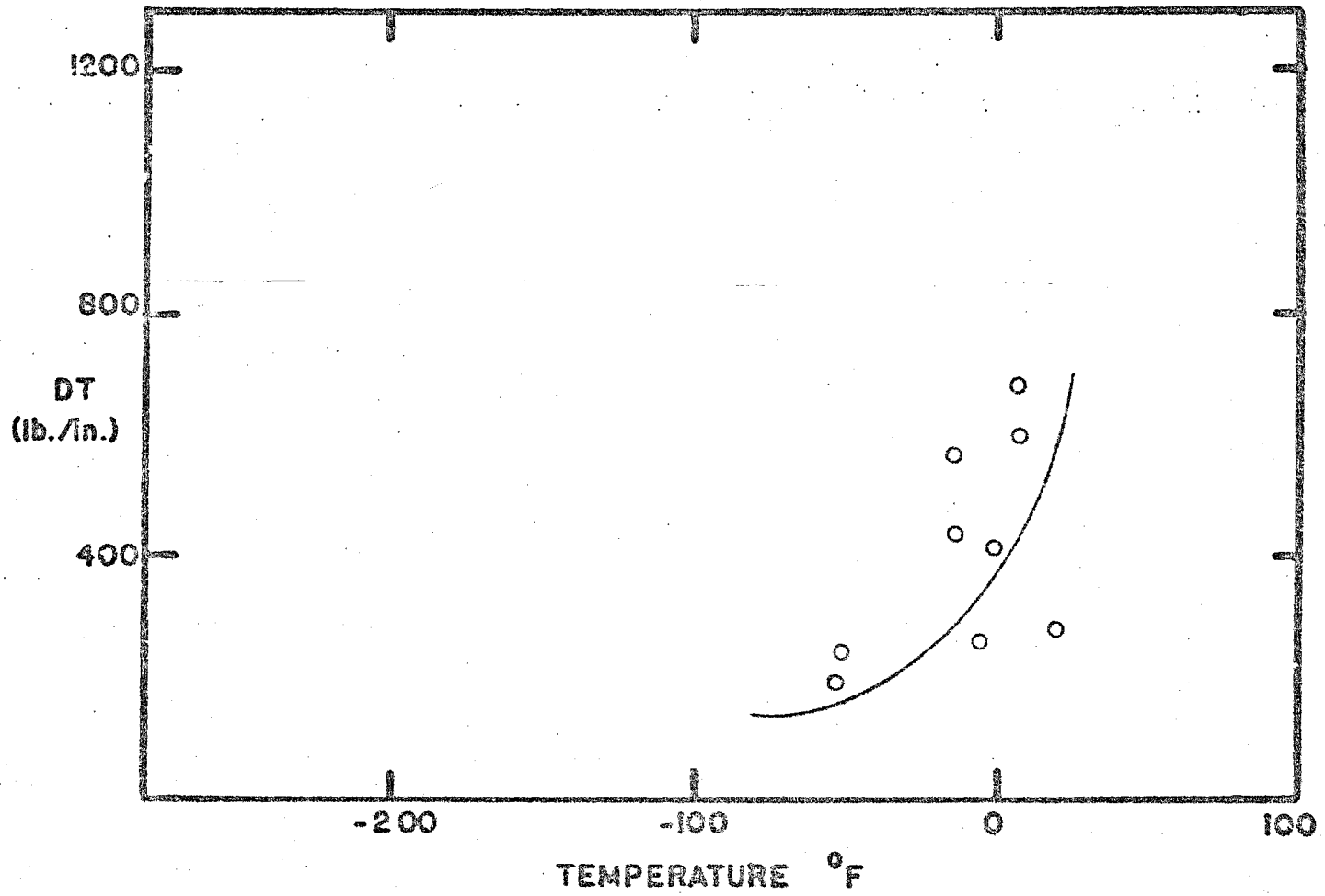

Fig. E-11 Dynamic Tear Data for A440 1" Material

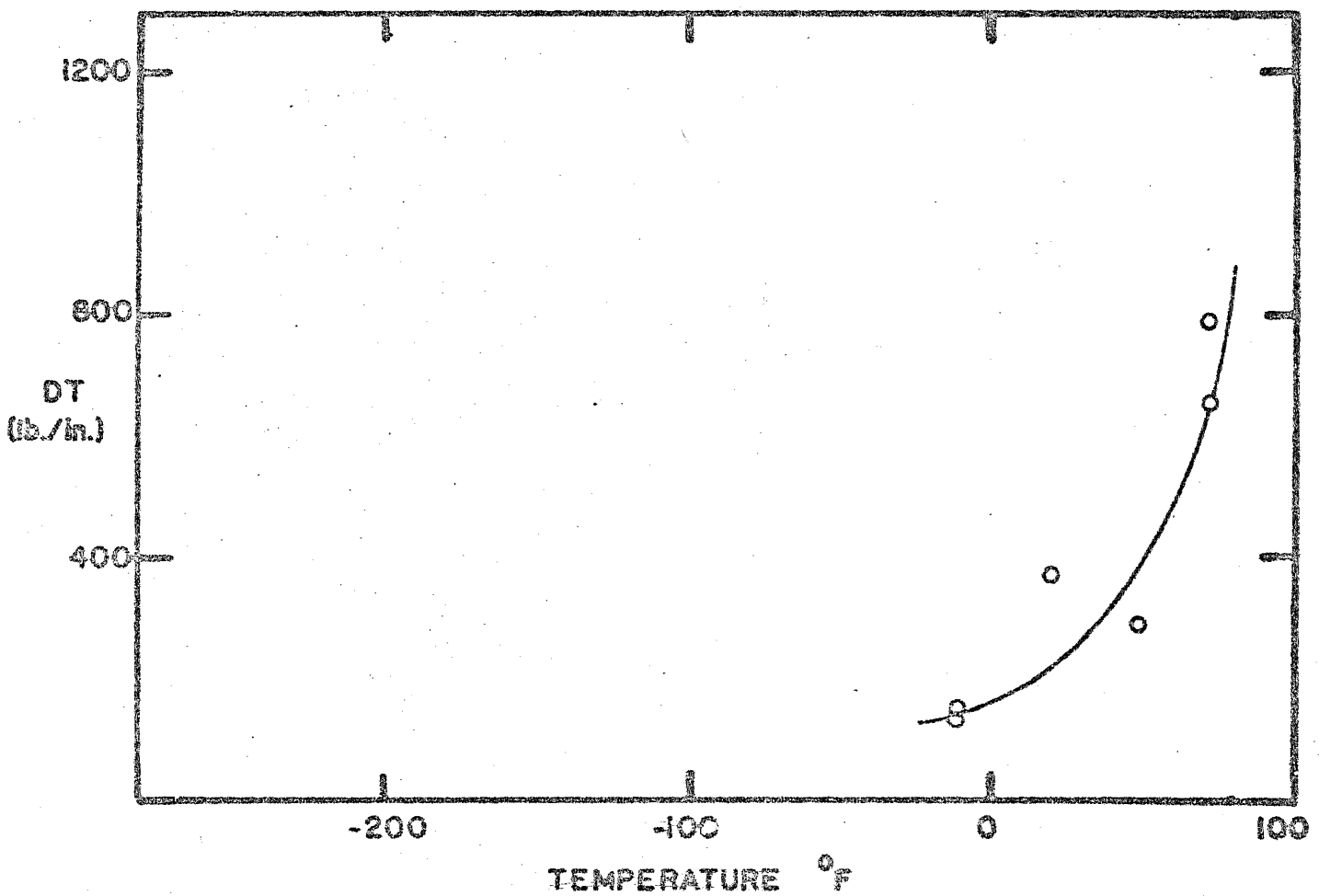

Fig. E-12 Dynamic Tear Data for A440 2" Material

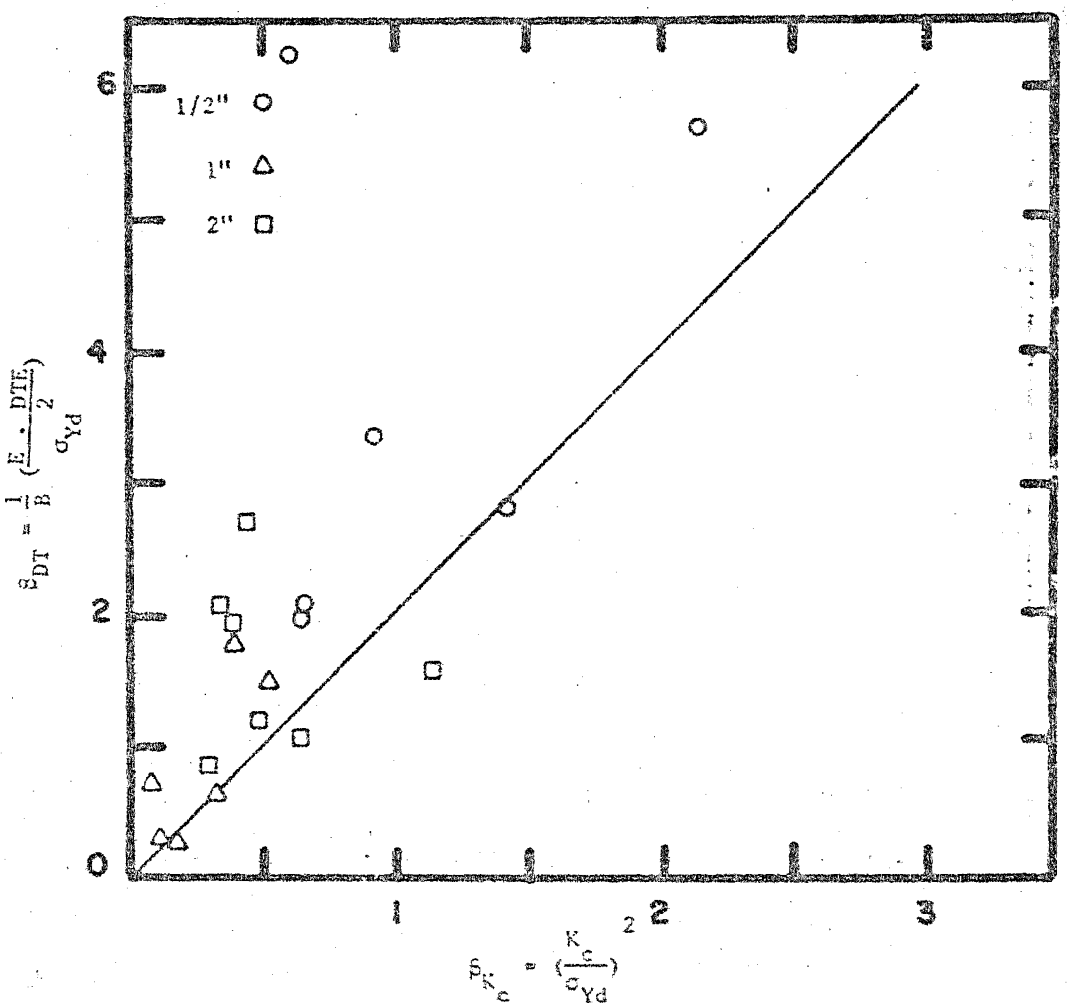

Fig. E-13 A440 β Data

TABLE E1.1* - A440 CHARPY DATA SUMMARY

Test	Material Thickness (in.)	T_{15} (° F)	T_{30} (° F)	T_{SH} (° F)	CVN_{SH} (ft.-lb.)
DS	0.5	- 25	- 10	50	65
DP	0.5	0	25	100	48
SS	0.5	- 150	- 140	- 50	44
SP	0.5	- 105	- 65	0	39
DS	1.0	0	25	0	> 80
DP	1.0	50	65	150	44
SS	1.0	- 135	- 75	- 50	32
SP	1.0	- 5	--	50	20
DS	2.0	70	150	--	> 60
DP	2.0	30	70	200	58
SS	2.0	- 135	- 95	100	58
SP	2.0	- 100	- 60	50	38

TABLE E1.2

Test	T	ΔT (° F)	ΔT_B (° F)
S	0.5	125	121
P	0.5	100	
S	1.0	135	137
P	1.0	50	
S	2.0	210	121
P	2.0	130	

*See Table A1.1 for designations

TABLE E2 - CHARPY TEST DATA

A440 1/2" (Notched) Slow Bend

Specimen No.	Temp. (° F)	Maximum Load (lb.)	Deflection at Maximum Load (in.)	Crack-Depth (in.)	Energy Absorbed		Shear (%)	Lateral Expansion (mils)
					Actual (ft.-lb.)	Normalized (ft.-lb.)		
128-SN	- 200	2575	0.044	0.079	4.7	4.7	0	5
108-SN	- 150	3250	0.096	0.079	17.6	17.6	0	20
94-SN	- 135	3150	0.110	0.079	38.0	38.0	40	36
22-SN	- 50	2950	0.120	0.079	44.0	44.0	95	54
82-SN	+ 74	2775	0.110	0.079	42.2	42.2	95	51

TABLE E2 - CHARPY TEST DATA

A440 1/2" (Notched) Dynamic

Specimen No.	Temp. (° F)	Maximum Load (lb.)	Deflection at Maximum Load (in.)	Crack-Depth (in.)	Energy Absorbed		Shear (%)	Lateral Expansion (mils)
					Actual (ft.-lb.)	Normalized (ft.-lb.)		
	- 100			0.079	4.5	4.5	0	5
	- 50			0.079	4.0	4.0	< 5	15
	- 50			0.079	13.0	13.0	< 5	8
	- 25			0.079	17.0	17.0	30	53
	- 25			0.079	55.0	55.0	85	21
	0			0.079	26.0	26.0	60	31
	0			0.079	60.0	60.0	95	54
	+ 50			0.079	65.0	65.0	100	61
	+ 50			0.079	63.0	63.0	100	58
	+ 100			0.079	60.5	60.5	100	50

TABLE E2 - CHARPY TEST DATA

A440 1/2" (Pre-Cracked) Slow Bend

Specimen No.	Temp. (° F)	Maximum Load (lb.)	Deflection at Maximum Load (in.)	Crack-Depth (in.)	Energy Absorbed		Shear (%)	Lateral Expansion (mils)
					Actual (ft.-lb.)	Normalized (ft.-lb.)		
203-SP	- 300	1850	0.026	0.126	1.52	1.78	0	4
204-SP	- 200	2150	0.031	0.128	2.38	2.81	0	4
205-SP	- 200	2275	0.026	0.131	2.83	3.40	0	4
206-SP	- 150	2200	0.072	0.132	9.47	11.40	< 5	12
207-SP	- 125	2075	0.031	0.114	2.47	2.81	0	4
208-SP	- 50	2175	0.064	0.116	30.50	35.00	100	32
209-SP	+ 75	1700	0.070	0.139	25.00	31.55	100	35
210-SP	+ 75	1675	0.068	0.140	25.00	31.80	100	32

TABLE E2 - CHARPY TEST DATA

A440 1/2" (Pre-Cracked) Dynamic

Specimen No.	Temp. (° F)	Maximum Load (lb.)	Deflection at Maximum Load (in.)	Crack-Depth (in.)	Energy Absorbed		Shear (%)	Lateral Expansion (mils)
					Actual (ft.-lb.)	Normalized (ft.-lb.)		
	- 100			0.140	2.00	2.48	0	4
	- 100			0.144	2.00	2.51	0	4
	- 50			0.126	4.00	4.70	0	4
	- 50			0.137	3.10	3.78	0	4
	0			0.151	15.50	19.90	45	14
	0			0.122	16.00	18.40	50	19
	+ 35			0.128	30.30	35.40	75	26
	+ 35			0.142	30.00	37.40	80	34
	+ 75			0.115	42.00	47.10	100	40
	+ 75			0.104	46.00	49.50	100	40
	+ 150			0.095	46.50	47.80	100	40
	+ 212			0.131	37.50	44.50	100	38
	+ 212			0.144	34.00	42.60	100	39

TABLE E2 - CHARPY TEST DATA

A440 1" (Notched) Slow Bend

Specimen No.	Temp. (° F)	Maximum Load (lb.)	Deflection at Maximum Load (in.)	Crack-Depth (in.)	Energy Absorbed		Shear (%)	Lateral Expansion (mils)
					Actual (ft.-lb.)	Normalized (ft.-lb.)		
130-SN	- 200	3125	0.068	0.079	11.54	11.54	0	11
107-SN	- 150	2900	0.057	0.079	6.32	6.32	0	5
78-SN	- 100	3400	0.140	0.079	33.84	33.84	0	27
98-SN	- 50	2525	0.070	0.079	22.40	22.40	85	27
158-SN	0	2425	0.066	0.079	22.20	22.20	--	25
138-SN	+ 75	3120	0.138	0.079	--	--	--	--

TABLE E2 - CHARPY TEST DATA

A440 1" (Notched) Dynamic

Specimen No.	Temp. (° F)	Maximum Load (lb.)	Deflection at Maximum Load (in.)	Crack-Depth (in.)	Energy Absorbed		Shear (%)	Lateral Expansion (mils)
					Actual (ft.-lb.)	Normalized (ft.-lb.)		
	- 100			0.079	5.0	5.0	0	6
	- 50			0.079	7.0	7.0	0	8
	- 50			0.079	8.0	8.0	0	8
	0			0.079	9.0	9.0	0	9
	0			0.079	14.0	14.0	< 5	20
	+ 25			0.079	37.0	37.0	10	36
	+ 25			0.079	42.0	42.0	10	37
	+ 50			0.079	61.0	61.0	60	53
	+ 50			0.079	43.0	43.0	40	40
	+ 100			0.079	77.0	77.0	100	64

TABLE E2 - CHARPY TEST DATA

A440 1" (Pre-cracked) Slow Bend

Specimen No.	Temp. (° F)	Maximum Load (lb.)	Deflection at Maximum Load (in.)	Crack-Depth (in.)	Energy Absorbed		Shear (%)	Lateral Expansion (mils)
					Actual (ft.-lb.)	Normalized (ft.-lb.)		
129-SP	- 200	1425	0.026	0.135	1.21	1.46	0	4
106-SP	- 150	1100	0.028	0.165	1.71	2.35	0	5
77-SP	- 100	1175	0.037	0.155	3.18	4.19	0	7
23-SP	- 50	1400	0.082	0.140	5.16	6.40	0	9
157-SP	0	1000	0.043	0.234	8.70	17.20	50	22
137-SP	+ 75	1540	0.525	0.156	15.00	19.80	75	25

TABLE E2 - CHARPY TEST DATA

A440 1" (Pre-cracked) Fast Bend

Specimen No.	Temp. (° F)	Maximum Load (lb.)	Deflection at Maximum Load (in.)	Crack-Depth (in.)	Energy Absorbed		Shear (%)	Lateral Expansion (mils)
					Actual (ft.-lb.)	Normalized (ft.-lb.)		
396-FP	- 170	1460	0.026	0.105	2.45	2.62	0	4
359-FP	- 97	1400	0.028	0.130	2.80	3.34	0	4
318-FP	- 50	1350	0.030	0.130	4.32	5.05	0	13
274-FP	0	850	0.016	0.185	4.40	6.60	0	12
240-FP	+ 50	1620	0.070	0.155	16.14	21.30	0	21

TABLE E2 - CHARPY TEST DATA

A440 1" (Pre-Cracked) Dynamic

Specimen No.	Temp. (° F)	Maximum Load (lb.)	Deflection at Maximum Load (in.)	Crack-Depth (in.)	Energy Absorbed		Shear (%)	Lateral Expansion (mils)
					Actual (ft.-lb.)	Normalized (ft.-lb.)		
	- 80			0.130	2.10	2.50	0	5
	- 25			0.140	2.00	2.48	0	4
	+ 25			0.125	4.10	4.10	0	3
	+ 75			0.156	33.20	43.70	60	49
	+150			0.130	32.30	36.50	85	43
	+212			0.125	34.50	40.40	90	28

TABLE E2 - CHARPY TEST DATA

A440 2" (Notched) Slow Bend

Specimen No.	Temp. (° F)	Maximum Load (lb.)	Deflection at Maximum Load (in.)	Crack-Depth (in.)	Energy Absorbed		Shear (%)	Lateral Expansion (mils)
					Actual (ft.-lb.)	Normalised (ft.-lb.)		
180-SN	- 200	3200		0.079	10.75	10.75	0	11
173-SN	- 150	3120		0.079	13.45	13.45	0	14
80-SN	- 100	3325	0.136	0.079	27.08	27.08	0	29
26-SN	- 50	3175	0.130	0.079	45.90	45.90	85	57
126-SN	0	3050	0.124	0.079	49.29	49.29	100	59
133-SN	+ 75	2995	0.124	0.079	60.04	60.04	100	55

TABLE E2 - CHARPY TEST DATA

A440 2" (Notched) Fast Bend

Specimen No.	Temp. (° F)	Maximum Load (lb.)	Deflection at Maximum Load (in.)	Crack-Depth (in.)	Energy Absorbed		Shear (%)	Lateral Expansion (mils)
					Actual (ft.-lb.)	Normalized (ft.-lb.)		
398-FN	-165	2650	0.068	0.079	14.66	14.66	0	17
397-FN	- 165	2100	0.048	0.079	7.20	7.20	0	5
362-FN	- 100	3280	0.100	0.079	20.93	20.93	0	19
361-FN	- 100	3220	0.098	0.079	21.53	21.53	< 5	20
322-FN	- 50	3500	0.145	0.079	27.58	27.58	< 5	29
323-FN	- 50	3500	0.125	0.079	34.61	34.61	< 10	27
266-FN	0	3310	0.136	0.079	42.65	42.65	40	40
243-FN	+ 50	3220	0.128	0.079	56.32	56.32	100	51

TABLE E2 - CHARPY TEST DATA

A440 2" (Notched) Dynamic

Specimen No.	Temp. (° F)	Maximum Load (lb.)	Deflection at Maximum Load (in.)	Crack-Depth (in.)	Energy Absorbed		Shear (%)	Lateral Expansion (mils)
					Actual (ft.-lb.)	Normalized (ft.-lb.)		
	0			0.079	7.0	7.0	0	9
	+ 50			0.079	12.0	12.0	0	16
	+ 50			0.079	11.0	11.0	0	15
	+ 75			0.079	22.0	22.0	0	24
	+ 100			0.079	30.0	30.0	0	35
	+ 100			0.079	21.0	21.0	< 10	26
	+ 150			0.079	31.0	31.0	[illegible]	36
	+ 150			0.079	30.5	30.5	[illegible]	35
	+ 200			0.079	44.0	44.0	80	43
	+ 200			0.079	53.0	53.0	90	57

TABLE E2 - CHARPY TEST DATA

A440 2" (Pre-cracked) Slow Bend

Specimen No.	Temp. (° F)	Maximum Load (lb.)	Deflection at Maximum Load (in.)	Crack-Depth (in.)	Energy Absorbed		Shear (%)	Lateral Expansion (mils)
					Actual (ft.-lb.)	Normalized (ft.-lb.)		
179-SP	- 200	1850	0.030	0.125	1.92	2.26	0	6
172-SP	- 150	1995	0.086	0.140	3.38	4.20	0	4
79-SP	- 100	2050	0.100	0.130	15.15	21.85	10	21
25-SP	- 50	1850	0.092	0.140	21.40	26.50	0	36
155-SP	0	1950	0.078	1.193	31.75	37.87	95	42
134-SP	+ 75	2075	0.082	0.090	33.75	37.80	100	36

TABLE E2 - CHARPY TEST DATA

A440 2" (Pre-cracked) Fast Bend

Specimen No.	Temp. (° F)	Maximum Load (lb.)	Deflection at Maximum Load (in.)	Crack-Depth (in.)	Energy Absorbed		Shear (%)	Lateral Expansion (mils)
					Actual (ft.-lb.)	Normalized (ft.-lb.)		
399-FP	- 161	3600	0.022	0.150	3.91	5.05	0	2
360-FP	- 98	2520	0.072	0.110	12.22	13.54	< 5	14
321-FP	- 50	2040	0.070	0.140	8.22	10.98	15	17
320-FP	- 50	1630	0.040	0.165	8.53	11.73	< 10	15
278-FP	0	2350	0.060	0.110	43.82	48.20	80	47
275-FP	0	2120	0.088	0.115	34.02	38.44	90	42
242-FP	+ 50	1900	0.088	0.130	32.35	38.65	95	40
241-FP	+ 50	2075	0.088	0.115	33.56	38.09	95	42

TABLE E2 - CHARPY TEST DATA

A440 2" (Pre-cracked) Dynamic

Specimen No.	Temp. (° F)	Maximum Load (lb.)	Deflection at Maximum Load (in.)	Crack-Depth (in.)	Energy Absorbed		Shear (%)	Lateral Expansion (mils)
					Actual (ft.-lb.)	Normalized (ft.-lb.)		
	- 50			0.180	2.5	3.62	0	4
	0			0.160	6.0	8.10	0	6
	+ 50			0.130	18.5	22.00	65	17
	+ 75			0.135	28.5	34.80	75	28
	+ 150			0.135	42.5	51.80	100	40
	+ 212			0.130	47.0	56.80	100	49

TABLE E3* - A440 K_c DATA

A440 1/2"

Nominal Yield Strength YS = 62.5 ksi

Specimen No.	B (in.)	Temp (°F)	A_o (in.)	F.A. ($in.^2$)	$P_{max.}$ (kips)	Time (sec)	K_c (ksi/in.)	G (lb/in)	DTE (lb/in)	β_{K_c}	β_{DT}	σ_{YD} (ksi)
1.013	0.5	- 100	0.700	1.150	11.7	8.0E-04	59.80	120.8	0.0	0.671	0.000	103.2
1.009	0.5	- 100	0.880	1.060	10.0	8.5E-04	59.66	120.2	0.0	0.671	0.000	103.0
1.015	0.5	- 100	0.660	1.170	15.0	1.1E-03	76.54	197.9	0.0	1.127	0.000	102.0
1.005	0.5	- 100	0.615	1.192	12.6	9.0E-04	59.85	121.0	347.2	0.679	1.946	102.8
1.001	0.5	- 96	0.610	1.183	17.0	1.0E-03	85.80	248.7	476.7	1.458	2.795	101.0
1.002	0.5	- 84	0.620	1.214	13.0	1.0E-03	61.05	125.9	355.9	0.739	2.089	99.4
1.014	0.5	- 60	0.690	1.172	12.0	9.0E-04	59.14	118.2	0.0	0.724	0.000	98.3
1.004	0.5	- 60	0.690	1.155	24.0	1.7E-03	0.00	0.0	0.0	0.000	0.000	93.7
1.006	0.5	- 50	0.600	1.200	13.0	8.5E-04	61.62	128.3	505.0	0.848	3.339	94.6
1.003	0.5	- 37	0.710	1.145	16.8	9.0E-04	96.21	312.7	817.5	2.160	5.647	92.6
1.010	0.5	- 25	1.090	0.955	7.2	4.5E-04	51.29	88.9	917.3	0.603	6.226	93.4
1.016	0.5	- 20	0.630	1.185	18.5	8.0E-04	101.19	345.9	0.0	2.488	0.000	90.7
Slow Bend Tests												
1.008	0.5	- 214	0.560	1.220	10.7	5.2E-01	47.27	75.5	0.0	0.388	0.000	107.3
1.007	0.5	- 151	0.730	1.135	10.7	4.0E-01	52.33	92.5	0.0	0.633	0.000	93.0

(See Table A3 for designations.

TABLE E3* - A440 K_c DATA

A440 1"

Nominal Yield Strength YS = 51.8 ksi

Specimen No.	B (in.)	Temp. (° F)	A_o (in.)	F.A. ($in.^2$)	$P_{max.}$ (kips)	Time (sec)	K_c (ksi/in.)	G (lb/in)	DTE (lb/in)	β_{K_c}	β_{DT}	σ_{YD} (ksi)
1.101	1.0	- 54.	0.950	2.000	16.2	1.2E-03	51.72	90.4	190.2	0.386	0.814	83.2
1.106	1.0	- 50	0.875	2.125	22.0	9.5E-04	68.63	155.1	242.8	0.677	1.033	83.4
1.118	1.0	- 40	0.900	2.100	21.6	9.0E-04	69.10	161.3	0.0	0.707	0.000	82.2
1.102	1.0	- 40	0.900	2.100	19.5	9.0E-00	66.54	149.6	0.0	1.165	0.000	61.7
1.115	1.0	- 12	0.950	2.050	15.8	6.0E-04	50.50	86.2	439.0	0.400	2.036	79.9
1.107	1.0	- 12	0.875	2.125	18.0	8.0E-04	54.61	100.7	564.7	0.479	2.684	78.9
1.116	1.0	- 5	0.950	2.050	17.6	5.0E-04	57.23	110.7	251.7	0.516	1.175	79.6
1.109	1.0	0	0.920	2.080	18.0	9.0E-04	57.40	111.3	0.0	0.554	0.000	77.1
1.111	1.0	0	0.920	2.080	14.8	6.0E-04	45.68	70.5	0.0	0.339	0.000	78.4
1.110	1.0	0	0.870	2.130	21.2	8.0E-04	66.35	148.7	0.0	0.733	0.000	77.5
1.117	1.0	0	0.880	2.120	16.9	5.0E-04	51.01	87.9	413.2	0.417	1.958	79.0
1.104	1.0	8	0.920	2.080	37.5	1.3E-03	0.00	0.0	680.8	0.000	3.574	75.1
1.105	1.0	8	0.970	2.030	26.5	8.0E-04	110.00	408.8	597.0	2.064	3.015	76.6
1.114	1.0	20	0.890	2.110	23.9	9.5E-04	80.98	221.5	284.4	1.174	1.507	74.7
1.113	1.0	40	0.880	2.120	21.2	7.0E-04	68.08	156.6	0.0	0.856	0.000	73.6
Slow Bend Tests												
1.108	1.0	-175	0.870	2.130	13.0	3.0E-01	37.61	47.8	0.0	0.183	0.000	88.0
1.103	1.0	-118	0.920	2.080	13.5	6.0E-01	41.53	58.3	0.0	0.302	0.000	75.6

*See Table A3 for designations.

TABLE E3* - A440 K_c DATA

A440 2"

Nominal Yield Strength YS = 62.5 ksi

Specimen No.	B (in.)	Temp. (°F)	A_o (in.)	F.A. ($in.^2$)	$P_{max.}$ (kips)	Time (sec)	K_c (ksi/in.)	G (lb/in)	DTE (lb/in)	β_{K_c}	β_{DT}	σ_{YD} (ksi)
1.201	2.0	- 10	0.965	4.070	29.0	1.0E-03	46.03	71.6	153.3	0.135	0.289	88.7
1.203	2.0	- 10	1.210	3.580	28.4	1.0E-03	57.61	112.1	140.8	0.211	0.265	88.7
1.207	2.0	20	0.920	4.160	27.4	5.0E-04	41.58	58.4	377.9	0.113	0.732	87.4
1.205	2.0	50	0.818	4.3	47.0	7.5E-04	70.16	166.3	291.5	0.356	0.624	83.1
1.206	2.0	72	0.900	4.200	46.2	7.5E-04	75.61	193.1	794.3	0.434	1.787	81.1
1.208	2.0	72	0.840	4.320	42.5	8.0E-04	63.83	137.6	652.8	0.311	1.475	80.9
Slow Bend Tests												
1.211	2.0	-124	1.180	3.640	26.2	4.5E-01	50.92	87.6	000.0	0.168	0.000	87.9
1.210	2.0	- 53	0.825	4.350	51.5	6.0E-01	81.46	224.2	000.0	0.545	0.000	78.0

*See Table A3 for designations

TABLE E4 - A440 R-CURVE INSTABILITY SUMMARY

Thickness (in.)	Test Temperature (^{o} F)	Fatigue Crack Length (in.)	K_c at Instability (psi)	Apparent Crack Length at Instability (in.)
1.0	- 70	6.10	33,243	6.23
1.0*	- 48	6.25	154,550	7.04
0.5**	-100	6.20	350,440	7.04
0.5***	- 50			
0.5****	- 30			

* Crack branching occurred at a of 7.65"

** Crack branching occurred at a of 6.85"

*** Plastic buckling of specimen, no crack propagation

**** Plastic buckling of specimen, no crack propagation

APPENDIX F - A441 DATA

This appendix contains the data collected for the 1/2", 1" and 2" thicknesses of the A441 material. This steel was supplied to the program by the Bethlehem Steel Corporation. The chemical analysis, physical properties and heat designations appear in Tables 1 and 2.

The data in this appendix is presented in the form of a Charpy summary, a detailed Charpy tabulation, a K_c tabulation, an R-curve summary and appropriate figures which best illustrate the data trends. Details of the test procedures and terminology can be found in appendices J, K, L and Chapter 2.

The A441 material was part of the Phase 1 program and as such there was not a large amount of material available for Phase 2 testing. Standard Charpy specimens were tested at two rates of loading while the precracked specimens were tested at three loading rates. The data are shown in Figures F-1 through F-6. A data summary is given in Table F-1 while Table F-2 presents the individual data. The standard specimens all showed a definite temperature shift between the slow and dynamic data. The shift was as expected for the 1/2" data. The 1" and 2" data exhibited a shift of about one-half that anticipated (28). The slow and fast precracked data showed zero shift for the three thicknesses. This was typical of results for all materials in the program. The slow and dynamic precracked data all showed definite temperature shifts but these shifts were less than Barsom's results (28).

The precracked data was also to the right of this standard Charpy data, (i.e., a higher transition temperature). It did not appear that the precracked data formed a lower bound for the standard Charpy data.

Being part of Phase 1, only K_c measurements were made on the A441 material. These K_c tests for the three thicknesses are shown in Figure F-7 through F-10. Table F-3 gives the individual data. It is particularly interesting to note that for the A441 material the static and dynamic K_c results do show temperature shifts, which are not consistent with Barsom's prediction (28). This is interesting because the other material tended to show shifts between the static and dynamic K_c data which were consistent with Barsom even when CVN data did not show a shift at the anticipated level. Thus for the A441 material both the CVN and K_c data exhibit temperature shifts not in agreement with Barsom. Also the CVN and K_c shifts for the A441 do not agree with each other for a given thickness. Another interesting observation relative to the A441 K_c data is the nice uniform trend shown in the CVN and static K_c data which show as the material gets thinner (goes from 2" to 1/2") at a given temperature and the toughness or fracture energy increases. This is as expected for a material such as the A441 where all three thicknesses were from the same heat. However, when examining the 1" and 2" dynamic K_c data it appears that there is no differences. The 1" data should be tougher than the 2" data but it is not. Although there is no obvious reason for this lack of consistency between the thicknesses for the dynamic K_c tests as found for the CVN and static K_c tests, the results do point to the fact that in fracture testing of bridge steel, certain results can be anticipated but

surprises should not be unexpected. This was found time and time again during the course of this investigation. With regard to K_c estimates from CVN the equation

$$K_{Ic} = \sqrt{A\ E\ CVN}$$

can be used satisfactorily with an A value of 5 as recommended by Barsom (28).

Material for R-curve testing was only available for the 1/2" thickness. The results of the tests are given in Table F-4. These results although not shown on Figure F-10 do generally agree with the static K_c levels shown in Figure F-10. This is consistent with previous results which point to the usefulness of the R-curve K estimates in extending the static K_c measurement to higher temperatures.

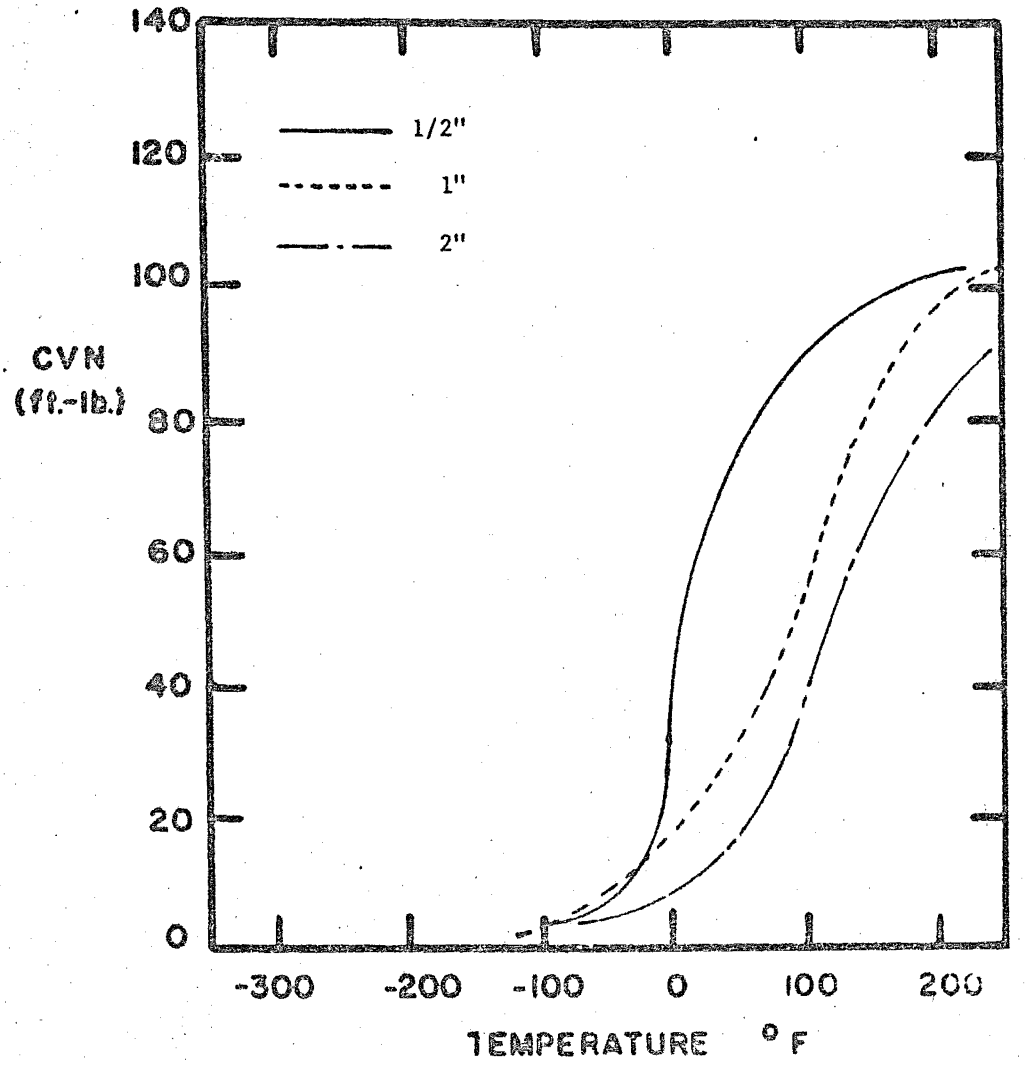

Fig. F-1a Composite Charpy Curves for A441 Material

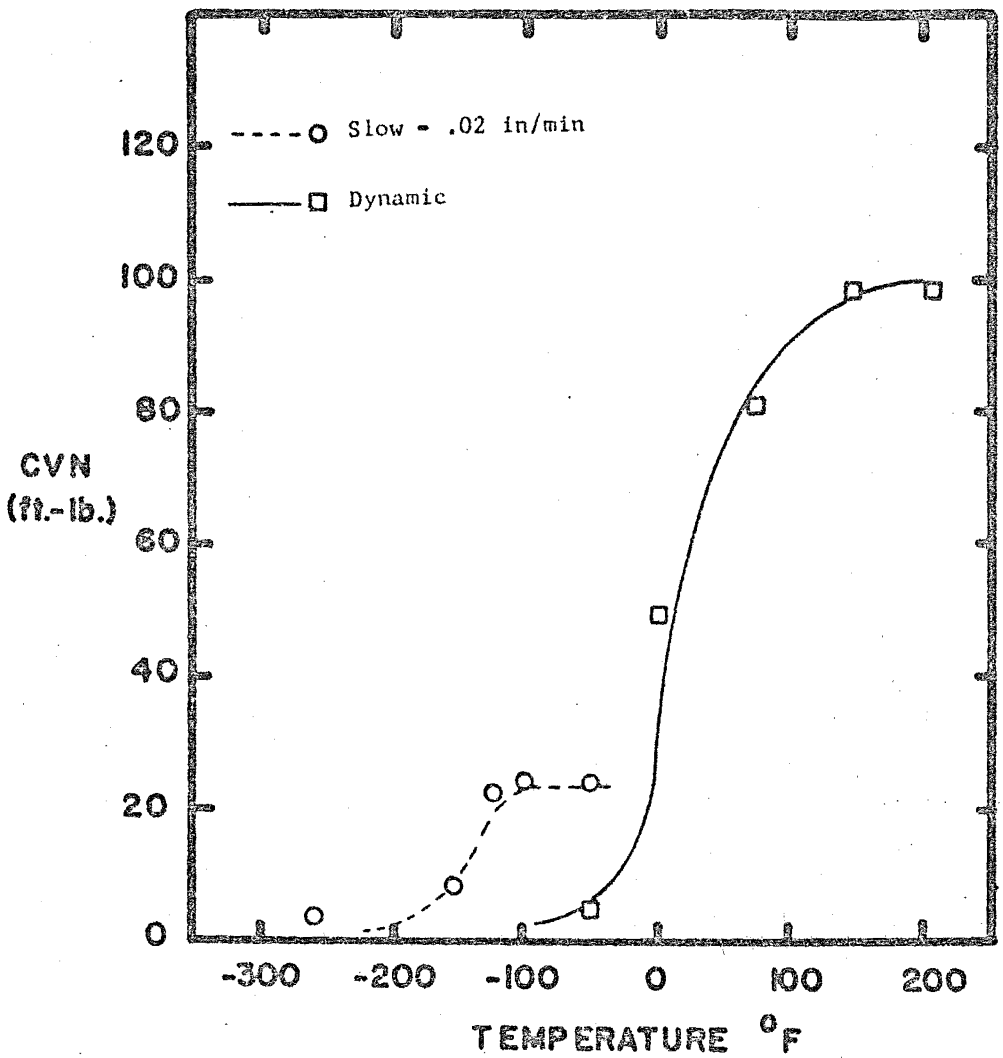

Fig. F-1 A441 1/2" Notched Charpy Data for Two Loading Rates

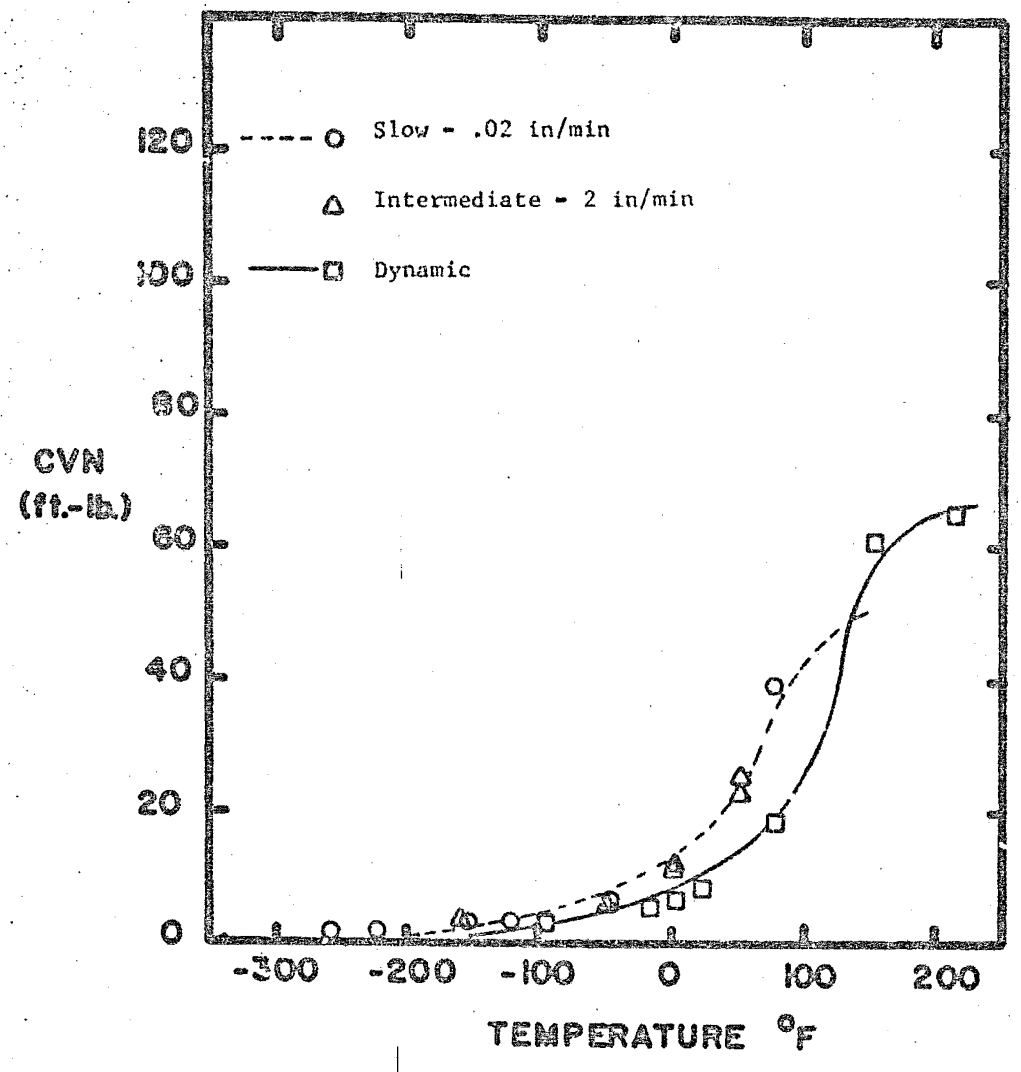

Fig. F-2 A441 1/2" Precracked Charpy Data for Three Loading Rates

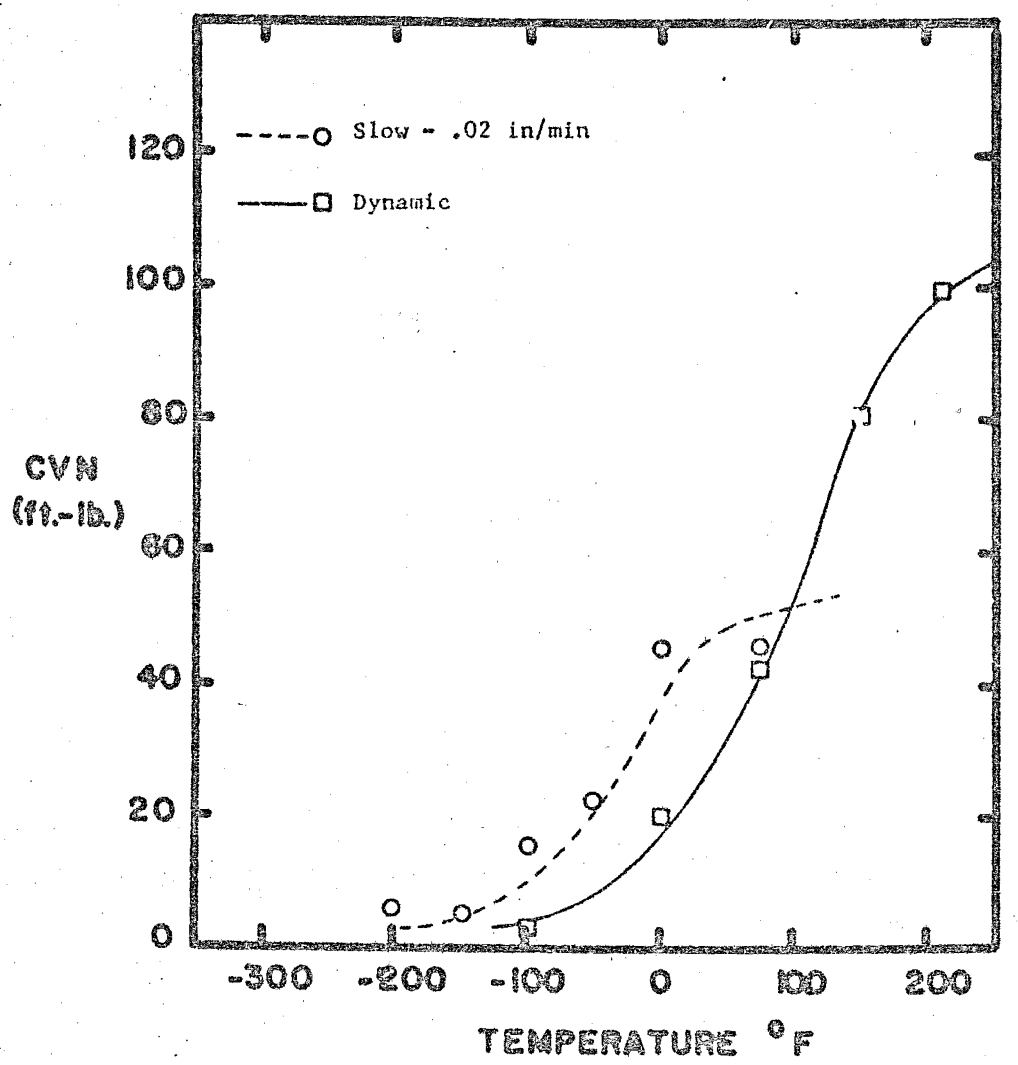

Fig. F-3 A441 1" Notched Charpy Data for Two Loading Rates

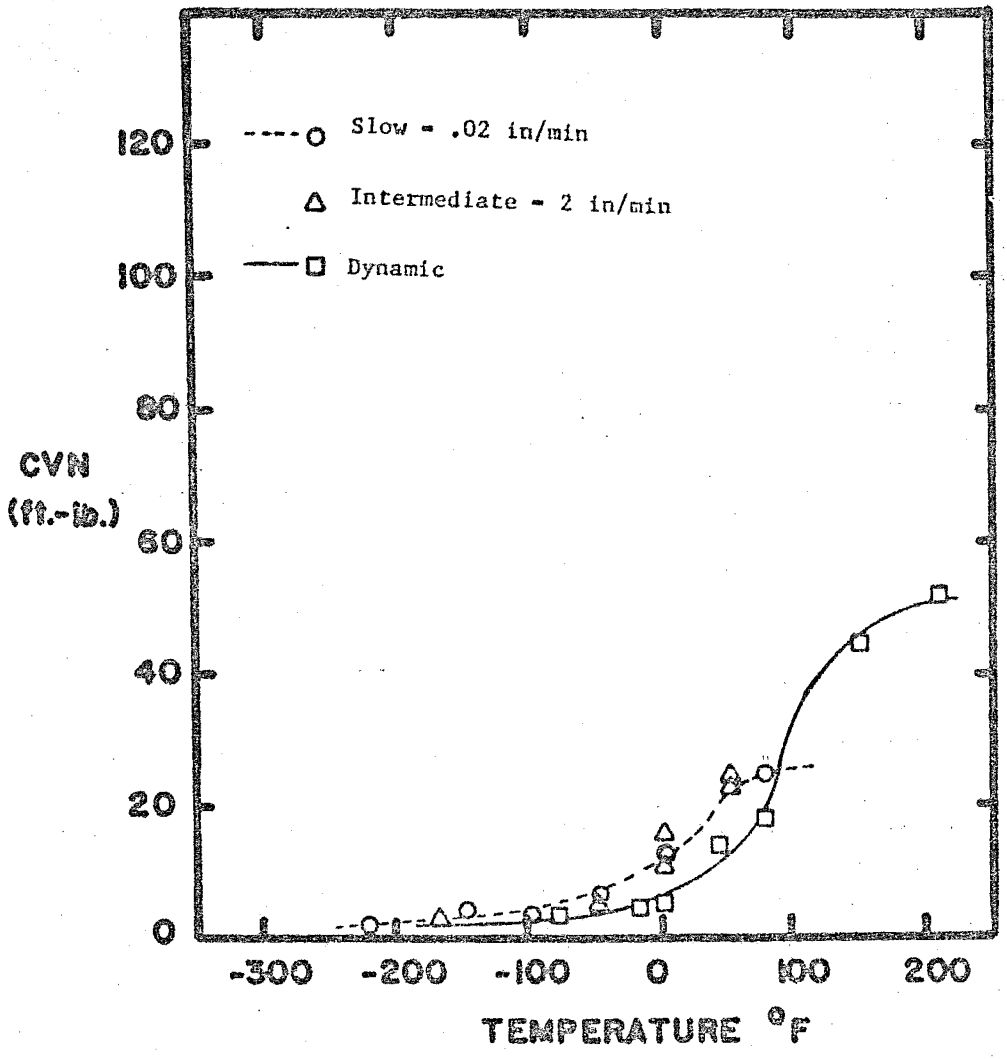

Fig. F-4 A441 1" Precracked Charpy Data for Three Loading Rates

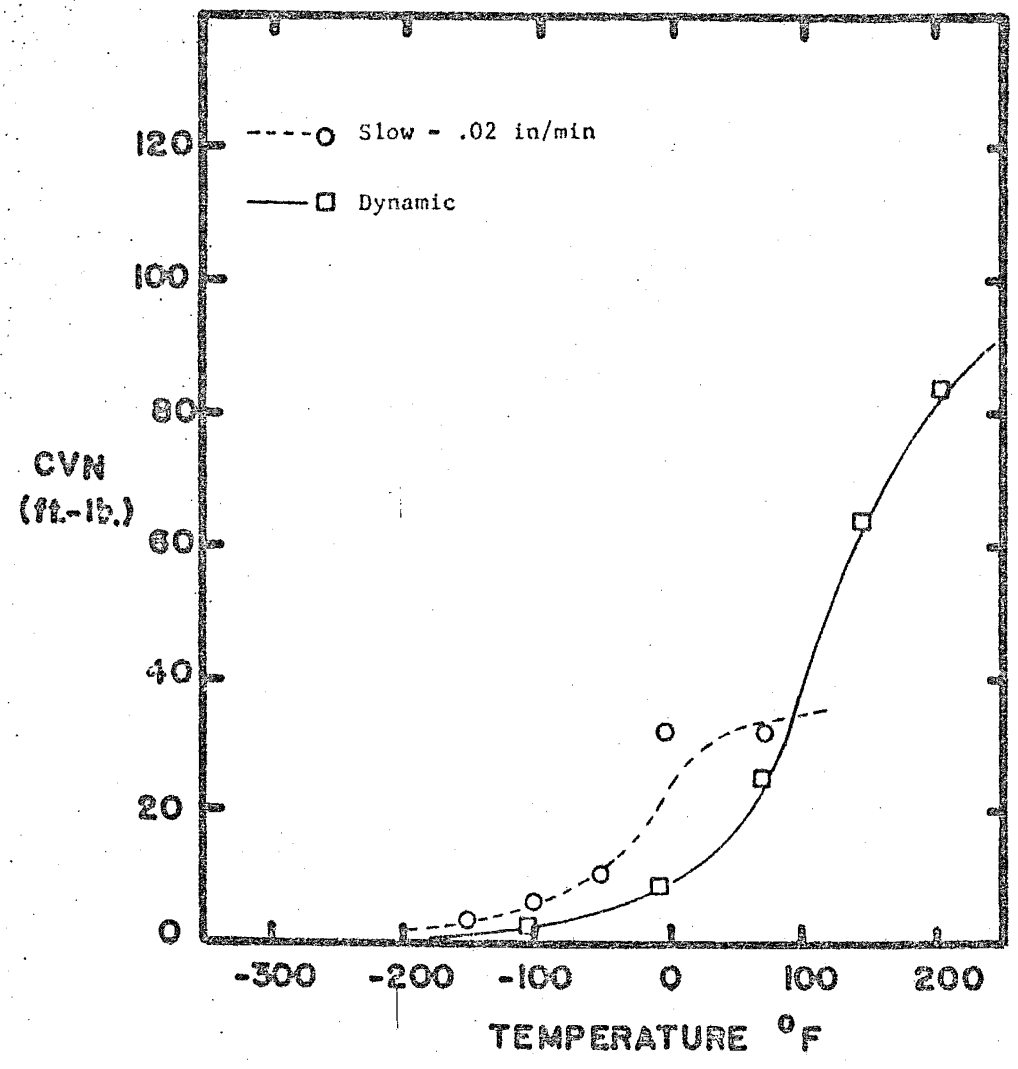

Fig. F-5 A441 2" Notched Charpy Data for Two Loading Rates

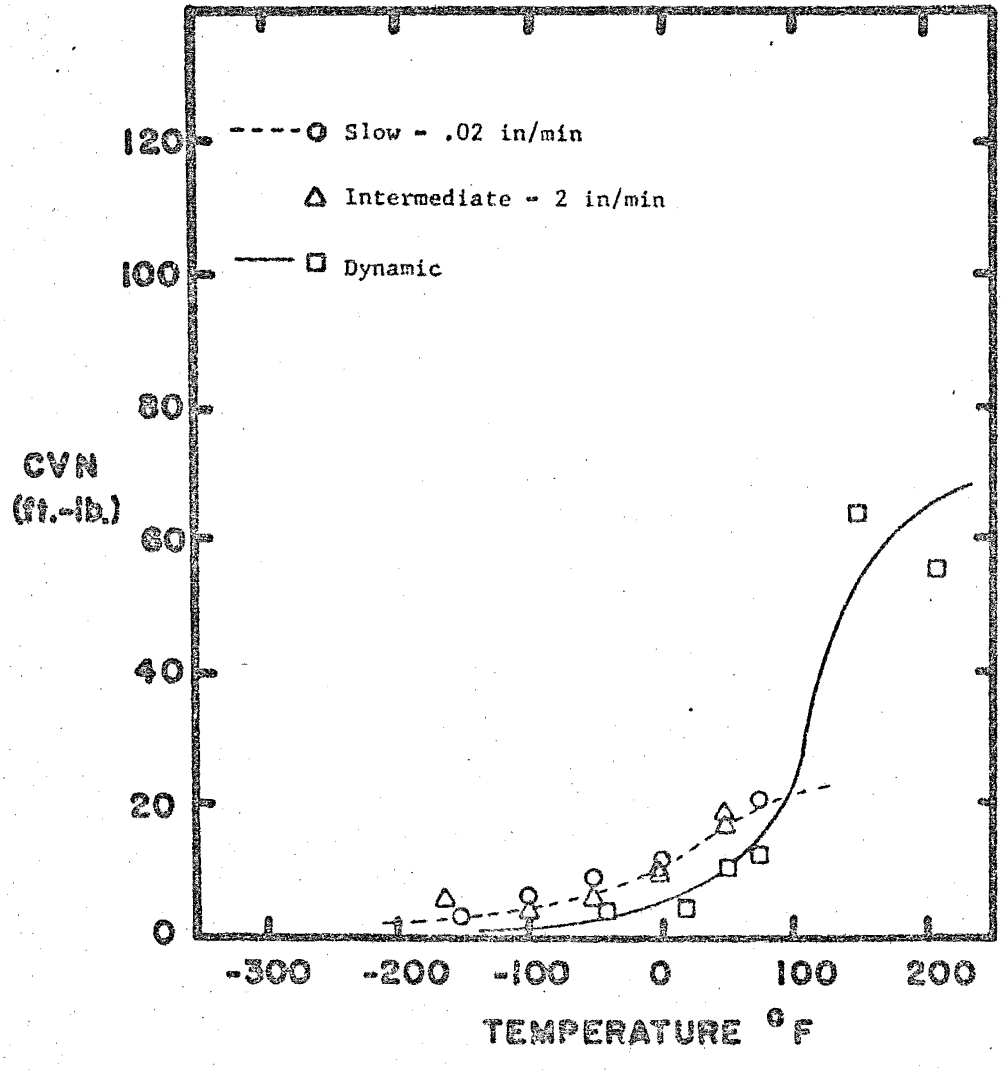

Fig. F-6 A441 2" Precracked Charpy Data for Three Loading Rates

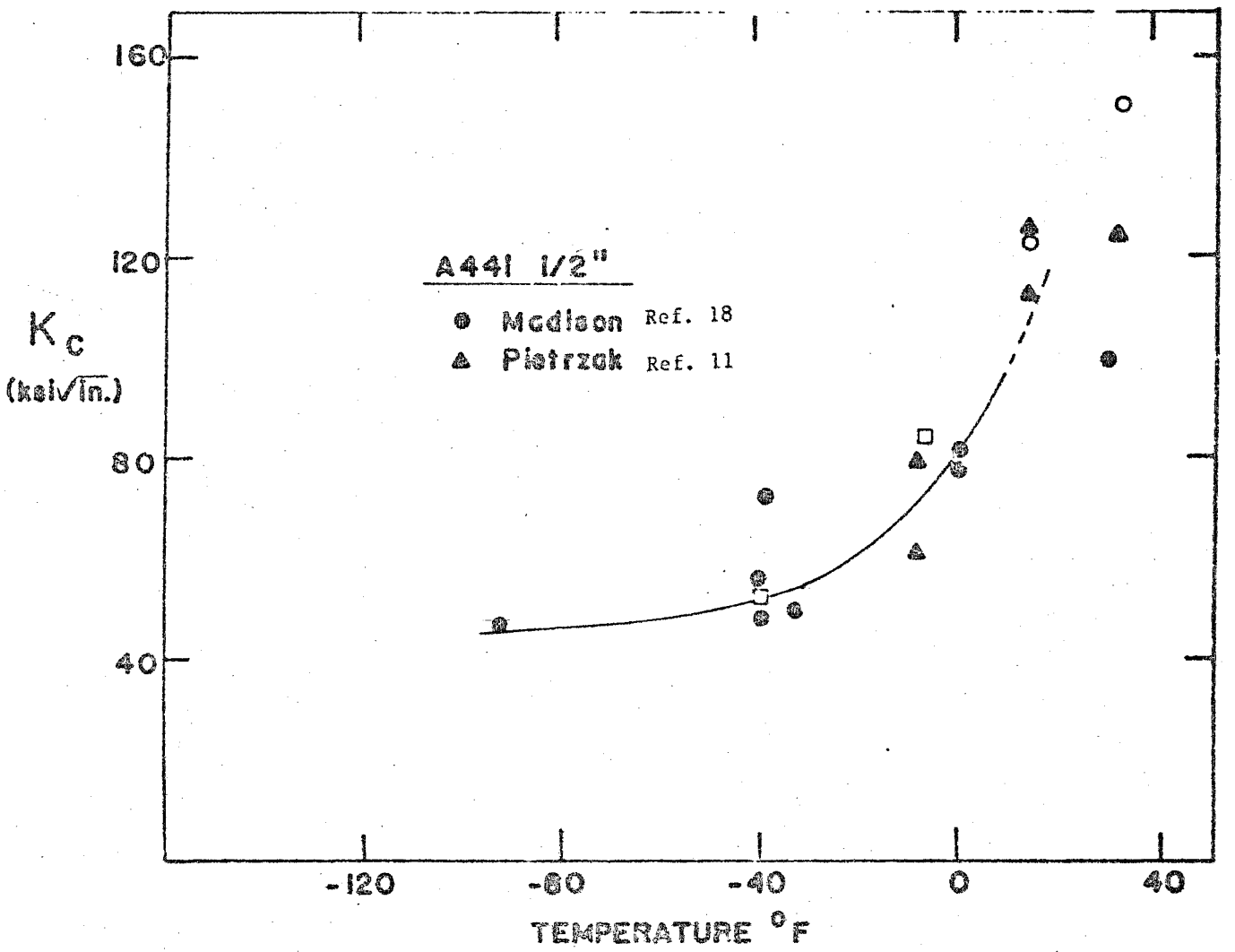

Fig. F-7 Filled Points show Dynamic K_c versus Temperature for A441 - 1/2" Plate. Circles show Estimates of Dynamic K_M from Thickness Reduction. Squares show Estimates of Dynamic K_c from Eqs. (20) and (7) from Phase I Report.

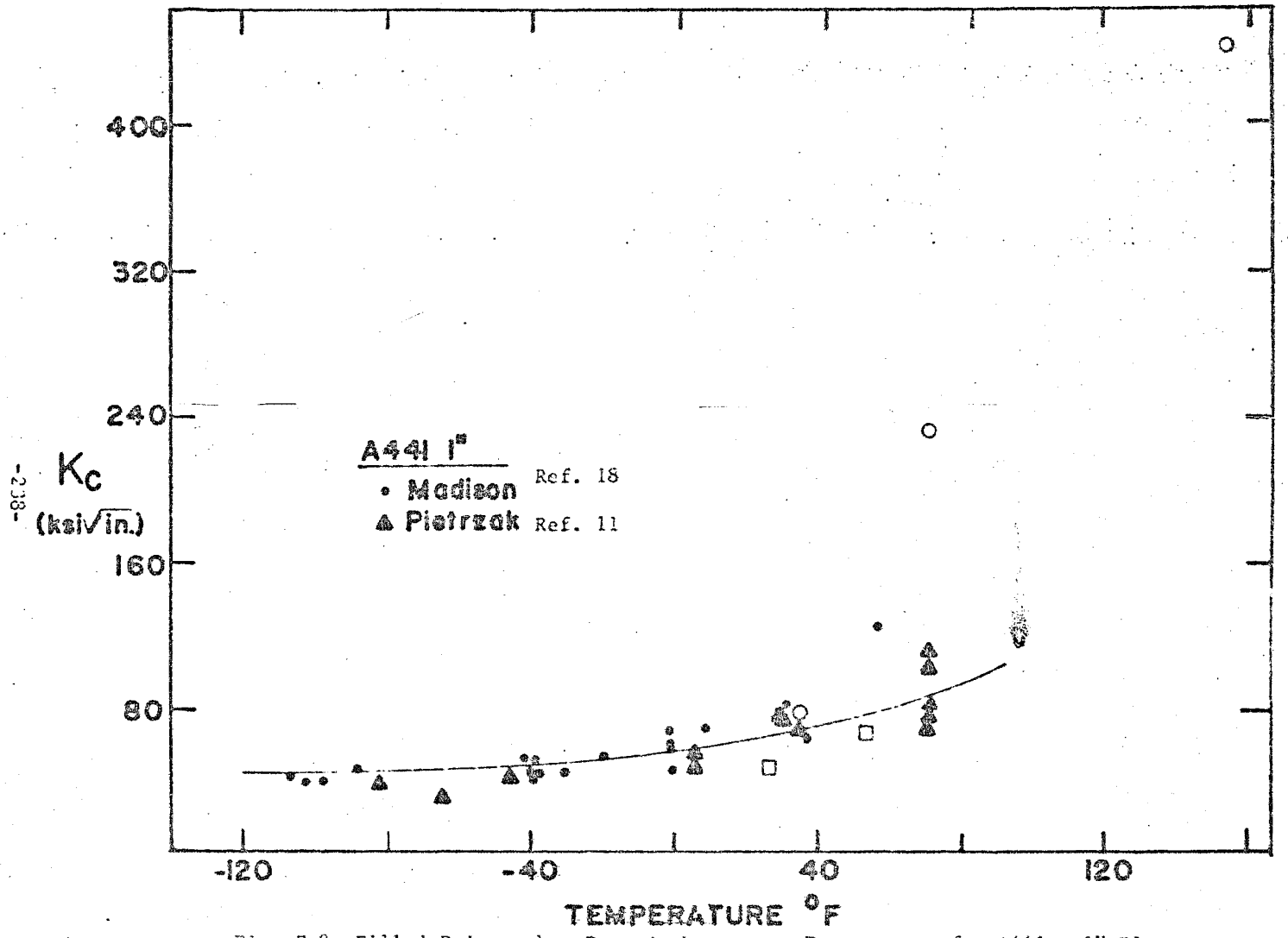

Fig. F-8 Filled Points show Dynamic K_c versus Temperature for A441 - 1" Plate. Circles show Estimates of Dynamic K_M from Thickness Reduction. Squares show Estimates of Dynamic K_c from Eqs. (20) and (7) from Phase I Report.

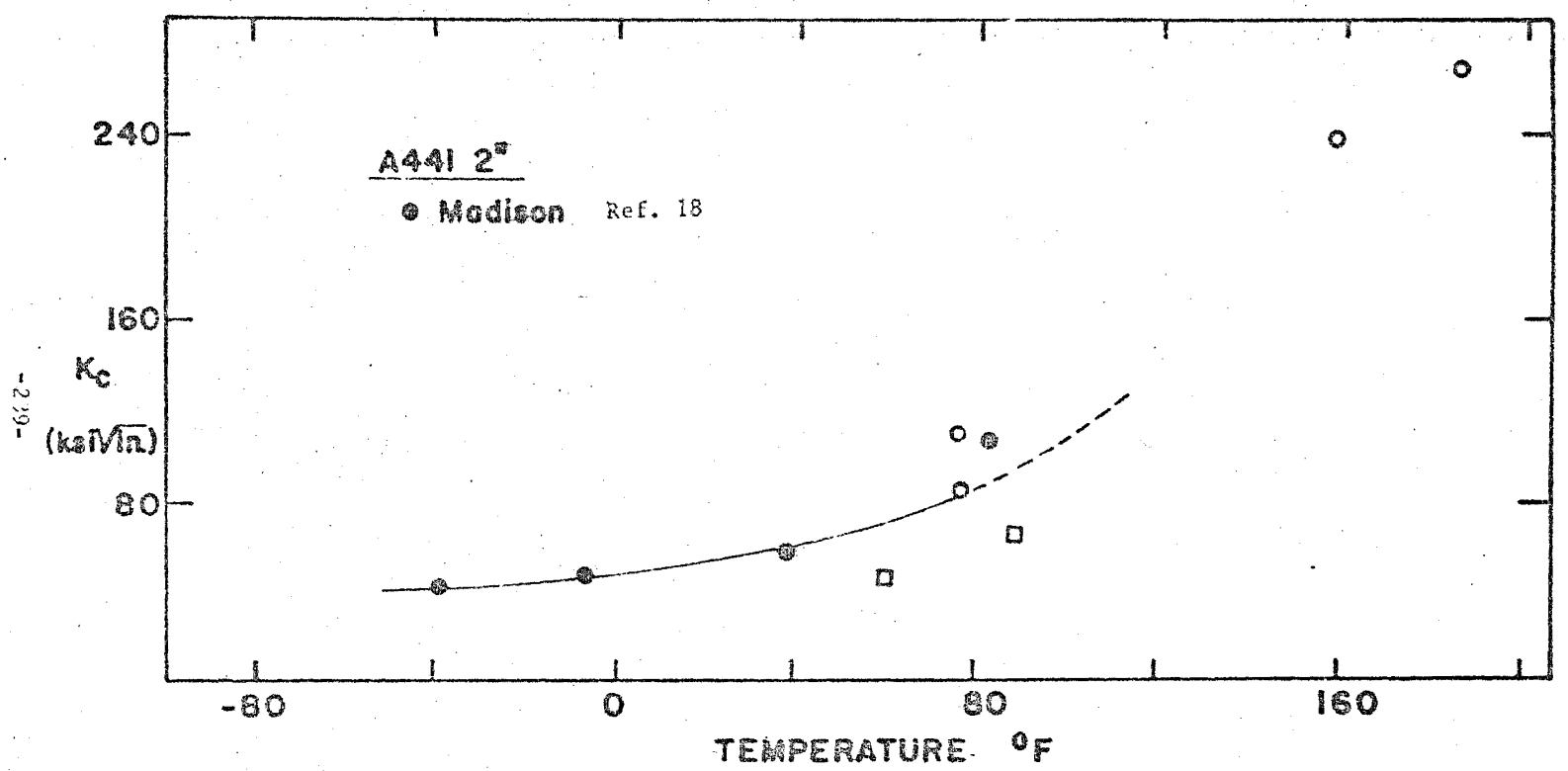

Fig. F-9 Filled Points show Dynamic K_c versus Temperature for A441 - 2" Plate. Circles show Estimates of Dynamic K_M from Thickness Reduction. Squares show Estimates of Dynamic K_c from Eqs. (20) and (7) from Phase I Report.

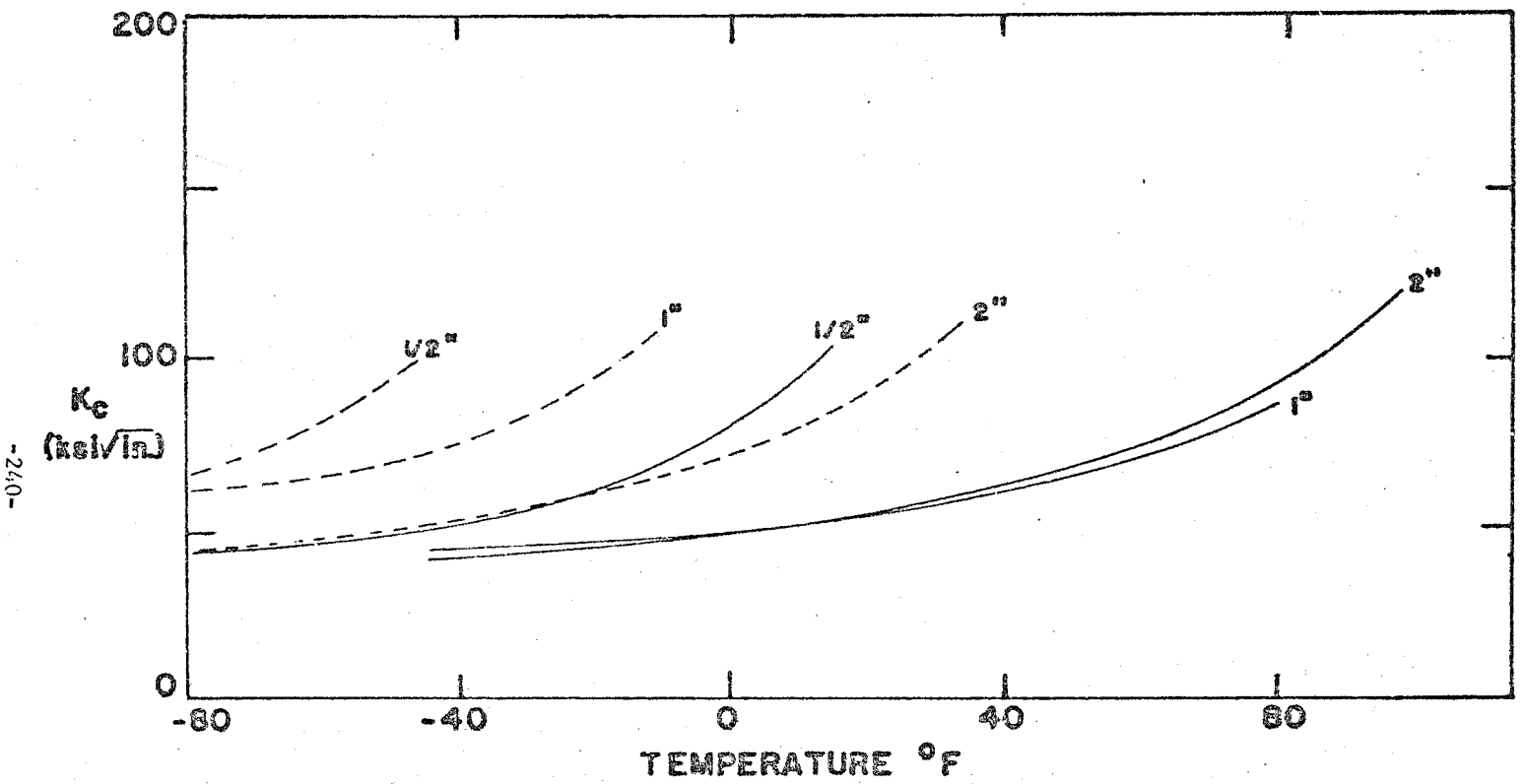

Fig. F-10 Trend Lines are shown (dashed) for Static K_c Values pertaining to 1/2", 1" and 2" with Thicknesses of A441 Plate. For Comparison, the Trend Lines Representing Dynamic K_c Values are shown (solid lines) copies from Figs. F-7, F-8 and F-9.

TABLE F1.1* - A441 CHARPY DATA SUMMARY

Test	Material Thickness (in.)	T_{15} (°F)	T_{30} (°F)	T_{SH} (°F)	CVN_{SH} (ft.-lb.)
DS	0.5	- 15	0	175	100
DP	0.5	60	120	200	65
SS	0.5	- 135	--	- 100	23
SP	0.5	15	70	> 75	> 40
DS	1.0	- 10	45	> 200	> 100
DP	1.0	65	90	> 200	> 50
SS	1.0	- 75	- 20	> 50	> 40
SP	1.0	35	--	75	25
DS	2.0	40	80	> 20	> 80
DP	2.0	80	115	> 200	> 60
SS	2.0	- 25	25	50	32
SP	2.0	40	--	75	22

TABLE F1.2

Test	t	ΔT (°F)	ΔT_B (°F)
S	0.5	115	130
P	0.5	45	
S	1.0	60	130
P	1.0	40	
S	2.0	65	130
P	2.0	40	

*See Table A1.1 for designations

TABLE F2 - CHARPY TEST DATA

A44[illegible] 1/2" (Notched) Slow Bend

Specimen No.	Temp. (° F)	Maximum Load (lb.)	Deflection at Maximum Load (in.)	Crack-Depth (in.)	Energy Absorbed		Shear (%)	Lateral Expansion (mils)
					Actual (ft.-lb.)	Normalized (ft.-lb.)		
100-SN	- 155	2800	0.054	0.079	7.85	7.85	0	10
202-SN	- 260	2450	0.036	0.079	3.00	3.00	0	5
96-SN	- 125	3300	0.112	0.079	22.30	22.30	15	26
65-SN	- 100	3400	0.122	0.079	24.43	24.43	30	27
12-SN	- 50	2750	0.122	0.079	24.30	24.30	30	26

TABLE F2 - CHARPY TEST DATA

A441 1/2" (Notched) Dynamic

Specimen No.	Temp. (° F)	Maximum Load (lb.)	Deflection at Maximum Load (in.)	Crack-Depth (in.)	Energy Absorbed		Shear (%)	Lateral Expansion (mils)
					Actual (ft.-lb.)	Normalized (ft.-lb.)		
	- 50			0.079	5.0	5.0	0	2
	0			0.079	49.0	49.0	30	46
	+ 75			0.079	81.0	81.0	80	70
	+ 150			0.079	98.0	98.0	100	81
	+ 212			0.079	98.0	98.0	100	78

TABLE F2 - CHARPY TEST DATA

A441 1/2" (Precracked) Slow Bend

Specimen No.	Temp. (° F)	Maximum Load (lb.)	Deflection at Maximum Load (in.)	Crack-Depth (in.)	Energy Absorbed		Shear (%)	Lateral Expansion (mils)
					Actual (ft.-lb.)	Normalized (ft.-lb.)		
99-SP	- 260	1050	0.020	0.190	0.95	1.54	0	4
114-SP	- 225	1225	0.032	0.160	1.00	1.35	0	5
101-SP	- 155	1475	0.032	0.135	1.87	2.28	0	6
95-SP	- 125	1225	0.022	0.170	2.58	3.02	0	6
64-SP	- 100	1500	0.031	0.140	1.96	2.43	0	8
11-SP	- 50	1750	0.040	0.140	5.30	6.67	< 5	10
194-SP	+ 75	1675	0.072	0.152	29.6	38.6	50	39

TABLE F2 - CHARPY TEST DATA

A441 1/2" (Precracked) Fast Bend

Specimen No.	Temp. (° F)	Maximum Load (lb.)	Deflection at Maximum Load (in.)	Crack-Depth (in.)	Energy Absorbed		Shear (%)	Lateral Expansion (mils)
					Actual (ft.-lb.)	Normalized (ft.-lb.)		
413	- 165	1200	0.028	0.105	4.00	4.15	0	2
375	- 100	1450	0.030	0.140	2.62	3.50	0	5
337	- 50	1800	0.036	0.125	5.15	6.08	< 5	11
336	- 50	1600	0.032	0.135	4.80	5.85	< 5	10
291	0	1650	0.040	0.140	9.16	11.35	< 15	16
290	0	2240	0.052	0.100	10.34	11.07	< 15	19
256	+ 50	1450	0.058	0.170	17.69	24.76	50	27
257	+ 50	1975	0.060	0.130	18.59	22.12	40	29

TABLE F2 - CHARPY TEST DATA

A441 1/2" (Precracked) Dynamic Tests

Specimen No.	Temp. (° F)	Maximum Load (lb.)	Deflection at Maximum Load (in.)	Crack-Depth (in.)	Energy Absorbed		Shear (%)	Lateral Expansion (mils)
					Actual (ft.-lb.)	Normalized (ft.-lb.)		
	- 100			0.135	2.2	2.68	0	4
	- 20			0.135	4.0	4.90	0	4
	0			0.125	5.0	5.85	0	7
	+ 20			0.120	7.0	8.00	0	10
	+ 75			0.190	11.5	17.80	20	15
	+ 150			0.130	52.5	60.50	100	51
	+ 212			0.130	56.0	64.5	100	53

TABLE F2 - CHARPY TEST DATA

A441 1" (Notched) Slow Bend

Specimen No.	Temp. (° F)	Maximum Load (lb.)	Deflection at Maximum Load (in.)	Crack-Depth (in.)	Energy Absorbed		Shear (%)	Lateral Expansion (mils)
					Actual (ft.-lb.)	Normalized (ft.-lb.)		
116-SN	- 200	2625	0.055	0.079	5.47	5.47	0	7
103-SN	- 150	2400	0.043	0.079	4.85	4.85	0	7
171-SN	- 100	3080	0.087	0.079	14.50	14.50	0	17
16-SN	- 50	3200	0.116	0.079	21.27	21.27	0	25
160-SN	0	3100	0.148	0.079	44.50	44.50	70	52
140-SN	+ 75	3000	0.138	0.079	45.00	45.00	75	58

TABLE F2 - CHARPY TEST DATA

A441 1" (Notched) Dynamic

Specimen No.	Temp. (°F)	Maximum Load (lb.)	Deflection at Maximum Load (in.)	Crack-Depth (in.)	Energy Absorbed		Shear (%)	Lateral Expansion (mils)
					Actual (ft.-lb.)	Normalized (ft.-lb.)		
	- 100			0.079	2.0	2.0	0	3
	0			0.079	19.0	19.0	10	15
	+ 75			0.079	41.5	41.5	30	37
	+ 150			0.079	80.0	80.0	70	75
	+ 212			0.079	99.0	99.0	95	84

TABLE F2 - CHARPY TEST DATA

A441 1" (Precracked) Slow Bend

Specimen No.	Temp. (° F)	Maximum Load (lb.)	Deflection at Maximum Load (in.)	Crack-Depth (in.)	Energy Absorbed		Shear (%)	Lateral Expansion (mils)
					Actual (ft.-lb.)	Normalized (ft.-lb.)		
115-SP	- 225	1675	0.032	0.135	1.67	2.07	0	4
102-SP	- 150	1250	0.026	0.140	3.17	3.93	0	5
170-SP	- 100	1700	0.032	0.125	2.27	2.66	0	7
13-SP	- 50	1500		0.140	5.00	6.20	5	12
159-SP	0	2000	0.062	0.130	11.83	12.60	20	19
139-SP	+ 75	1575		0.162	18.03	24.25	50	34

TABLE F2 - CHARPY TEST DATA

2441 1" (Precracked) Fast Bend

Specimen No.	Temp. (°F)	Maximum Load (lb.)	Deflection at Maximum Load (in.)	Crack-Depth (in.)	Energy Absorbed		Shear (%)	Lateral Expansion (mils)
					Actual (ft.-lb.)	Normalized (ft.-lb.)		
412	- 170	1050	0.028	0.140	2.12	2.65	0	3
376	- 100	1300	0.020	0.125	2.66	3.20	0	4
339	- 50	1920	0.040	0.110	4.67	5.17	0	12
338	- 50	1400	0.029	0.130	4.60	5.49	0	9
293	0	1500	0.036	0.140	9.28	11.51	0	18
292	0	1700	0.061	0.160	11.60	15.61	10	20
259	+ 50	2370	0.080	0.120	19.49	19.49	15	27
258	+ 50	1880	0.070	0.150	18.02	23.88	40	32

TABLE F2 - CHARPY TEST DATA

A441 1" (Precracked) Dynamic

Specimen No.	Temp. (° F)	Maximum Load (lb.)	Deflection at Maximum Load (in.)	Crack-Depth (in.)	Energy Absorbed		Shear (%)	Lateral Expansion (mils)
					Actual (ft.-lb.)	Normalized (ft.-lb.)		
	- 80			0.180	2.0	2.90	0	3
	- 20			0.135	3.5	4.27	0	5
	0			0.135	4.0	4.88	0	6
	+ 40			0.150	10.5	13.60	5	13
	+ 75			0.156	13.3	17.50	10	16
	+ 150			0.140	35.5	44.00	80	38
	+ 212			0.208	31.0	51.00	100	39

TABLE F2 - CHARPY TEST DATA

A441 2" (Notched) Slow Bend

Specimen No.	Temp. (° F)	Maximum Load (lb.)	Deflection at Maximum Load (in.)	Crack-Depth (in.)	Energy Absorbed		Shear (%)	Lateral Expansion (mils)
					Actual (ft.-lb.)	Normalized (ft.-lb.)		
174-SN	- 150	2320	0.036	0.079	3.03	3.03	0	4
67-SN	- 100	2450	0.052	0.079	6.20	6.20	0	6
14-SN	- 50	2800	0.069	0.079	10.00	10.00	0	14
162-SN	0	3275	0.156	0.079	31.50	31.50	10	34
141-SN	+ 75	3000	0.136	0.079	31.40	31.40	30	40

TABLE F2 - CHARPY TEST DATA

A441 2" (Notched) Dynamic

Specimen No.	Temp. (° F)	Maximum Load (lb.)	Deflection at Maximum Load (in.)	Crack-Depth (in.)	Energy Absorbed		Shear (%)	Lateral Expansion (mils)
					Actual (ft.-lb.)	Normalized (ft.-lb.)		
	- 100			0.079	2.0	2.0	0	6
	0			0.079	8.5	8.5	0	12
	+ 75			0.079	25.0	25.0	25	25
	+ 150			0.079	64.0	64.0	70	54
	+ 212			0.079	84.0	84.0	95	66

TABLE F2 - CHARPY TEST DATA

A441 2" (Precracked) Slow Bend

Specimen No.	Temp. (° F)	Maximum Load (lb.)	Deflection at Maximum Load (in.)	Crack-Depth (in.)	Energy Absorbed		Shear (%)	Lateral Expansion (mils)
					Actual (ft.-lb.)	Normalized (ft.-lb.)		
175-SP	- 150	1850	0.030	0.125	2.00	2.35	0	5
66-SP	- 100	1700	0.046	0.145	4.44	5.62	0	6
15-SP	- 50	1450	0.058	0.156	6.33	8.38	0	12
161-SP	0	1900	0.058	0.145	8.67	10.95	0	19
142-SP	+ 75	2100	0.094	0.130	15.40	19.90	50	32

TABLE F2 - CHARPY TEST DATA

A441 2" (Precracked) Fast Bend

Specimen No.	Temp. (° F)	Maximum Load (lb.)	Deflection at Maximum Load (in.)	Crack-Depth (in.)	Energy Absorbed		Shear (%)	Lateral Expansion (mils)
					Actual (ft.-lb.)	Normalized (ft.-lb.)		
377	- 100	1425	0.028	0.150	3.20	4.20	0	5
341	- 50	1560	0.028	0.135	4.10	5.00	0	8
340	- 50	1000	0.022	0.190	3.40	5.12	0	8
296	0	1750	0.060	0.130	7.80	9.30	0	14
295	0	2020	0.076	0.140	8.31	10.31	0	16
294	0	1420	0.628	0.135	8.74	10.67	0	18
261	+ 50	2245	0.076	0.120	15.69	18.04	20	23
260	+ 50	2220	0.060	0.115	14.49	16.40	< 10	24

TABLE F2 - CHARPY TEST DATA

A441 2" (Precracked) Dynamic

Specimen No.	Temp. (° F)	Maximum Load (lb.)	Deflection at Maximum Load (in.)	Crack-Depth (in.)	Energy Absorbed		Shear (%)	Lateral Expansion (mils)
					Actual (ft.-lb.)	Normalized (ft.-lb.)		
	- 40			0.150	2.0	2.58	0	4
	+ 20			0.125	3.2	3.74	0	4
	+ 50			0.156	7.2	9.50	0	14
	+ 75			0.130	10.0	11.90	< 5	14
	+ 150			0.125	54.5	63.70	80	50
	+ 212			0.135	45.0	55.0	90	49

TABLE F3.1

DYNAMIC K_c AND K_M VALUES FOR 1/2 INCH A441 PLATE

A441, B = 1/2 in., Dynamic Loading

Specimen Number	Max. Load (kips)	B (in.)	Temp. (^{o}F)	σ_{YS} (ksi)	K_c (ksi $\sqrt{in}$)	K_M (ksi $\sqrt{in}$)
A023	26.25	0.492	83.0	74.9	> 125	--
A024	27.50	0.492	83.0	73.2	> 125	
A025	12.00	0.493	- 8.0	84.6		--
A026	14.50	0.486	- 8.0	84.0	79.6	--
A029	18.00	0.483	32.0	78.7	124.6	150.6
A030	22.00	0.476	32.0	78.7	> 125	--
A031	18.50	0.482	14.0	81.0	126.1	123.4
A032	17.50	0.476	14.0	81.0	112.8	126.0

TABLE F3.2

DYNAMIC K_c AND K_M VALUES FOR 1 INCH A441 PLATE

A441, B = 1 in., Dynamic Loading

Specimen Number	Max. Load (kips)	B (in.)	Temp. (°F)	σ_{YS} (ksi)	K_c (ksi $\sqrt{in}$)	K_M (ksi $\sqrt{in}$)
A114	30.00	0.935	154.0	69.8	> 125	443.4
A119	33.00	0.964	81.0	73.6	> 125	--
A120	24.50	0.970	81.0	73.5	> 125	--
A121	20.00	0.971	32.0	78.2	73.9	81.3
A122	20.00	0.970	32.0	78.3	75.4	--
A124	11.25	0.977	-80.5	92.1	39.4	--
A125	15.00	0.976	7.7	79.3	51.0	--
A126	13.25	0.974	-35.5	91.7	45.2	--
A127	12.50	0.936	-44.5	86.7	43.3	--
A128	15.75	0.971	7.7	79.0	55.1	--
A129	15.38	0.955	7.7	79.1	55.1	--
A131	9.50	0.967	-62.5	91.5	32.4	--
A134	24.00	0.971	72.0	73.5	111.3	--
A135	21.00	0.977	72.0	73.0	83.8	--
A139	25.50	0.967	72.0	71.9	> 125	--
A140	25.50	0.961	72.0	71.9	> 125	--
A142	19.00	0.950	36.5	76.0	71.0	--
A143	30.00	0.968	72.0	72.5	> 125	--
A144	26.50	0.978	72.0	72.7	> 125	--
A145	23.00	0.957	72.0	73.5	104.7	232.5
A146	22.50	0.948	72.0	74.1	105.4	--
A147	20.00	0.982	72.0	77.8	73.8	--
A149	26.00	0.985	72.0	72.4	> 125	--
A150	16.50	0.964	72.0	75.8	71.0	--
A153	18.50	0.960	72.0	77.8	67.8	--

TABLE F3.3

DYNAMIC K_c AND K_M VALUES FOR 2 INCH A441 PLATE

A441, B = 2 in., Dynamic Loading

Specimen Number	Max. Load (kips)	B (in.)	Temp. (^oF)	σ_{YS} (ksi)	K_c (ksi $\sqrt{in}$)	K_M (ksi $\sqrt{in}$)
A223	36.50	1.956	83.0	73.2	102.7	--
A224	36.50	1.956	83.0	73.2	102.8	--
A225	21.00	1.955	- 5.8	83.2	48.1	--
A226	21.00	1.955	- 5.8	83.2	48.3	--
A229	55.00	1.958	188.0	67.5	> 125	267.3
A230	52.50	1.942	160.0	69.9	> 125	237.0
A231	36.90	1.946	77.0	73.8	> 125	110.6
A232	36.25	1.939	77.0	73.8	> 125	83.9

TABLE F4 - A441 R-CURVE INSTABILITY SUMMARY

Thickness (in.)	Test Temperature ($^{\circ}$ F)	Fatigue Crack Length (in.)	K_c at Instability (psi)	Apparent Crack Length at Instability (in.)
0.5*	- 50	6.3	169,376	6.85
0.5	- 95	6.3	66,070	6.66

*Crack branching occurred at crack length of 8.3"

APPENDIX G - A588 DATA

This appendix contains the data collected for the 1/2", 1" and 2" thicknesses of the A588 material. This steel was supplied to the program by the Bethlehem Steel Corporation. The chemical analysis, physical properties and heat designations appear in Tables 1 and 2.

The data in this appendix is presented in the form of a Charpy summary, a detailed Charpy tabulation, a K_c tabulation, an R-curve summary and appropriate figures which best illustrate the data trends. Details of the test procedures and terminology can be found in appendices J, K and L and Chapter 2.

Standard Charpy specimens were tested at two loading rates. Precracked Charpy specimens were also tested but at three loading rates rather than two. The Charpy data is presented in Figures G-1 through G-6. Data tabulations are given in Tables G-1 and G-2. The results from the precracked slow and fast Charpy tests indicated that there was no temperature shift for these two speeds. For both the standard and precracked Charpy specimens there was a definite temperature shift. The observed shift for the standard specimens was not consistent with predictions of Barsom (28). For the 1/2" material the results gave a higher shift while for the 2" material the results were lower than expected. Due to strange results from the slow test of the standard 1" Charpy specimens, it was impossible to discern a shift for the 1" material. It was also noted that the shift for the precracked

specimens tended to be less than predicted values. This behavior is in agreement with tests of the other material in this program. The precracked results showed much higher transition temperature than the standard specimens and the precracked tests results do not appear to form a lower bound for the standard data.

The K_c and D.T. tests for the three thicknesses of A588 are shown in Figures G-7 through G-9. Table G-3 tabulates these data. As with most of the other materials tested in this program the transition in standard CVN, K_c and D.T. curves occurred over the same temperature range for a given thickness. A shift between the static K_c and the dynamic K_c test results is noted for a given thickness. These shifts for the 1/2" and 1" materials are in general agreement with Barsom (28). The data for the 2" material does not allow a meaningful evaluation of the temperature shift. These A588 K_c data as with other data from the program point to the presence of a temperature shift as proposed by Barsom (28) even when the CVN results do not clearly show such a shift. The equation

$$K_{Ic} = \sqrt{A\ E\ CVN}$$

for correlating K_c and CVN data is quite effective for the 1" and 2" materials if A is taken as 5. However, for the 1/2" material an A value of 15 will provide good results. Figure G-10 shows β_{DT} vs. β_{K_c}. For β_{K_c} less than 1 it appears that a fair correlation between K_c and D.T. can be made. This result confirms other test data from this program.

R-curve tests were run on the 1/2" and 1" materials. The results of these tests are tabulated in Table G-4. In all of the R-curve tests of the A588 materials there was not any stable crack growth detected. All crack growth was unstable and caused the specimens to split in half. In four of the tests crack velocities were great enough to cause crack branching. Figures G-7 and G-8 show the K_c estimates from the R-curve tests. As with the other materials, the K estimate prove very useful in extending the static K_c measurements to higher temperatures.

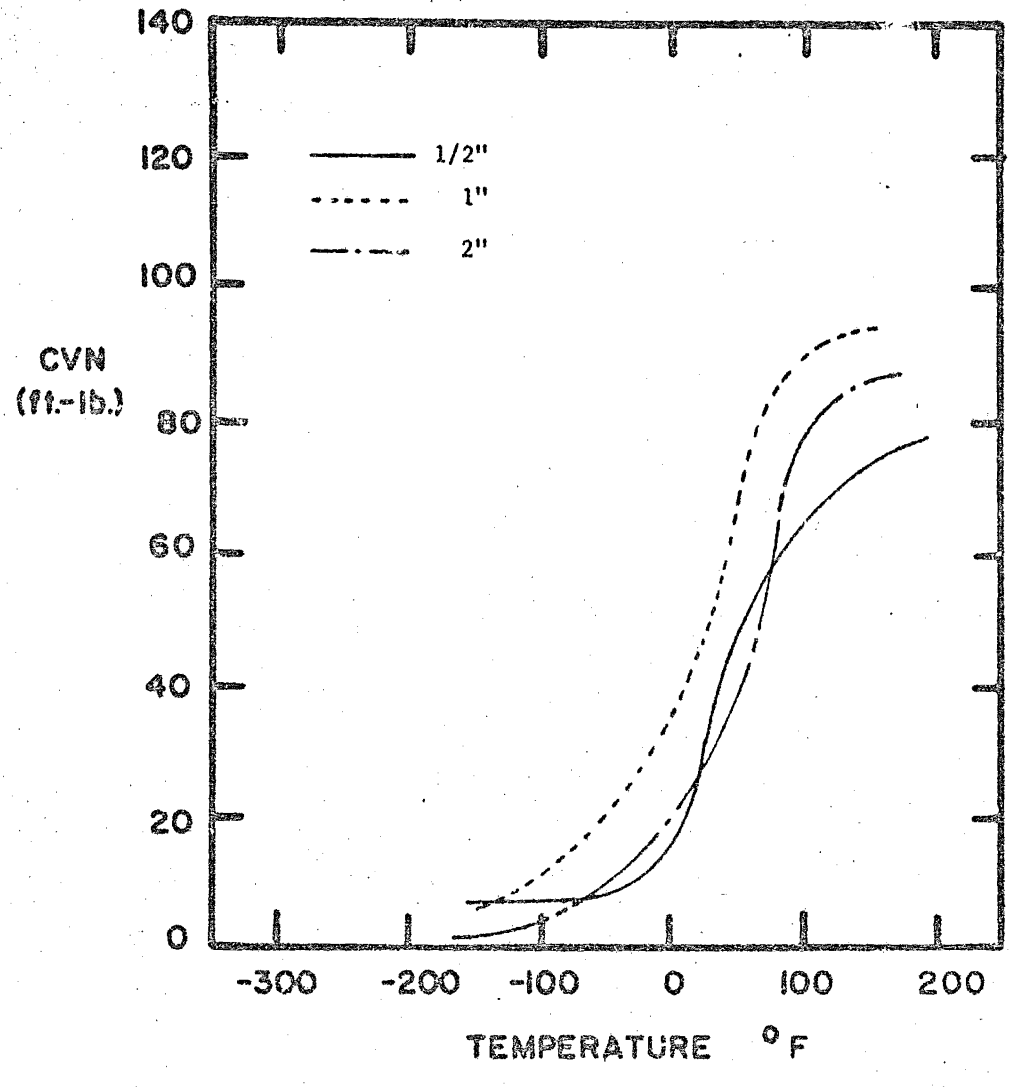

Fig. G-1a Composite Charpy Curves for A588 Material

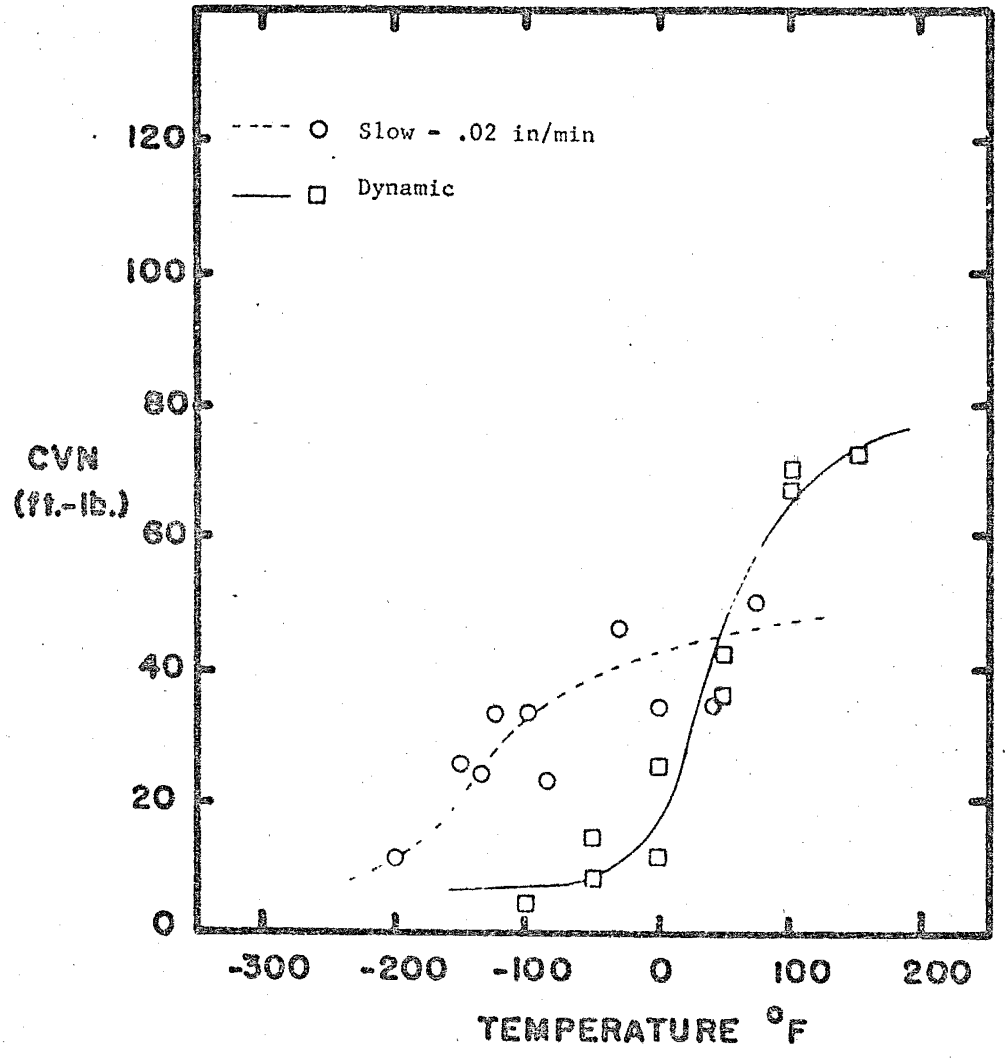

Fig. G-1 A588 1/2" Notched Charpy Data for Two Loading Rates

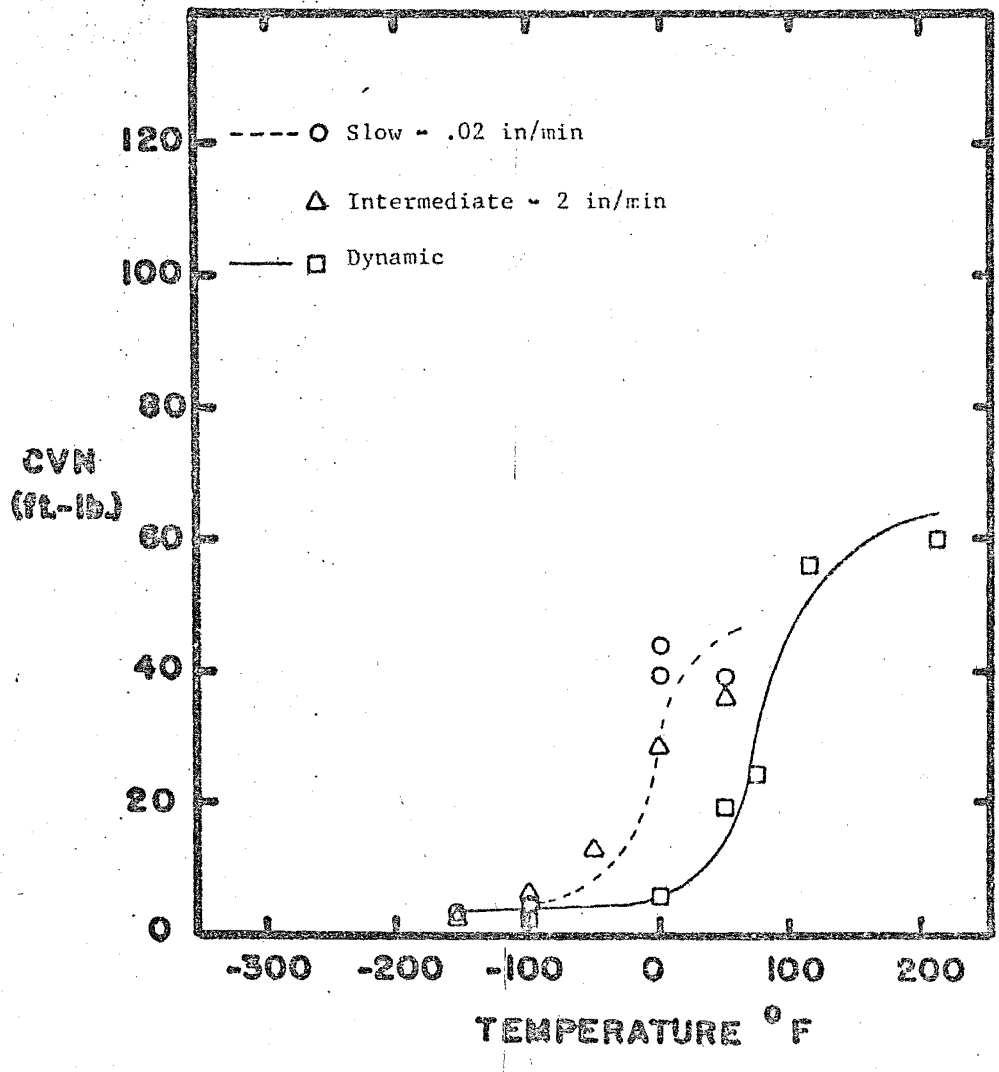

Fig. G-2 A588 1/2" Precracked Data for Three Loading Rates

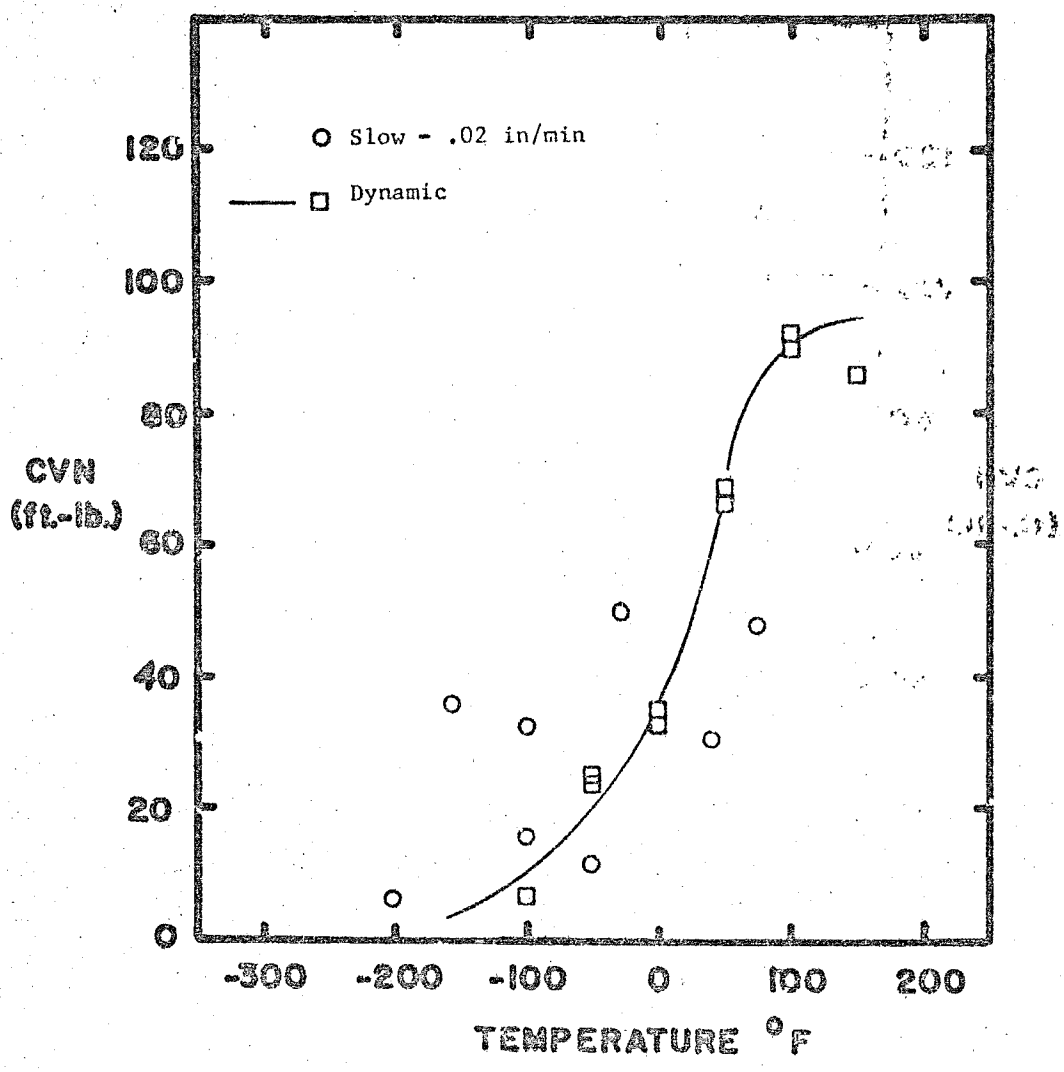

Fig. G-3 A588 1" Notched Charpy Data for Two Loading Rates

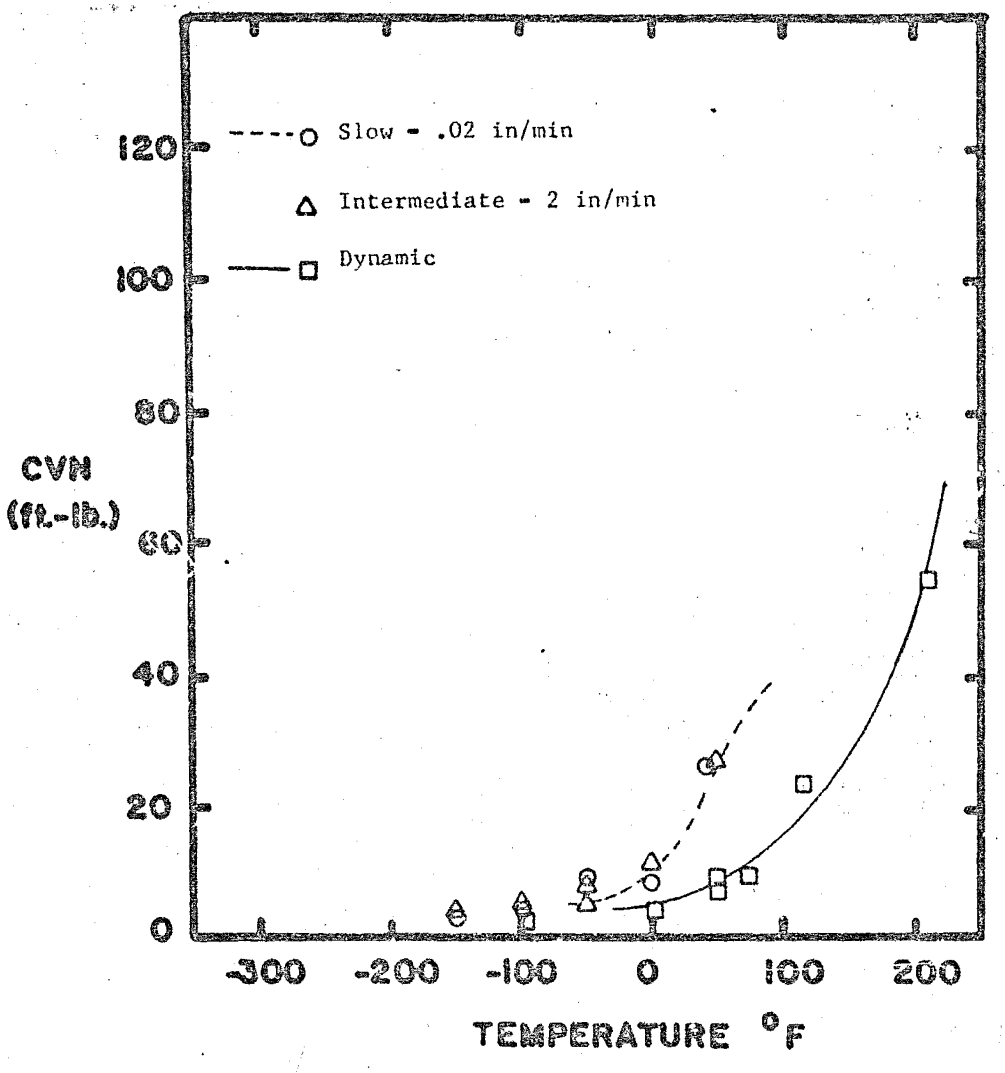

Fig. G-4 A588 1" Precracked Data for Three Loading Rates

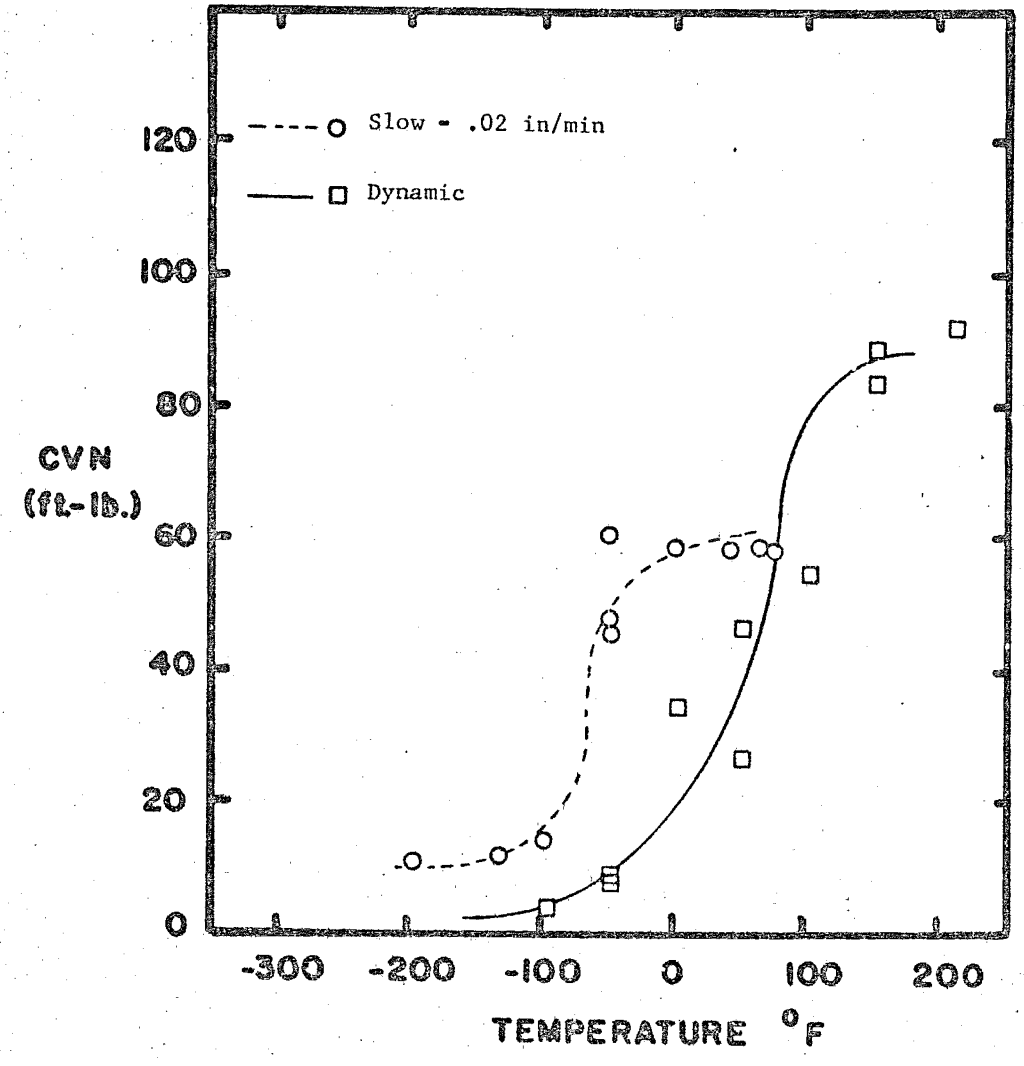

Fig. G-5 A588 2" Notched Charpy Data for Two Loading Rates

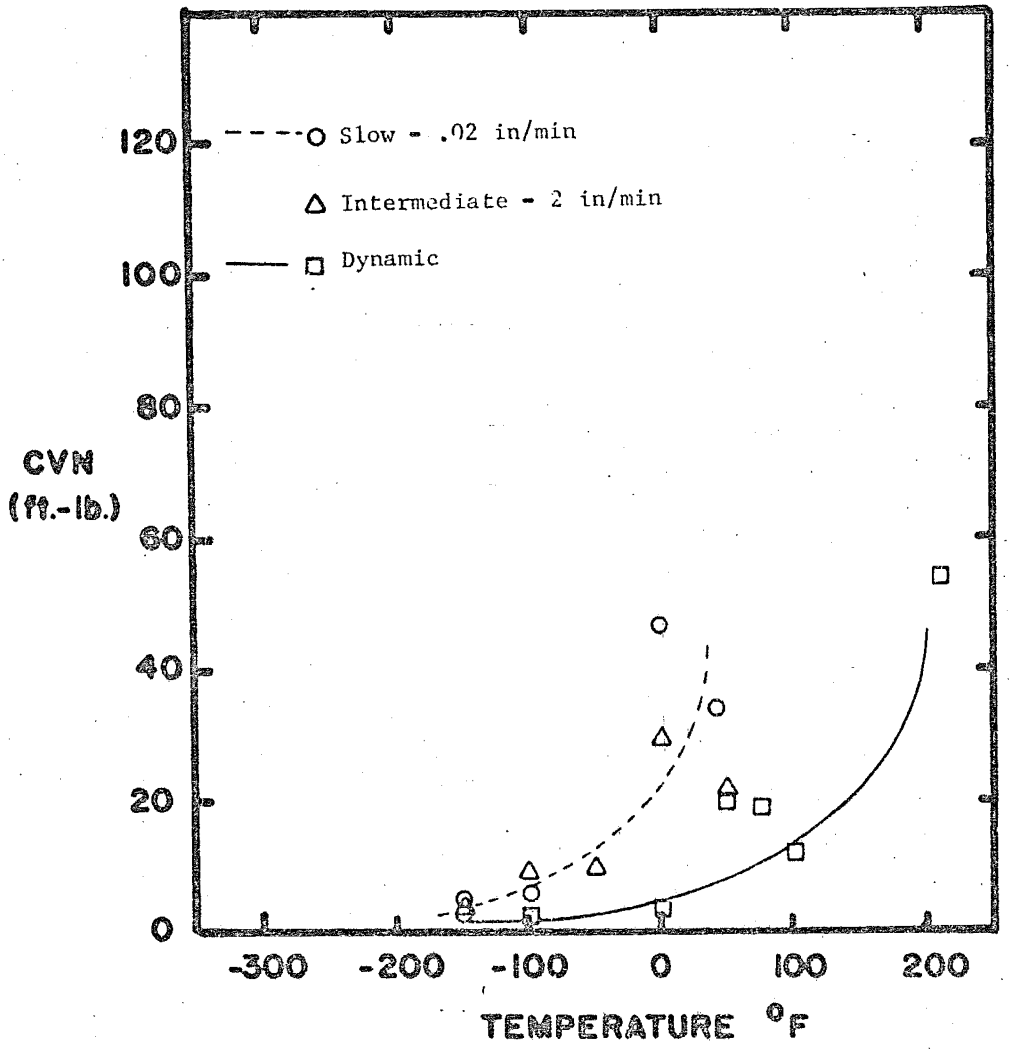

Fig. G-6 K_c Data for A588B 1/2" Material

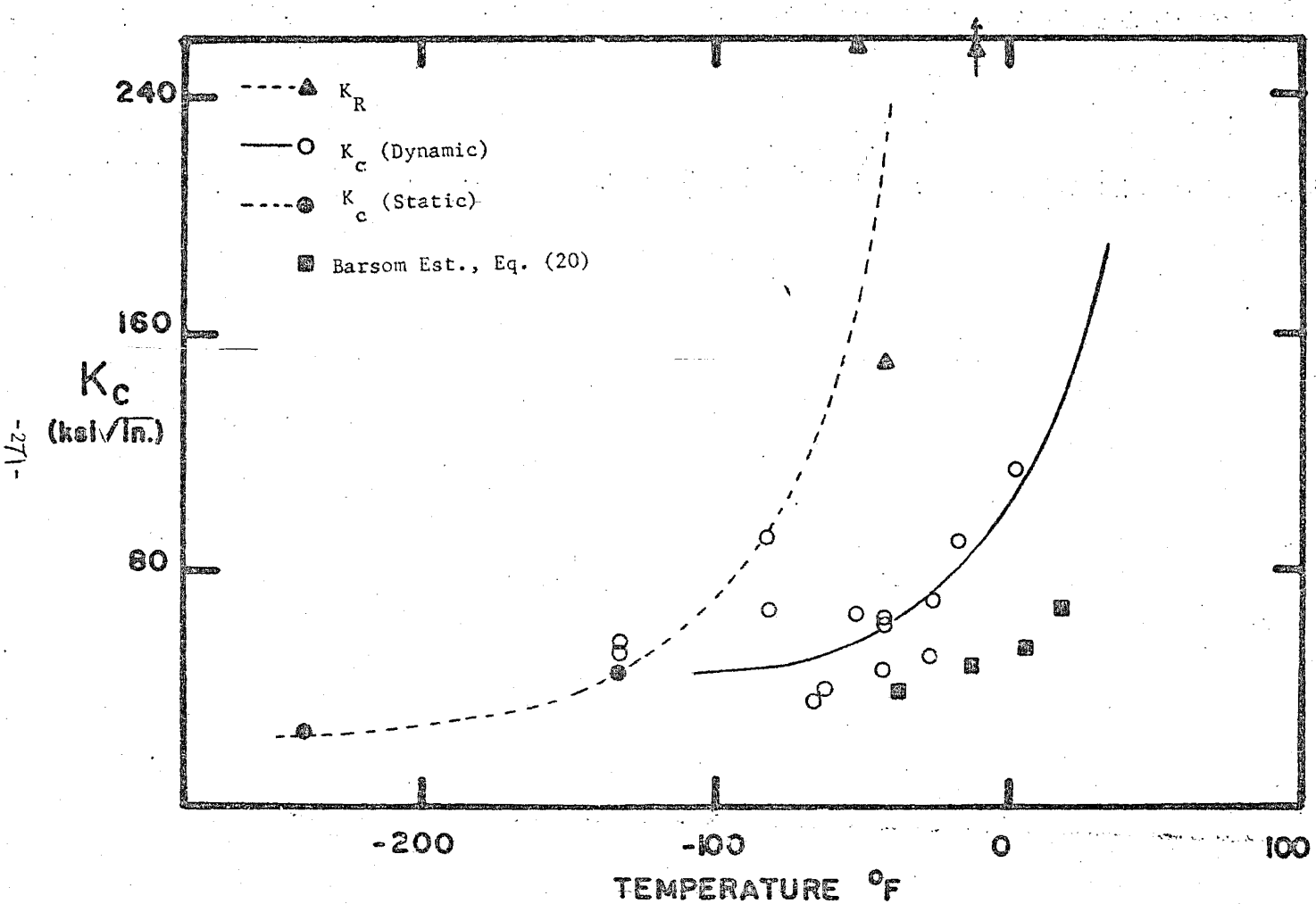

Fig. G-7 K_c Data for A588B 1/2" Material

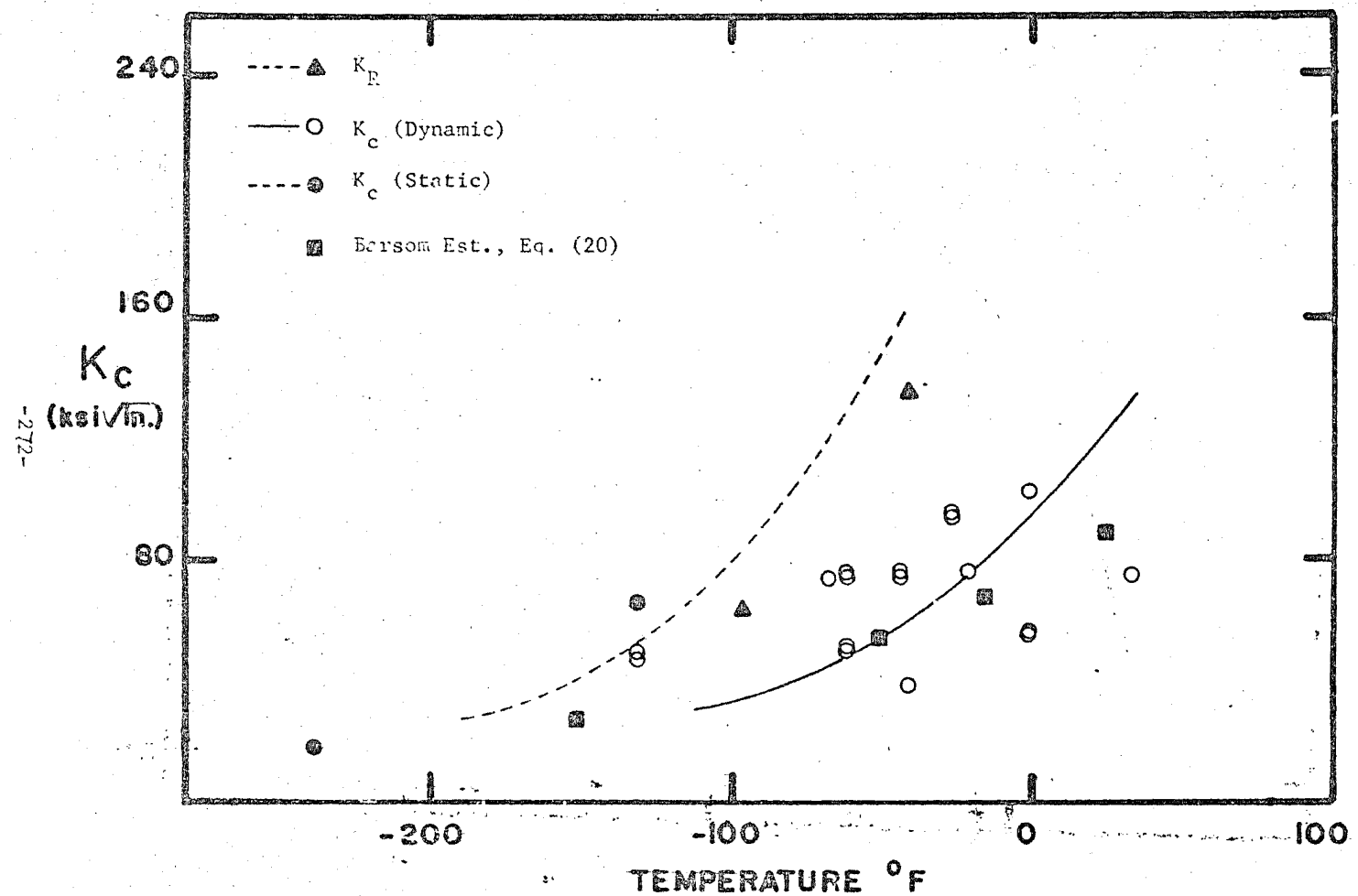

Fig. C-8 K_c Data for A588B 1" Material

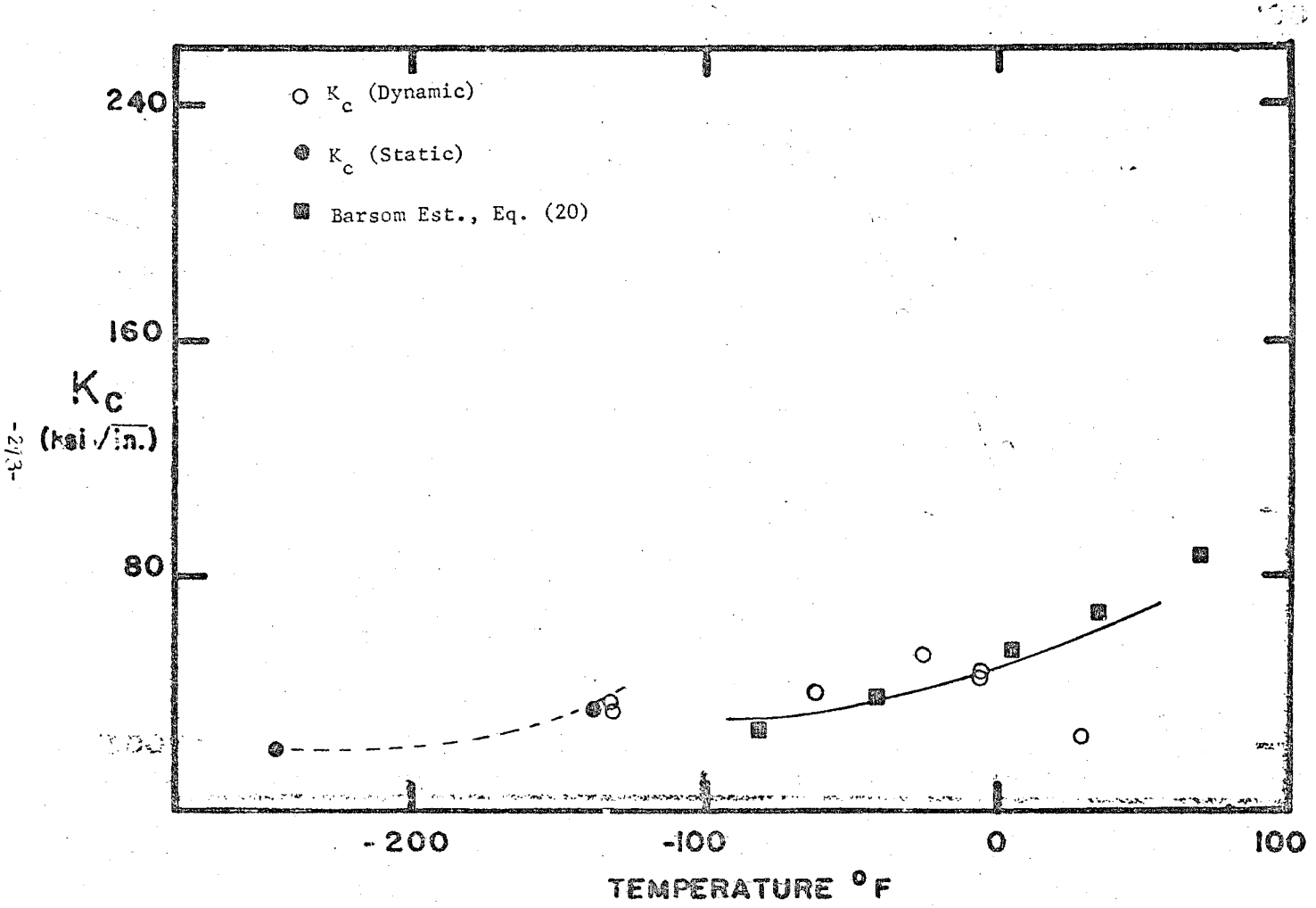

Fig. G-9 K_c Data for A588B 2" Material

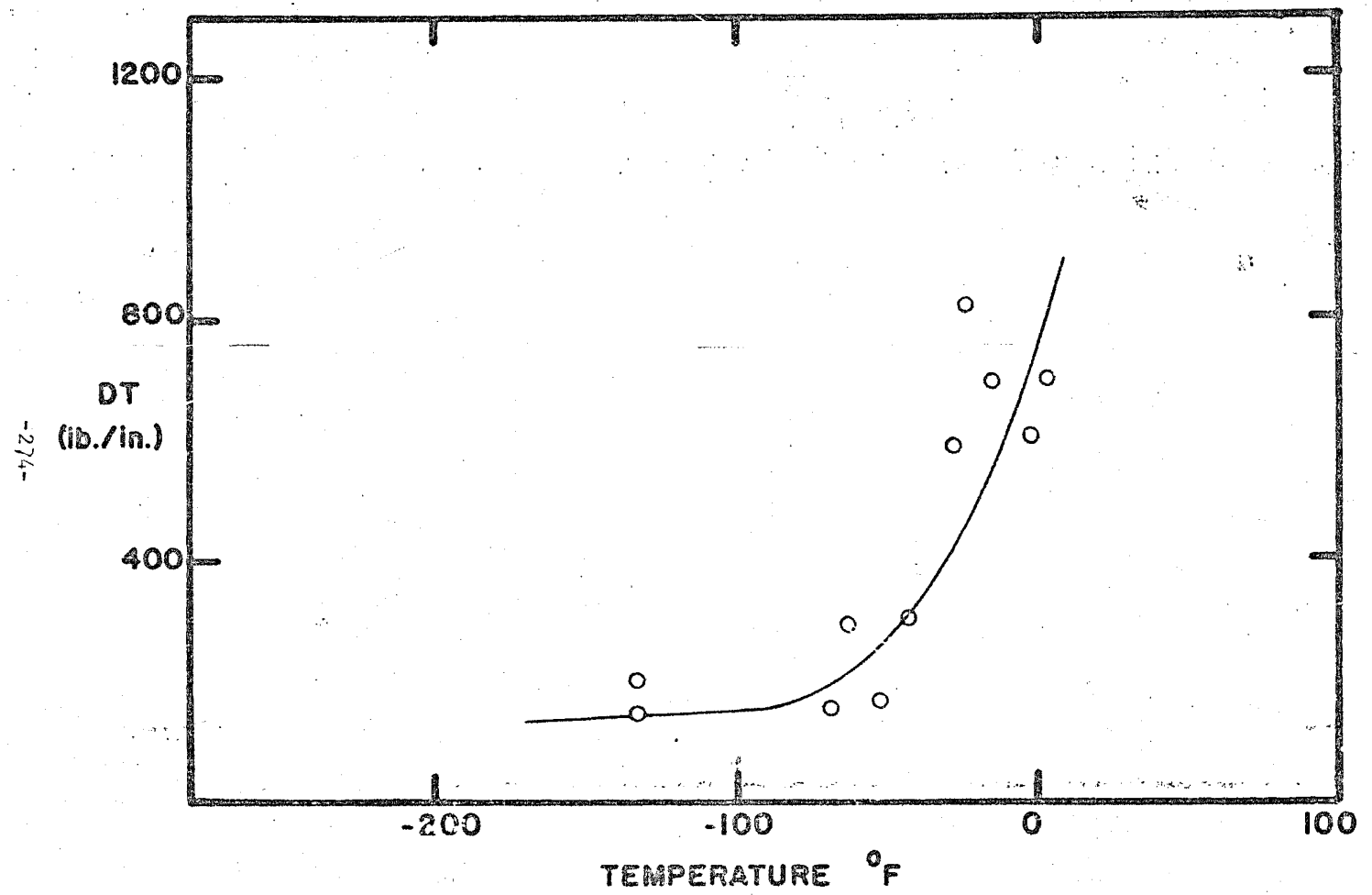

Fig. C-10 Dynamic Tear Data for A588L - 1/2" Material

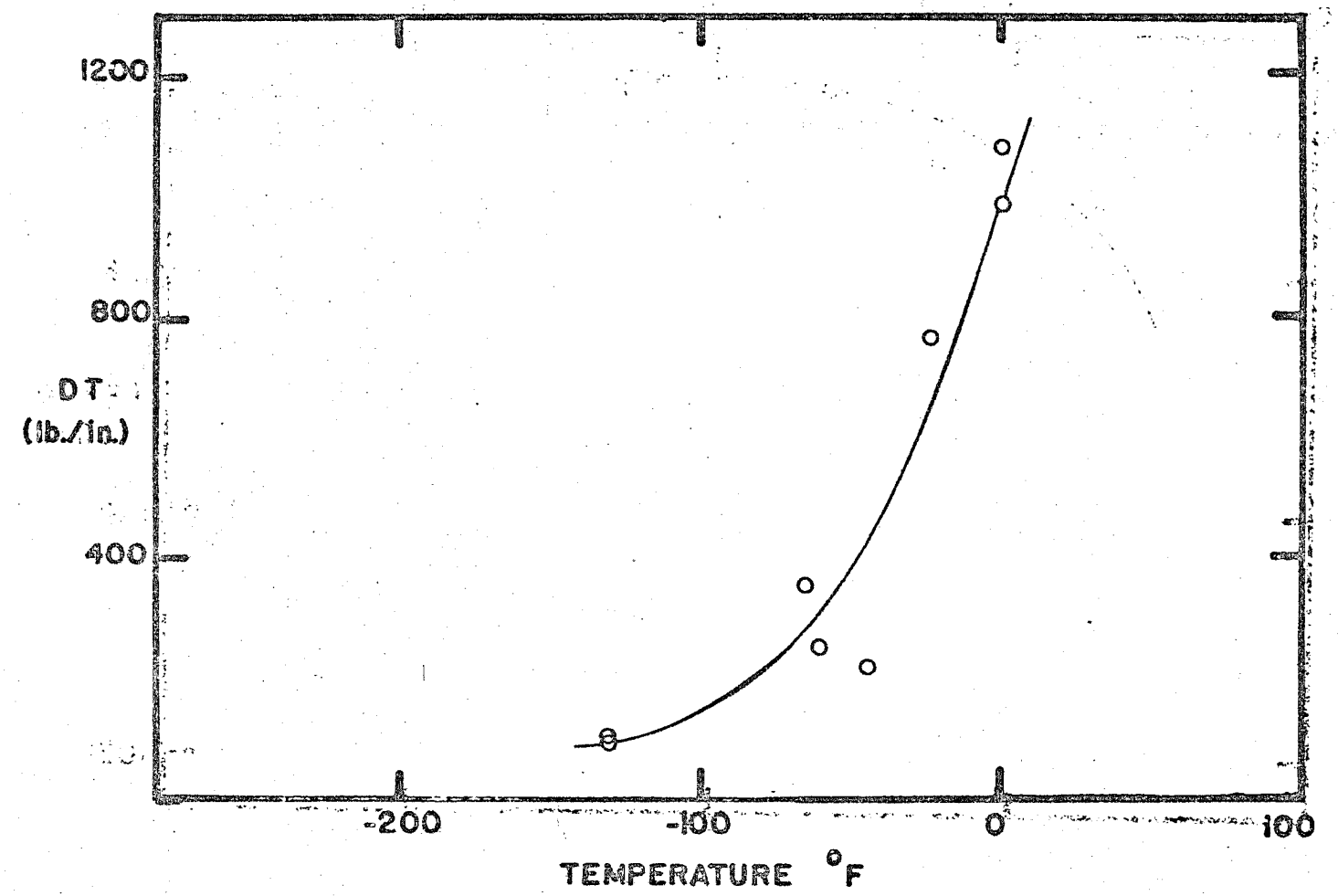

Fig. C-11 Dynamic Tear Data for A588B - 1" Material

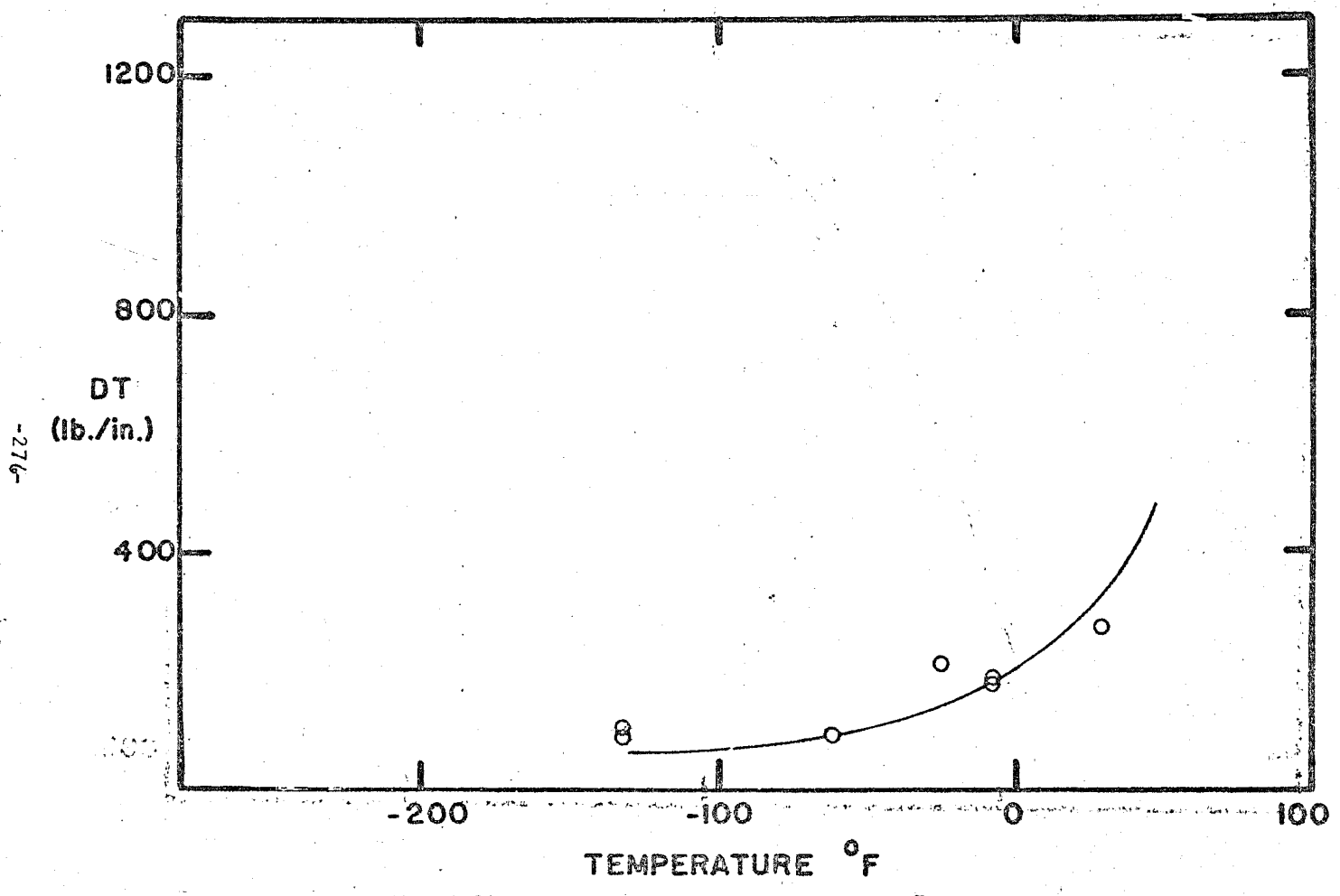

Fig. G-12 Dynamic Tear Data for A588B - 2" Material

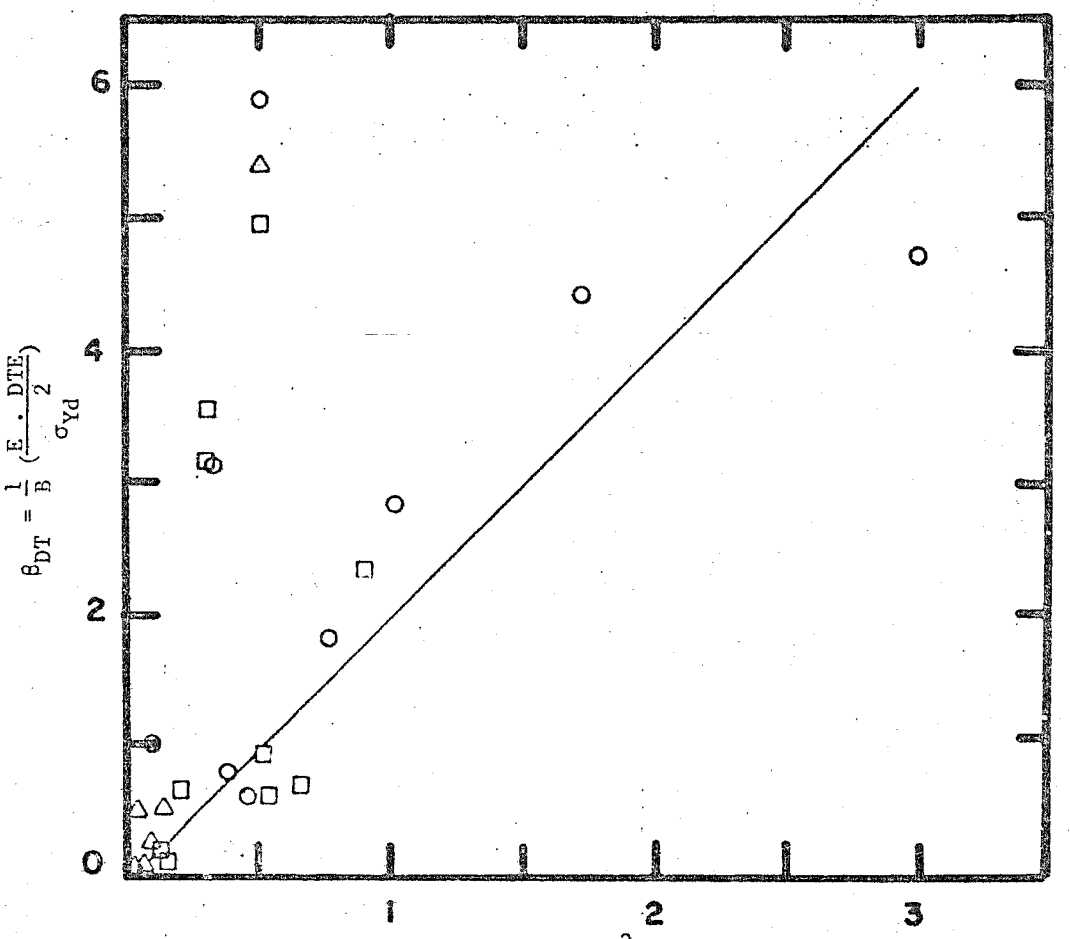

Fig. G-13 A588B β Data

TABLE G1.1* - A588 CHARPY DATA SUMMARY

Test	Material Thickness (in.)	T_{15} (° F)	T_{30} (° F)	T_{SH} (° F)	CVN_{SH} (ft.-lb.)
DS	0.5	- 10	25	150	80
DP	0.5	50	70	175	65
SS	0.5	- 175	- 110	0	50
SP	0.5	- 25	0	50	48
DS	1.0	- 75	- 15	125	95
DP	1.0	100	160	--	> 60
SS	1.0	--	--	--	--
SP	1.0	25	60	--	> 35
DS	2.0	- 15	35	150	90
DP	2.0	110	180	--	> 60
SS	2.0	- 100	- 75	0	60
SP	2.0	- 25	25	--	> 50

TABLE G1.2

Test	t	ΔT (° F)	ΔT_B (° F)
S	0.5	160	112
P	0.5	70	
S	1.0	--	111
P	1.0	75	
S	2.0	85	121
P	2.0	135	

*See Table A1.1 for designations.

TABLE G2 - CHARPY TEST DATA

A588B 1/2" (Notched) Slow Bend

Specimen No.	Temp. (°F)	Maximum Load (lb.)	Deflection at Maximum Load (in.)	Crack-Depth (in.)	Energy Absorbed		Shear (%)	Lateral Expansion (mils)
					Actual (ft.-lb.)	Normalized (ft.-lb.)		
183-SN	- 200	3470	0.067	0.079	10.75	10.75	0	12
112-SN	- 150	3725	0.120	0.079	25.00	25.00	0	24
97-SN	- 125	3675	0.146	0.079	33.00	33.00	0	23
88-SN	- 135	3570	0.124	0.079	23.35	23.35	0	30
63-SN	- 85	3650	0.117	0.079	22.11	22.11	< 5	25
52-SN	- 30	3425	0.120	0.079	46.07	46.07	85	55
35-SN	+ 40	3350	0.116	0.079	35.50	35.50	100	52
144-SN	+ 75	3400	0.130	0.079	50.40	50.40	100	56
222-SN	0	4130	0.120	0.079	34.00	34.00	< 10	32
229-SN	- 100	4225	0.146	0.079	32.80	32.80	< 5	31

TABLE G2 - CHARPY TEST DATA

A588B 1/2" (Notched) Dynamic

Specimen No.	Temp. (°F)	Maximum Load (lb.)	Deflection at Maximum Load (in.)	Crack-Depth (in.)	Energy Absorbed		Shear (%)	Lateral Expansion (mils)
					Actual (ft.-lb.)	Normalized (ft.-lb.)		
	- 100			0.079	4.0	4.0	0	12
	- 50			0.079	8.0	8.0	0	11
	- 50			0.079	14.0	14.0	0	22
	0			0.079	25.0	25.0	< 5	9
	0			0.079	11.0	11.0	< 5	30
	+ 50			0.079	42.0	42.0	30	41
	+ 50			0.079	36.0	36.0	20	34
	+ 100			0.079	70.0	70.0	100	60
	+ 100			0.079	67.0	67.0	100	58
	+ 150			0.079	72.5	72.5	100	60

TABLE G2 - CHARPY TEST DATA

A588B 1/2" (Pre-Cracked) Slow Bend

Specimen No.	Temp. (° F)	Maximum Load (lb.)	Deflection at Maximum Load (in.)	Crack-Depth (in.)	Energy Absorbed		Shear (%)	Lateral Expansion (mils)
					Actual (ft.-lb.)	Normalized (ft.-lb.)		
486-SP	- 150	2800	.040	.105	3.77	4.11	0	4
485-SP	- 160	1960	.030	.145	2.12	2.68	0	6
232-SP	- 100	2150	.067	.150	4.65	6.11	< 5	11
221-SP	0	2700	.070	.135	36.20	39.00	80	40
218-SP	0	3500	.100	.080	43.80	44.00	85	51
215-SP	+ 41	3250	.061	.140	37.40	38.60	90	41

TABLE G2 - CHARPY TEST DATA

A588B 1/2" (Pre-Cracked) Fast Bend

Specimen No.	Temp. (° F)	Maximum Load (lb.)	Deflection at Maximum Load (in.)	Crack-Depth (in.)	Energy Absorbed		Shear (%)	Lateral Expansion (mils)
					Actual (ft.-lb.)	Normalized (ft.-lb.)		
444-FP	- 155	1120	.034	.150	2.50	3.23	0	4
392-FP	- 100	1600	.036	.175	4.30	6.20	0	8
357-FP	- 50	1960	.052	.145	9.61	12.20	10	17
311-FP	0	1620	.072	.190	18.80	28.30	80	29
314-FP	+ 50	2370	.072	.120	25.40	29.30	100	41

TABLE G2 - CHARPY TEST DATA

A588B 1/2" (Pre-Cracked) Dynamic

Specimen No.	Temp. (° F)	Maximum Load (lb.)	Deflection at Maximum Load (in.)	Crack-Depth (in.)	Energy Absorbed		Shear (%)	Lateral Expansion (mils)
					Actual (ft.-lb.)	Normalized (ft.-lb.)		
	- 100			0.120	2.00	2.30	0	5
	0			0.155	4.00	5.30	< 10	8
	+ 50			0.115	16.50	19.40	40	25
	+ 75			0.135	20.00	24.40	60	25
	+ 116			0.090	53.00	56.00	100	54
	+ 212			0.140	49.00	60.50	100	44

TABLE G2 - CHARPY TEST DATA

A588B 1" (Notched) Slow Bend

Specimen No.	Temp. (° F)	Maximum Load (lb.)	Deflection at Maximum Load (in.)	Crack-Depth (in.)	Energy Absorbed		Shear (%)	Lateral Expansion (mils)
					Actual (ft.-lb.)	Normalized (ft.-lb.)		
184-SN	- 200	2740	0.068	0.079	6.20	6.20	0	9
113-SN	- 160	3400	0.166	0.079	35.20	35.20	< 5	38
81-SN	- 100	3100	0.182	0.079	32.20	32.20	10	37
53-SN	- 30	3100	0.160	0.079	49.48	49.48	45	57
36-SN	+ 40	3300	0.126	0.079	25.60	25.60	30	28
145-SN	+ 75	3200	0.116	0.079	47.80	47.80	100	47
231-SN	- 100	3750	0.080	0.079	15.27	15.27	< 5	18
238-SN	- 50	3050	0.079	0.070	11.61	11.61	0	12

TABLE G2 - CHARPY TEST DATA

A588B 1" (Notched) Dynamic

Specimen No.	Temp. (°F)	Maximum Load (lb.)	Deflection at Maximum Load (in.)	Crack-Depth (in.)	Energy Absorbed		Shear (%)	Lateral Expansion (mils)
					Actual (ft.-lb.)	Normalized (ft.-lb.)		
	- 100			0.079	6.5	6.5	0	6
	- 50			0.079	25.0	25.0	0	24
	- 50			0.079	24.5	24.5	0	25
	0			0.079	35.0	35.0	< 5	34
	0			0.079	33.0	33.0	< 5	34
	+ 50			0.079	66.0	66.0	20	59
	+ 50			0.079	69.0	69.0	20	61
	+ 100			0.079	92.0	92.0	85	75
	+ 100			0.079	90.0	90.0	95	70
	+ 150			0.079	86.0	86.0	100	71

TABLE G2 - CHARPY TEST DATA

A588B 1" (Pre-Cracked) Slow Bend

Specimen No.	Temp. (° F)	Maximum Load (lb.)	Deflection at Maximum Load (in.)	Crack-Depth (in.)	Energy Absorbed		Shear (%)	Lateral Expansion (mils)
					Actual (ft.-lb.)	Normalized (ft.-lb.)		
489	- 150	2100	0.036	0.140	3.69	4.58	0	10
488	- 150	1650	0.032	0.155	3.34	4.40	0	11
233	- 100	1800	0.040	0.160	3.34	5.50	0	10
224	- 50	2580	0.054	0.120	8.60	9.89	< 5	14
219	0	1700	0.048	0.150	7.00	9.00	0	12
216	+ 40	2300	0.070	0.130	22.60	26/30	40	29

TABLE G2 - CHARPY TEST DATA

A588B 1" (Pre-Cracked) Fast Bend

Specimen No.	Temp. (° F)	Maximum Load (lb.)	Deflection at Maximum Load (in.)	Crack-Depth (in.)	Energy Absorbed		Shear (%)	Lateral Expansion (mils)
					Actual (ft.-lb.)	Normalized (ft.-lb.)		
445-FP	- 150	1850	0.051	0.125	3.52	4.14	0	4
393-FP	- 100	2000	0.032	0.140	4.42	5.50	0	5
226-FP	- 50	1800	0.036	0.150	5.80	7.50	0	8
225-FP	- 50	2010	0.032	0.125	4.10	4.85	0	14
312-FP	0	2060	0.056	0.130	9.28	11.07	< 20	15
315-FP	+ 50	2275	0.122	0.120	23.31	26.80	60	33

TABLE G2 - CHARPY TEST DATA

A588B 1" (Pre-Cracked) Dynamic

Specimen No.	Temp. (° F)	Maximum Load (lb.)	Deflection at Maximum Load (in.)	Crack-Depth (in.)	Energy Absorbed		Shear (%)	Lateral Expansion (mils)
					Actual (ft.-lb.)	Normalized (ft.-lb.)		
	- 100			0.115	2.00	2.34	0	4
	0			0.145	3.00	3.78	0	4
	+ 50			0.115	6.00	7.02	< 5	8
	+ 50			0.170	6.50	8.95	< 10	10
	+ 75			0.120	8.00	9.20	15	11
	+ 116			0.140	18.50	22.80	50	22
	+ 212			0.145	43.00	54.00	100	54

TABLE G2 - CHARPY TEST DATA

A588B 2" (Notched) Slow Bend

Specimen No.	Temp. (° F)	Maximum Load (lb.)	Deflection at Maximum Load (in.)	Crack-Depth (in.)	Energy Absorbed		Shear (%)	Lateral Expansion (mils)
					Actual (ft.-lb.)	Normalized (ft.-lb.)		
186-SN	- 200	3470	0.046	0.079	10.70	10.70	0	7
91-SN	- 135	3200	0.074	0.079	11.75	11.75	0	14
59-SN	- 50	3125	0.194	0.079	47.50	47.50	35	57
37-SN	+ 40	2975	0.158	0.079	58.00	58.00	100	65
34-SN	+ 63	2975	0.170	0.079	58.17	58.17	100	66
146-SN	+ 75	2900	0.160	0.079	58.20	58.20	100	64
230-SN	- 100	3620	0.074	0.079	13.64	13.64	0	14
227-SN	- 50	3650	0.164	0.079	45.00	45.00	10	45
228-SN	- 50	3665	0.160	0.079	60.30	60.30	40	62
223-SN	0	3750	0.176	0.079	58.00	58.00	25	56

TABLE G2 - CHARPY TEST DATA

A588B 2" (Notched) Dynamic

Specimen No.	Temp. (° F)	Maximum Load (lb.)	Deflection at Maximum Load (in.)	Crack-Depth (in.)	Energy Absorbed		Shear (%)	Lateral Expansion (mils)
					Actual (ft.-lb.)	Normalized (ft.-lb.)		
	- 100			0.079	3.5	3.5	0	4
	- 50			0.079	8.0	8.0	0	7
	- 50			0.079	8.5	8.5	0	10
	0			0.079	34.0	34.0	0	22
	+ 50			0.079	26.0	26.0	< 5	26
	+ 50			0.079	46.0	46.0	15	40
	+ 100			0.079	54.0	54.0	30	49
	+ 150			0.079	83.0	83.0	85	66
	+ 150			0.079	88.5	88.5	100	76
	+ 212			0.079	91.5	91.5	100	69

TABLE G2 - CHARPY TEST DATA

A588B 2" (Pre-Cracked) Slow Bend

Specimen No.	Temp. (° F)	Maximum Load (lb.)	Deflection at Maximum Load (in.)	Crack-Depth (in.)	Energy Absorbed		Shear (%)	Lateral Expansion (mils)
					Actual (ft.-lb.)	Normalized (ft.-lb.)		
490-SP	- 150	1775	0.038	0.150	5.03	6.50	< 5	12
487-SP	- 150	1600	0.039	0.165	3.41	4.70	0	6
234-SP	- 100	2400	0.054	0.140	4.95	6.14	0	9
220-SP	0	2850	0.096	0.140	44.10	54.70	90	50
217-SP	43	2560	0.076	0.125	28.50	34.20	70	40

TABLE G2 - CHARPY TEST DATA

A588B 2" (Pre-Cracked) Fast Bend

Specimen No.	Temp. (° F)	Maximum Load (lb.)	Deflection at Maximum Load (in.)	Crack-Depth (in.)	Energy Absorbed		Shear (%)	Lateral Expansion (mils)
					Actual (ft.-lb.)	Normalized (ft.-lb.)		
446-FP	- 150	1220	0.032	0.170	3.60	5.06	0	4
394-FP	- 100	1900	0.052	0.135	8.02	9.76	0	11
358-FP	- 50	2300	0.054	0.125	8.37	9.84	< 5	12
313-FP	0	2120	0.070	0.120	25.40	29.29	20	26
316-FP	+ 50	3000	0.080	0.110	19.11	21.10	50	44

TABLE G2 - CHARPY TEST DATA

A588B 2" (Pre-Cracked) Dynamic

Specimen No.	Temp. (° F)	Maximum Load (lb.)	Deflection at Maximum Load (in.)	Crack-Depth (in.)	Energy Absorbed		Shear (%)	Lateral Expansion (mils)
					Actual (ft.-lb.)	Normalized (ft.-lb.)		
	- 100			0.150	2.00	2.58	0	3
	0			0.130	3.00	3.58	0	9
	+ 50			0.135	16.50	20.00	20	14
	+ 75			0.110	17.00	18.90	30	13
	+ 100			0.100	11.00	11.90	20	54
	+ 212			0.140	44.00	54.00	100	45

TABLE G3.1 - A588B K_c DATA

A588B 1/2"

Nominal Yield Strength YS = 68.5 ksi

Specimen No.	B (in.)	Temp. (° F)	A_o (in.)	F.A. ($in.^2$)	$P_{max.}$ (kips)	Time (sec)	K_c (ksi√in.)	G (lb/in)	DTE (lb/in)	β_{K_c}	β_{DT}	σ_{YD} (ksi)
4.001	0.5	- 130	0.800	1.100	10.0	8.5E-04	54.76	101.3	137.5	0.452	0.614	115.1
4.002	0.5	- 130	0.800	1.100	9.3	8.0E-04	50.61	86.5	181.1	0.385	0.805	115.4
4.003	0.5	- 80	0.930	1.035	10.5	7.5E-04	65.90	146.7	000.0	0.777	0.000	105.8
4.017	0.5	- 80	0.820	1.090	15.0	1.4E-03	90.35	275.8	000.0	1.527	0.000	103.4
4.013	0.5	- 65	0.880	1.060	6.0	5.0E-04	34.36	39.9	141.5	0.215	0.762	104.8
4.018	0.8	- 60	0.860	1.712	11.2	8.0E-04	39.95	53.9	287.4	0.191	1.017	102.2
4.015	0.5	- 50	0.700	1.150	12.5	6.0E-04	64.50	140.5	167.0	0.803	0.954	101.8
4.009	0.5	- 40	0.880	1.060	10.0	1.0E-03	60.04	121.8	000.0	0.743	0.000	98.5
4.008	0.5	- 40	0.885	1.057	7.6	7.0E-04	44.60	67.2	000.0	0.400	0.000	99.8
4.016	0.5	- 40	0.950	1.025	9.5	1.0E-03	60.65	124.3	297.4	0.758	1.813	98.5
4.006	0.8	- 23	0.860	1.712	13.8	7.0E-04	50.07	84.7	820.1	0.330	3.194	97.5
4.004	0.5	- 23	0.830	1.085	11.9	7.5E-04	69.87	164.9	453.5	1.033	2.840	97.2
4.011	0.5	- 15	1.090	0.955	11.5	8.0E-04	89.19	268.8	684.8	1.727	4.400	96.0
4.014	0.5	0	1.100	0.950	18.3	8.0E-04	00.00	000.0	618.9	0.000	4.131	94.2
4.010	0.5	5	1.100	0.950	13.2	8.5E-04	113.49	435.1	694.7	2.952	4.713	93.4
4.012	0.5	25	0.850	1.075	20.8	1.3E-04	00.00	000.0	000.0	0.000	0.000	97.6
Slow Bend Tests												
4.005	0.5	- 238	0.940	1.030	4.0	3.0E-01	23.30	18.3	000.0	0.072	0.000	123.1
4.007	0.5	- 130	0.900	1.050	7.5	4.0E-04	44.02	65.5	000.0	0.275	0.000	118.7

*See Table A3 for designations

TABLE G3.2 - A588B K_c DATA

A588B 1"

Nominal Yield Strength YS = 68.1 ksi

Specimen No.	B (in.)	Temp. (°F)	A_o (in.)	F.A. ($in.^2$)	$P_{max.}$ (kips)	Time (sec)	K_c (ksi/in.)	G (lb/in)	DTE (lb/in)	β_{K_c}	β_{DT}	σ_{YD} (ksi)
4.101	1.0	- 130	0.940	2.060	14.5	9.5E-04	44.19	66.0	99.0	0.147	0.221	115.3
4.102	1.0	- 130	0.910	2.090	16.0	9.5E-04	47.73	77.0	86.1	0.172	0.192	115.3
4.104	1.0	- 65	1.350	1.650	15.7	1.0E-03	74.42	187.1	349.1	0.524	0.978	102.8
4.105	1.0	- 23	1.065	1.935	24.4	7.5E-04	93.05	292.5	762.8	0.905	2.359	97.8
4.107	1.0	- 60	0.920	2.080	16.0	7.5E-04	48.62	79.9	242.3	0.222	0.675	103.1
4.117	1.0	0	0.970	2.030	16.6	8.0E-04	53.34	96.1	1081.8	0.317	3.564	94.8
4.118	1.0	0	0.975	2.025	17.2	6.0E-04	55.76	105.0	989.6	0.339	3.197	95.7
4.110	1.0	35	0.975	2.025	22.0	7.0E-04	74.76	188.8	201.5	0.669	0.714	91.4
4.111	1.0	- 43	0.980	2.020	22.5	7.5E-04	75.74	193.8	213.9	0.567	0.626	100.6
4.113	1.0	- 40	0.900	2.100	12.6	6.5E-04	37.07	46.4	000.0	0.136	0.000	100.6
4.114	1.0	- 60	0.910	2.090	16.0	8.0E-04	48.09	78.1	000.0	0.219	0.000	102.8
4.106	1.0	0	0.890	2.110	30.0	1.2E-03	101.75	349.7	000.0	1.184	0.000	93.5
4.112	1.0	- 20	0.950	2.050	22.8	9.0E-04	75.09	190.5	000.0	0.601	0.000	96.8
4.115	1.0	- 60	1.020	1.980	21.6	9.0E-04	74.93	189.7	000.0	0.535	0.000	102.4
4.116	1.0	- 60	1.110	1.890	20.0	9.0E-04	75.33	191.7	000.0	0.541	0.000	102.4
Slow Bend Tests												
4.106	1.0	- 238	0.835	2.165	7.3	2.5E-01	18.71	11.8	000.0	0.023	0.000	124.4
4.108	1.0	- 131	0.920	2.080	21.0	7.0E-01	66.37	148.8	000.0	0.492	0.000	94.6

*See Table A3 for designations.

TABLE G3.3 - A588B K_c DATA

A588B 2"

Nominal Yield Strength YS = 62.5 ksi

Specimen No.	B (in.)	Temp. (^{o}F)	A_o (in.)	F.A. (in.^{2})	$P_{max.}$ (kips)	Time (sec)	K_c (ksi/in.)	G (lb/in)	DTE (lb/in)	β_{K_c}	β_{DT}	σ_{YD} (ksi)
4.205	2.0	- 130	0.890	4.220	22.5	8.0E-04	32.22	35.1	79.6	0.043	0.098	109.4
4.206	2.0	- 130	0.900	4.200	25.0	8.0E-04	36.49	45.0	97.1	0.056	0.120	109.4
4.204	2.0	- 60	0.865	4.270	27.5	8.5E-04	39.33	52.3	74.5	0.084	0.120	96.0
4.207	2.0	- 23	0.940	4.120	32.5	9.8E-04	50.99	87.8	209.7	0.159	0.380	90.3
4.201	2.0	- 5	1.320	3.360	21.0	5.0E-04	46.07	71.7	187.5	0.130	0.340	90.3
4.202	2.0	- 5	1.165	3.670	22.5	5.5E-04	42.27	60.4	176.6	0.110	0.323	90.0
4.211	2.0	- 30	1.100	3.800	15.0	7.0E-04	25.92	22.7	262.1	0.046	0.533	85.3
Slow Bend Tests												
2.208	2.0	- 245	0.750	4.500	16.5	3.0E-01	20.15	13.7	000.0	0.014	0.000	119.8
4.203	2.0	- 137	1.250	3.500	16.8	4.2E-01	33.70	38.4	000.0	0.070	0.000	90.2

*See Table A3 for designations.

TABLE G4 - A588 K-CURVE INSTABILITY SUMMARY

Thickness (in.)	Test Temperature (^{o} F)	Fatigue Crack Length (in.)	K_c at Instability (psi)	Apparent Crack Length at Instability (in.)
0.5	- 95	6.30	63,844	6.42
0.5**	- 40	6.25	135,474	7.43
0.5***	- 10	6.25	347,118	7.91
1.0****	- 50	6.20	217,147	7.24
1.0*****	- 40	6.23*	150,000	6.42

*Average crack length, fatigue crack front slanted through thickness

**Crack branching occurred at crack length of 7.05"

***Crack branching occurred at crack length of 7.15"

****Crack branching occurred at crack length of 6.65"

*****Crack branching occurred at crack length of 7.15"

APPENDIX H - A514 DATA

This appendix contains the data collected for the 1/2", 1" and 2" thicknesses of the A514 material. This steel was supplied to the program by the Bethlehem Steel Corporation. The chemical analysis, physical properties and heat designations appear in Tables 1 and 2.

The data in this appendix is presented in the form of a Charpy summary, a detailed Charpy tabulation, a K_c tabulation, and appropriate figures which best illustrate the data trends. Details of the test procedures and terminology can be found in appendices J, K and L and Chapter 2.

Standard and precracked Charpy tests were made on all three thicknesses of the A514 material. The tests were carried out at three speeds except for the 1" standard specimens which were only tested at two speeds. Figures H-1 through H-6 show the data while Table H-1 and H-2 provide data in tabular form. The slow and fast loading rate data for both standard and precracked specimens did not show any temperature shift. The slow and dynamic data did show a definite temperature shift. For all three thicknesses the standard test results showed a much greater shift than predicted by Barsom (28). The precracked results for the 1/2" and 1" material were in fair agreement with Barsom. The 2" precracked shift was much greater than anticipated. The precracked Charpy data showed a much higher transition temperature

than the standard data. Also it does not appear that the precracked data forms a lower bound for the standard Charpy data.

The K_c tests for the A514 material were carried out during Phase 1 of the project. D.T. measurements were not obtained. Figures H-7 through H-9 show the K_c results. Individual results are given in Table H-3. For the particular range of temperatures tested it is not possible to make a very meaningful assessment of the formula

$$K_{Ic} = \sqrt{A\ E\ CVN}$$

for correlating K_c and CVN data. The Charpy curves are well into their upper shelf regions at the point where the K_c tests were made.

R-curves were attempted for the A514 1/2" and 1" material. However no useful data was obtained from these tests. The plates were only tested down to -100° F and for these tests no crack growth occurred.

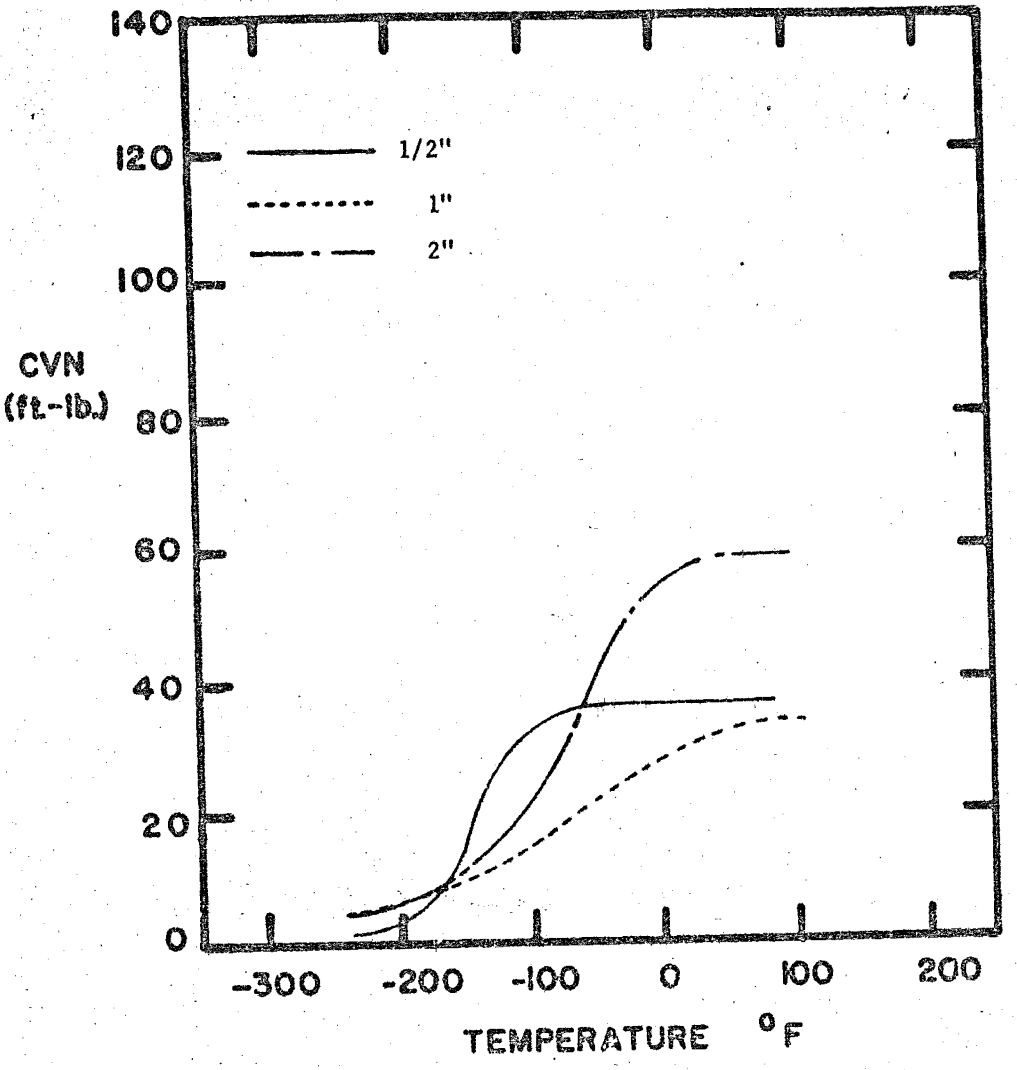

Fig. H-1a Composite Charpy Curves for A514 Material

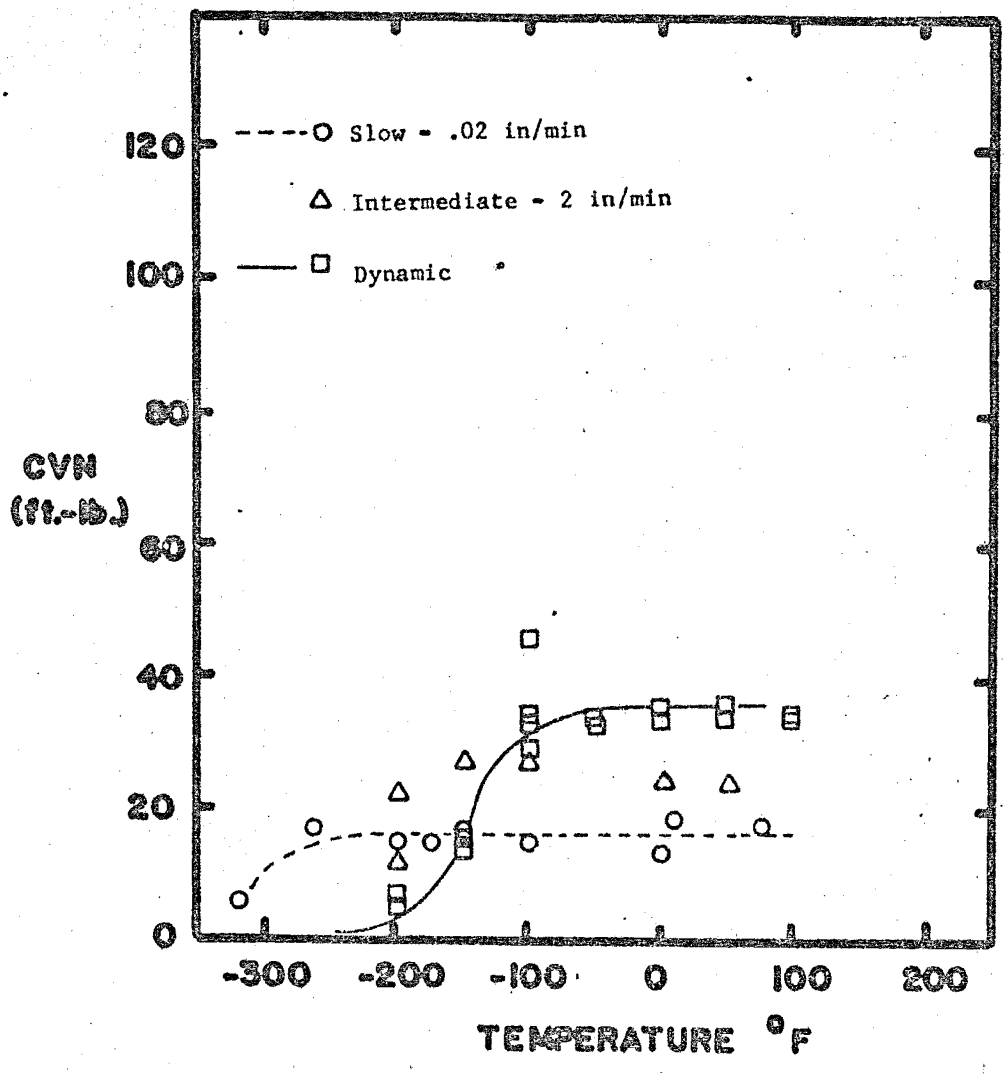

Fig. H-1 A514 1/2" Notched Charpy Data for Three Loading Rates

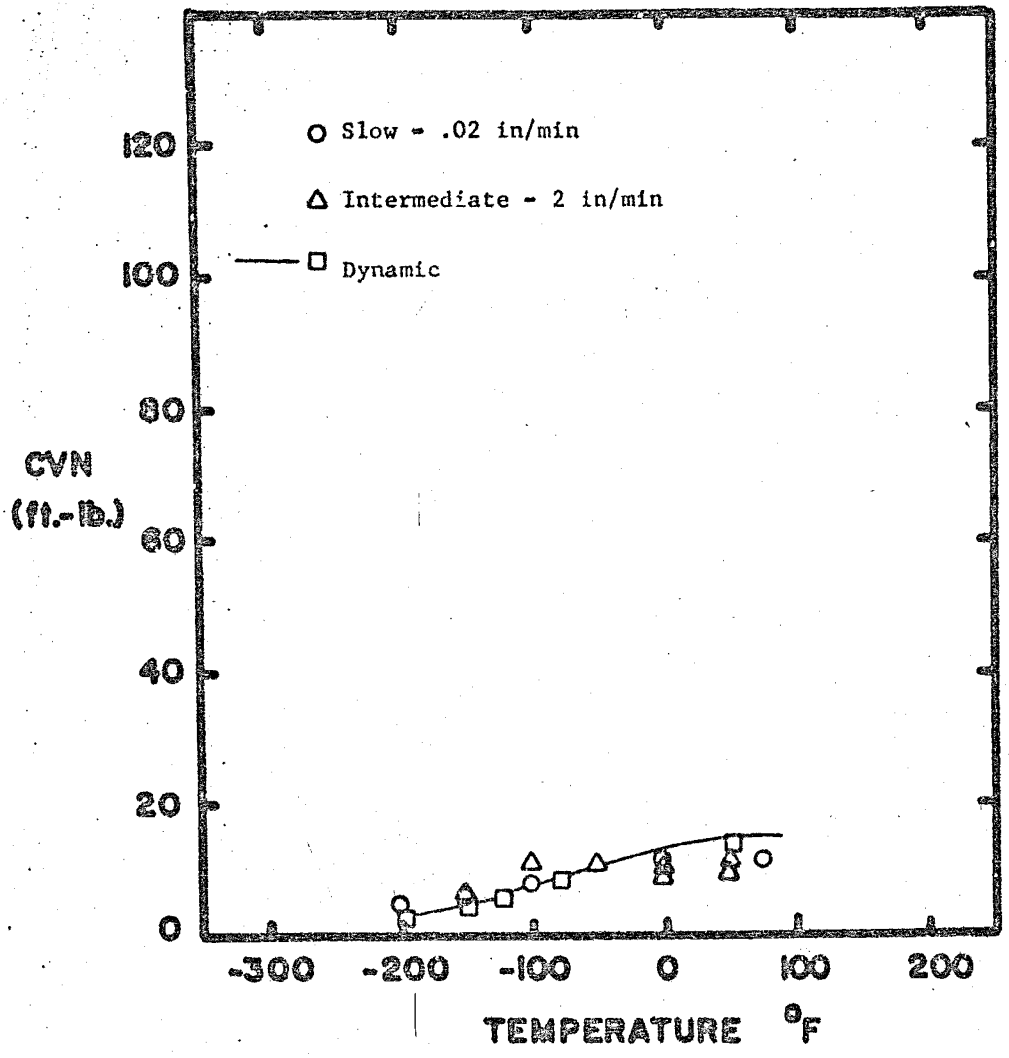

Fig. H-2 A514 1/2" Precracked Data for Three Loading Rates

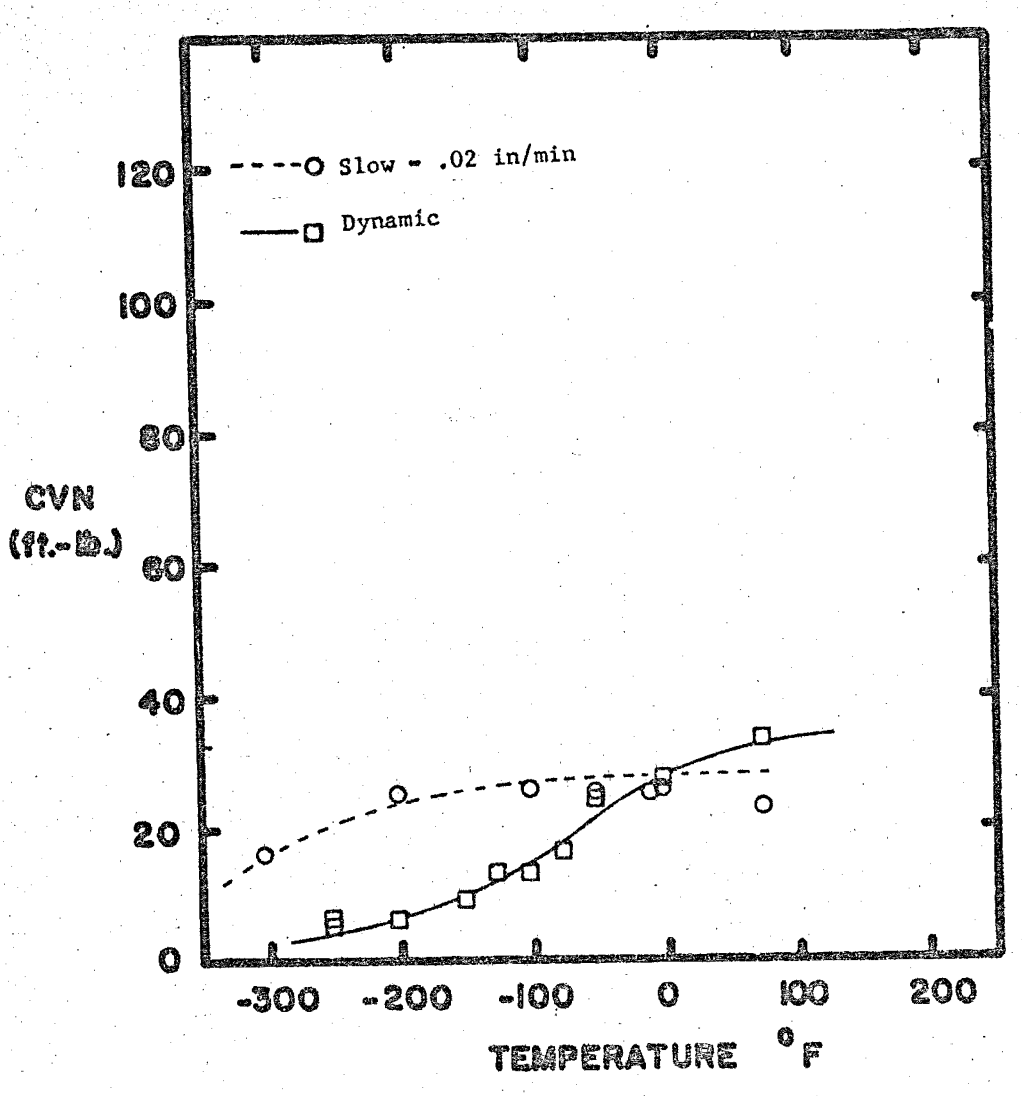

Fig. H-3 A514 1" Notched Charpy Data for Two Loading Rates

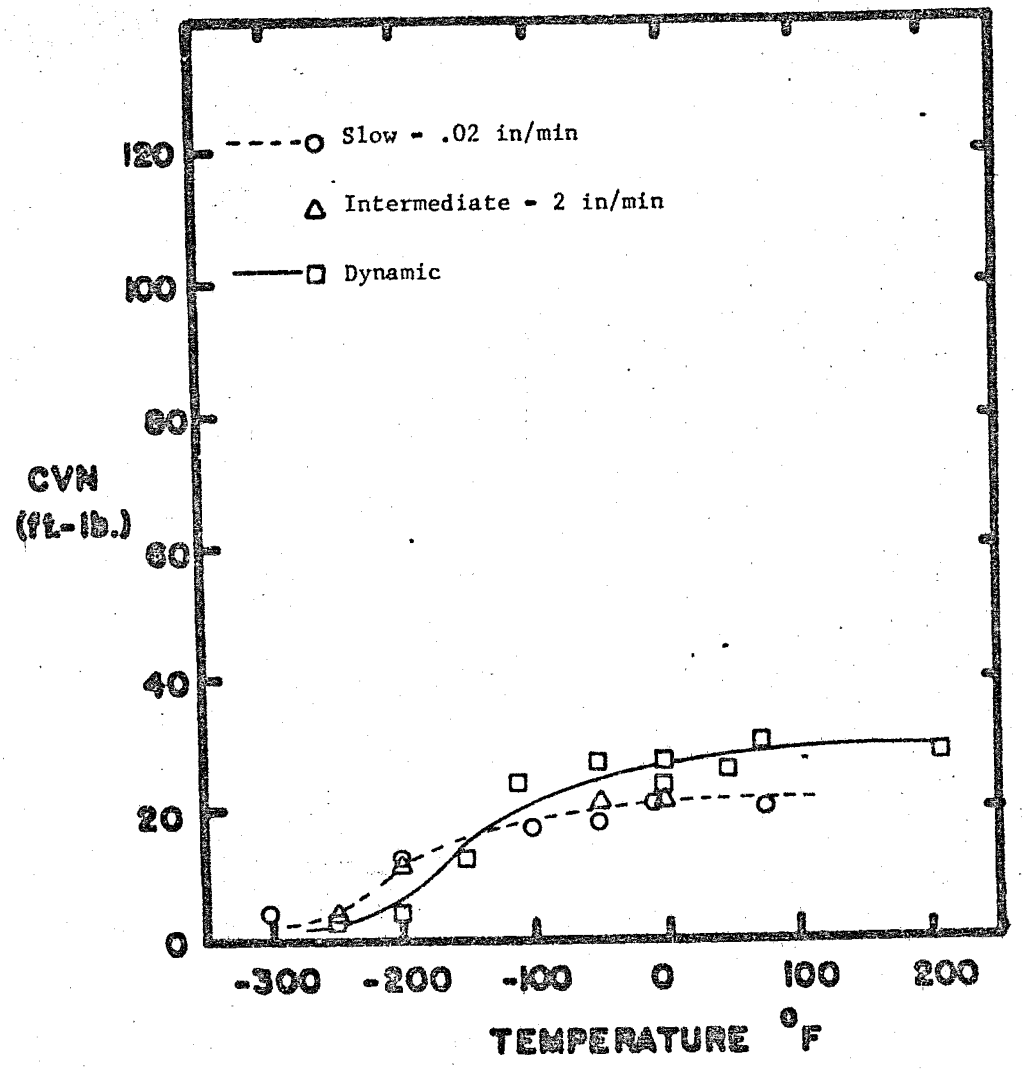

Fig. H-4 A514 1" Precracked Data for Three Loading Rates

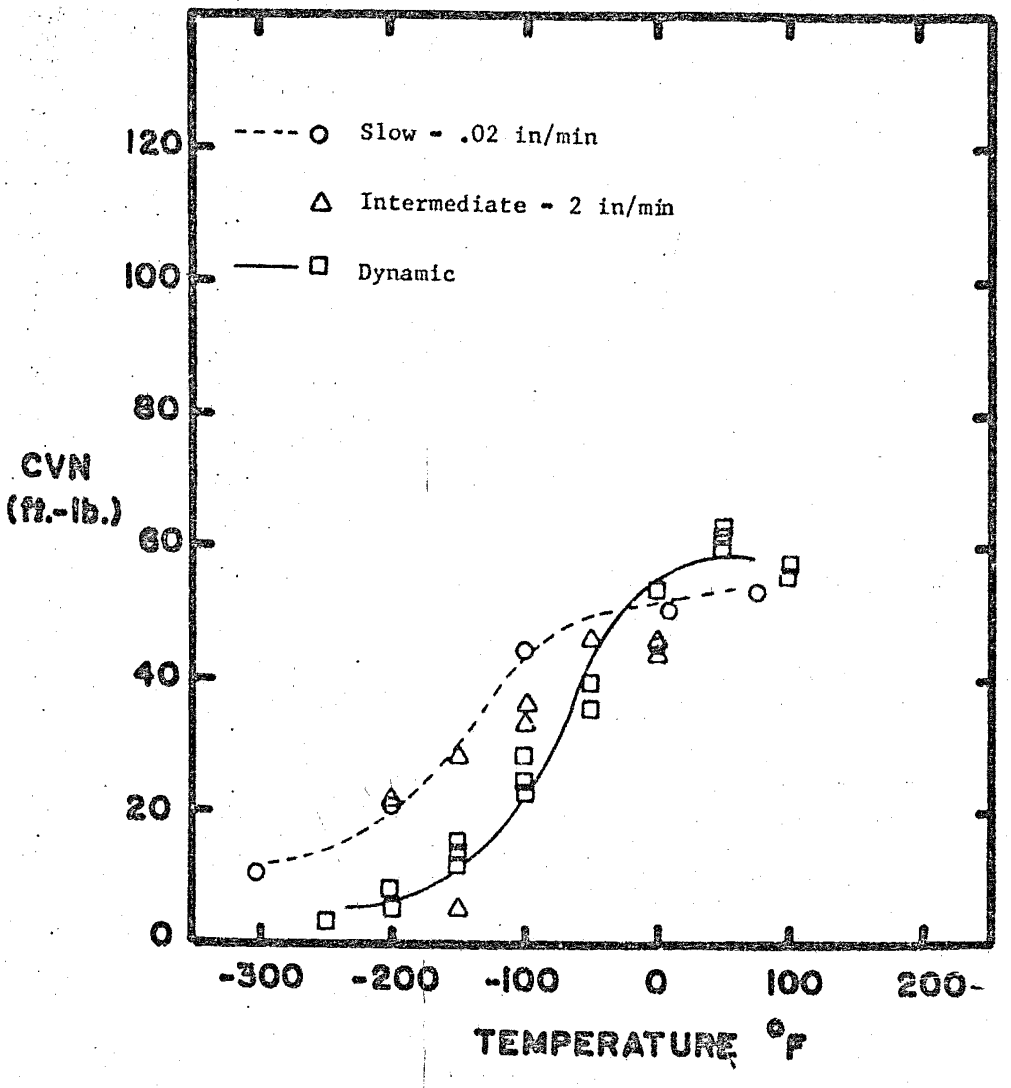

Fig. H-5 A514 2" Notched Charpy Data for Three Loading Rates

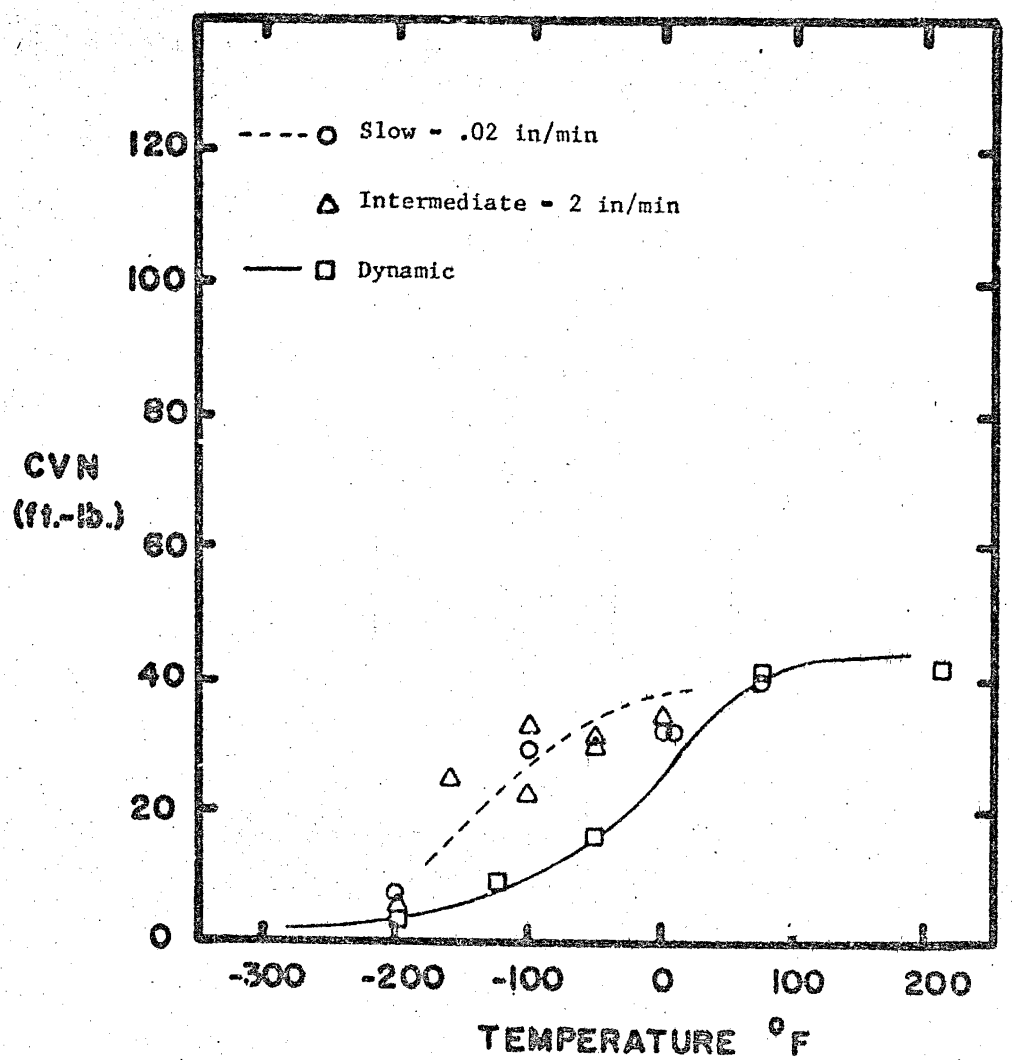

Fig. H-6 A514 2" Precracked Data for Three Loading Rates

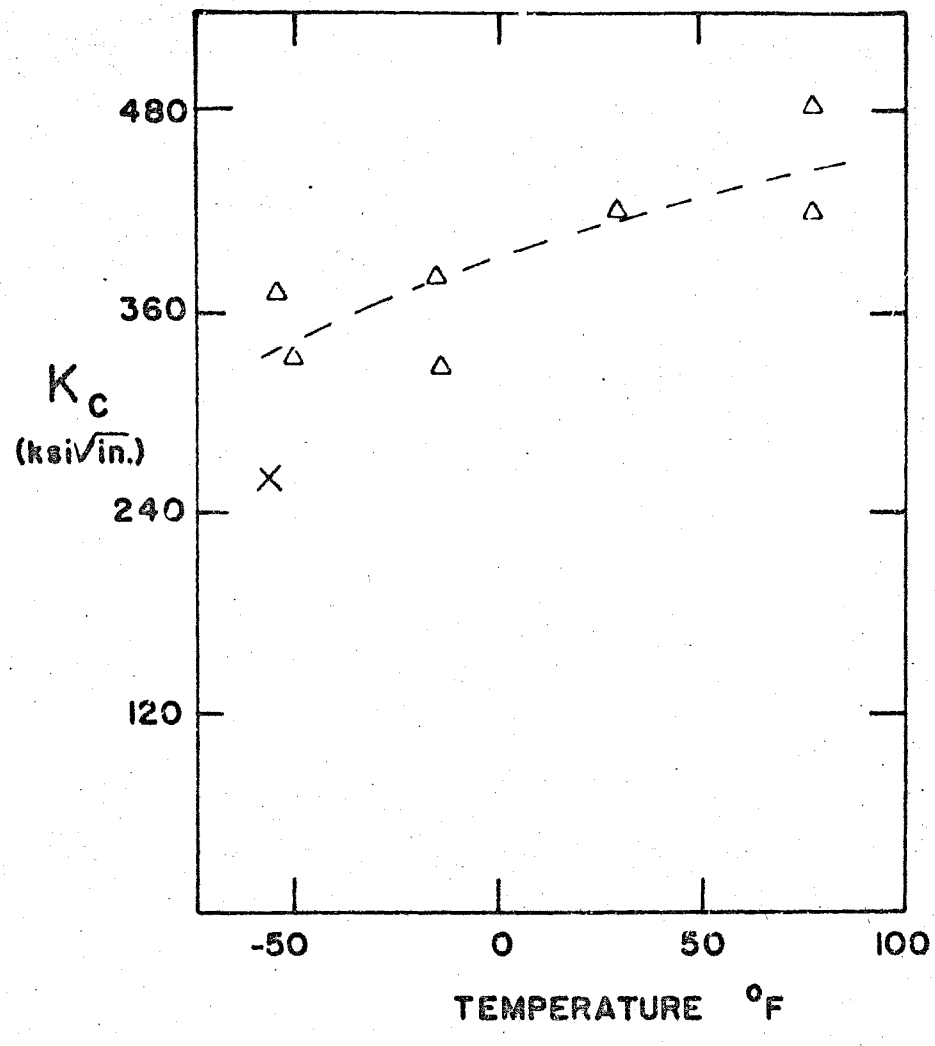

Fig. H-7 Triangles show Estimates of Dynamic K_M for 1/2" A514 Plate. X symbol show Estimates of Dynamic K_c from Eqs. (17, 18, 7) of Phase I Report

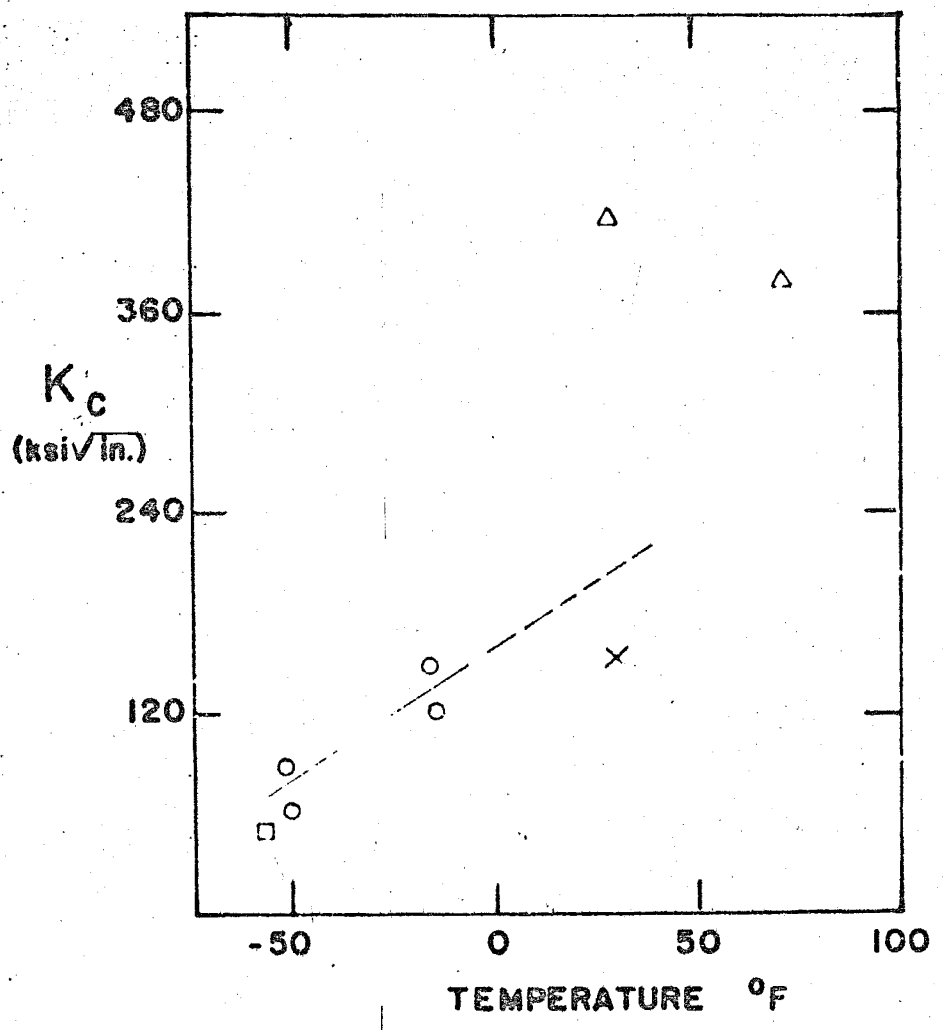

Fig. H-8 Circles show Dynamic K_c Measurements for 1" A514 Plate. Triangles show Estimates of Dynamic K_M from the Crack-Arrest Bend-Angle Method. Squares and X symbols show Estimates of Dynamic K_c from Eqs. (20) and (7) and from Eqs. (17, 18, 7) respectively from Phase I Report.

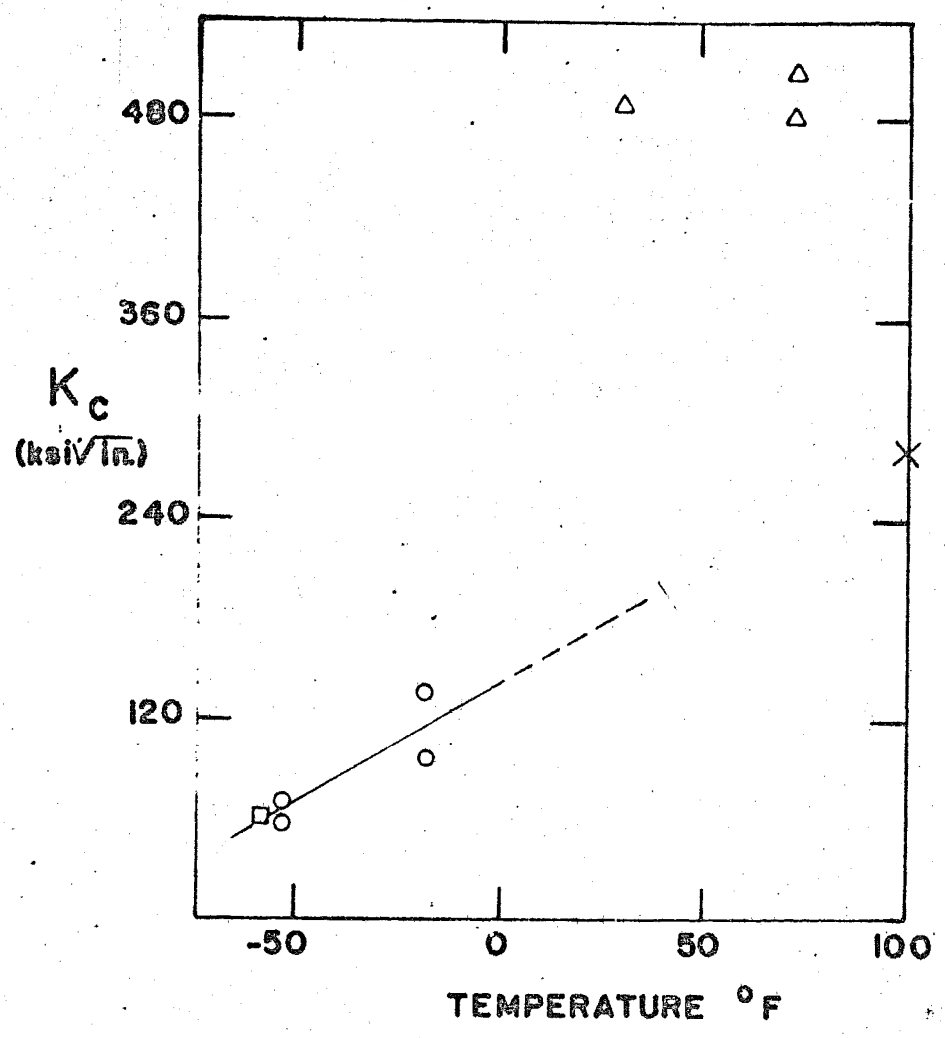

Fig. H-9 Circles show Estimates of Dynamic K_c for 2" A514 Plate. Triangles show Estimates of Dynamic K_M from the Crack-Arrest Bend-Angle Method.
Squares and X symbols show Estimates of Dynamic K_c from Eqs. (20) and (7) and from Eqs. (17, 18, 7) respectively from Phase I Report

TABLE H1.1* - A514 CHARPY DATA SUMMARY

Test	Material Thickness (in.)	T_{15} (°F)	T_{30} (°F)	T_{SH} (°F)	CVN_{SH} (ft.-lb.)
DS	0.5	- 150	- 110	- 50	35
DP	0.5	--	--	75	15
SS	0.5	- 250	--	- 225	16
SP	0.5	--	--	75	14
DS	1.0	- 100	20	75	33
DP	1.0	- 145	--	50	28
SS	1.0	- 320	--	- 100	27
SP	1.0	- 150	--	0	20
DS	2.0	- 125	- 75	50	58
DP	2.0	- 50	20	100	43
SS	2.0	- 240	- 150	0	52
SP	2.0	- 160	- 80	50	38

TABLE H1.2

Test	t	ΔT (°F)	ΔT_B (°F)
S	0.5	110	24
P	0.5	0	
S	1.0	200	52
P	1.0	0	
S	2.0	95	55
P	2.0	105	

*See Table A1.1 for designations

TABLE H2 - CHARPY TEST DATA

A514 1/2" (Notched) Slow Bend

Specimen No.	Temp. (° F)	Maximum Load (lb.)	Deflection at Maximum Load (in.)	Crack-Depth (in.)	Energy Absorbed		Shear (%)	Lateral Expansion (mils)
					Actual (ft.-lb.)	Normalized (ft.-lb.)		
118-SN	- 175	6000	0.074	0.079	14.30	14.30	0	4
110-SN	- 150	6000	0.066	0.079	16.30	16.30	0	6
69-SN	- 100	5600	0.066	0.079	14.20	14.20	5	5
70-SN	- 100	5850	0.064	0.079	14.00	14.00	5	5
2-SN	0	3000	0.050	0.079	12.80	12.80	30	7
40-SN	+ 10	5700	0.062	0.079	17.80	17.80	40	6
132-SN	+ 75	5640	0.064	0.079	16.40	16.40	40	8
199-sn	- 200	6400	0.066	0.079	14.80	14.80	0	4
201-SN	- 265	6400	0.069	0.079	16.80	16.80	0	3
196-SN	- 320	3375	0.050	0.079	5.00	5.00	0	3

TABLE H2 - CHARPY TEST DATA

A514 1/2" (Notched) Fast Bend

Specimen No.	Temp. (° F)	Maximum Load (lb.)	Deflection at Maximum Load (in.)	Crack-Depth (in.)	Energy Absorbed		Shear (%)	Lateral Expansion (mils)
					Actual (ft.-lb.)	Normalized (ft.-lb.)		
466	- 200	5550	0.056	0.079	10.06	10.06	—	5
464	- 200	5800	0.044	0.079	21.10	21.10	—	5
419	- 140	6450	0.072	0.079	24.00	24.00	—	6
418	- 150	5600	0.060	0.079	26.00	26.00	—	6
379	- 100	5500	0.060	0.072	27.20	27.20	—	8
299	0	5750	0.076	0.076	23.30	23.00	—	9
265	+ 50	5500	0.056	0.056	22.70	22.70	—	7

TABLE H2 - CHARPY TEST DATA

A514 1/2" (Notched) Dynamic

Specimen No.	Temp. (° F)	Maximum Load (lb.)	Deflection at Maximum Load (in.)	Crack-Depth (in.)	Energy Absorbed		Shear (%)	Lateral Expansion (mils)
					Actual (ft.-lb.)	Normalized (ft.-lb.)		
	- 200			0.079	6.0	6.0	0	4
——	- 200			0.079	4.0	4.0	0	4
	- 150			0.079	11.5	11.5	0	6
	- 150			0.079	14.0	14.0	0	13
	- 150			0.079	11.5	11.5	< 5	10
	- 100			0.079	45.0	45.0	< 5	22
	- 100			0.079	28.5	28.5	10	20
	- 100			0.079	32.0	32.0	15	17
	- 100			0.079	33.0	33.0	15	—
	- 50			0.079	32.0	32.0	15	32

TABLE H2 - CHARPY TEST DATA

A514 1/2" (Notched) Dynamic (Continued)

Specimen No.	Temp. (° F)	Maximum Load (lb.)	Deflection at Maximum Load (in.)	Crack-Depth (in.)	Energy Absorbed		Shear (%)	Lateral Expansion (mils)
					Actual (ft.-lb.)	Normalized (ft.-lb.)		
	- 50			0.079	33.0	33.0	20	27
	- 50			0.079	31.0	31.0	25	—
	0			0.079	35.5	35.5	80	—
	0			0.079	35.5	35.5	70	39
	0			0.079	33.0	33.0	100	41
	+ 50			0.079	33.0	33.0	100	47
	+ 50			0.079	35.0	35.0	100	42
	+ 50			0.079	35.0	35.0	100	44
	+ 100			0.079	33.5	33.5	100	45
	+ 100			0.079	32.5	32.5	100	45

TABLE H2 - CHARPY TEST DATA

A514 1/2" (Pre-Cracked) Slow Bend

Specimen No.	Temp. (° F)	Maximum Load (lb.)	Deflection at Maximum Load (in.)	Crack-Depth (in.)	Energy Absorbed		Shear (%)	Lateral Expansion (mils)
					Actual (ft.-lb.)	Normalized (ft.-lb.)		
117	-,200	2825	0.036	0.130	3.00	3.55	0	4
109	- 150	3000	0.038	0.125	3.80	4.40	0	3
68	- 100	2925	0.040	0.145	5.50	7.05	< 10	3
1	0	2950	0.038	0.156	8.30	11.00	60	3
39	+ 10	2750	0.042	0.140	7.70	9.50	60	2
131	75	2750	0.039	0.156	7.00	11.00	60	3

TABLE H2 - CHARPY TEST DATA

A514 1/2" (Pre-Cracked) Fast Bend

Specimen No.	Temp. (° F)	Maximum Load (lb.)	Deflection at Maximum Load (in.)	Crack-Depth (in.)	Energy Absorbed		Shear (%)	Lateral Expansion (mils)
					Actual (ft.-lb.)	Normalized (ft.-lb.)		
469	- 250	2200	0.025	0.130	3.78	4.48	—	2
463	- 200	2975	0.028	0.145	4.41	5.60	—	3
417	- 150	1710	0.040	0.150	5.07	6.45	—	2
378	- 100	3050	0.037	0.145	7.70	10.00	—	2
343	- 50	2750	0.036	0.145	8.00	10.08	—	5
342	- 50	2750	0.038	0.120	9.20	10.58	—	5
300	0	3120	0.040	0.124	9.18	10.33	—	5
297	0	2730	0.036	0.145	6.98	8.76	—	3
262	+ 50	2810	0.038	0.130	7.65	9.13	—	6
263	50	3090	0.040	0.130	8.95	10.63	—	6

TABLE H2 - CHARPY TEST DATA

A514 1/2" (Pre-Cracked) Dynamic

Specimen No.	Temp. (° F)	Maximum Load (lb.)	Deflection at Maximum Load (in.)	Crack-Depth (in.)	Energy Absorbed		Shear (%)	Lateral Expansion (mils)
					Actual (ft.-lb.)	Normalized (ft.-lb.)		
	- 200			0.180	1.50	2.28	0	4
	- 150			0.145	3.00	3.78	0	4
	- 125			0.145	4.00	5.04	< 5	4
	- 80			0.156	6.20	8.20	15	6
	+ 50			0.160	9.80	13.20	20	6
	+ 75			0.160	10.00	13.10	25	5
	75			0.180	8.00	12.20	25	6

TABLE H2 - CHARPY TEST DATA

A514 1" (Notched) Slow Bend

Specimen No.	Temp. (° F)	Maximum Load (lb.)	Deflection at Maximum Load (in.)	Crack-Depth (in.)	Energy Absorbed		Shear (%)	Lateral Expansion (mils)
					Actual (ft.-lb.)	Normalized (ft.-lb.)		
191-SN	- 300	5010	0.060	0.079	17.15	17.15	< 20	15
119-SN	- 200	4300	0.090	0.079	26.29	26.29	40	20
72-SN	- 100	4500	0.065	0.079	26.93	26.93	100	18
18-SN	- 50	4100	0.062	0.079	26.20	26.20	100	22
46-SN	- 10	3600	0.071	0.079	25.60	25.60	100	21
4-SN	0	4375	0.060	0.079	27.80	27.80	100	22
148-SN	+ 75	4150	0.058	0.079	23.40	23.40	100	20

TABLE H2 - CHARPY TEST DATA

A514 1" (Notched) Dynamic

Specimen No.	Temp. (° F)	Maximum Load (lb.)	Deflection at Maximum Load (in.)	Crack-Depth (in.)	Energy Absorbed		Shear (%)	Lateral Expansion (mils)
					Actual (ft.-lb.)	Normalized (ft.-lb.)		
	- 150			0.079	10.0	10.0		
	- 125			0.079	14.0	14.0		
	- 100			0.079	14.5	14.5		
	- 75			0.079	17.0	17.0		
	- 50			0.079	25.0	25.0		
	0			0.079	28.0	28.0		
	+ 75			0.079	34.5	34.5		
	- 200			0.079	7.0	7.0	0	4
	- 250			0.079	6.0	6.0	0	3
	- 250			0.079	7.0	7.0	0	4

TABLE H2 - CHARPY TEST DATA

A514 1" (Pre-Cracked) Slow Bend

Specimen No.	Temp. (° F)	Maximum Load (lb.)	Deflection at Maximum Load (in.)	Crack-Depth (in.)	Energy Absorbed		Shear (%)	Lateral Expansion (mils)
					Actual (ft.-lb.)	Normalized (ft.-lb.)		
190-SP	- 300	2870	0.045	0.130	3.60	4.30	0	3
120-SP	- 200	3000	0.060	0.152	9.79	12.75	20	7
71-SP	- 100	2700	0.043	0.140	14.25	17.80	80	14
17-SP	- 50	2500	0.042	0.140	14.40	17.90	100	16
45-SP	- 10	2900	0.052	0.135	17.65	21.46	100	18
3-SP	0	2950	0.042	0.140	18.85	23.40	100	17
147-SP	+ 75	2750	0.043	0.130	17.10	20.20	100	18

TABLE H2 - CHARPY TEST DATA

A514 1" (Pre-Cracked) Fast Bend

Specimen No.	Temp. (° F)	Maximum Load (lb.)	Deflection at Maximum Load (in.)	Crack-Depth (in.)	Energy Absorbed		Shear (%)	Lateral Expansion (mils)
					Actual (ft.-lb.)	Normalized (ft.-lb.)		
465	- 200	3650	0.040	0.130	12.43	14.80	15	8
435	- 160	5400	0.060	0.130	24.50	29.00	> 50	20
344	- 50	3130	0.048	0.125	18.53	21.80	90	14
301	0	2850	0.040	0.130	18.23	21.75	100	12

TABLE H2 - CHARPY TEST DATA

A514 1" (Pre-Cracked) Dynamic

Specimen No.	Temp. (° F)	Maximum Load (lb.)	Deflection at Maximum Load (in.)	Crack-Depth (in.)	Energy Absorbed		Shear (%)	Lateral Expansion (mils)
					Actual (ft.-lb.)	Normalized (ft.-lb.)		
	- 250			0.130	2.50	2.70	0	5
	- 200			0.130	4.00	4.35	0	4
	- 150			0.130	10.50	12.50	25	8
	- 110			0.135	20.00	24.20	40	11
	- 50			0.135	22.30	27.20	75	19
	0			0.156	20.00	27.40	80	16
	0			0.134	18.00	23.40	100	17
	+ 50			0.125	22.50	26.30	100	16
	+ 75			0.145	24.10	30.50	100	24
	+ 212			0.150	21.00	27.00	100	19

TABLE H2 - CHARPY TEST DATA

A514 2" (Notched) Slow Bend

Specimen No.	Temp. (°F)	Maximum Load (lb.)	Deflection at Maximum Load (in.)	Crack-Depth (in.)	Energy Absorbed		Shear (%)	Lateral Expansion (mils)
					[illegible]	Normalized (ft.-lb.)		
193-SN	- 300	4500	0.068	0.079	10.03	10.03	0	4
122-SN	- 200	5700	0.088	0.079	19.97	19.97	< 5	14
74-SN	- 100	4325	0.054	0.079	43.76	43.76	85	34
6-SN	0	4250	0.08	0.079	45.00	45.00	100	31
42-SN	+ 10	4150	0.096	0.079	50.00	50.00	100	42
84-SN	+ 74	4050	0.094	0.079	53.00	53.00	100	43

TABLE H2 - CHARPY TEST DATA

A514 2" (Notched) Fast Bend

Specimen No.	Temp. (°F)	Maximum Load (lb.)	Deflection at Maximum Load (in.)	Crack-Depth (in.)	Energy Absorbed		Shear (%)	Lateral Expansion (mils)
					Actual (ft.-lb.)	Normalized (ft.-lb.)		
468	- 200	2680	0.048	0.079	4.90	4.90	0	4
471	- 200	5050	0.060	0.079	21.71	21.71	0	8
438	- 150	4920	0.080	0.079	24.00	24.00	< 5	14
437	- 150	4600	0.087	0.079	27.50	27.50	< 10	13
383	- 100	4700	0.090	0.079	33.00	33.00	15	22
382	- 100	4700	0.078	0.079	35.90	35.90	15	22
347	- 50	4400	0.060	0.079	46.50	46.50	75	38
303	0	4250	0.080	0.079	46.11	46.11	95	39
304	0	4250	0.080	0.079	45.34	45.34	95	34

TABLE H2 - CHARPY TEST DATA

A514 2" (Notched) Dynamic

Specimen No.	Temp. (° F)	Maximum Load (lb.)	Deflection at Maximum Load (in.)	Crack-Depth (in.)	Energy Absorbed		Shear (%)	Lateral Expansion (mils)
					Actual (ft.-lb.)	Normalized (ft.-lb.)		
	- 250			0.079	3.0	3.0	0	3
	- 200			0.079	8.0	8.0	0	3
	- 200			0.079	5.0	5.0	0	3
	- 200			0.079	6.0	6.0		
	- 150			0.079	12.0	12.0	0	10
	- 150			0.079	15.0	15.0	< 5	7
	- 150			0.079	13.0	13.0		9
	- 100			0.079	28.0	28.0	95	25
	- 100			0.079	23.0	23.0	85	21
	- 100			0.079	24.0	24.0	100	21

TABLE H2 - CHARPY TEST DATA

A514 2" (Notched) Dynamic (Continued)

Specimen No.	Temp. (°F)	Maximum Load (lb.)	Deflection at Maximum Load (in.)	Crack-Depth (in.)	Energy Absorbed		Shear (%)	Lateral Expansion (mils)
					Actual (ft.-lb.)	Normalized (ft.-lb.)		
	- 50			0.079	39.0	39.0	100	24
	- 50			0.079	35.0	35.0	100	25
	0			0.079	53.0	53.0	100	27
	0			0.079	53.5	53.5	100	29
	+ 50			0.079	63.0	63.0	100	26
	+ 50			0.079	60.0	60.0	100	26
	+ 50			0.079	61.0	61.0	100	25
	+ 100			0.079	55.5	55.5	100	28
	+ 100			0.079	57.0	57.0	100	25

TABLE H2 - CHARPY TEST DATA

A514 2" (Pre-Cracked) Slow Bend

Specimen No.	Temp. (° F)	Maximum Load (lb.)	Deflection at Maximum Load (in.)	Crack-Depth (in.)	Energy Absorbed		Shear (%)	Lateral Expansion (mils)
					Actual (ft.-lb.)	Normalized (ft.-lb.)		
192-SP	- 300	2750	0.038	0.135	3.90	4.60	0	4
121-SP	- 200	2875	0.042	0.135	5.70	6.90	< 5	5
73-SP	- 100	2750	0.034	0.150	22.60	29.17	85	23
5-SP	0	1625	0.048	0.171	22.80	32.30	100	21
41-SP	+ 10	2700	0.050	0.140	25.40	31.40	100	27
83-SN	+ 74	2325	0.058	0.155	30.70	40.00	100	29

TABLE H2 - CHARPY TEST DATA

A514 2" (Pre-Cracked) Fast Bend

Specimen No.	Temp. (°F)	Maximum Load (lb.)	Deflection at Maximum Load (in.)	Crack-Depth (in.)	Energy Absorbed		Shear (%)	Lateral Expansion (mils)
					Actual (ft.-lb.)	Normalized (ft.-lb.)		
470	- 250	2220	0.026	0.125	4.25	4.90	0	2
467	- 200	2860	0.054	0.120	6.06	7.00	< 5	4
436	- 155	2500	0.033	0.125	5.30	6.30	< 5	4
381	- 100	3000	0.050	0.140	26.20	32.90	60	24
380	- 100	2900	0.040	0.130	19.00	22.01	40	15
302	0	2730	0.056	0.135	27.00	33.02	100	26
345	- 50	2920	0.060	0.125	26.00	36.60	100	26
346	- 50	2650	0.053	0.150	22.70	30.50		24

TABLE H2 - CHARPY TEST DATA

A 514 2" (Pre-Cracked) Dynamic

Specimen No.	Temp. (°F)	Maximum Load (lb.)	Deflection at Maximum Load (in.)	Crack-Depth (in.)	Energy Absorbed		Shear (%)	Lateral Expansion (mils)
					Actual (ft.-lb.)	Normalized (ft.-lb.)		
	- 200			0.156	2.2	2.9	0	4
	- 125			0.140	7.2	8.9	10	4
	- 50			0.150	12.5	16.1	15	9
	+ 75			0.145	33.0	41.6	100	25
	+ 212			0.156	32.0	42.2	100	28

APPENDIX H3.1

DYNAMIC K_c AND K_M VALUES FOR 1/2 INCH A514 PLATE

Specimen Number	Initial Crack Length a (inches)	Test Temperature T (^{o}F)	Dynamic Yield Stress σ_{Yd} (ksi)	Net Ligament (L_N) (inches)	Bend Angle A (radians)	Max. Load (kips)	K_c (ksi/in)	K_M (ksi/in)
03	0.825	- 55	156	--	--	--	--	--
04	0.8	- 55	156	1.70	0.038	--	--	378
06	0.8	- 50	156	1.95	0.026	--	--	339
07	0.8	- 15	152	1.95	0.028	--	--	334
012	0.8	- 15	152	1.90	0.035	--	--	382
08	0.8	+ 30	147	1.35	0.068	--	--	425
010	0.8	+ 76	143	1.86	0.049	--	--	425
011	0.8	+ 76	143	0.96	0.118	--	--	460

APPENDIX H3.2

DYNAMIC K_c AND K_M VALUES FOR 1 INCH A514 PLATE

Specimen Number	Initial Crack Length a (inches)	Test Temperature T (^{o}F)	Dynamic Yield Stress σ_{Yd} (ksi)	Net Ligament (L_N) (inches)	Bend Angle A (radians)	Max. Load (kips)	K_c (ksi/in)	K_M (ksi/in)
CVN	--	- 54	142	--	--	--	45	--
15	0.766	- 53	142	--	--	31.2	91.4	--
16	0.778	- 50	140	--	--	23.0	66.0	--
17	0.783	- 15	138	--	--	40.0	127.3	--
18	--	- 15	138	--	--	45.0	150.8	
111	--	- 15	138	--	--	--	--	--
114	--	- 12	137	0.64	0.122	--	--	393
110	--	+ 30	131	1.47	0.063	--	--	420
CVN	--	+ 32	--	--	--	--	155	--
113	--	+ 72	127	1.80	0.045	--	--	387

APPENDIX H3.3

DYNAMIC K_c AND K_M VALUES FOR 2 INCH A514 PLATE

Specimen Number	Initial Crack Length a (inches)	Test Temperature T (^oF)	Dynamic Yield Stress σ_{Yd} (ksi)	Net Ligament (L_N) (inches)	Bend Angle A (radians)	Max. Load (kips)	K_c (ksi/in)	K_M (ksi/in)
CVN	--	- 60	141	--	--	--	58	--
26	0.83	- 56	140	--	--	42.5	63.6	--
27	0.79	- 54	139	--	--	53.0	78.3	--
28	0.78	- 19	134	--	--	67.5	102.7	--
29	0.80	- 19	134	--	--	85.0	141.4	--
212	--	+ 30	130	1.48	0.045	--	--	492
210	--	+ 74	125	1.88	0.026	--	--	490
216	--	+ 74	125	2.05	0.035	--	--	518
CVN	--	+ 90	123	--	--	--	256	--

APPENDIX I THE LEAK-BEFORE-BURST TOUGHNESS CRITERION

The leak-before-burst (LBB) toughness criterion has been sometimes termed a twice-plate-thickness critical crack size criterion. It was originally developed for application to pressure vessels based on the idea that a part-through crack, after spreading through the plate thickness, might have a total length of about 2B. If the fracture toughness was then large enough to prevent onset of rapid fracturing, leakage would provide warning of the presence of the crack prior to sudden bursting of the vessel. Although structural components such as those used in steel bridges were not considered in first applications of LBB criterion, one can see that such an application might be justified. For example, the tensile residual stress field adjacent to a line of welding tends to have lateral dimensions comparable to the thicknesses of the welded components. If one assumes that a crack might form across such a region of high stress, then the toughness necessary to prevent rapid crack propagation should increase with the crack size and thus with the plate thickness. In addition the fracture toughness required to prevent crack propagation obviously increases with increase of stress level. The LBB criterion is responsive both to plate thickness and to stress level. This can be written as

$$K_c^2 = \frac{\sigma_L^2 \, \pi \cdot B}{1 - \frac{1}{2}\left(\frac{\sigma_L}{\sigma_{YS}}\right)^2} \qquad \text{(I-1)}$$

where σ_L is the applied stress, B is the plate thickness and σ_{YS} is the material's yield strength. The toughness estimates provided by equation (I-1) can be adjusted with regard to degree of conservatism by elevating σ_L above the nominal tensile stress expected to occur during service.

From equation (5) of the text, equation (I-1) can be re-written as

$$\frac{1}{B}\left(\frac{K_c}{\sigma_{YS}}\right)^2 = \beta_c = \frac{\pi y^2}{1 - \frac{1}{2} y^2}$$

where $y = \sigma_L/\sigma_{YS}$. Equation (7) of the text provides the empirical relationship

$$\beta_c = \beta_{Ic}\,(1 + 1.4\,\beta_{Ic}^2)$$

Assuming the approximation provided by equation (7) is acceptable,

$$\frac{\pi y^2}{1 - \frac{1}{2} y^2} = \beta_{Ic}\,(1 + 1.4\,\beta_{Ic}^2) \qquad \text{(I-2)}$$

Because

$$\beta_{Ic} = \frac{1}{B}\left(\frac{K_{Ic}}{\sigma_{YS}}\right)^2 .$$

Equation (I-2) permits a determination of K_{Ic} from given values of σ_L, σ_{YS} and B. In this discussion, the interest is primarily on dynamic

fracture toughness. Thus σ_{Yd} will be used in place of σ_{YS} and K_{Id} in place of K_{Ic}.

As an illustration, assume a 1" plate of A441 steel with σ_{YS} = 57 ksi at room temperature. Assume we want the LBB value of K_{Id} at 0° F. It is first necessary to estimate σ_{Yd}. The procedure for doing this shown below as Steps 1 and 2 follows the method outlined in Ref. (14).

(1) Assume σ_{Yd} is the same as the static σ_{YS} at an absolute temperature (T') which is 7/12 times the absolute temperature of interest (T).
Since T = 459° R, T' = 267° F.

(2) Assume the elevation of σ_{YS} at T' over σ_{YS} at 529° F (70° F) is given in units of ksi by the
$$\frac{14,500}{T'} = \frac{14,500}{529} = 27 \text{ ksi}$$

(3) Assume σ_L = 1/2 (57 ksi) = 28.5 ksi
Then
$$y = \frac{28.5}{84} = 0.34 \qquad \text{(I-3)}$$
Evaluating the left side of equation (I-2) we now have
$$\beta_{Ic} (1 + 1.4 \beta_{Ic}^2) = 0.382$$

(4) Several approximation guesses or use of a graph results in β_{Ic} = 0.332.

(5) No use has yet been made of the plate thickness. Evidently the values of K_{Ic} for 1/2", 1", and 2" plates can be calculated using the equation
$$K_{Id} = \sigma_{Yd} (0.332B)^{1/2}$$

For the 1" plate one obtains

$$K_{Id} = 48.4 \text{ ksi}\sqrt{\text{in}}$$

If one now desires to use K_{Id} above to specify material procurement standards, then one of the correlations between K_{Id} and CVN can be used to determine the appropriate CVN level.

APPENDIX J K_c MEASUREMENTS

J.1 K_c Specimen Preparation

The test specimen configuration for all K_c tests in this program is shown in Figure J-1. All of the specimens were saw-cut from the original plate with their long dimension in the rolling direction. This resulted in a crack toughness characterization pertaining to crack motion perpendicular to the rolling direction of the steel. This direction was studied because the resistance of the steel to crack propagation in this direction is higher and more uniform than for crack motion parallel to the rolling direction. Besides, in structural applications the rolling direction is usually made to correspond to the direction of largest tension.

After the individual test specimens were saw-cut from the plates the top and bottom surfaces of the specimens were shaped to assure parallel surfaces. This was done to assure specimen stability during the fatigue cracking process. The sides of the specimens to be used in the thickness reduction technique were surface ground to assure a uniform thickness throughout an individual specimen. For the thickness reduction specimens the tolerance in the thickness direction was ± 0.001 in. The surfaces of the remaining specimens were left in "as received" condition. A 90° Chevron notch was machined in the center of the specimen as shown in Figure J-1. The recommended angles

of taper, α, for the notch are 45^{o}, 45^{o} and 29^{o} respectively for the 1/2", 1" and 2" thicknesses. The Chevron notch was used to help initiate crack growth in the fatigue process.

The fatigue crack growth was done on a 10-ton Amsler Vibrophore, which is a high frequency fatigue testing machine. The test specimens were placed into the machine in a 3-point bend arrangement, and the fatigue cracking was done in two stages, a fast and a slow growth portion. During the fast growth stage, the crack was driven down into the specimen to the depth, α_F. The main purpose of this fast growth portion was to get the crack well into the specimen in a short period of time. Accordingly, no fatigue cracking criteria was followed during this particular portion of crack growth. As mentioned above, the only requirement adhered to was to get the fatigue cracking done quickly. Approximately 20 minutes was considered acceptable. The criteria followed in the slow growth portion of the fatigue cracking process was that the average crack growth rate over the slow growth distance, α_S, be equal to or less than 1 microinch/cycle when practical.

In many instances during the fatigue cracking process the crack in the test specimen tended to grow faster on one side than on the other. In order to straighten out the crack leading edge a steel wedge was forced into the machine notch on the side of the specimen where the crack was longer. This prevented the longer side of the crack from cycling through the complete stress range, thereby slowing its growth rate, while allowing the other and shorter crack to continue to grow. When the edges of the crack reached equal length on both

sides of the specimen the wedge was removed and the regular fatigue cracking process was continued.

J.2 K_c Test Apparatus

This section describes the various apparatuses used in determining the dynamic and static K_c values.

J.2.1 Dynamic K_c

The dynamic fracture tests were done in a drop-weight tear test machine, shown in Figures J-2 and J-3. This machine was adapted from drawings supplied by the Naval Research Laboratory. The main uprights of the machine are two W12x85 columns to which are bolted fabricated tee-sections along which the drop-weight rides. The bolts allow for realignment of the rail system. The drop-weight machine has a drop-height capacity of approximately 20 feet. There are side grooves in the drop-weight which cause it to ride along the web of the tee-section. A close tolerance of 1/16 in. exists between the falling weight and the rail system so that upon release there is negligible "wobbling" or locking of the weight along the rails.

The weight of the falling mass is 400 pounds. In a previous study the original weight, 200 pounds, was doubled in size in order that lower drop-heights could be used in the dynamic tests to impart the same amount of energy to the test specimens as would a smaller weight falling from a greater height. This was done to help lessen the influence of the test specimen's inertia on the load record. The additional weight also doubled the energy capacity of the drop-weight

machine. The original weight used by Madison and Luft (19) was increased by bolting onto it two plates weighing approximately 100 pounds each. These plates were set on opposite sides of the original weight.

The drop-weight is raised and lowered to the required drop-heights by means of a 2-ton overhead crane. Once the weight has been positionedd positioned at the required elevation above the test specimen it is released by an electromagnetic release mechanism. After the weight fractures the specimen, the falling weight is stopped by two shock absorbing supports.

At the bottom of the drop-weight is the tup which serves also as the load dynamometer. The tup is positioned snugly in a recess at the bottom of the weight and is fasteneed into place by a long bolt passing vertically through the weight to its top. The tup is the load measuring part of the test apparatus, and it is shown in Figure J-4. The load dynamometer was machined from 4340 steel and it was heat treated to Rc 50. Two four-arm bridges are instrumented onto the tup with a 500 ohm strain gage passing across each arm of the bridge. The resistance of the gages was increased from 240 ohms in order to give the load signal greater sensitivity. Two bridges were placed on the tup as a precautionary measure in case one bridge failed in operation by shearing off due to the repeated shock loadings. A four-arm bridge is used to measure the axial load in the dynamometer, and by its very use, any bending that might occur in the tup upon impact with the test specimen is removed from the load signal.

As an aid in decreasing the influence of the specimen's inertia on the load record, 3/4 in. long, 1/2 in. diameter half-rounds were used during each drop-weight fracture test. The position of the pad relative to the test specimen is shown in Figure J-5. When the tup makes contact with the half-round, a considerable amount of deformation occurs in the pad with a corresponding large amount of energy absorption. This cushions the application of the load onto the test specimen and, as a result, stretches out the loading time. The half-round cushions were machined from unhardened drill rod.

The loading dynamometer has a 147° included angle ground into its tip. The original tip shape of the tup was semi-circular. The mild-angled tip is used to reduce the resistance of the half-round cushions to initial deformation.

The load signal is recorded on a Tektronix Type 549 storage oscilloscope with a "Type-Q Transducer and Strain Gage Preamp Plug-In Unit" used to monitor the signal. This particular oscilloscope is equipped with a delay mechanism whereby the start of the trace can be delayed for a specific time interval and then started and stored on the oscilloscope screen.

A photocell is attached to the drop-weight machine, as shown in Figure J-3, and when the weight is released and starts its free fall, a shutter attached to the drop-weight breaks the light beam of the photo-cell and sends a triggering signal to the oscilloscope to initiate the sweep of the trace. Depending on the drop-height of the particular test, a corresponding particular delay time is set on the oscilloscope's delay mechanism. When the triggering signal is

monitored by the oscilloscope the delay mechanism is activated, and when the set delay time passes, the load signal from the four-arm bridge of the tup is recorded and stored on the oscilloscope. The intention of the delay mechanism is to set, as the delay time, the time required for the drop-weight to pass the photo-cell and make contact with the test specimen. In this way the trace recorded on the oscilloscope will show a record of the load in the tup beginning with first contact against the test specimen. These delay times vary depending on the initial height of the drop-weight before release. These times were initially measured by a method of trial whereby the weight was dropped onto a solid bar from a definite prescribed height and the delay times were varied until the load signal was properly recorded on the oscilloscope. A polaroid camera is used to take a picture of the load signal stored on the oscilloscope screen in order to have a permanent record of each fracture test.

On the surface of the test specimens opposite the Chevron notch a 1/16 in. diameter hole was drilled 3/4 in. deep into the specimen at the center-thickness, offset 1 inch on either side of the plane of the notch. Into this hole was placed a chromel-alumel thermocouple which provided for the recording of the specimen temperature before each test. The specimens were heated in an oven or cooled in a household refrigerator, in a deep freeze, or by means of dry ice depending on the required test temperature.

J.2.2 Static K_c

Static K_c tests are conducted on a standard 120 kip Tinius-Olsen hydraulic tensile testing machine at a crosshead speed of 1 inch

per minute. The same instrumentation is used to record load for the static tests as for the impact tests. The instrumented tup is mounted in the head of the testing machine and the load record is taken from the oscilloscope trace. Loading times for these tests were of the order of one second.

J.2.3 Thickness Reduction Measurement

In the thickness reduction technique a Gaertner Series M1200 traveling microscope was used to measure the thickness reductions on slices cut from the fractured specimens. The microscope has a range of 2 inches and can read directly down to 0.0001 in. Since thickness (or thickness reduction) measurements were required at different normal separations from the brittle or flat portion of the fracture surface, calibrated movement perpendicular to the fracture surface, or in other words, movement perpendicular to that furnished by the microscope travel was required. To furnish this the shimming assemblage shown in Figure J-6 was machined, assembled, and mounted to the base of the microscope. This setup allowed for movement in 0.005 in. increments away from the fracture surface and perpendicular to the thickness direction.

To aid in these thickness reduction measurements slices were saw-cut from the fractured specimen. These slices furnished two surfaces whose edges corresponded to the thickness or thickness reduction profile at specific locations away from the end of the fatigue crack. These slices conveniently fitted into the shimming assemblage, as shown in Figure J-6, for thickness measurements.

J.3 K_c Test Procedure

This section describes the various methods and test procedures employed in determining K_c.

J.3.1 Dynamic K_c Procedure

On the day previous to testing, the specimens to be tested were placed in the required test-temperature atmosphere and were allowed to stay in this temperature for 12 hours or more. This assured uniform temperature distribution in each specimen.

Knowing the testing conditions - temperature, specimen size and yield strength - the general results of the particular test were estimated based on the experience acquired from previous tear-tests. Having some idea of the general outcome of the test a sufficient drop-height was selected. The height was kept near the minimum necessary to induce fracture upon impact of the drop-weight onto the test specimen. This practice also tended to reduce the test specimen's inertial effect on the load record. After the drop-height was selected a corresponding delay time was set on the oscilloscope. Also, having some general idea of the expected fracture load, the magnitude of the intervals on the ordinate axis of the oscilloscope screen was set.

After all systems were checked and found to be functioning properly, a final temperature reading was taken of the test specimen. The temperature was recorded, and the specimen was immediately placed onto the test fixture of the drop-weight machine. The specimen was

aligned so that the load dynamometer would hit the specimen directly over the fatigue crack. Then the required number of half-round cushions were placed on the specimen. The number of cushions varied depending on the expected magnitude of the fracture load. The safety pin was now removed from the release mechanism, and the drop-weight was raised to its required height. After reaching this height the drop-weight was released immediately and the test specimen was fractured. Except in the case of occasional maladjustments of the electronic equipment, a load-time signal was recorded and stored on the oscilloscope screen. A polaroid photograph was taken of the trace.

Since each dynamic fracture test required approximately one minute to complete once the specimen was taken from its test-temperature atmosphere, no facilities were used to keep the specimen in its test-temperature atmosphere while seated on the dynamic test fixture. Any temperature gradient within the test specimen was assumed negligible.

J.3.2 Static K_c Procedure

The procedure for cooling the static K_c specimens is identical to those described for the dynamic measurements. The instrumentation is also the same. The only differences between the two measurements is the use of a Tinius-Olsen hydraulic testing machine rather than a falling weight to load the specimen.

J.3.3 K_c Measurement by Thickness Reduction

A number of the dynamically tested specimens were measured for thickness reduction. One-half of the fractured specimen was selected

and a slice was taken from it as shown in Figure J-7. The saw-cuts were made so that the slice represented the measurement positions B/2 and 3B/4 away from the end of the fatigue crack. These slices were also wet ground to remove the rough edges resulting from sawing. The edges of each slice were also gently finished with a fine emergy cloth to remove burrs resulting from the grinding. This resulted in true thickness contours at the measurement positions. The slice was now ready for thickness reduction measurements.

Before any measurements could be taken the microscope was first aligned as perfectly as possible with the shimming assemblage which was mounted to the base of the microscope. This meant that the microscope traveled parallel to the edges of the assemblage and perpendicular to its sides. The slice was then placed on the sliding measuring platform and clamped in position, as shown in Figure J-6. With the turn-screw in its loosened position the sliding platform was manually pushed back and forth while the edge of the slice was aligned with the y-direction crosshair of the microscope. This guaranteed that the slice was positioned parallel to the sides of the shimming setup.

The turn-screw was tightened with no shims. The microscope was then moved until its x-direction crosshair was aligned parallel to a "weighted" fracture surface or zero position. The word, "weighted", is used because the unevenness of the actual fracture surface required judgment in the selection of an average position. This movement of the microscope in aligning the x-direction crosshair does not hamper the other fixed alignments. The steps in the alignment of the microscope and slice are illustrated in Figure J-8.

The remaining procedure consisted of measuring the thickness reduction at various distances from the fracture surface. This was done by inserting 0.005 in. shims in the frame as shown in Figure J-8. At each new distance from the fracture surface the thickness reduction was measured.

Now that the test procedure has been described, a few additional words are needed concerning the previously described slicing procedure. In this procedure it was explained how a slice was removed from one-half of the fractured specimen. Care should be taken in selecting the proper half to use for the slice. That half of the specimen should be used which retains both shear lips upon fracture. The typical slice in Figure J-7 is an example of such a selection. This type of slice permits the measurement of the thickness below the fracture surface because of the physical presence of the shear lips.

If the shear lips are shared between both halves, personal judgment should be used in selecting which half of the specimen to slice. If this situation is so pronounced that thickness measurements are not possible across the slice because of the absence of material at one edge of the slice, a different measuring procedure is required. This missing material corresponds to the shear lip existing on the other half of the fracture specimen. For this situation the measuring procedure is exactly the same except that the slice is shimmed so that measurements can be made at equal distances above and below the fracture surface at equal distances, and the measurements are made from the centerline of the slice out to the edge of the slice where the shear lip exists. The total thickness for a particular distance

away from the fracture surface is, therefore, taken to be the sum of the two half-thickness measurements made above and below the fracture surface at the same distance. The centerline of the slice must be physically scribed onto the slice for this method. The remaining measurement setups are the same.

J.3.4 Bend Angle K_c Measurement Procedure

In several of the drop-weight tear tests the test specimen failed to fracture completely due to its high degree of toughness at near room temperatures. The drop-weight was usually at its maximum safe operating drop-height for such a test. This maximum safe height was decided to be 10 feet, and a greater height was not used in fear of damaging the load dynamometer or the strain gages instrumented onto it.

After such a test the partically fractured specimen was removed from the drop-weight machine, and the bend angle, A, was measured by means of a protractor. The specimen was then placed into the deep freeze or in contact with dry ice. After being in this cold atmosphere for several hours it was again placed into the dro-weight machine where the fracture of the specimen was completed. No data was required during this second drop. Its purpose was just to complete the break of the specimen.

Inspection of the fracture surface of the broken specimen clearly distinguished to what depth the crack moved during the first drop of the weight at the warmer temperature. The remaining ligament cross-section was more brittle in texture compared to the ductile failure

plane of the initial drop. This difference in appearance easily led to the location of the final crack arrest position resulting from the first drop and accordingly showed the cross-section of the previously unbroken ligament. Since the final crack arrest position was never perfectly straight, a "weighted" straight position was selected along the actual arrest edge.

J.4 K_c Data Analysis

The material presented in this section describes the data reduction techniques employed to calculate K_c from the experimental measurements.

J.4.1 Dynamic and Static K_c Calculations

Using a boundary collocation technique Gross and Srawley developed an expression for K for single-edge-cracked plate specimens in 3-point bending (21). This expression for K is represented by a fourth degree polynomial of the following form with values of the coefficients A_i furnished for values of a/W up to 0.6:

$$Y = \frac{K\ B\ W^2}{1.5\ PL\ \sqrt{a}} = A_o + A_1\left(\frac{a}{W}\right) + A_2\left(\frac{a}{W}\right)^2 + A_3\left(\frac{a}{W}\right)^3 + A_4\left(\frac{a}{W}\right)^4 \quad \text{(J-1)}$$

where

Y = dimensionless ratio

B = specimen width

W = specimen depth

P = applied load

L = span length

a = effective crack length

A_i = coefficients whose values are dependent on the specimen's L/W ratio

The coefficients for the above equation have been developed for L/W ratios of 8 and 4 and are shown in Figure J-9.

Since the same 3-point bend configuration was used in the dynamic fracture tests, the above K calibration was employed for the solution of the dynamic K_c values. However, due to a specimen length-to-width ratio of 3.33 which was the L/W ratio used in this program, a set of coefficients, differing from those developed by Gross and Srawley, had to be derived for use in equation (J-1).

This new set of coefficients was obtained (19) by simply linearly extending those values of A_i recommended by Gross and Srawley to the L/W value of 3.33. The results of this extension are presented also in Figure J-9. As a check, a compliance calibration was made by Luft (19) for a bend specimen whose L/W ratio was 3.33 and it was shown that the above linear extension of the Gross-Srawley data was valid.

Using the equation for the plastic zone size, r_Y, equation (4) in an adjusted form

$$K = \sigma_{YS}\sqrt{2\pi r_Y} \qquad \text{(J-2)}$$

and substituting this expression into equation (J-1) results in

$$\frac{r_Y}{W} = \frac{P^2 L^2}{B^2 \sigma_{YS}^2 W^4} \frac{2.25}{2\pi} \left(\frac{a}{W} Y\right)^2. \qquad \text{(J-3)}$$

Equations (J-2) and (J-3) were used to solve for K_c. This was done by a simple computer program. The flow chart of the computer program is shown in Figure J-10. Essentially the method of solution involves an iterative process where a value of (r_Y/W) is assumed, and this value is used, in turn, to calculate another (r_Y/W) value by means of equation (J-3) remembering that

$$\frac{a}{W} = \frac{a_o}{W} + \left(\frac{r_Y}{W}\right)_{\text{assumed}}.$$

When the difference between the assumed and calculated values of (r_Y/W) is equal to or less than 0.0001 inches the iterative process is stopped and a K value evaluated using equation (J-2). The computer solution was the method used in all the K_c computations both static and dynamic.

The values of P and a used in equation (J-3) corresponded to the maximum load determined from the load records and the fatigue crack length respectively. The value of σ_{YS} was that value of yield strength which was appropriate for the particular test temperature and testing speed. This value was determined from the equation

$$(\sigma_{YS}) = (\sigma_{YS})\Big|_{+\,75^{o}\,F,\ t_o} + \frac{174{,}000\ \text{ksi}}{\log(2 \times 10^{10} f)(T + 459)} - 27.4\ \text{ksi} \qquad \text{(J-4)}$$

where

t = loading time to maximum load

t_o = time of load application for a static test (50 sec.)

T = testing temperature in ^{o} F

This expression was suggested by Irwin (14) as a best fit for data on A302B steel from Ripling and for data on three Ni-Cr forging steels from Wessel. It takes into account both the strain rate and the material temperature on the yield strength. This equation is considered tc furnish best fit conditions for any structural steel whose static yield strength is not greater than approximately 120 ksi. Madison (18) and Luft (19) showed that A441 steel behavior agreed approximately with this equation.

J.4.2 Investigations into a Typical Load Record Response

Figure J-11 shows a sketch of a typical load record as recorded and stored on the oscilloscope after each successful fracture test.

The sketch includes two different types of load response, one represented by the solid curve and the other by the dashed curve. The solid line depicts a load record resulting when the half-round steel cushions are used during the fracture test. These cushions stretched out the loading time, from zero to maximum load, to approximately 0.5 to 1.5 milliseconds. These loading times resulted in values for the inverse of loading time (1/t) which guaranteed load responses that would lead to minimum K_c levels. During this loading period small slope changes were often observed in the load record. It is uncertain whether these are vestiges of an inertial influence or are due to deformation behavior of the half-round cushion. The maximum recorded load was taken as the fracture load, P_c, which was used in all the K_c calculations. After reaching maximum load, the load record fell off either sharply or gradually, depending on the severity of the type of fracture.

In a majority of the load records, oscillations beyond the maximum load point were found to exist that were periodic in nature, as shown in Figure J-11, and so a study was made into the possible sources of vibration in the test setup during a drop-weight tear test. The oscillations were observed after the maximum load and while a load was still being applied to the test specimen. It was felt that vibrations were interacting with the actual fracture process because the drop-weight was actually fracturing the specimen during this time period. The results of the study of expected vibration time periods is shown in Figure J-12.

First investigated was the reflected wave motion in the drop-weight caused by its initial sudden contact with the test specimen. This wave motion corresponds to the travel of a compression wave up from the tup to the top of the weight where it is reflected back down to the tup as a tensile wave. The period for one such complete cycle was calculated to be 2.3×10^{-4} sec.

Investigated next was the bending response of the test specimen. In these calculations the specimen was considered to be a spring with the 400 lb. weight vibrating above it. The spring constant for the specimen was calculated taking into consideration the crack in the specimen. The period for this response was found to be 8.4×10^{-3} sec. These vibrations could not appear on the trace because fracture of the test specimen occurs within the first quarter of that time period.

The last type of vibration investigated was the shear wave motion in the test specimen. This study is directly analogous to the reflected wave motion in the drop-weight, described previously, except

that in this instance the path of travel of the reflected wave is from the center of the test specimen, where the tup strikes, to either of the specimen's supports and back to the center. The wave motion involved is a shear wave motion and can be regarded as a high frequency contribution to bending of the specimen. The period for this complete cycle was calculated to be 0.8×10^{-4} sec.

Measuring the period of the oscillations visible in the load records resulted in a period whose value was approximately 4.0×10^{-4} sec. This value is in reasonable agreement with the calculated value of the period for the reflected wave response. In fact it is felt that these oscillations do originate from these reflected waves, and that the difference that exists between the calculated and measured values of the periods may be caused by camping.

If the half-round steel cushions are not used during a fracture test, the resulting load record is depicted by the dashed curve in Figure J-11. The shape of the rising portion of the curve is similar to that when a pad is used. Some cushioning resulted from the indentation of the tup into the test specimen. The loading time for this type of load record corresponds nearly to the shear wave period and represents the main inertial response of the test specimen to the rapidly applied load. This load record cannot be regarded as valid because it is elevated by the inertia of the test specimen. Studies by Madison (18) and Luft (19) indicated that the second load maximum was in approximate agreement with the bending moment in the specimen, measured directly by strain gages on the specimen.

J.4.3 Calculation of K_c from Bend-Angle Data

As an attempt at formulating a plasticity based fracture toughness characterization, a bend-angle type of K_c measurement procedure was explored. As in the thickness reduction technique it was reasoned that in the dynamic fracture tests the K value driving the crack increased until the critical K level was attained whereupon unstable crack propagation began. Again the K level increased to the plateau value with increased fracture surface roughening. However, due to a lack of available energy caused by an insufficient drop height the fracture process ceased and the crack arrested. Resulting was a partially fractured specimen with a measurable bend-angle, A.

Using these considerations it was felt that the K level corresponding to the crack arrest would represent the plateau value since it was at this value that the crack was propagating when it arrested. Accordingly it was reasoned that the K value resulting from any bend-angle type computation would be a plateau value.

The bend-angle technique consisted of measuring the bend-angle after the initial partial fracture, completing the fracture of the specimen at a very cold temperature, measuring the depth of the net ligament resulting from the first drop and calculating the crack opening stretch, δ, using simple geometry, Figure J-13. The specimen was assumed to rotate about a plastic hinge whose center of rotation was at the middle of this net ligament. The δ value was calculated at the crack arrest point using $\delta = 0.5\ L_N\ A$, equation (12). The "effective" K_c value was calculated from the above δ value using equation (8)

In such a procedure it is desirable to obtain crack arrest near the one-half point of the original net section. This assists in obtaining a crack arrest K value pertaining to a low constraint portion of the R-curve. Excessively small values of the remaining net ligament are undesirable because the contribution to the total bend-angle from previous positions of the crack may then be too large.

J.4.4 Calculation of K_c by Thickness Reduction

Since the choice of position relative to the fracture surface at which to measure thickness reduction is somewhat arbitrary, various positions were tried. These initial trials were examined with a view of producing a consistent set of K_c measurements for all plate thicknesses tested. The position which is currently being employed is given by the equation

$$S = \frac{B}{3} f\left(\frac{r_Y}{B}\right) \qquad \text{(J-5)}$$

where S is the distance from the fracture plane and

$$f\left(\frac{r_Y}{B}\right) = \frac{\left(\frac{r_Y}{B}\right)^{1/3}}{1 + 2\left(\frac{r_Y}{B}\right)^{1/2}} \qquad \text{(J-6)}$$

Equation (J-5) was selected because it provides a simple monotonic increase of S with r_Y/B up to the point $r_Y = B$ where 100 percent shear is anticipated. For values of r_Y/B greater than 1, S was taken as B/9.

The calculation of K from the thickness reduction is made by equating the thickness reduction at the point of measurement to the crack opening stretch, δ. Now by using $\delta = K_c^2/E\,\sigma_Y$, equation (8) can be calculated. From this value r_Y is calculated and with this value

a check of S given by equation (J-5) is made. If the two values agree the calculation is stopped. If they do not, a new δ is measured at the S value just calculated. This procedure is continued until convergence is obtained. To start the calculation, the intial trial value of S was chosen as $S_o = B/9$.

An example of a typical iterative procedure is given in Appendix O. Due to the physical arrangement of the thickness reduction measuring device, it proved convenient to obtain a series of δ values at 0.005 increments in S. To obtain δ values between these, linear interpolation was used.

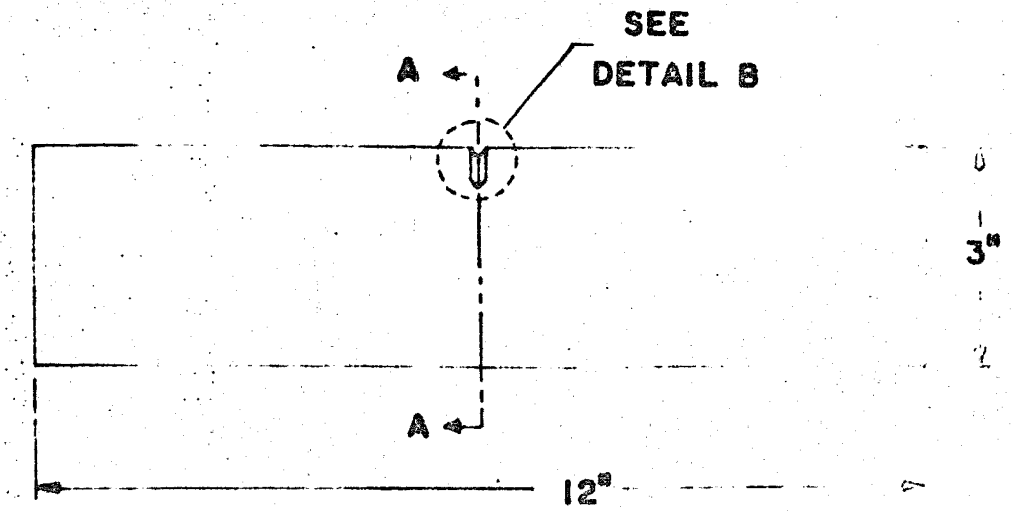

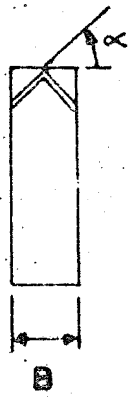

B = PLATE THICKNESS	α
1/2"	45°
1"	45°
2"	29°

SECTION A-A

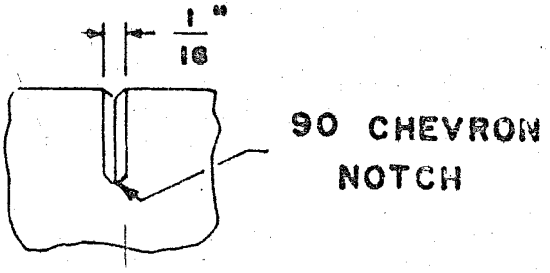

DETAIL B

Fig. J-1 Lehigh Test Specimen

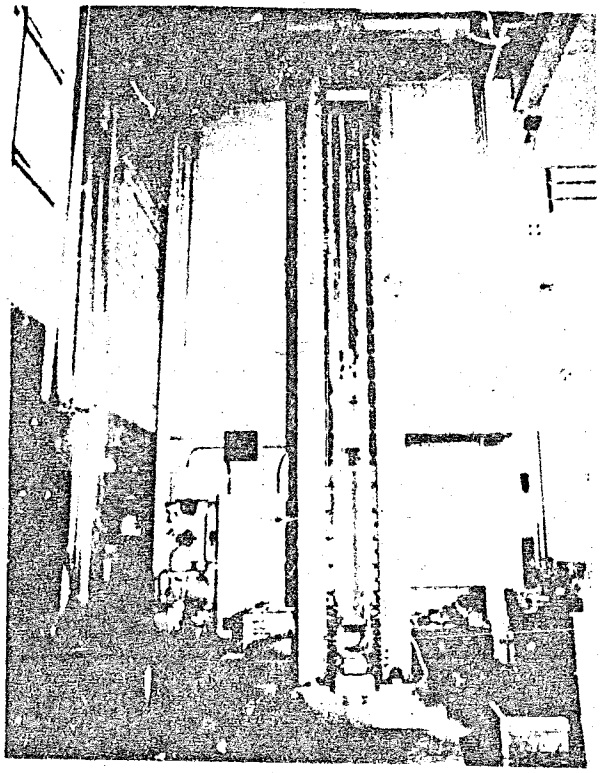

Fig. J-2 The Lehigh Impact Test Machine

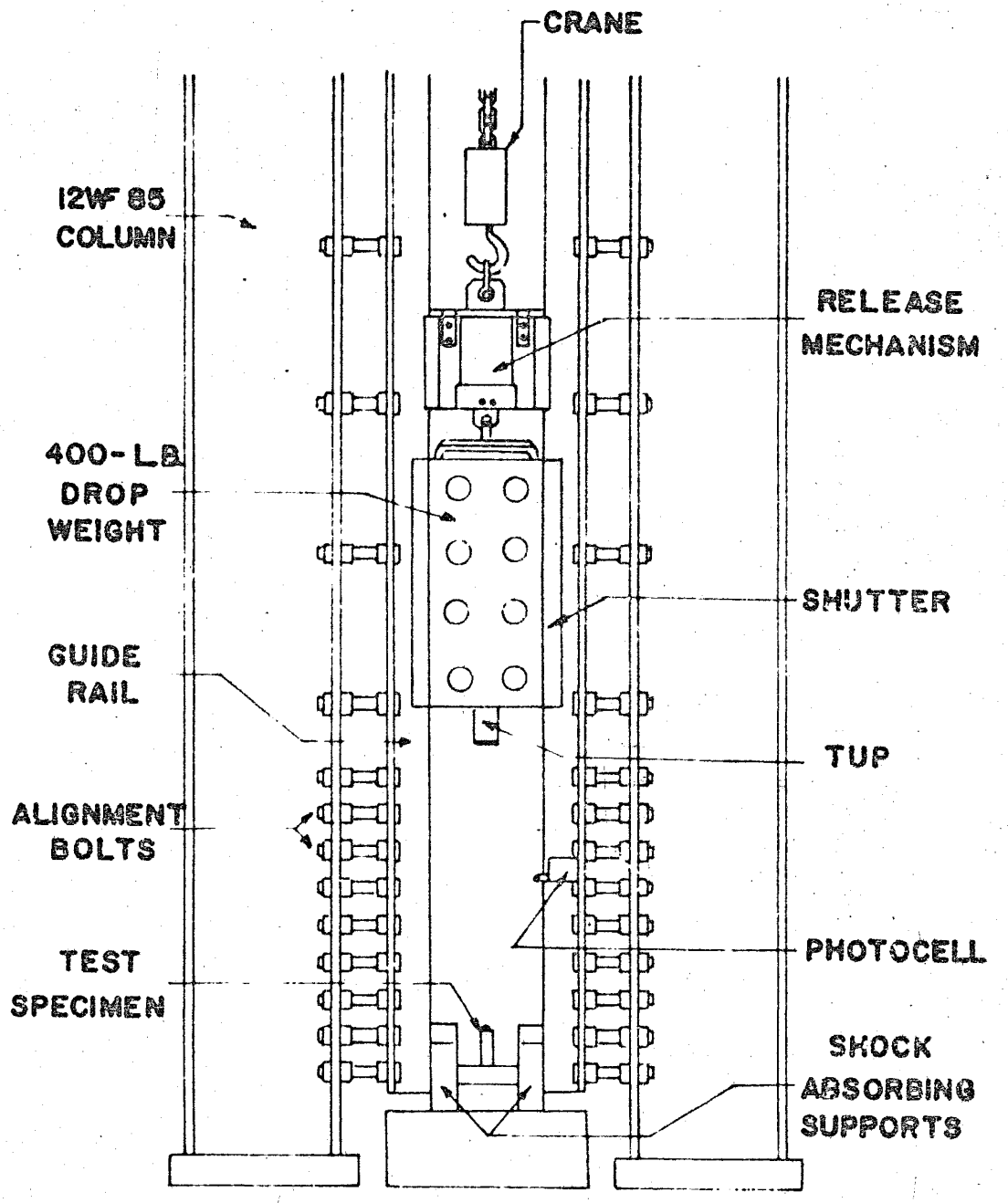

Fig. J-3 Lehigh Drop-Weight Tear Test Machine

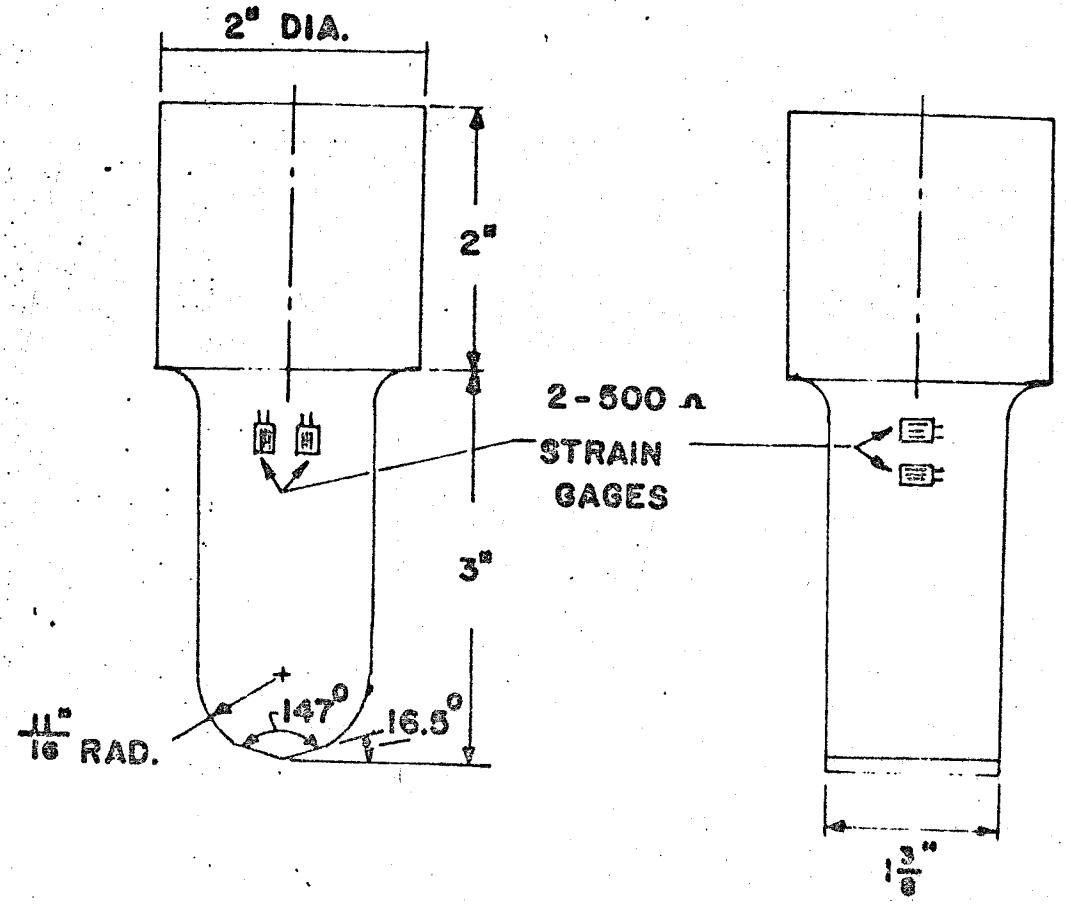

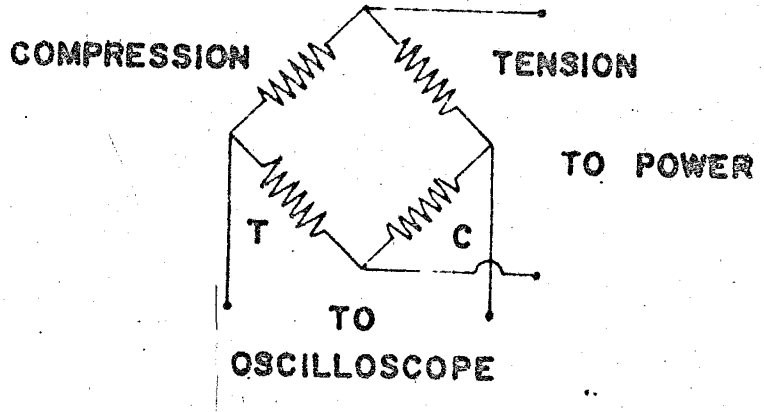

Fig. J-4 Load Dynamometer (Tup)

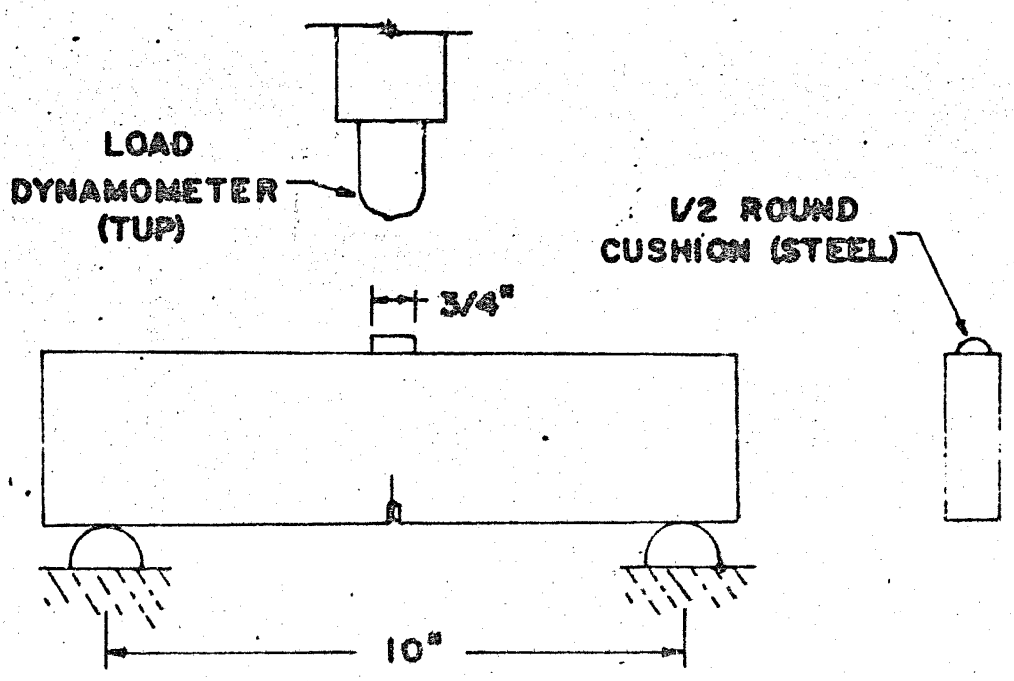

Fig. J-5 Padded Test Specimen on Test Fixture

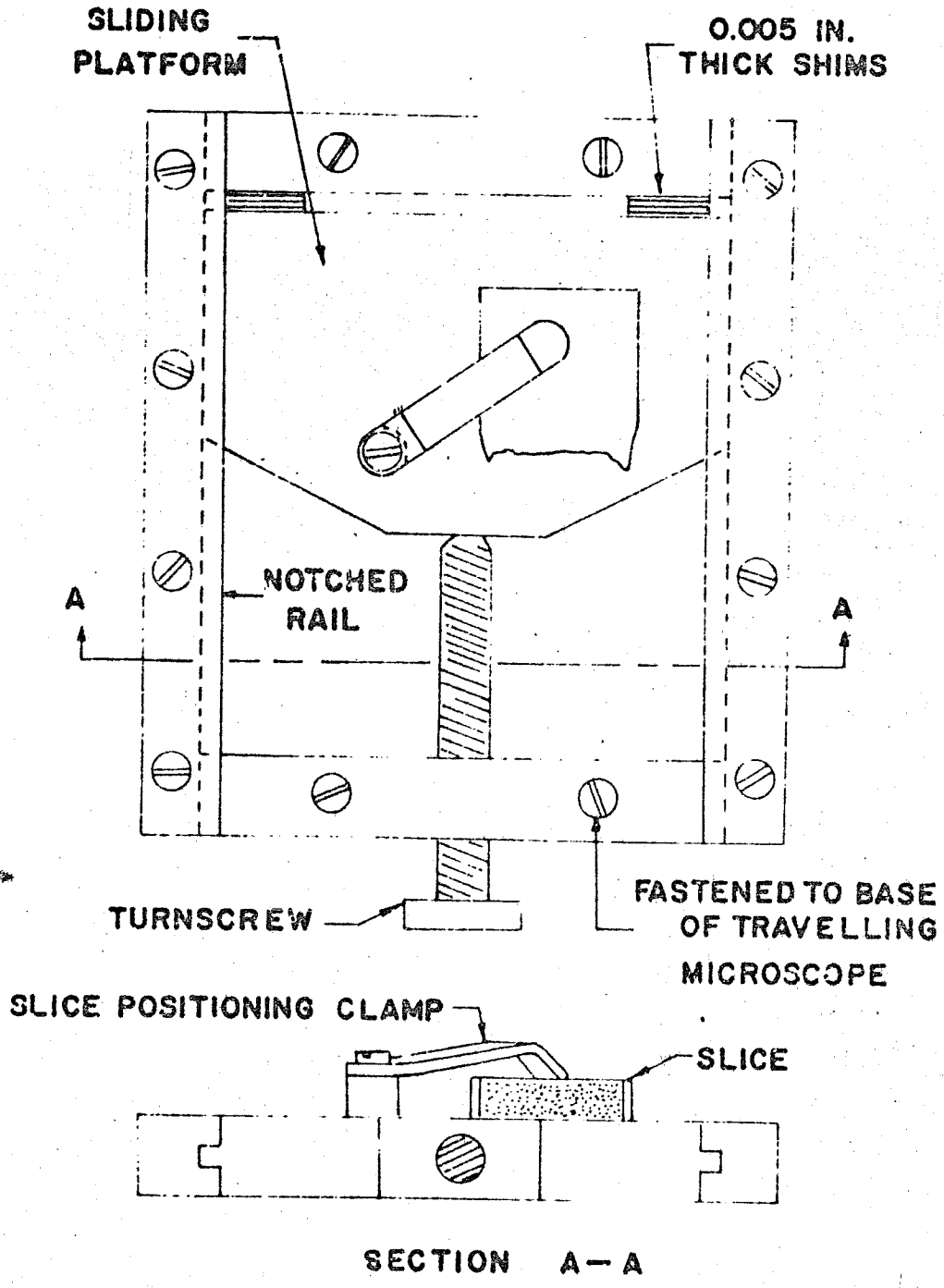

Fig. J-6 Shimming Assemblage

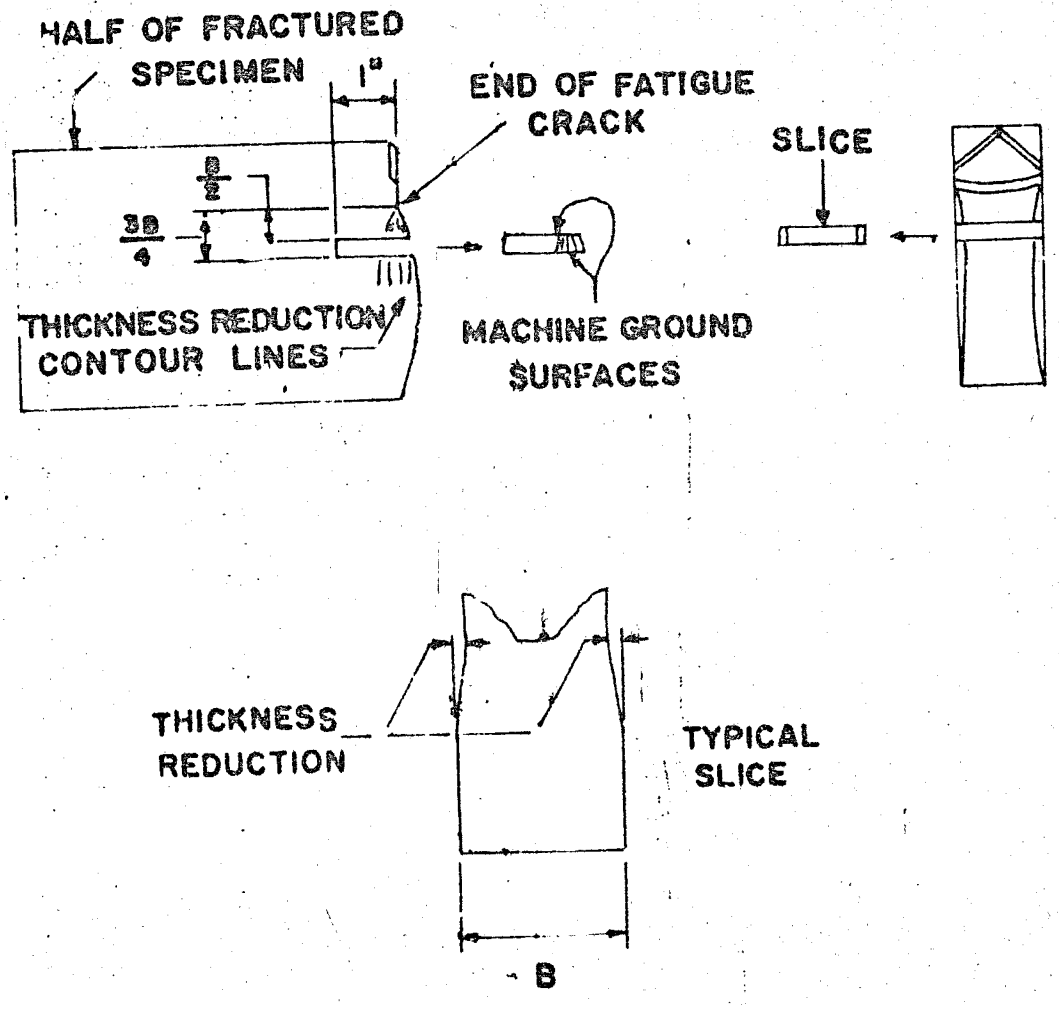

Fig. J-7 Slicing Technique Employed in Thickness Reduction Procedure

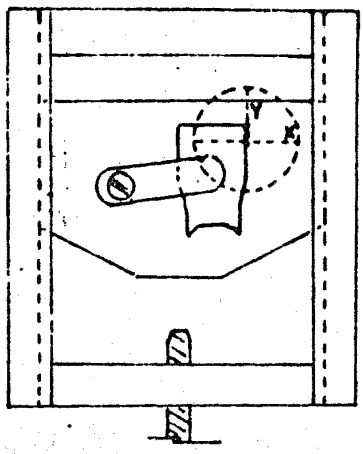

(1) POSITION EDGE OF SLICE PARALLEL TO Y-DIRECTION CROSSHAIR.

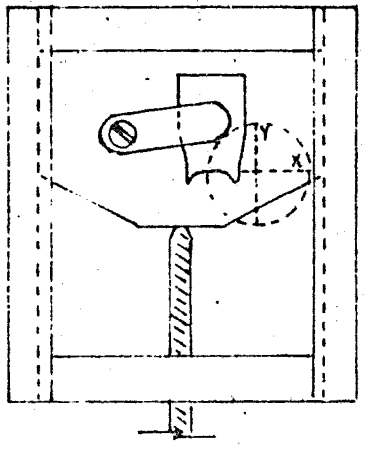

(2) POSITION X-DIRECTION CROSSHAIR PARALLEL TO BRITTLE PORTION OF FRACTURE SURFACE (ZERO POSITION).

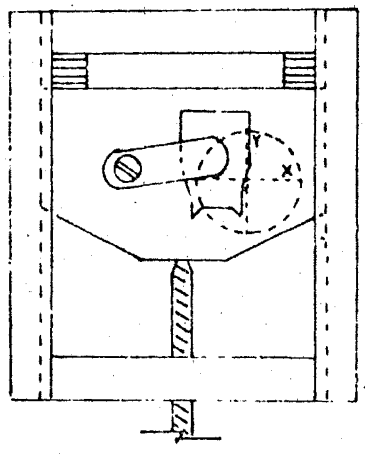

(3) SHIM AND MEASURE THE THICKNESS REDUCTION AWAY FROM FRACTURE SURFACE.

Fig. J-8 Alignment Procedure of Slice Prior to Thickness Reduction Measurements

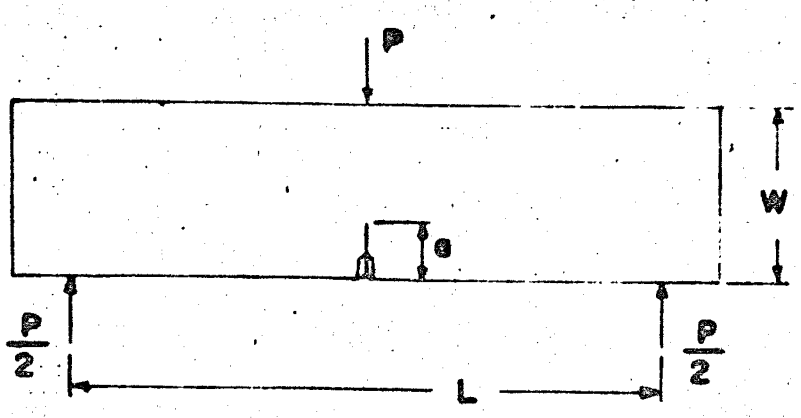

$$Y = \frac{KBW^2}{1.5PLV\overline{a}} = A_0 + A_1\left(\frac{a}{W}\right) + A_2\left(\frac{a}{W}\right)^2 + A_3\left(\frac{a}{W}\right)^3 + A_4\left(\frac{a}{W}\right)^4$$

THIS EXPRESSION WAS DEVELOPED BY GROSS AND SRAWLEY FOR SPECIMENS WHOSE L/W RATIOS ARE EITHER 8 OR 4. (ASTM STP 410)

L/W	A_0	A_1	A_2	A_3	A_4
8	+1.96	-2.75	+13.66	-23.98	+25.22
4	+1.93	-3.07	+14.53	-25.11	+25.80
3.33	+1.93	-3.12	+14.68	-25.30	+25.90

Fig. J-9 K Calibration for Lehigh Test Specimen

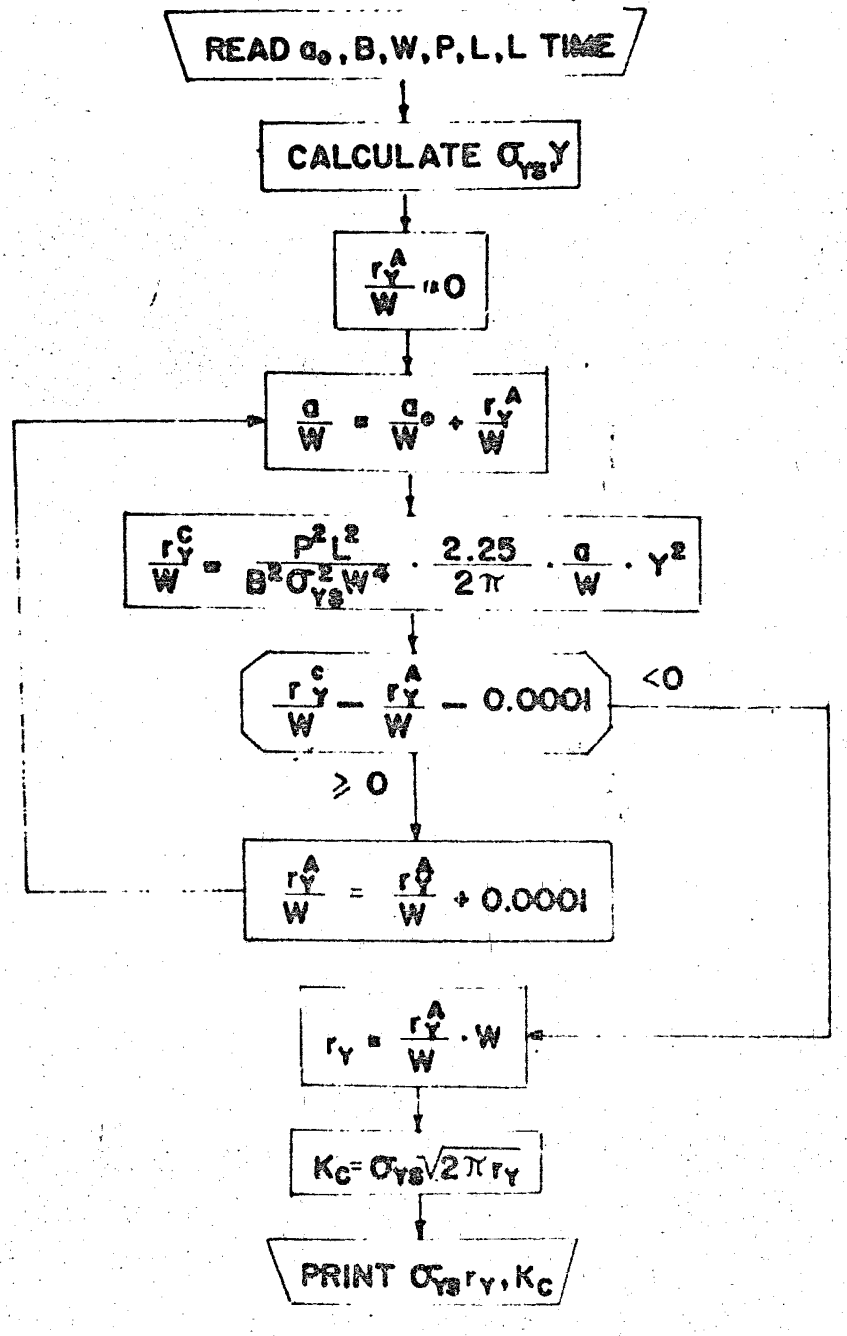

Fig. J-10 Flow Chart for the Computer Solution for K_c

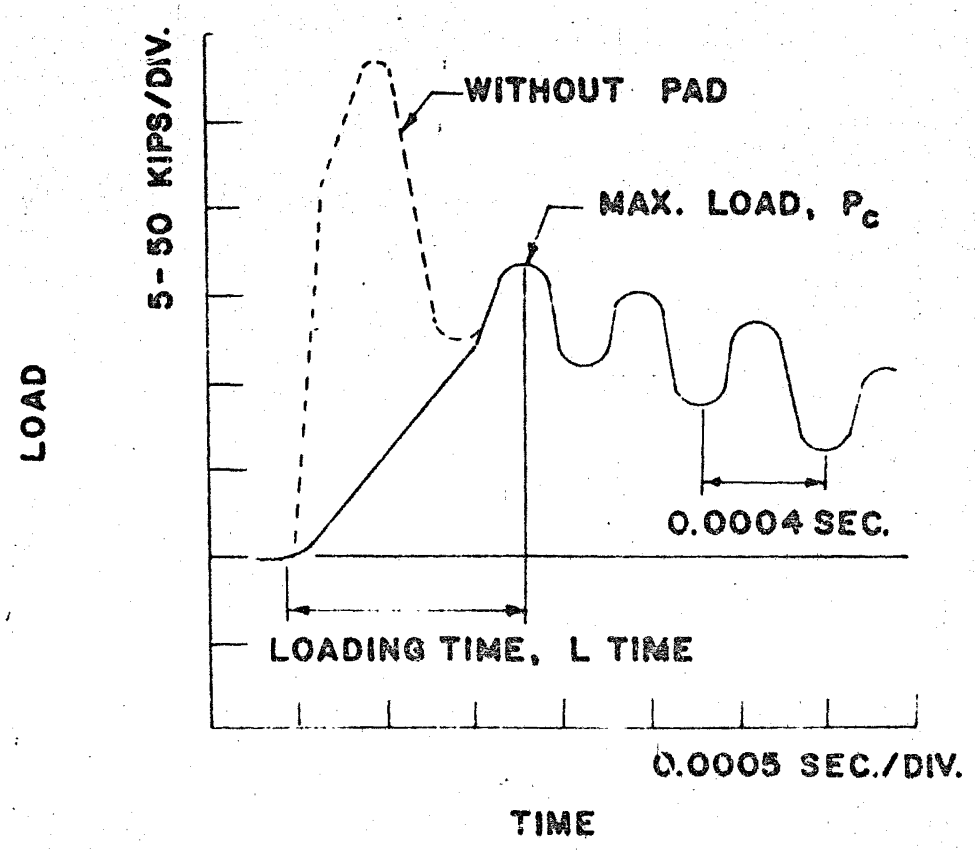

Fig. J-11 Typical Load-Time Record

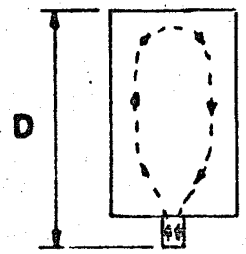

① REFLECTED WAVE MOTION

V = VELOCITY = $\sqrt{\frac{E}{\rho}}$

T' = PERIOD = $\frac{2D}{V}$

$T = 23 \times 10^{-4}$ SEC.

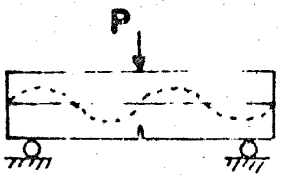

② BENDING WAVE MOTION

T' = PERIOD = $2\pi\sqrt{\frac{M'}{K'}}$

WHERE $K' = \frac{1}{C}$

$T = 8.4 \times 10^{-3}$ SEC.

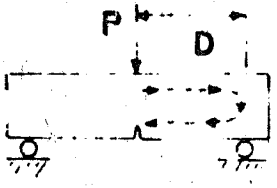

③ SHEAR WAVE MOTION

V = VELOCITY = $\sqrt{\frac{G}{\rho}}$

T' = PERIOD = $\frac{2D}{V}$

$T = 0.8 \times 10^{-4}$ SEC.

Fig. J-12 Investigations into a Typical Load-Time Record Response

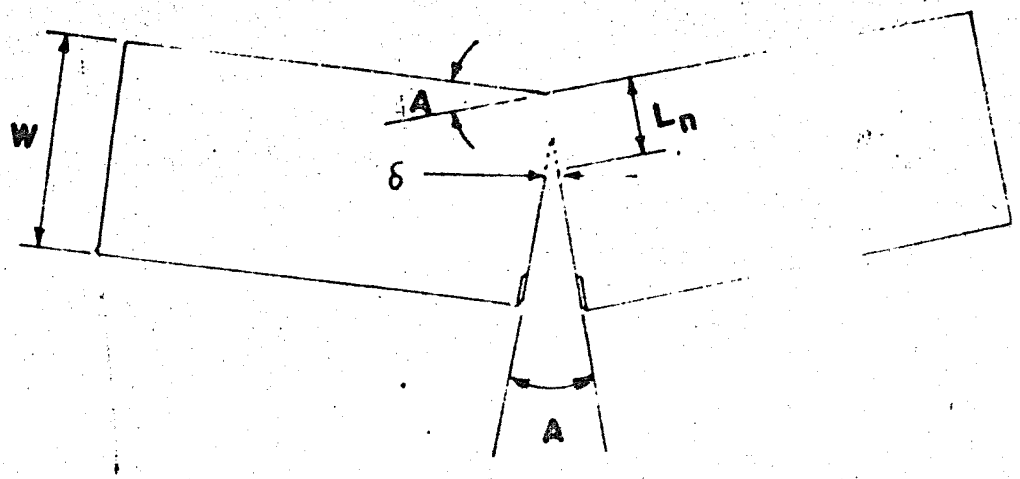

$$\delta = \frac{1}{2} L_n A$$

Fig. J-13 Typical Partially Fractured Test Specimen used in Bend Angle Procedure

APPENDIX K R-CURVE MEASUREMENTS

K.1 R-Curve Specimen Preparation

A crack-line-loaded compact tension specimen was employed for the determination of R-curves. The specimen had an h/W ratio of 0.6. W was 19.166 inches and h was 11.5 inches. These proportions correspond to those recommended in ASTM Standard E 399-70 (5). The important details of the specimen are shown in Figure K-1.

All specimens were flame cut from the original plate so that the direction of crack propagation was normal to the rolling direction as was the case for the K_c specimens. After flame cutting the specimen was a 24" x 24" square. At this point approximately 1/2 inch was saw-cut from each edge so that a specimen slightly larger than 23" x 23" was produced. The next procedure called for final milling of the edges to give a 23" x 23" square $\pm$ 0.005 inches. This square was then machined to provide the loading hole, initial Chevron notch, tapped holes at positions V_1 and V_2 and a series of holes at the specimen corners for handling purposes. The Chevron notch was used to assist the fatigue precracking. No attempt was made to remove the mill scale from any of the specimens. In fact the thicknesses of all specimens, except for the K_c specimens used for thickness reduction measurements, were the as-received nominal values.

The next step in the preparation of the R-curve specimen was to fatigue precrack each specimen approximately 0.5 inches past the Chevron notch. This produced an initial crack length of 6.25 inches or an a_o/W of 0.326. The fatigue precracking was done on a 20,000 pound M.T.S. electrohydraulic closed-loop test system. Loading plates were attached to the specimen as shown in Figures K-2 and K-3. The load levels for precracking were maintained at a 15,000 pound maximum and a 2000 pound minimum at a cyclic frequency of 10 H_Z. This gives an approximate K value of $K = 1.66\ P/B$ or for the 1/2" plate a K_{max} of 50 ksi$\sqrt{in}$ and a ΔK of 43.4 ksi$\sqrt{in}$. The same load levels were used for both 1/2" and 1" thick specimens. Typical precracking times were approximately 16 hours to precrack a 1 inch specimen.

K.2 R-Curve Test Apparatus and Procedures

In a series of recent papers Heyer and McCabe (7, 22, 23) have described a procedure for obtaining R-curves from crack line loaded compact tension specimens. Their test consisted of wedge loading a compact tension specimen while monitoring the crack surface displacements at two definite positions relative to the load line. By this technique they were able to measure large portions of an R-curve from a single test. This method also has the advantage of allowing crack length and load to be determined without monitoring crack length or load directly. These are determined through the use of compliance curves. This enables testing to be carried out, if desired, in enclosed chambers for temperature or environmental control where it

would be difficult to measure crack length visually. The test apparatus described in this section is almost identical to the one used by Heyer and McCabe.

The test apparatus used for the R-curve measurements consists of seven primary components. These are test base, wedge, sector and wedge block combination, two DCDT displacement transducers, a D.C. power supply, an X-Y recorder, and a 20,000 pound M.T.S. test system.

The essential operating features of the R-curve measuring system are not complicated. The test specimen is placed on the horizontal test base which is mounted approximately 12 inches above the M.T.S. base. This is shown in Figures K-4 and K-5. The sectors, wedge blocks and wedge are inserted next. This is shown in Figure K-6. The two DCDT displacement transducers are now mounted at the V_1 and V_2 positions. The transducers used are Hewlett Packard type 24DCDT with a stroke of $\pm$ 0.5 inches. These have an output of approximately 25 volts DC/inch for a 24 Volt DC input. The power supply used to provide the DC input is a H. P. Harrison Laboratory Model 6204B. The transducer output is recorded on a Honeywell X-Y recorder. At this point the wedge is connected to the hydraulic ram of the M.T.S. system by means of a clevis arrangement.

After checking the alignment of the specimen and wedge and the operation of the transducers and the X-Y recorder, the test is begun. This is accomplished by moving the ram of the M.T.S. system down at a controlled rate. This in turn pulls the wedge down and through the specimen forcing the wedge blocks to drive the sectors into the

specimen. During this course of action the output of the V_1 and V_2 transducers are recorded on the X-Y recorder.

The enclosed angle of the wedge is approximately 1-1/2 degrees. The wedge and wedge-blocks were made of tool steel while the sectors were made from a Maraging 250 grade of steel. So far this combination of materials has proved adequate. The relief portion of the wedge blocks which can be seen in Figures K-1 and K-4 allow for line contact at a given position on the sectors. It also offers accommodation to the rotation of the sectors as the specimen deforms.

The R-curve testing procedure for low temperature testing is essentially identical to the procedure already described. The only difference is that the test base and specimen are enclosed in an insulated box. The cooling of the specimen is provided by either a controlled flow of cold nitrogen or packing with dry ice, or a combination of both.

K.3 R-Curve Data Analysis

A very common way of obtaining the stress intensity factor, K, for a particular geometry is to study the change of compliance of the specimens as a function of crack length (25). Although the geometry of the R-curve specimen used in this study was very nearly identical to the ASTM E-399 specimen for $h'' = 0.6$, it was felt that the difference in loading was sufficient to warrant a K calibration study. This was also necessary to determine the relationship between the V_1/V_2 ratio and (a/w)

To date two 3/4" 7075-T6 full size aluminum specimens have been employed in calibration experiments. The calibration experiments were run on the M.T.S. test system. This was accomplished by attaching straps to the Maraging 250 sectors and loading the same through the sectors. This is shown in Figure K-7. For a particular crack length the specimen compliance in terms of V_1/P and V_1/V_2 was determined. The compliance readings were taken at 1/2 inch crack intervals starting from a crack length of 5.75 or $a/W = 0.3$. A 1/16 inch wide saw-cut was used to extend the crack after each reading. To convert V_1 to the displacement of the load line, V_L, the method employed by Heyer was used (22). This is $V_L = [a/(a + 3.5)]\, V_1$. Plots of $(E\ B\ V_L)/P$ and V_1/V_2 are shown in Figures K-8 and K-9.

The results for V_1/V_2 from both calibration experiments exhibited very good repeatability or agreement. This was not the case for the $[(E\ B\ V_L)/P]$ data. However, if one ignores the first set of V_1 data from Plate 1, since this was the first attempt to use the transducers, the results from Plate 2 show agreement with the general trend reported by Roberts (24). The major difference is a vertical translation of the data. This type of phenomena is discussed by Heyer (22). It is his technique to establish one base line $[(E\ B\ V)/P]$ curve and to correct this to fit the compliance of a particular test specimen.

Since there is general agreement with the results of Roberts (24) in terms of shape of the $[(E\ B\ V_L)/P]$ curve, his results were used for calculations of stress intensity factors. This involves use of the customary proportionality of K^2 to the derivative of the compliance with respect to the crack length.

Once the V_1 versus V_2 record is obtained from a R-curve test the data reduction is quite simple. First a/W is determined from V_1/V_2. With a/W and V_1, P is determined from the (E B V)/P versus a/W curve. These two values, a/W and P, are sufficient to determine K and subsequently the R-curve.

If desired, the formula for K given in ASTM standard E-399

$$K = \frac{P}{BW^{1/2}} \left[29.6 \left(\frac{a}{W}\right)^{1/2} - 185.5 \left(\frac{a}{W}\right)^{3/2} + 655.7 \left(\frac{a}{W}\right)^{5/2} - 1017.0 \left(\frac{a}{W}\right)^{7/2} + 638.9 \left(\frac{a}{W}\right)^{9/2}\right] \qquad \text{(K-1)}$$

can be used in place of the tabulated data of Roberts (24).

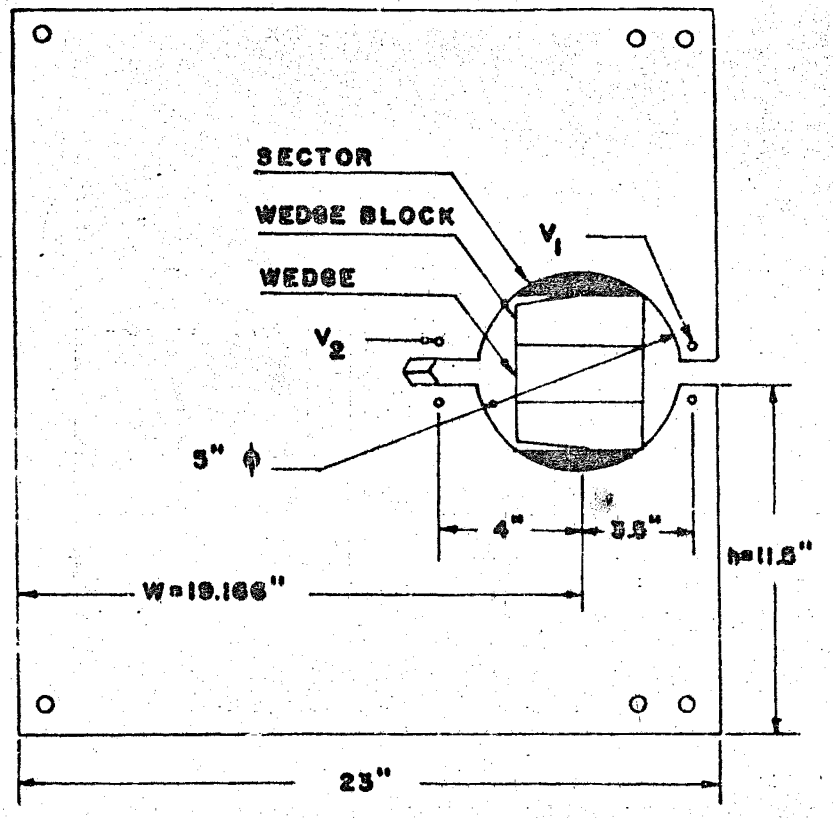

Fig. K-1 R-Curve Specimen

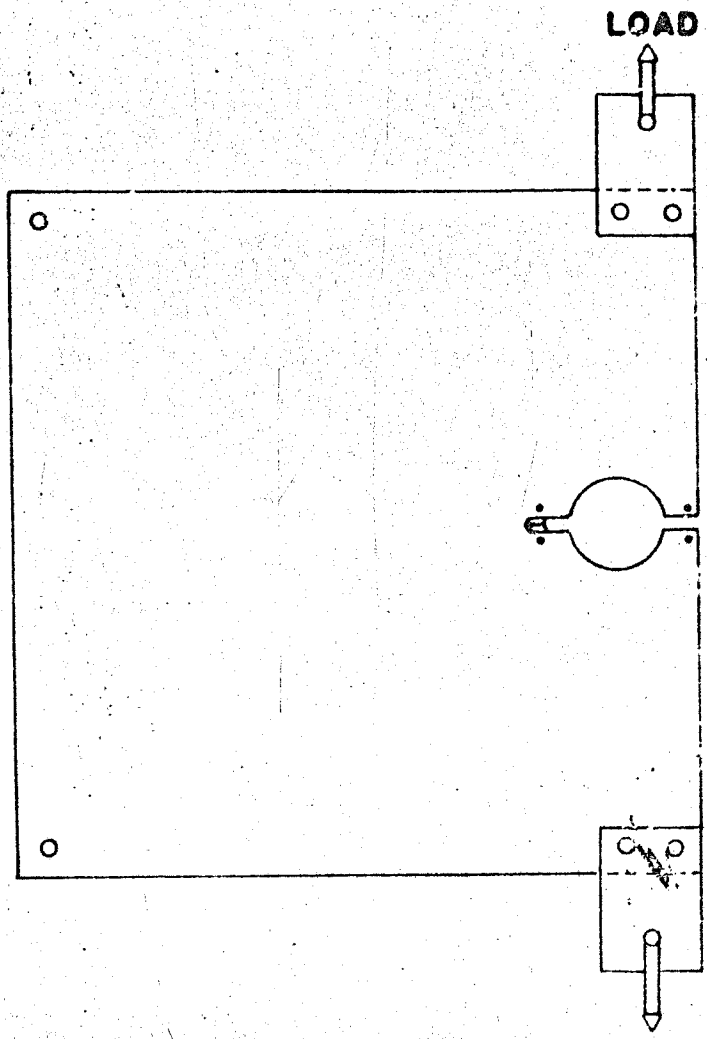

Fig. K-2 Pre-Cracking Fixtures

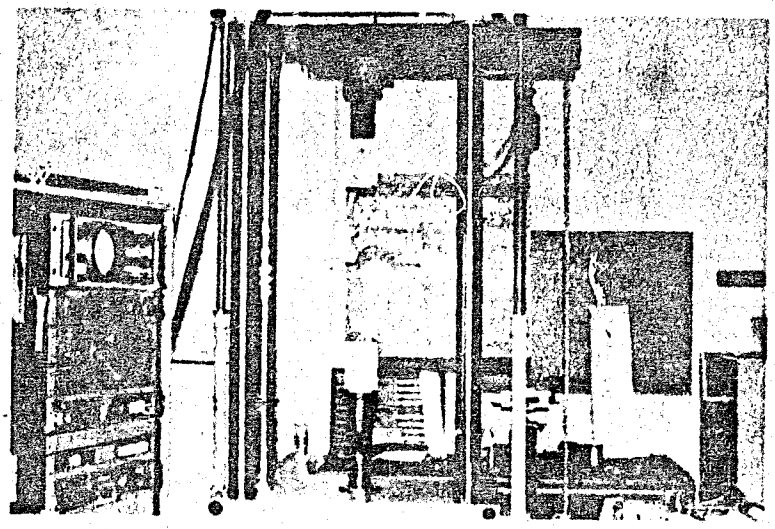

R-Curve Specimen being Pre-cracked in M.T.S. Machine

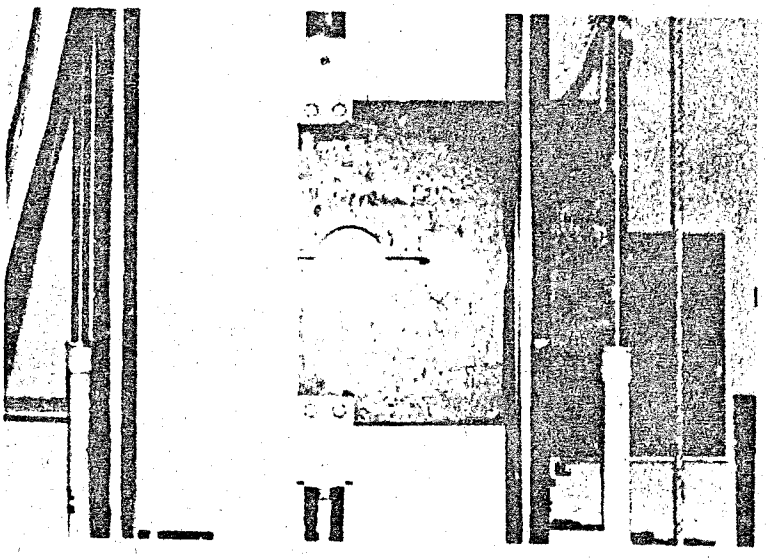

Closeup of R-Curve Specimen

Fig. K-3 Pre-Cracking Arrangement for R-Curve Specimens

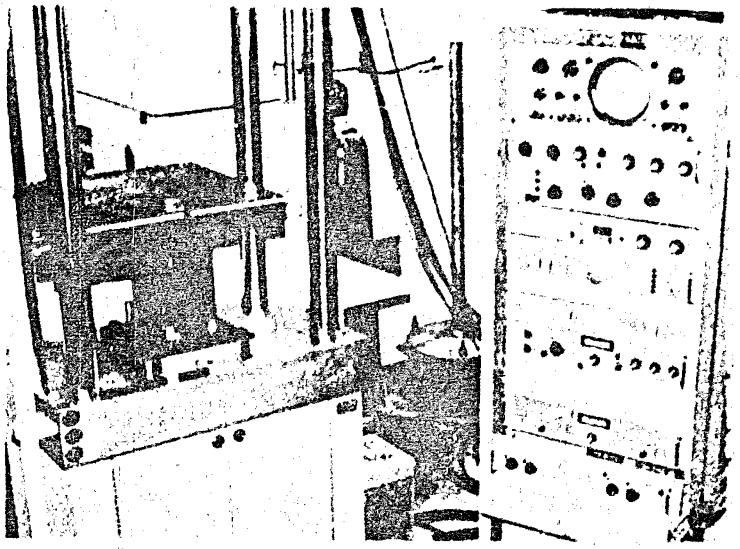

M.T.S. Machine with R-Curve Test Base and Specimen Mounted

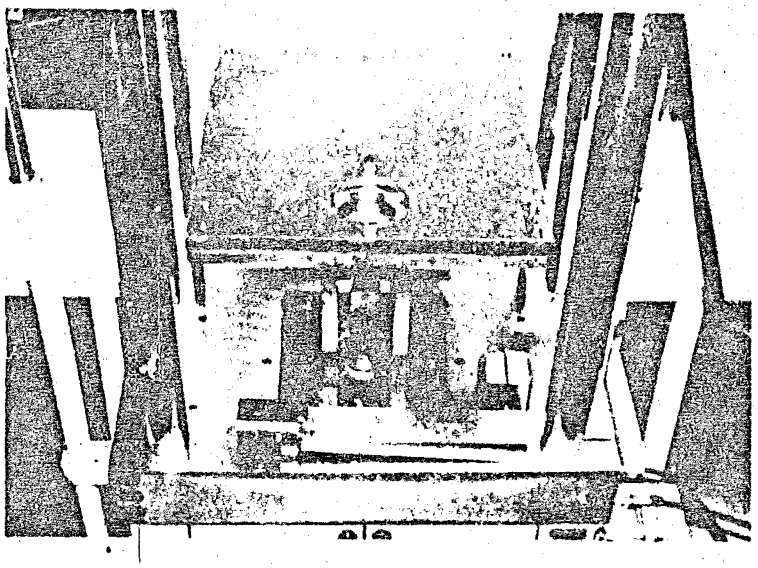

Closeup of R-Curve Test Base and Specimen

Note: Wedge and Clevis in foreground

Fig. K-4 R-Curve Test Base and Specimen

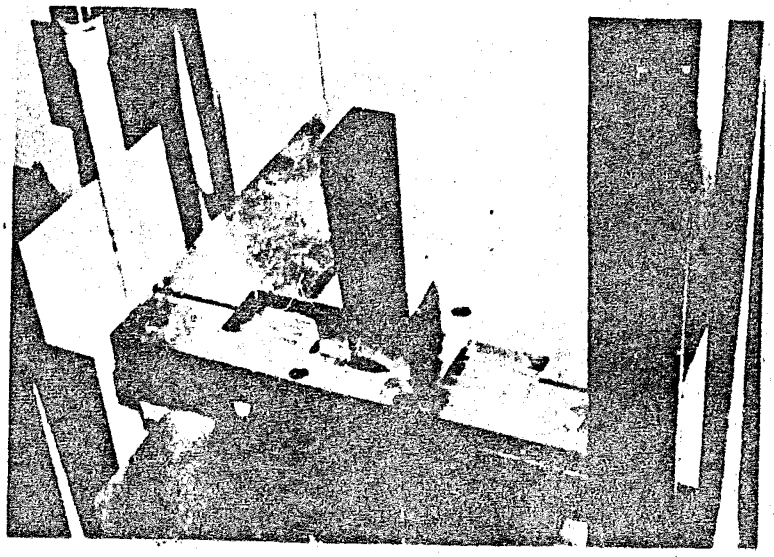

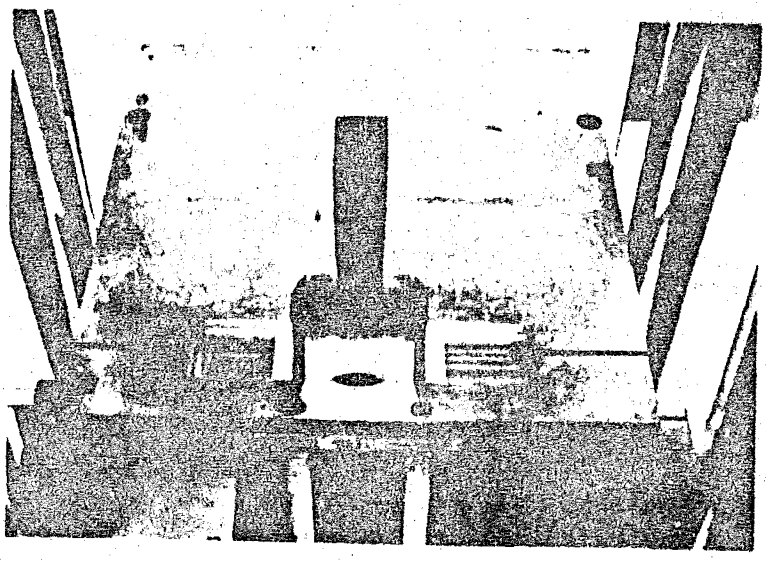

Fig. K-5 Closeup Views of R-Curve Test Base with Wedge and Wedge Block-Sector Inserted

Fig. K-6 Two Views of R-Curve Test System

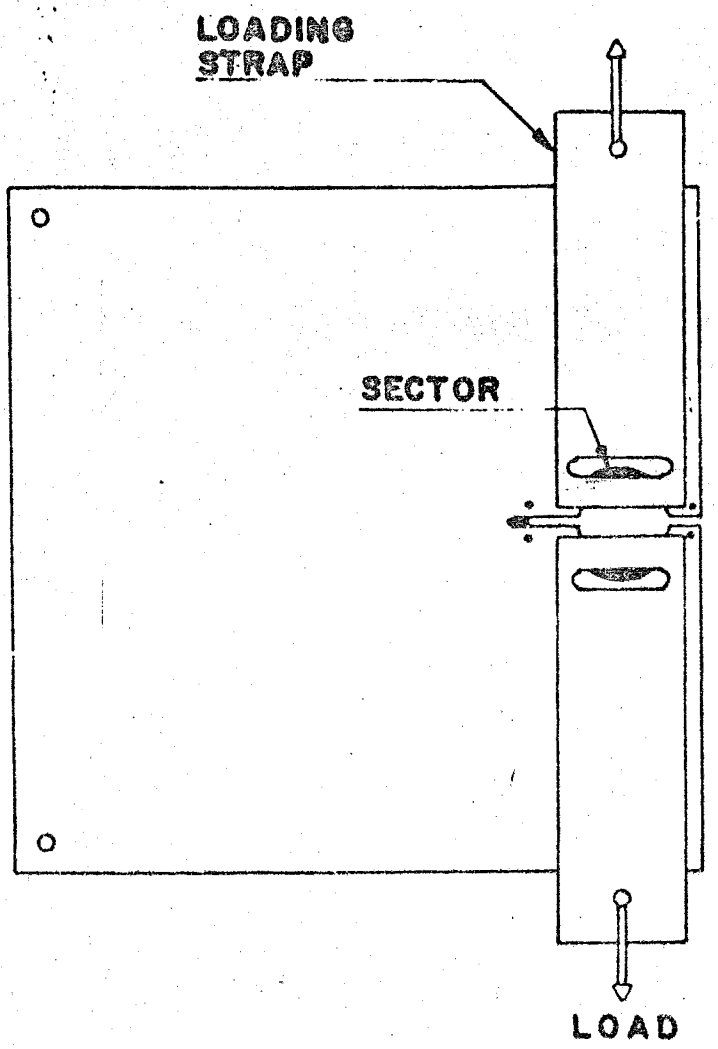

Fig. K-7 Compliance Measurement Fixtures

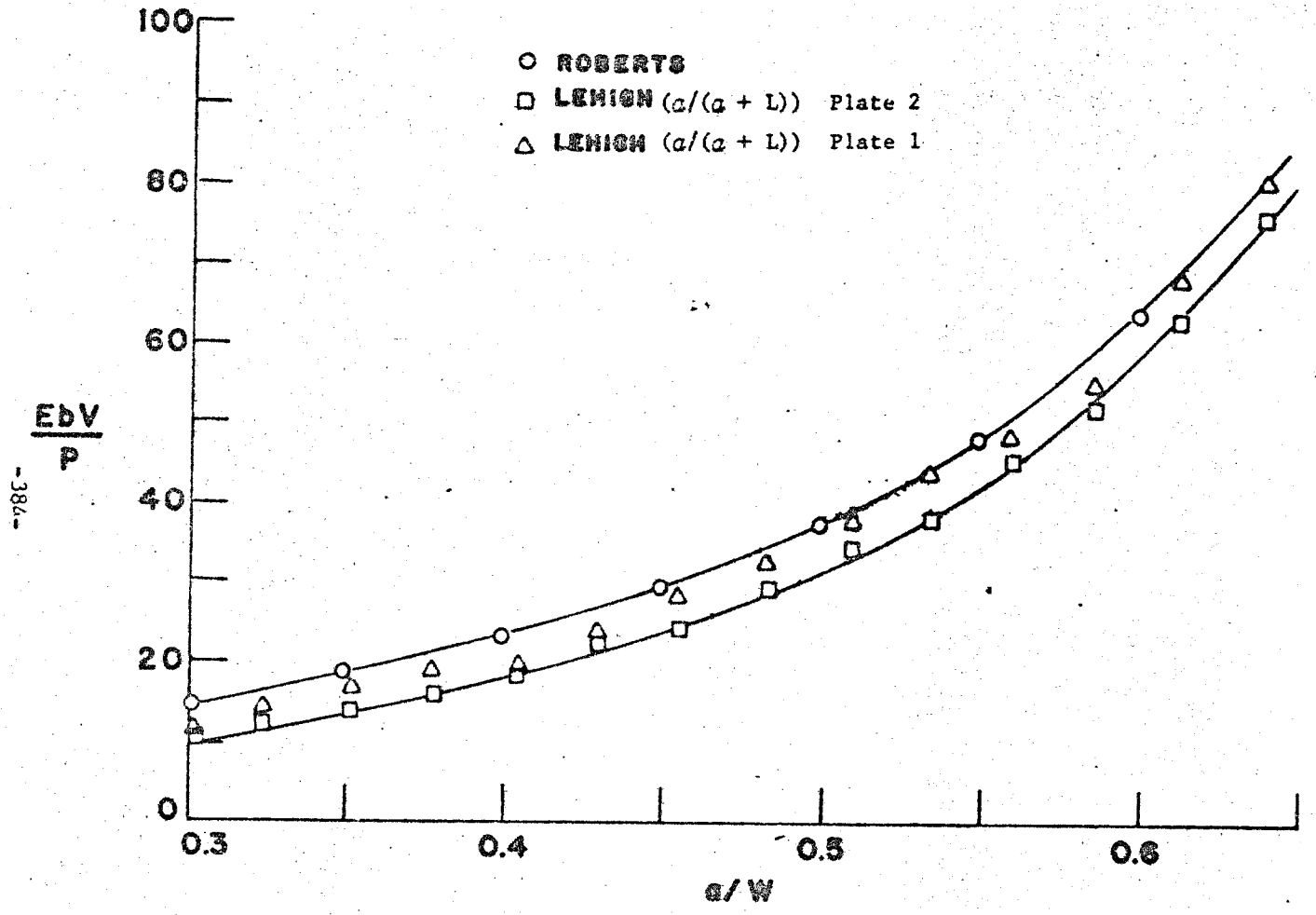

Fig. K-8 $\frac{E\,b\,V}{P}$ versus $\frac{a}{W}$

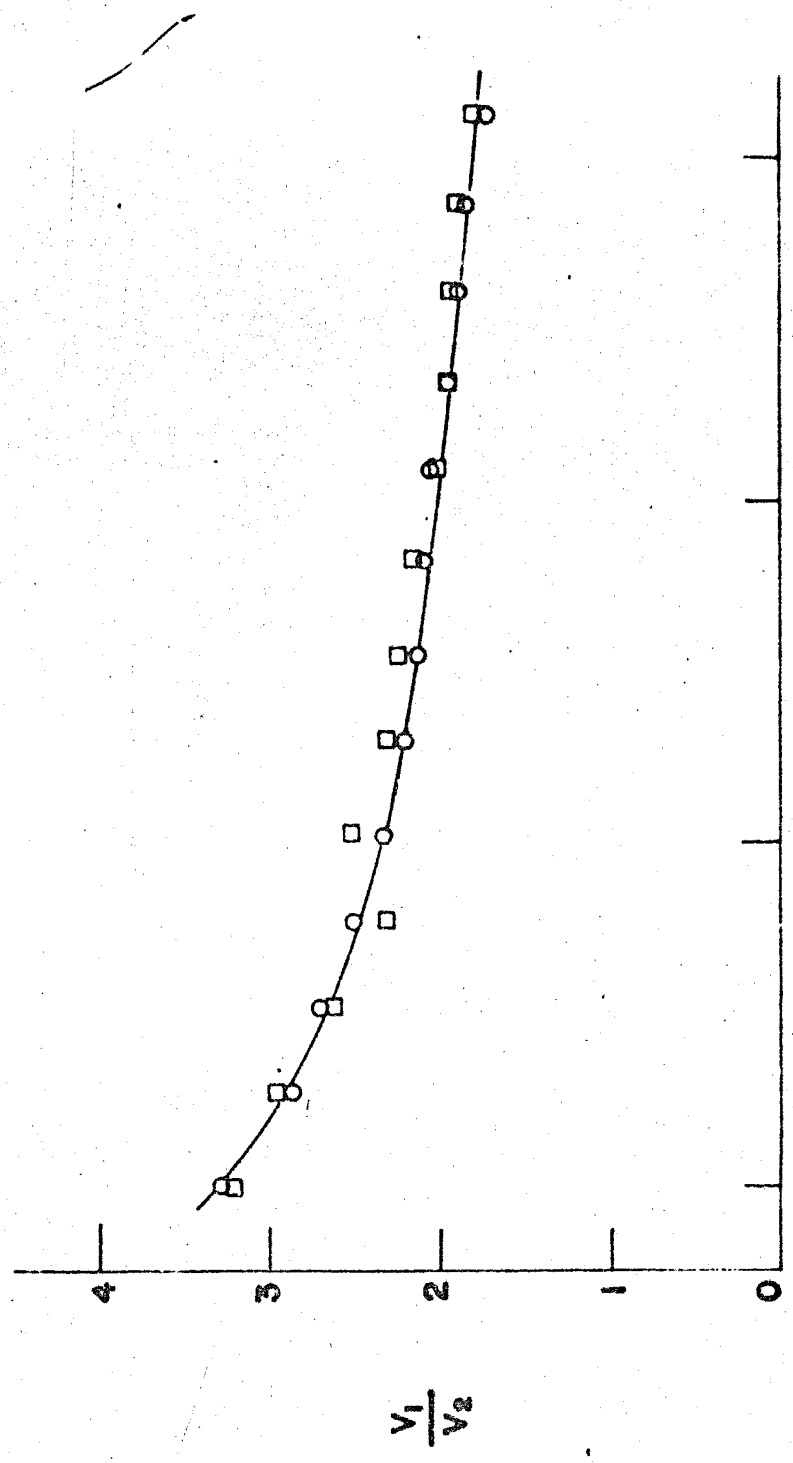

Fig. K-9 V_1/V_2 Compliance Curve

APPENDIX L CHARPY AND DYNAMIC TEAR MEASUREMENTS

L.1 Charpy Measurements

Standard V-notch Charpy specimens were manufactured according to ASTM standard A370-71 (20). These specimens were tested dynamically as per the specification as well as at a slow speed and intermediate test speed. For the slow and intermediate tests, the tests were performed on an Instron Test Machine at crosshead speeds of .02 in/min. and 2.0 in/min., respectively. The specimen temperatures were maintained by a constant temperature bath. For the slow and intermediate Charpy tests the energy absorbed was determined from the individual load displacement records. Precracked Charpy specimens were also tested at the same three test speeds as described above. The major difference in these tests were that the specimens were pre-cracked on a Manlabs Fatigue Precracker to a depth of approximately 0.05" below the notch. All energy levels for the precracked specimens were normalized to the standard notch depth so that the precracked data could be compared to the standard Charpy data.

L.2 Dynamic Tear Measurements

The energy absorbed in fracturing the A7, A440, A242, A588 and SAE 1035 dynamic K_c specimens were measured by absorbing the residual energy in the striking weight and tup by means of soft Aluminum blocks.

APPENDIX M - BEAM FATIGUE TESTS

M.1 Introduction

Fracture toughness testing as described in other portions of this report appear to give meaningful answers to fracture behavior of structural steels. The conventional method to design of structural members by limiting the applied stress to a value below the yield strength of the material tends to be inadequate in the presence of a sharp flaw (crack) and under conditions conducive to brittle fracture in the material. The reason for such an inadequacy is due to the very high localized stresses in the vicinity of the crack tip. As already discussed, factors influencing fracture behavior of a structural member are, apart from chemical composition and conventional mechanical properties, temperature, strain rate sensitivity and thickness of the member. It has been found from various test results, including results from the present program, that it is very difficult (for a given type of material) to define fracture toughness in any empirical or theoretical form which would describe the relative influence of all the various factors involved. Thus in many cases one is restricted to individually specified test data for engineering application.

In order to translate test data into an ability to predict fracture behavior of structural members, suitable analysis methods and

experimental verification must be sought. The analysis approach used in the present program utilized linear elastic fracture mechanics concepts. The method basically involves determination of a critical stress intensity factor which is a function of crack geometry, specimen size and the nature of applied stresses.

Four standard AISC 14 X 30, A36 rolled I beams with coverplates which were used earlier in a fatigue life study, were used for the exploratory experimental verification of proposed analysis methods. Details of beam specimen material, prior fatigue load history and other relevant factors are summarized in Table 1.

M.2 Stress Intensity Factor Estimation

In the present tests the cracked beams which were tested were not typical of what would be expected in service. Actual service cracks would generally tend to be semi-elliptical part-through cracks and they would not be as large as the ones tested in this work. However, since the four beams were available for the test, an examination of their fracture behavior was made.

Due to the complex shape of the cracks in the test beams more than one method of calculating K was potentially available for some of the beams. Test beam CPA 331(A) shown in Figure M-6 can be thought of as a beam cracked through the flange and into the web. Test beam CPA 332 (B) shown in Figure M-7 can be thought of as either a beam cracked through the flanges and into the web (the remaining flange material producing forces to reduce the K level) or as a beam where the flange

crack is viewed as an eccentrically located through-crack in a finite plate. Test beam TAA 341 (B) shown in Figure M-7 can be thought of as a cracked beam where the crack is modeled as an edge crack in a finite plate. Test beam TAA 332 (A) shown in Figure M-8 can be modeled as either a beam cracked through the flange and into the web (the remaining flange material producing forces to reduce the K level) or as an edge crack in a finite plate.

For the beams where the crack is viewed as through the flange and into the web, consider a beam with rectangular cross-section subjected to bending (Figure M-1). As per linear elastic fracture mechanics analysis the value of the stress intensity factor, K, at the crack tip is given by

$$K = \frac{6M}{b\,W^{3/2}\left(1 - \left(\frac{a}{W}\right)\right)^{3/2}}\, g\left(\frac{a}{W}\right) \qquad \text{(M-1)}$$

where

M = applied bending moment

W = specimen width

a = crack length

$g\left(\frac{a}{W}\right)$ = correction factor to include finite-width effects (see Table in Figure M-1)

Since I beams were used in the experimental work, a method of analysis was adopted which allowed the above equation to be used. The flexural strength of a beam subject to bending is primarily a

function of its section moment of inertia. In the present method, the test beam is considered as an equivalent beam, with thickness equal to the thickness of web (b) of the original beam and depth ($\bar{W}$), such that the moment of inertia of the beam remains unchanged. Thus the depth of the equivalent beam is calculated from the equation

$$\bar{W} = (12\ I/b)^{1/3} \qquad \text{(M-2)}$$

where I is the moment of inertia of the test beam. Figure M-2 shows details of the cross-section of the test beam and corresponding beam with rectangular cross-section. In order to calculate the equivalent crack length ($\bar{a}$), the crack tip is fixed at the same location as in the test beam, with reference to its centerline. Thus we have

$$\bar{a} = a_o + \frac{\bar{W} - W}{2} \qquad \text{(M-3)}$$

Equation (M-1) is now applicable for K value estimate.

For the case where the beam is modeled as an edge crack in a finite plate, the stress intensity factor can be written as

$$K = \sigma\sqrt{\pi a}\ \ f(\tfrac{a}{W}) \qquad \text{(M-3)}$$

where σ is the flange stress, a is the crack length and $f(a/W)$ is a function of the ratio of crack length to flange width. Values of $f(a/W)$ can be found in Reference (32). For the case of the eccentrically located through crack the stress intensity factor is given as (32)

$$K = \sigma\sqrt{\pi a}\ \ f(\lambda, \delta) \qquad \text{(M-4)}$$

where λ and δ refer to the relative position of the crack with respect

to the finite plate. Again σ and a are the flange stress and crack length respectively.

M.3 Procedure for Critical Load Calculations

In the case of a structural member failing by fracture, the failure criteria should be based on fracture toughness, K_c, values for the material. As the applied loads reach a critical value, the corresponding stress-intensity fracture, K, reaches the fracture toughness value of the material. It is important, however, to note that the choice of fracture toughness value will depend upon proper judgment of loading conditions and the actual test temperature.

Figure M-3a shows dynamic fracture toughness data obtained from 12" x 3" x flange thickness specimens cut from one of the test beams. Also shown in Figure M-3a is R-curve data for the A36 material tested in this program. The R-curve data can be used to estimate the values of K_c for slow loading. Figure M-3b gives CVN values for the flange material.

M.4 Experimental Procedure

The four beams chosen generally contained three-ended cracks generated from the weld joint (coverplate to the beam) during an earlier fatigue loading. One beam was tested under static load, at -50° F. A three-point bend test setup (Figure M-4) was used for the purpose. SR-4 strain gages were mounted in the vicinity of the crack tip to qualitatively monitor crack tip loading. Load was applied in

increments of 5000 lbs. by means of 100 kip capacity hydraulic jacks, up to a point where the test beam failed to take additional load. A split insulation box was used to chill the beam portion containing the crack. The desired temperature was maintained for at least 15 minutes prior to the test as well as during testing.

The remaining three beams were tested under semi-dynamic loading conditions (corresponding to loading rates of the order of 8000 lbs./sec.) and at temperatures in the neighborhood of -50° F. The test setup was essentially similar to that used for the first test except that a 300 kip Baldwin Universal testing machine was used to execute fast loading. Figure M-5 shows the general setup for the three tests. Fast loading was achieved by starting the top crosshead in motion and loading the beam as the moving crosshead made contact. The load and loading times was monitored by means of a Hewlett-Packard X-Y recorder. In all cases the test temperature was maintained at least for 15 minutes before the test started.

M.5 Discussion of Test Results

A summary of K-value estimates in terms of the applied load P for the beam specimens is given in Table M-2. It should be noted although an attempt to increase loading speed in the last three tests was made, that the loading rates were all approximately equal for the four tests. The test temperatures were also approximately equal at about -60° F. For this loading rate and temperature the yield strength of the A36 material will be elevated to about 46 ksi.

Coupled with the K-value estimates in Table M-2, estimates of K_c are needed to evaluate the test results. If it is suspected that cracking produced large loading rates at the crack tip as the crack began to run, K_c can have a low value of about 40 ksi $\sqrt{in}$ as seen in Figure M-3a. If the behavior is static, it is possible to use the R-curve results shown in Figure M-3a to estimate K_c. However, these results are not for the same A36 as found in the beams. It is possible to use the temperature shift discussed in Chapter 2 to estimate K_c from the CVN data in Figure M-3b. Using a shift temperature of 150° F and Barsom's results, equation (20), it is possible to estimate K_c. Using all of these places K_c for static conditions at upwards of 150 ksi $\sqrt{in}$. Thus there is an uncertainity in K_c which places its value between 40 and 150 ksi $\sqrt{in}$.

At attempt is made through the following discussion of each test, to account for the difference in observed results and predictions from the proposed analysis method.

M.5.1 Beam CPA 331(A)

The loading configuration and initial flaw size are shown in Figure M-6. For this beam the flange had been completely cracked during the fatigue testing and the crack had progressed 3.5 inches into the web. For the remaining section of this test beam, the plastic limit load is about 28 kips. Using a K_c of about 150 ksi $\sqrt{in}$ and the value of K given in Table M-2, K = 5P, gives a fracture load of about 30 kips. Thus considering the two calculated loads it would be expected that

this beam would fail by plastic yielding rather than fracturing. This was the case for this beam.

M.5.2 Beam CPA 332(B)

The loading configuration and initial flaw size are shown in Figure M-7. For this beam two calculations of K were made as shown in Table M-2. For the web crack K, $K = 2.52P$ and for the eccentrically loaded through crack K, $K = 1.03P$. Examining these two results indicates that if both K calculations are valid and K_c is similar at both crack tips, then the web crack will run first. If this occurs then the critical load will be for a K_c of 150 ksi $\sqrt{in}$, 60 kips. This is exactly the load at which the beam failed. Although such agreement is nice it is viewed as quite fortuitous. Also upon examination of the failed section it was not possible to decide which crack tip ran first.

M.5.3 Beam TAA 341(B)

The loading configuration and initial flaw size are shown in Figure M-8. For this beam K was calculated on the basis of an edge crack as shown in Table M-2. K is $K = 1.02P$. Thus for a K_c of 150 ksi $\sqrt{in}$ a critical load of 147 kips would be needed. For this beam, failure occurred by web buckling at about 95 kips and the test was stopped. This result tends to be consistent with the K calculations.

M.5.4 Beam TAA 332(A)

The loading configuration and initial flaw size are shown in Figure M-9. For this beam the K was calculated on the basis of a web crack, K = 2.32P and as an edge crack, K = 2.8P. This result coupled with a K of 150 ksi $\sqrt{in}$ give a failure load of 53 kips for the edge crack. In this particular test the failure load was 77 kips which is in fair agreement with the predicted value.

M.6 Summary

Meaningful stress analysis in terms of applied stresses or applied loads is an important step to translate any mechanical property of the material (as obtained from standard material tests) to predict structural behavior. Fracture analysis, complicated as it is in practical applications, will eventually be a simplified engineering estimate type analysis. The presently proposed methods to predict failure loads for a structural I beam assume (after visual inspection) rather ideal models of the beam. The mode of failure is anticipated (as an engineering judgment) based on the nature of load application, test temperature and a study of brittle-ductile transition behavior of the material from fracture toughness and Charpy V-notch test data.

It would appear, based on the present results, that the critical load for beam fracture can be predicted quite readily. However, it is cautioned that the present results be viewed with great care.

There are a great number of uncertainties involved in the calculations, a few of which are:

1. the value of K_c chosen on a judgment basis.
2. the crack lengths were not corrected for plasticity by an r_Y factor.
3. residual stresses are not accounted for.

TABLE H-1 TEST BEAM PRIOR HISTORY

Beam No.	$N_{Failure}$ (cycles)	S_{min} (ksi)	S_r (ksi)	
CPA 331A	16,613,000	10	5	all at end of flange coverplate
CPA 332B	8,451,200	10	5	
PAA 332A	3,170,200	10	12	
PAA 341B	48,200	10	18	

Note: All Beams are:

W14 X 30 ASTM A36

1/4" weld at ends of coverplates (Manual)

Average yield point (static) for all beams is 34.4 ksi

TABLE M-2 K ESTIMATES

Beam*	Loading Configuration	Loading Type	M (in-kips)	K Web Crack (ksi/in)	K Edge Crack (ksi/in)	K Eccentric Center Crack (ksi/in)
CPA 331A	Fig. M-6	Static	19.5P	5.0P	--	--
CPA 332B	Fig. M-7	Semi-Static	13.9P	2.52P	--	1.03P
TAA 341B	Fig. M-8	Semi-Static	13.3P	--	1.02P	--
TAA 332A	Fig. M-9	Semi-Static	12.5P	2.32P	2.80P	--

*Test Temperature N -50° F

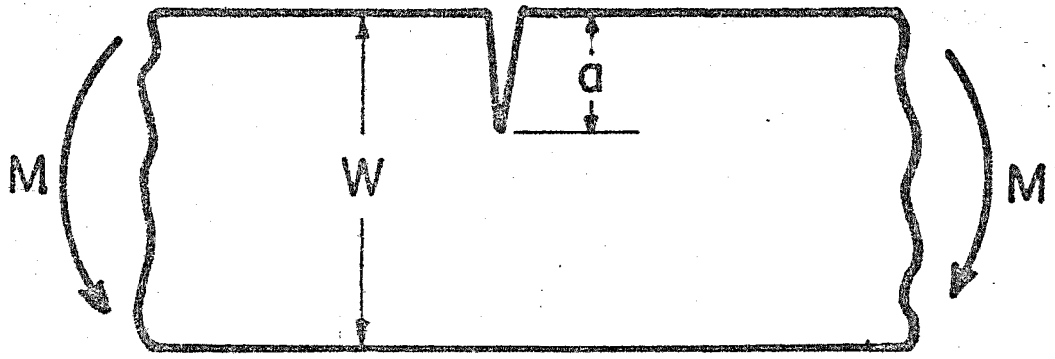

$$K = \frac{6M}{W^{3/2}\,(1 - \frac{a}{W})^{3/2}}$$

a/W	g (a/W)
0.5	0.36
0.1	0.49
0.2	0.60
0.3	0.66
0.4	0.69
0.5	0.72
0.6	0.73

Fig. M-1 Theoretical K Calibration

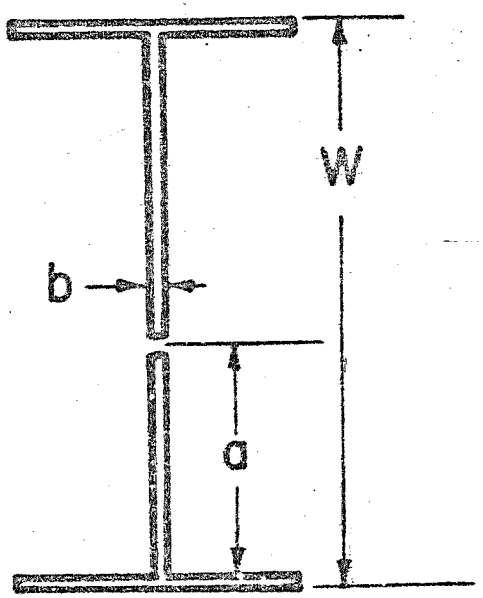

TEST BEAM CROSS-SECTION

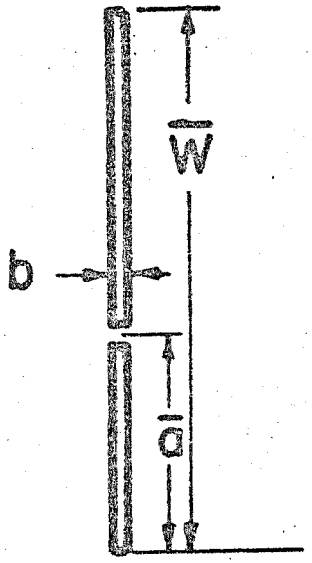

EQUIVALENT BEAM CROSS-SECTION

Fig. M-2 Test Beam Model

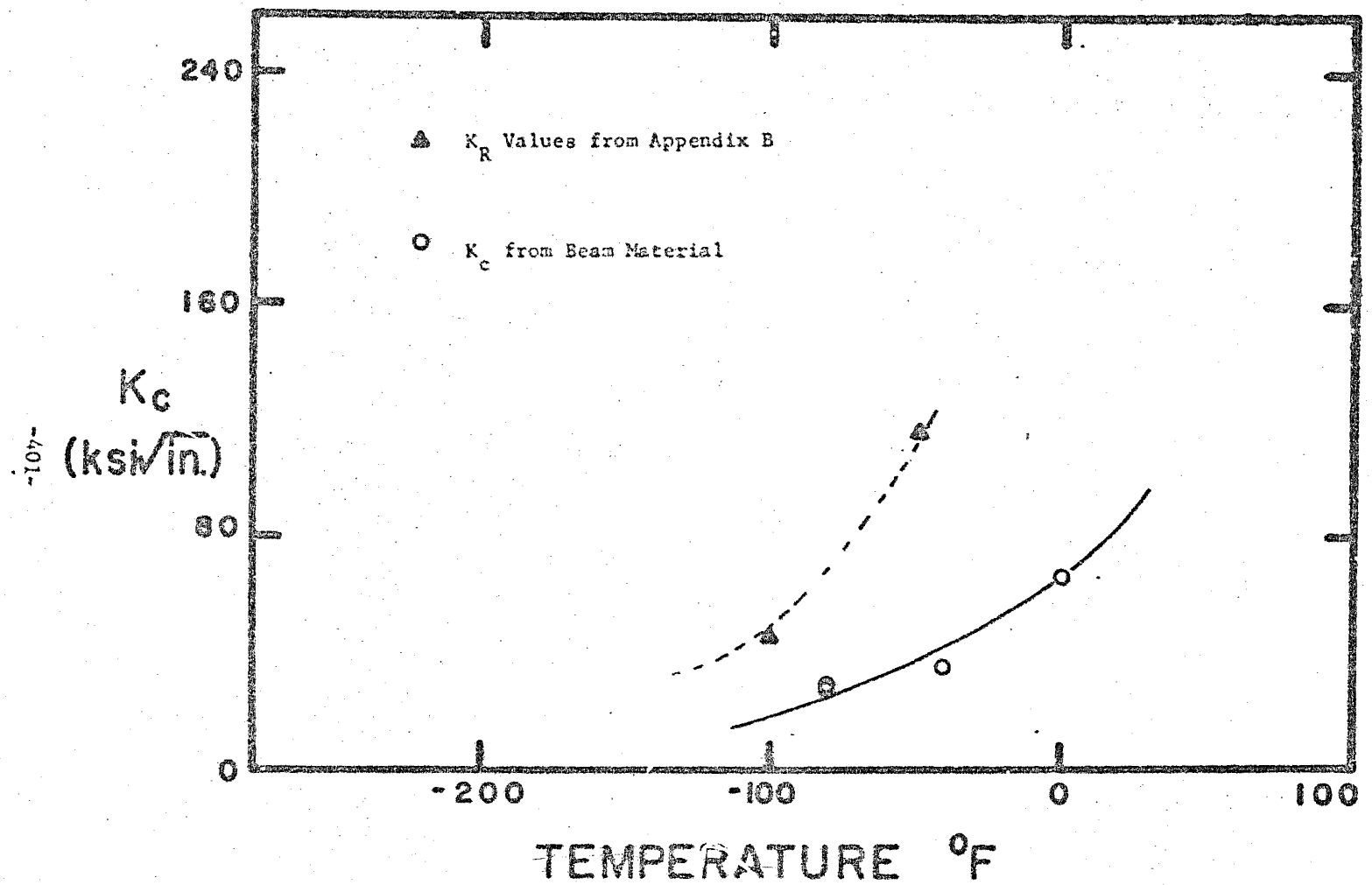

Fig. M-3(a) K_c Data for A36 Beams

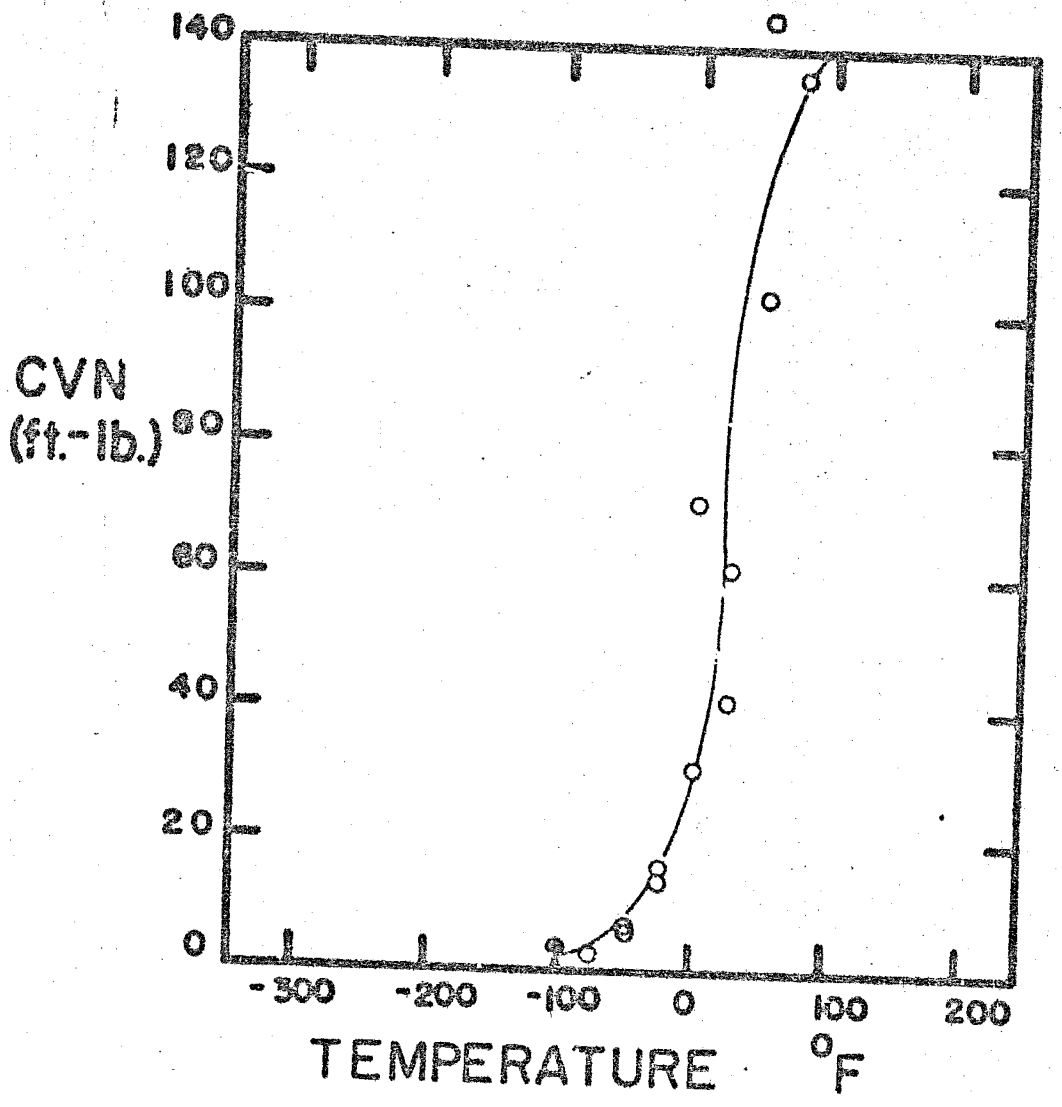

A36 1/2" Nocched Charpy Data (Specimens from Fracture Test Beams)

Fig. M-3(b) CVN Data for A36 Beams

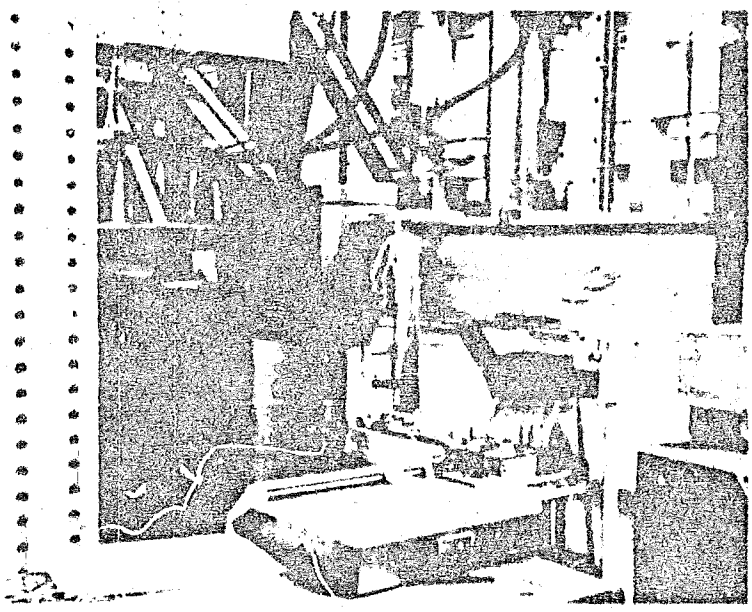

Fig. M-4 Test No. 1 Setup

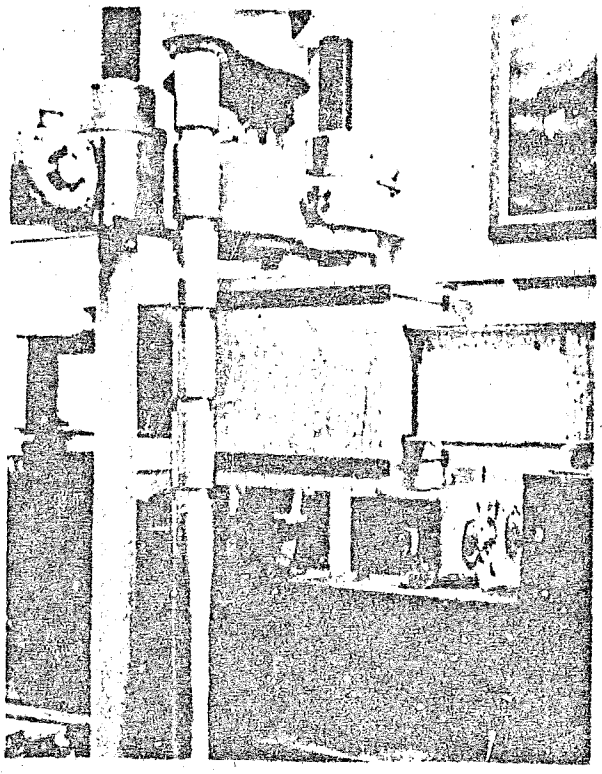

Fig. M-5 Test Beam and Cooling Box in 300 kip Baldwin Testing Machine

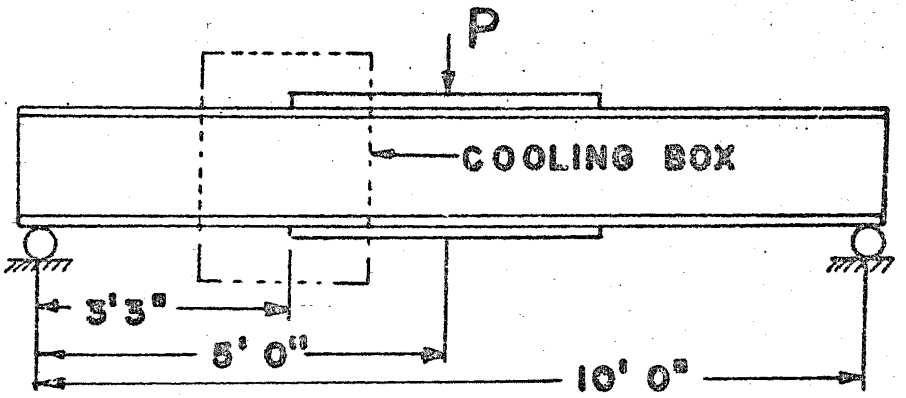

Fig. M-6(a)

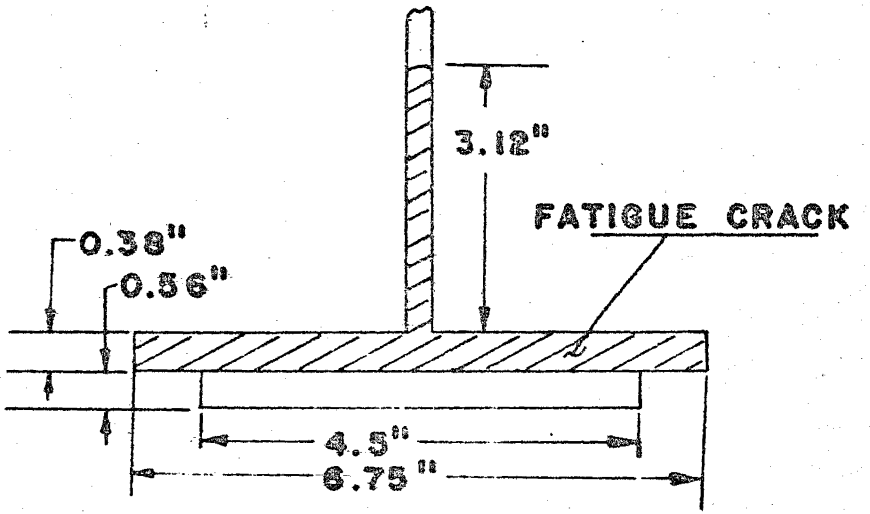

Fig. M-6(b) Test Beam CPA331(a)

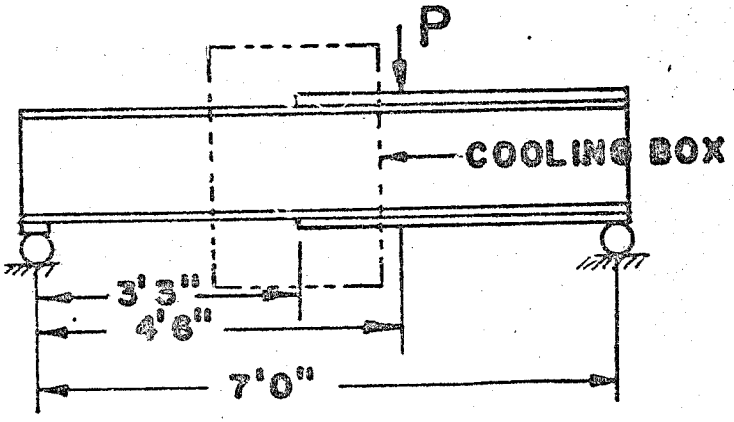

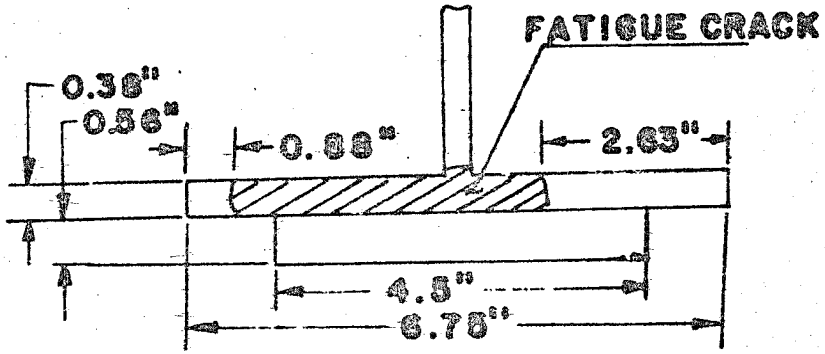

Fig. M-7 Test Beam CPA332(a)

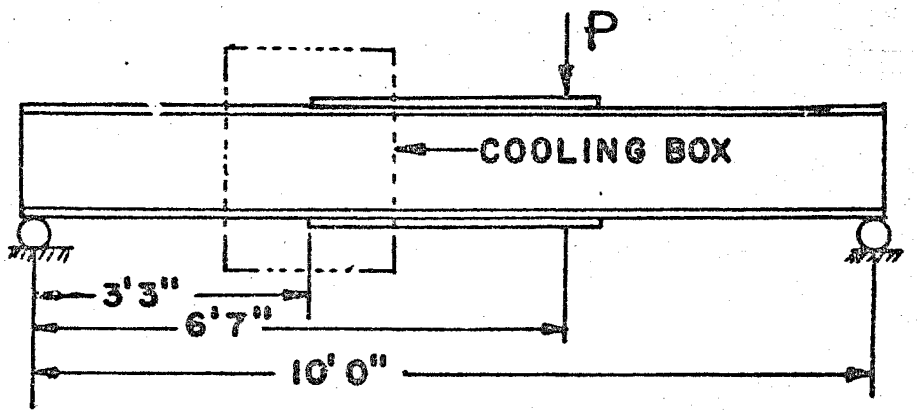

Fig. M-8(a) Schematic of Test Setup

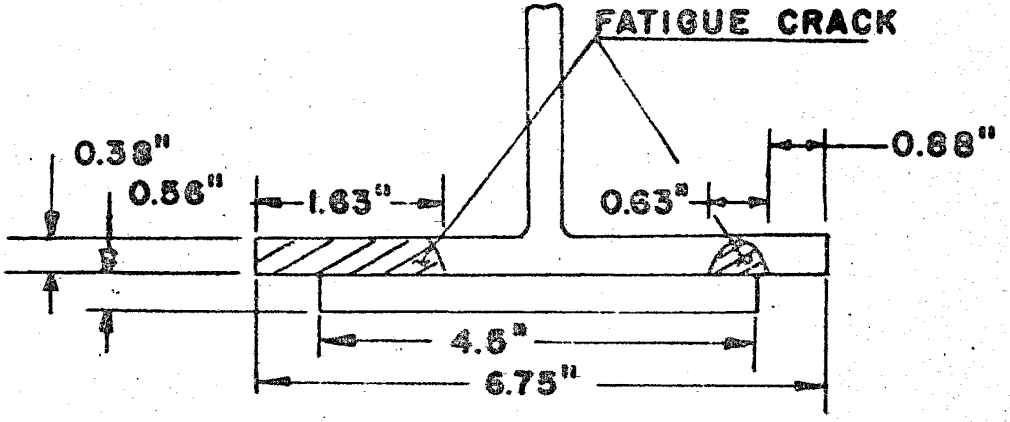

Fig. M-8(b) Test Beam TAA341(b)

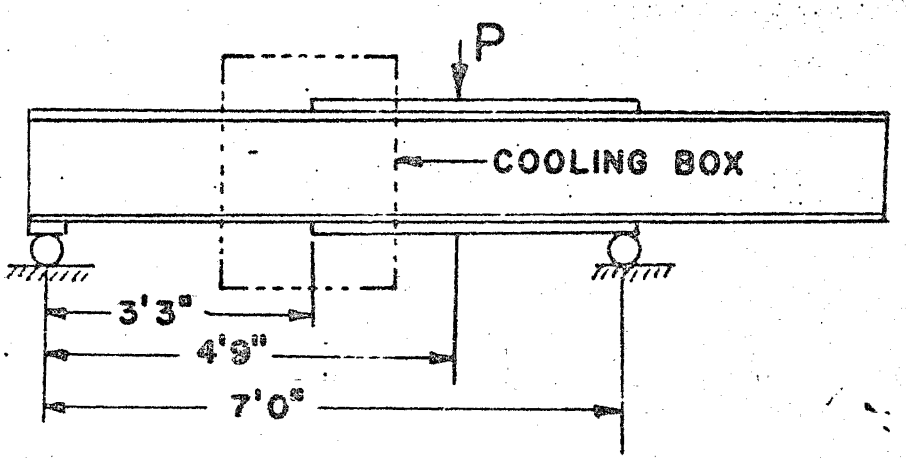

Fig. M-9(a) Schematic of Test Setup

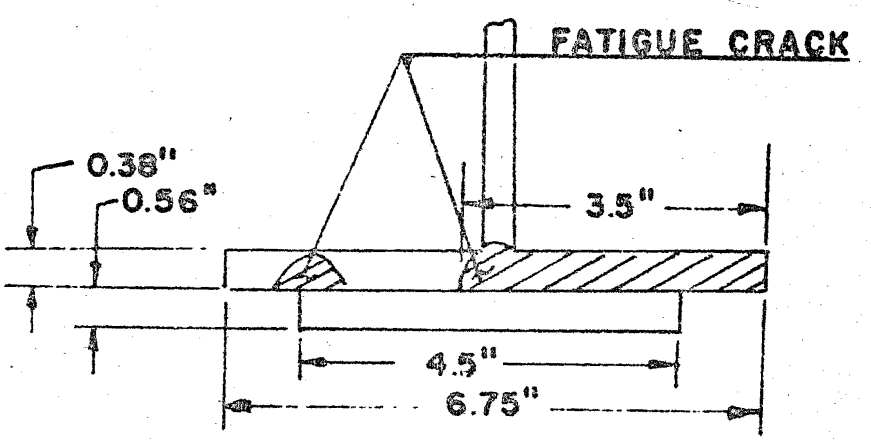

Fig. M-9(b) Test Beam TAA332(a)

APPENDIX N

SAMPLE K_c CALCULATION FROM THICKNESS-REDUCTION MEASUREMENTS

A441 Steel - 1 inch thickness, 36.5° F B = 0.9502 in.

$$S_o = \frac{B}{9} = 0.1056 \text{ in.}$$

$$r_Y = \frac{E\,\delta}{2\pi\,\sigma_Y} = 62.82\,\delta$$

S	X_1	X	B'	δ
0.110	1.0144	1.9624	0.9480	0.0022
0.105	1.0146	1.9622	0.9476	0.0026
0.100	1.0147	1.9618	0.9471	0.0031
0.095	1.0149	1.9615	0.9466	0.0036

S_n	δ	r_Y	r_Y/B	f
0.1056	0.00255	0.1602	0.1690	0.3034
0.0991	0.00349	0.2192	0.231	0.3129
0.0991	0.00318	0.2004	0.211	0.3103
0.0983	0.00327	0.2054	0.216	0.3110
0.0985	0.00325	0.2042	0.215	0.3108
0.0984				

$$K_M = \sigma_{YS}\sqrt{2\pi\, r_Y} = 86.0 \text{ ksi } \sqrt{\text{in.}}$$

K_c = 71.0 ksi $\sqrt{\text{in}}$ (calculated from maximum load)

Note: S, S_n, X_1, X_2, B', δ, r_Y → in.

REFERENCES

1. Highway Accident Report
   "Collapse of U. S. 35 Highway Bridge, Point Pleasant, West Virginia, December 15, 1967"
   Report NTSB-HAR-71-1, National Transportation Safety Board, 1971

2. W. F. Brown, Jr. (editor)
   "Introduction to Fracture Toughness Testing and Its Applications",
   ASTM STP 381

3. W. F. Brown, Jr. and J. E. Srawley
   "Plane Strain Crack Toughness Testing of High Strength Metallic Materials",
   ASTM STP 410

4. P. C. Paris and G. C. Sih
   "Stress Analysis of Cracks in Fracture Toughness Testing and Its Application", ASTM STP 381

5. ASTM
   "Tentative Method of Test for Plane-Strain Fracture Toughness of Metallic Materials",
   ASTM Designation E399-70T

6. W. F. Brown, Jr. and J. E. Srawley
   "Fracture Toughness Testing Methods in Fracture Toughness Testing and Its Applications",
   ASTM STP 381

7. R. H. Heyer and D. E. McCabe
   "Plane-Strain Fracture Toughness Testing Using a Crack-Line Loaded Specimen",
   Paper presented at the National Symposium on Fracture Mechanics, Lehigh University, June 1969

8. J. A. Begley and J. D. Landes
   "The J-Integral as a Failure Criterion",
   Paper presented at the National Symposium on Fracture Mechanics, University of Illinois, August 1971

9. G. R. Irwin, B. Lingaraja and H. Tada
   "Interpretations of the Crack Opening Dislocation Concept",
   Fritz Engineering Laboratory Report 358.2, June 1969

REFERENCES (continued)

10. C. M. Carman and G. R. Irwin
"Crack Opening Stretch and Thickness Contraction in Relation to R-Curves",
Paper presented at National Symposium on Fracture Mechanics, Carnegie-Mellon University, August 1960; also Frankford Arsenal Report R-2029, 1972

11. G. R. Irwin and K. Pietrzak
"Fracture Toughness Evaluation of Structural Steels",
Fritz Engineering Laboratory Report 366.2, June 1971

12. A. A. Wells
"Houdremont Lecture"
British Welding Journal, p. 2, 1965

13. ASTM
"ASTM Standard E-208 for DWT-NDT Fracture Testing"

14. G. R. Irwin
"Linear Fracture Mechanics, Fracture Transition, and Fracture Control",
Engineering Fracture Mechanics, Vol. 1, pp. 241-257, 1968

15. J. M. Barsom and S. T. Rolfe
"Correlations Between K_{Ic} and Charpy V-Notch Results in the Transition-Temperature Range",
ASTM STP 466, p. 281, 1970

16. H. T. Corten and R. H. Sailors
"Relationship Between Material Fracture Toughness Using Fracture Mechanics and Transition Temperature Tests",
University of Illinois T and AM Report No. 346, August 1971

17. C. N. Freed and R. J. Goode
"Correlations of Two Fracture Toughness Tests for Titanium and Ferrous Alloys",
NRL Report 6740, January 1969

18. R. B. Madison
"Application of Fracture Mechanics to Bridges",
Ph.D. Dissertation, Lehigh University, 1969,
Fritz Engineering Laboratory Report 335.2

19. D. E. Luft, R. B. Madison and G. R. Irwin
"Measurement of Dynamic K_c from the Drop-Weight Tear Test",
Fritz Engineering Laboratory Report 335.1, Lehigh University, 1969

REFERENCES (continued)

20. ASTM
"ASTM Standard A-370-71",
Vol. 31, ASTM Standards, 1971

21. B. Gross and J. E. Srawley
"Stress Intensity Factors for Three-Point Bend Specimen by Boundary Collocation",
Technical Note D-3092, NASA, December 1965

22. R. H. Heyer and D. E. McCabe
"Crack Growth Resistance in Plane-Stress Fracture Testing",
Presented at the Fourth National Symposium on Fracture Mechanics, Carnegie-Mellon Institute, August 24-26, 1970

23. R. H. Heyer and D. E. McCabe
"R-Curve Determination Using a Crack-Line-Wedge-Loaded (CLWL) Specimen",
Presented at ASTM E-24 Meeting, Hawthorne, California, September 29, 1971

24. E. Roberts, Jr.
"Elastic Crack-Edge Displacements for the Compact Tension Specimens",
Materials Research and Standards, MTRSA, Vol. 9, No. 2, p. 27

25. G. R. Irwin et al
"Basic Aspects of Crack Growth and Fracture",
NRL Program 6598, November 21, 1967

26. J. W. Fisher, K. H. Frank, M. A. Hirt and B. M. McNamee
"Effect of Weldments on the Fatigue Strength of Steel Beams",
NCHR Program Report 102, Highway Research Board, 1970

27. G. R. Irwin
"Structural Aspects of Brittle Fracture",
Applied Materials Research, Vol. 3, No. 2, p. 65, 1964

28. H. M. Branson
"Toughness Criteria for Bridge Steels",
Technical Report No. 5 for AISI Project 168, February 8, 1973

29. W. S. Pellini
"Advances in Fracture Toughness Characterization Procedures and in Quanitative Interpretations to Fracture - Safe Design for Structural Steels", NRL Report 6713, April 1968

30. E. A. Lange, P. P. Puzak and L. A. Cooley
"Standard Method for 5/8 Inch Dynamic Tear Test"
NRL Report 7159, August 1970.

31. L. A. Cooley and E. A. Lange
"Vertical Drop-Weight Machine for Conduting Drop-Weight NDT, Drop-Weight Tear and Dynamic Tear Tests", NRL Report 6993, January 1970.

32. G. C. Sih, "Handbook of Stress-Intensity Factors", Institute of Fracture and Solid Mechanics, Lehigh University, 1973.

GPO 884-514

END

DATE

FILMED

3-24-75

NTIS